Kun Liu · Daifen Chen · Serhiy Serbin ·
Volodymyr Patlaichuk *Editors*

# Gas Turbines Structural Properties, Operation Principles and Design Features


Springer

# Gas Turbines Structural Properties, Operation Principles and Design Features

Kun Liu · Daifen Chen · Serhiy Serbin ·
Volodymyr Patlaichuk
Editors

# Gas Turbines Structural Properties, Operation Principles and Design Features


Springer

*Editors*
Kun Liu
Jiangsu University of Science
and Technology
Zhenjiang, Jiangsu, China

Daifen Chen
Jiangsu University of Science
and Technology
Zhenjiang, Jiangsu, China

Serhiy Serbin
Admiral Makarov National University
of Shipbuilding
Mykolayiv, Ukraine

Volodymyr Patlaichuk
Admiral Makarov National University
of Shipbuilding
Mykolayiv, Ukraine

ISBN 978-981-99-0976-6 ISBN 978-981-99-0977-3 (eBook)
https://doi.org/10.1007/978-981-99-0977-3

Jointly published with Shanghai Scientific and Technical Publishers



This Springer imprint is published by the registered company Springer Nature Singapore Pte Ltd.
The registered company address is: 152 Beach Road, #21-01/04 Gateway East, Singapore 189721, Singapore

# Preface

The book provides an insight into the development, the current state of the worldwide variety of Marine gas turbines and its achievements.

For the first time ever in the educational literature, the book presents a detailed introduction and discussion of the gas turbine marine engine markets, major global manufacturers of marine gas turbines, and the main technical characteristics of different gas turbine engines types, which allows us to be more familiar with their types, dimensions, special features, and structures.

The major global manufacture of marine gas turbines, gas turbine engine classification, thermodynamic basics, geometric characteristics, application and thermal analyzing of working cycle, design and operation of the components, and efficiency improving methods are clearly presented and illustrated, because it is the main power installation of the marine.

The greatest attention has been given to marine gas turbines, which have great advantages as compared to other types of heat engines and different turbine engines. Of undoubted interest is the main ways of increasing the GTU efficiencies.

On top of that, this book also shows the working principles axial turbine, the design feature of the partial turbine stage, flow force action and peculiarities, and energy conversion processes in the multi-ring stage.

The book contains a lot of illustrations and rich figures, which are mainly published for the first time; they help get a better understanding of the educational content. The actual operations and designs of different modern ship gas turbine engines, thermal and principal schemes of marine gas turbines given in the book all offer ample opportunities for their application in the students' individual work.

The book content is systematized in such a way that the reader could navigate through it easily at the self-study of the subject. This is particularly the case for extramural and distance learning.

Zhenjiang, China — Kun Liu
Zhenjiang, China — Daifen Chen
Mykolayiv, Ukraine — Serhiy Serbin
Mykolayiv, Ukraine — Volodymyr Patlaichuk

# Contents

**Part I Operation Principles**

**1 Power Generation Market for Gas Turbines** ..... 3

**2 General Information About Turbine Design and Operation** ..... 11

**3 Thermodynamic Basics of the Turbine Theory** ..... 31

**4 Flow in the Plane Turbine Channels** ..... 49

**5 Features of the Actual Profile Flow. Cascade Loss Classification** ..... 59

**6 Gas Turbine Engine Classification** ..... 75

**7 Simple Cycle Gas Turbine Units** ..... 87

**8 The Features of GTU Thermal Calculation** ..... 99

**9 Thermal Calculation of the Simple Cycle Gas Turbine Unit** ..... 109

**Part II Design Features**

**10 Advantages and Disadvantages of the Power Plants with Gas Turbine Units** ..... 125

**11 Combined Marine Power Plants with Gas Turbine Engines** ..... 143

**12 Design and Operation of the Gas Turbine Parts. Inlet Casings of the Gas Turbine Unit** ..... 151

**13 Compressor Part of the Gas Turbine Unit** ..... 159

**14 Compression Work and Efficiency of the Compressor Stage** ..... 175

**15 Combustion Chambers of the Gas Turbine Units** ..... 193

**16 Turbine Part of the Gas Turbine Units** ..... 215

**17 Improving the Efficiency of the Gas Turbine Units** ..... 243

# Part I
# Operation Principles

# Chapter 1
# Power Generation Market for Gas Turbines


Forecast International predicts that the power generation market for gas turbines will continue to contract as it has done for the past five years. Sales in the ten-year period 2019–2028 will total $96.045 billion, 10.6% less than last year's sales projection for the 2018–2027 period [1, 2].

At present, General Electric (GE) controls 47.4% of the projected market by value, Siemens 21.9% and Mitsubishi Hitachi Power Systems (MHPS) 19.3%. These three OEMs (original equipment manufacturer) control 88.6% of the total market. The remaining 11.4% is comprised of a dozen or more companies led by Ansaldo Energia at 6.3%, followed by Mitsubishi Heavy Industries (MHI) at 3.3% and Solar Turbines at 3.3%. The remaining group of manufacturers collectively account for less than 1%.

The industrial and marine power generation market is shown in Fig. 1.1 [1, 2].

This market assessment of the marine gas turbine sector is based on the Forecast International Industrial and Marine Gas Turbine Database [1], a comprehensive listing of more than 41,150 gas turbine installations, of which 3,916 (9.51%) are gas turbines used for propulsion and 933 (2.27%) are gas turbines used for onboard power generation.

The marine gas turbine market is presented in Fig. 1.2 [1].

The startling thing about the marine gas turbine market is just how few companies are actually involved in it. During the 1980s, the major players absorbed the minor ones and the industry consolidated to just six players. Of these, Pratt & Whitney and Perm provided mostly aircraft engines for using on hovercraft and other air cushion vehicles. This is a very limited market, accounting for only 3% of the number of gas turbines supplied to the marine market. Vericor owes its position to its provision of gas turbines for the U.S. Navy Landing Craft, Air Cushion (LCAC) program. However, the follow-on program to the LCAC, the Ship-to-Shore Connector, will use Rolls-Royce MT7 gas turbines, suggesting that Vericor will not be participating in the future marine gas turbine market to the same extent. Thus, the key players in the marine gas turbine market are GE, Rolls-Royce and Zorya-Mashproekt. GE is



K. Liu et al. (eds.), *Gas Turbines Structural Properties, Operation Principles and Design Features*, https://doi.org/10.1007/978-981-99-0977-3_1

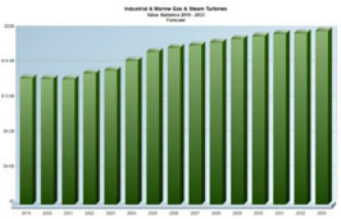

(a) industrial and marine gas and steam turbines

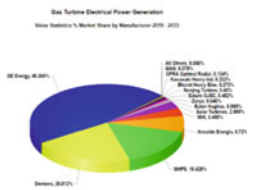

(b) gas turbine electric power generation (by manufactures)

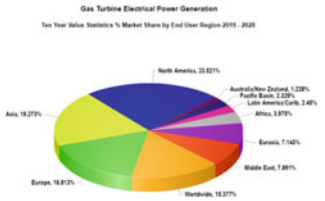


(c) gas turbine electric power generation (by region)

**Fig. 1.1** Industrial and marine power generation market

undoubtedly the market leader with nearly half the market, while Rolls-Royce and Zorya-Mashproekt split the rest between them [1].

To some extent, this concentration of the market into a few key suppliers is disguised by the fact that licensed production accounts for a significant number of gas turbines. Rolls-Royce and GE both have licensees in Japan, and GE has also licensed the LM2500 to Italy, India, Norway and Korea. Zorya-Mashproekt has sold production licenses to India and China. In computing the market share of the primary companies listed above, production by licensees is included within the totals.

### General Electric

General Electric Company (https://www.geaviation.com/marine) is one of the largest and most diversified industrial corporations in the world. GE traces its beginnings to Thomas A. Edison, who established his Electric Light Company in 1878. In 1892, Edison General Electric Company and Thomson-Houston Electric Company merged to form the General Electric Company.

Since the time of General Electric's incorporation in 1892, the company has developed, manufactured, and marketed a wide variety of products for the generation, transmission, distribution, control, and utilization of electricity. Over the years, the development and application of related and new technologies have considerably broadened the scope of GE's activities and those of its affiliates. The company's products include lamps, motors, locomotives, major appliances for the home, industrial electronic products and components, electrical distributions and control equipment, power generation and delivery products, nuclear power support services and fuel assemblies, and commercial and military aircraft jet engines. It also produces

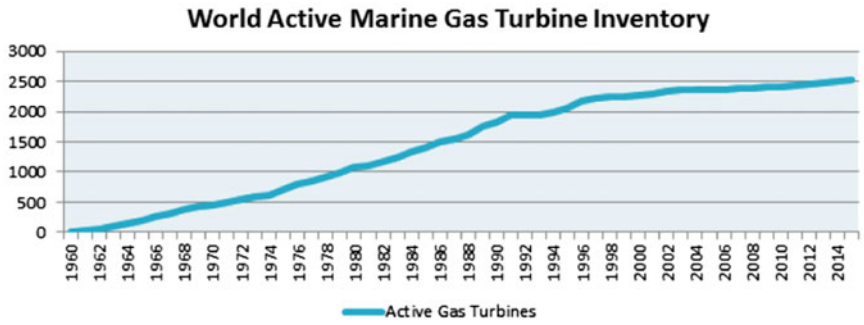


(a) marine gas turbine inventory

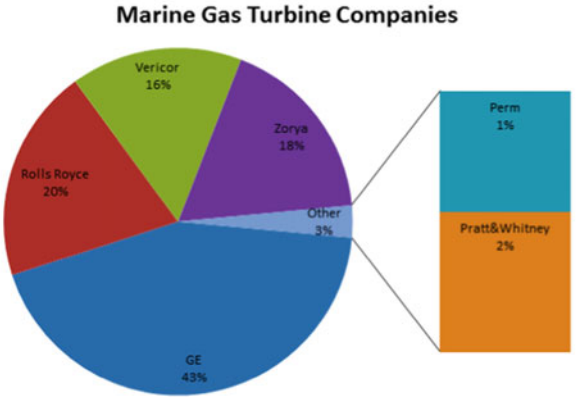


(b) marine gas turbine companies

**Fig. 1.2** Marine gas turbine market

engineered plastics, silicones, and cutting materials, as well as a wide variety of high-technology products used in aerospace, defense, and medical diagnostic applications. General Electric employs about 307,000 people worldwide [1].

Fully 95% of the marine propulsion gas turbines delivered by GE or its licensees are LM2500s of varying types. The LM1500 is long out of production and its support is in the hands of small aftermarket companies. The LM1600 has reached the end of its production life, while the LM500 achieved a limited degree of success as a power unit for fast attack craft but has never moved outside that niche [1].

The LM6000 appears to have achieved the most success as a power unit for offshore oil applications. Currently, there are 14 LM6000 gas turbines operating in marine installations, such as on floating production storage and off-loading (FPSO) vessels in the harsh North Sea environment. These engines had accumulated over

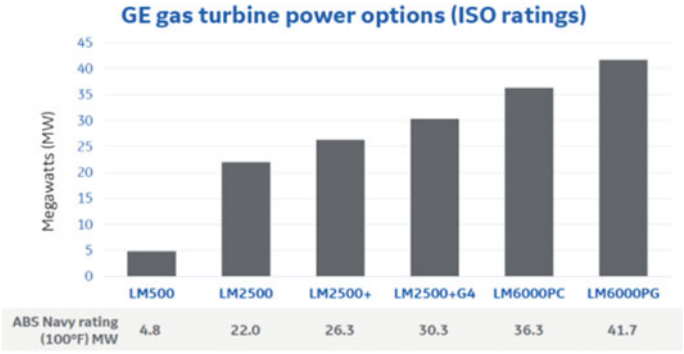


(a) gas turbine power options

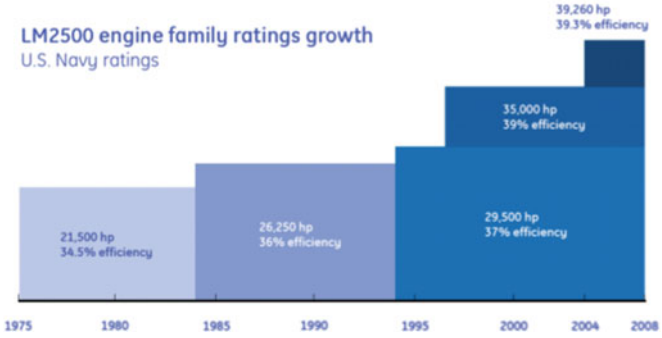


(b) LM2500 engine family rating grows

**Fig. 1.3** Parameters of marine GE turbines

260,000 fired hours in service by 2003. In April 2015, the LM6000 PC and PG models received Lloyd's Register's Design Appraisal Document to the Marine Naval Vessel Rules (NVR).

The newest model can operate in both simple-cycle and combined-cycle modes, and will quickly be available in both standard and DLE combustion models, capable of burning natural gas, fuel oil, or both in a dual-fuel capacity. The LM2500+G4, in combined-cycle mode relative to the LM2500+, will have more power, plus a 0.8% heat rate advantage.

Parameters of marine GE turbines are presented in Fig. 1.3 [3].

**Rolls-Royce**

Rolls-Royce (https://www.rolls-royce.com) was established in 1904 in Manchester, England when C.S. Rolls and Henry Royce joined forces to produce and market the

latter's automobiles in the United Kingdom. The company moved to Derby in 1908, and it involved in the production of aircraft engines for the Royal Fighting Corps during World War I. In the ensuing years, Rolls-Royce produced a wide variety of piston engines, and during World War II the company handled the lead development of the Whittle gas turbine engine. After the war ended, Rolls-Royce continued to refine its capabilities in both aero and industrial/marine gas turbine engines [1].

During the 1960s, Rolls-Royce began the development of the RB211 turbofan engine. The RB211 design featured the use of a new carbon-fiber material—Hyfil that was lighter than aluminium and stronger than steel. However, the protracted and costly development of the Hyfil resulted in substituting Hyfil components with those made of titanium. The subsequent redesign, labor, and material costs escalated rapidly, culminating in the company declaring bankruptcy in 1971. At that time, the restructured, nationalized Rolls-Royce Ltd. concern was formed, with Rolls-Royce Motors Ltd restructured as a separate public company. Rolls-Royce Motors Ltd was currently a company of the Vickers plc group.

In 1995, Rolls-Royce expanded its presence in its largest market, the U.S., through the acquisition of Allison Engine Company. The acquisition gave Rolls-Royce a firm base from which its engines could compete for U.S. military programs. In November 1999, Rolls-Royce completed the purchase of Vickers plc, further enhancing its global position in marine power systems. The company was divested from Vickers Defence Systems in late 2002 [1].

As evidenced by the pie chart, Rolls-Royce has a much more diversified product portfolio than General Electric and has exploited advancing gas turbine design technology to the fullest. It was making major inroads into General Electric's once-solid monopoly of U.S. Navy gas turbine supply. With the success of the MT30 in securing contracts at the high end of the power spectrum and the emergence of the MT7 as a viable contender at the low end, Rolls-Royce has revitalized its product line. This will continue to be the case if the developing use of integrated full electric propulsion emphasizes the value of the MT7 as a ship service generator that contributes its output to the electricity pool of the ship. Marine gas turbines delivered by Rolls-Royce are shown in Fig. 1.4 [1].

**Zorya-Mashproekt**

Zorya-Mashproekt (https://zmturbines.com/en/about-company/) is a Ukrainian company founded in the early 1950s. Since the middle 1950s, the Enterprise has been designing and producing marine gas turbine propulsion plants for displacement ships, hovercrafts, and hydrofoils. Zorya-Mashproekt has developed and produced unique reversible gas turbine plants which allow the ship to change immediately the direction of movement [1].

Since the late 1960s, the Enterprise has been shipping gas turbines for electricity-generating plants and since 2010 the completed power generation units have been delivered to the customers.

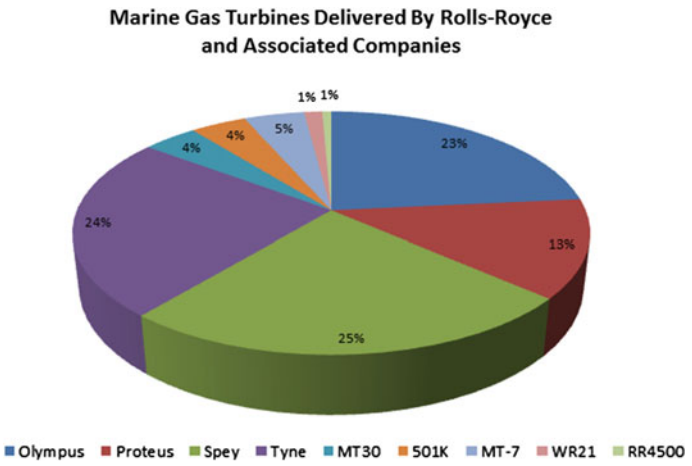


**Fig. 1.4** Marine gas turbine delivered by Rolls-Royce

In the 1970s Zorya-Mashproekt released gas turbines for natural gas pumping units. Over the past 65 years, the Enterprise has developed gas turbine plants available in the power range from 100 to 11 MW. Today the Enterprise produces 3–25 MW gas turbine engines. Every engine has several modifications for different applications. The design features of engines and their characteristics are constantly being improved. They are able to run on different grades of gaseous and liquid fuels. The Enterprise has developed and manufactured the gear boxes for all types of displacement ships and step-up gears for the driving system of electric generators, compressors, and pumps. The gear boxes have a variable gear ratio and can engage/disengage power inputs.

The modern gas turbines produced by Zorya-Mashproekt are referred to as the UGT series (UGT apparently simply standing for Ukrainian Gas Turbine), with "UGT" followed by a number that is the listed output of the gas turbine in question measured in kilowatts. Thus, the UGT 25,000 is a Ukrainian Gas Turbine rated at 25,000 kW.

Historically, Zorya's biggest—indeed only—market was the warship production of the Soviet Union. Nearly all Russian gas turbine-powered warships use machinery from this plant, the only exceptions being a few air cushion landing craft that uses aero-derived gas turbines.

Marine gas turbines delivered by Zorya are presented in Fig. 1.5 [1].

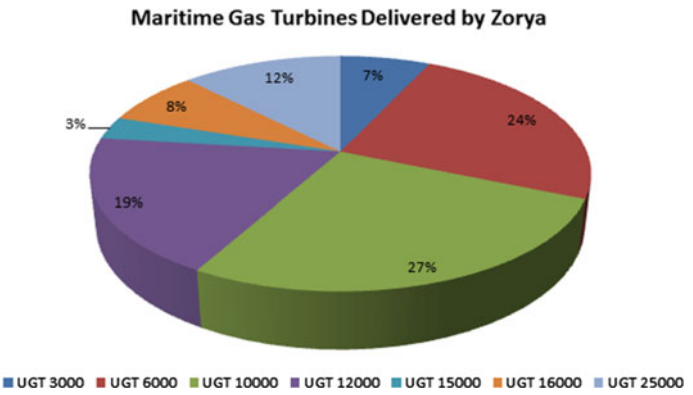


**Fig. 1.5** Marine gas turbine delivered by Zorya-Mashproekt

## References

1. Slade SL (2015) Competing manufacturers of marine gas turbines. A special descriptive market analysis. Forecast Int. http://www.fi-powerweb.com/Downloads/Competing-Manufacturers-of-Marine-Gas-Turbines.pdf
2. Worldwide gas turbine report, TMI Staff & Contributors (2020). https://www.turbomachinerymag.com/worldwide-gas-turbine-report/
3. Building on a marine power legacy. http://www.mce-asic.co.uk/marine/systems/propulsion-systems/docs/ge-experience.pdf

# Chapter 2
# General Information About Turbine Design and Operation


## 2.1 Design and Principle of Operation of the Simplest Axial Turbine

The turbine is a rotary engine designed to transform the reserve of the working fluid potential energy into mechanical energy [1].

The working body of the steam and gas turbines is, respectively, the water vapor or gas (or a mixture of gases), and the reserve of its potential energy is determined by the excess pressure and the temperature in the initial state.

We consider the design and principle of the operation of the turbine, the schematic diagram of which is shown in Fig. 2.1. The axial turbine is the turbine in which the flow of the working fluid is parallel to the shaft [1].

The main elements of the turbine are the nozzles 1, formed by the nozzle blades (the vanes) fixed in the housing 4, and the rotor (working) blades 2, collected along the rim of the disk 3. A set of the nozzle vanes or the static guide vanes accelerates and adds swirl to the fluid and directs it to the next ring of the turbine blades mounted on a turbine rotor. The disk is made together with the shaft 7 or separately and then connected rigidly with it. The shaft, together with all the parts mounted on it, forms the rotating part of the turbine—the rotor.

The position of the rotor relative to the housing is fixed by the journal bearings 6 and 13 and the thrust bearing 12. The bearings are mounted in chairs 9 and 11 connected to the lower half of the housing. With the assistance of the chairs, the turbine is fixed to the base. The housing has pipes for supplying the working fluid (the inlet pipe) and for the outlet (the exhaust pipe). Where the shaft exits the housing to isolate the internal cavities from the environment, the outer seals 5 and 10 are provided. The power generated by the turbine is transmitted to the consumer via the flange or the coupling 8. The nozzles and the working ring are formed by special-profile blades and have the appearance of a grid of blades. In these grids, the working process is carried out.



K. Liu et al. (eds.), *Gas Turbines Structural Properties, Operation Principles and Design Features*, https://doi.org/10.1007/978-981-99-0977-3_2

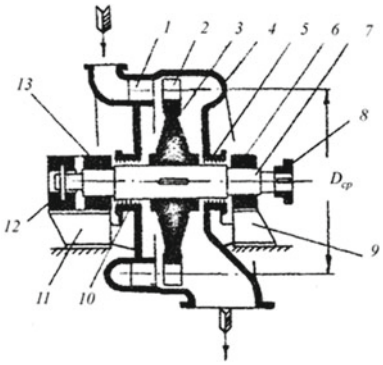


**Fig. 2.1** Diagram of the simplest axial turbine

The combination of the nozzles and the working ring placed behind it together with the bearing parts is the turbine stage. From this point of view, the concerned turbine is a single-stage.

The conversion of the potential energy of the working fluid into kinetic is due to its expansion in the blade channels. The pressure of the working fluid decreases and the velocity relative to the channel walls increases. Against this background, the concepts of "expansion" and "conversion of potential energy into kinetic" are further identified and used as equivalents for convenience.

The diagram of the flowing part of the turbine stage, as well as the scan of a cylindrical section of its average diameter on the plane in the form of profile grids, are shown in Fig. 2.2. The identification of the characteristic stage cross sections: 0—in front of the nozzle blade; 1—behind the nozzle blade (before the rotor blade); 2behind the rotor blade (behind the stage). The corresponding indexes will also denote all the parameters in these sections.

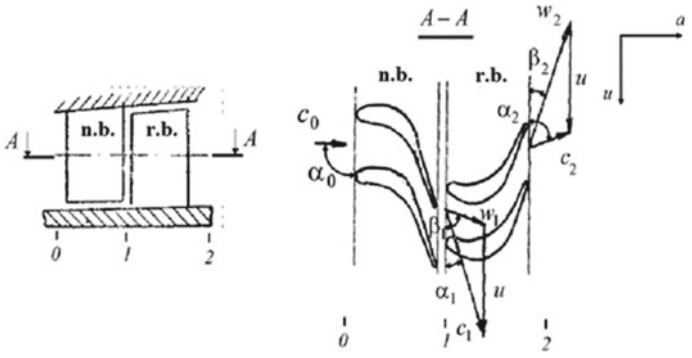


**Fig. 2.2** Diagram of the turbine stage. (n.b.—a nozzle blade; r.b.—a rotor blade)

We assume that all parameters change only within the cascade of the turbine blades, and remain unchanged before the stage, behind it, and in the gap between the cascades.

The working body in the cascades is involved in the complex motion, so we will distinguish its velocity—the *absolute c*—is the relative stationary elements of the turbine, and the *transport u*—is the velocity of the channel relative to the fixed elements, and the *relative w*—is the velocity relative to the walls of the channel. In this case, according to the law of mechanics is the following:

$$\vec{c} = \vec{w} + \vec{u}. \tag{2.1}$$

For the fixed (nozzle) blade cascade $u = 0$ and therefore $c = w$, for the rotor blade cascades the circumferential velocity of the blades is the transport velocity ($u = \pi\, D\, n$, where $D$ is the cross-section diameter, m; $n$ is the rotor speed, $s^{-1}$), and Eq. (2.1) is used in full form.

In determining the directions of the flow velocities (the angles to the frontal cascade plane) we will use $\alpha$ for the absolute velocities and $\beta$ for the relative velocities. The nozzle stream of the working fluid flows with some absolute velocity $c_0$ at an angle $\alpha_0$. In the nozzle blades, the working fluid expands, its pressure decreases, and the velocity increases to $c_1$. The nozzle exit flow angle $\alpha_1$ is determined by the shape of the profiles and their location in the cascade.

The gas flow with the absolute velocity $c_1$ and the kinetic energy corresponding to it flows to the rotor blade cascade. In the inlet cascade section, the flow has a relative velocity $w_1$, which according to (2.1) the following:

$$\vec{w}_1 = \vec{c}_1 - \vec{u}.$$

The implementation of the last ratio is graphically depicted on the cross-section of the rotor blade cascade (the direction $u$ coincides with the direction of the movement of the rotor blades). The vectors $c_1$, $w_1$ and $u$ form the so-called inlet velocity triangle for the rotor blade cascade.

The velocity triangles may be drawn for both the inlet and outlet sections of any turbomachine. The vector nature of the velocity is utilized in the triangles, and the most basic form of the velocity triangle consists of the circumferential velocity, the absolute velocity and the relative velocity of the fluid making up three sides of the triangle.

The relative velocity of the gas outlet from the rotor blade cascade depends on whether the expansion in the blade channels continues or not (if "yes", $w_2 > w_1$), as well as the energy losses in the channels. The direction of the velocity $w_2$ (the angle $\beta_2$) is determined by the shape of the profiles of the working blades and their location in the cascade.

According to (2.1), the absolute gas velocity at the stage outlet $c_2$ is equal to the sum of the relative $w_2$ and the transport $u$ velocities (see the outlet velocity triangle); and $c_2 < c_1$, which is the result of converting the kinetic energy of the stream into the work.

As gas flows through the cascade, the acting on the blades forces arose. The total force $P$ which is acting on the rotor blades can be conditionally divided into two components: the circumferential force $P_u$ and the axial force $P_a$ (Fig. 2.3), so that

$$P = \sqrt{P_u^2 + P_a^2}.$$

The tangential component is the driving force that executes the useful work in the turbine.

The nozzles may be arranged throughout the circumference or only part of it. Then the turbine stage is called the stage with the partial inlet of the working fluid or partial stage that is characterized by the inlet rate as the following:

$$e = \frac{l_{\text{act}}}{\pi D_m},$$

where $D_m$ is the medium stage diameter; $l_{\text{act}}$ is the length of the active arc (the inlet arc) at the medium diameter.

It is obviously, that in stages with the full inlet of the working fluid $e = 1$.

When rotating the partial stage, the rotor blades pass alternately the active zone, when the working fluid comes from the nozzle channels, and the idle zone when they interact with the stagnant substance. Therefore, the partial causes additional and sometimes very significant stage losses. However, in some cases it is used in stages with low flow rates: at low flow rates and full inlet, the stage may have too short blades or small diameters, resulting in losses even greater than in the partial stage. In addition, the design of the small diameter turbines can have design difficulties. Therefore, it is more appropriate to apply a partial stage of a larger diameter with blades of the acceptable length than a stage with a full inlet.

The turbine as an engine differs from the piston engine by a number of essential features.

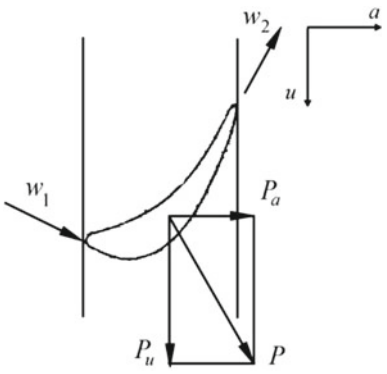


**Fig. 2.3** Components of the aerodynamic force

The first power feature is the dual transformation of energy. The potential energy of the working fluid is at first converted into the flow kinetic energy, and then the flow kinetic energy is converted into the mechanical energy of the turbine rotor rotation. In this case, the flow velocities reached values up to 500 m/s and above. In piston engines, the potential energy of the working fluid is converted directly into mechanical work, due to its pressure on the piston when expanding in the cylinders, without the acquisition of tangible speeds.

The second feature of the turbine—kinematic—is to immediately obtain the rotational motion as a result of the flow force on the rotor blades. The turbine, unlike the piston engines, does not need additional mechanisms, such as the crankshafts, which convert the reciprocating piston motion into the rotational crankshaft motion.

The third feature is the working process continuity. The workflow occurs in the nozzles and rotor blade channels, it is always opened for the working fluid, which moves continuously from the inlet to the outlet turbine section. The workflow does not contain cycles or the discrete-time periods typical of reciprocating engines. The turbine rotor rotates with a constant frequency. The exceptions are the gas turbines which are operating on a cycle with an isochoric heat supply in the combustion chamber. However, at present, this type of engine has no practical application.

Due to the above referred turbine characteristics, it is possible to realize the high flow velocities and the rotor movement. The high-speed turbines, however, in many cases require the use of a downshift between them and the consumer, such as a propeller on ships.

## 2.2 Impulse and Reaction Stages

Depending on the organization of the energy transformation processes, the turbine stages are impulse (active), reaction and impulse (active) with reaction [1].

In the impulse stage conversion of the potential energy into kinetic energy is carried out completely in the nozzles, and in the rotor blade cascade, there is only the conversion of the flow of kinetic energy into the mechanical work. Thus, the processes of the energy transformation are separated by territoriality: each of the transformation stages is carried out in its own separate stage element. The work in the rotor blade cascade of the impulse stage is performed due to the stream turning in blades, i.e. as a result of the active action of the flow substance. The active flow action is due to the occurrence of the centrifugal forces in the working fluid when it is flowing inside a curved channel.

The working fluid at high pressure enters through a stationary nozzle of a turbine; as a result, the pressure of the fluid is decreased and it is increased in fluid velocity (Fig. 2.4). As a result of the increased velocity, the working fluid passes through the nozzle in the form of a high-speed jet. This is a high-velocity jet hit of the properly shaped turbine blade; as a result, the flow direction is changed. The effect of this change in direction of the fluid flow will produce an impulse force. This force causes the blade movement, thereby the rotor starting to rotate.

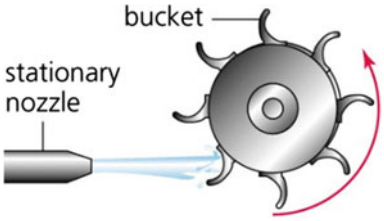


**Fig. 2.4** The impulse turbine principle

The applied force to the blade is developed by causing the fluid to change the direction of flow (Newton's 2nd Law—change of momentum). The change of momentum produces the impulse force.

In the reaction stage, the conversion of the potential energy into kinetic energy occurs approximately equally in the nozzles and in the rotor blade cascade. In the rotor blade cascade, therefore, along with the conversion of the kinetic energy into work, there is a further expansion of the working fluid. The result of the expansion of the working fluid is a reactive force that is acting on the blades. The work in the reaction stage is carried out partly due to the turn of the flow, and partly due to the reactive action of the jet. Thus, in the case of the reaction turbine, the moving blades of a turbine are shaped in such a way that the working fluid expands and drops in pressure as it passes through them. As a result of the pressure decrease in the moving blade, a reaction force will be produced. This force will make the blades rotate.

A comparison of impulse and reaction turbine principles is presented in Fig. 2.5.

The intermediate stage type is the impulse (active) stage with a reaction. In this stage, the expansion of the working fluid is carried out mainly in the nozzles and only to a small extent—in the rotor blade cascade.

**Changing of pressure and velocity in stages**. Let's take a look at how the working fluid and the flow parameters change in different type stages, using the previously entered notations of sections for velocities and angles.

From the definition of the impulse stage, since the expansion of the working fluid occurs only in the nozzles, the following:

$$p_1 < p_0; \quad c_1 > c_0;$$

$p_2 = p_1$ and $w_2 = w_1$ (in the absence of losses).

Figure 2.6a shows the graphs of pressure $p$ and velocities $c$ and $w$ of the impulse stage. There is lack of expansion in the rotor blade cascade results in a constant pressure in the rotor blade cascade and in a constant relative velocity (in the absence of losses). In the actual process, the exit relative velocity $w_2$ is slightly less than $w_1$.

The velocity triangles of the impulse stage are constructed taking into account the above-mentioned velocity ratios of this stage.

For the reaction stage, the ratios are the following:

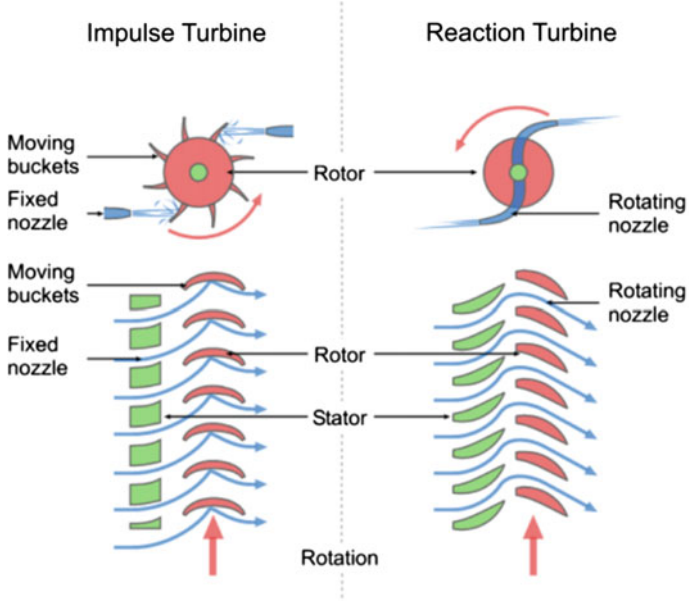


**Fig. 2.5** Comparison of impulse and reaction turbine principle

$$p_1 < p_0; \quad c_1 > c_0;$$
$$p_2 < p_1; \quad w_2 > w_1.$$

The graphs of pressure and the velocities of this stage are shown in Fig. 2.6b. The pressure decreases both in the nozzles and in the rotor blade cascade, and the velocities (respectively absolute and relative) are increased. With close quantities of the potential energy converted into kinetic energy inside the nozzle and rotor blade cascade, the outlet velocity of the working fluid will also be close in magnitude.

The velocity triangles usually depict the superposed vertices and the rotation by 90° compared to Fig. 2.6. In this form, the typical triangles of impulse and reaction stages are shown in Fig. 2.7. There are also characteristics ratios of velocities and angles.

The angles of the velocity triangles are counted at the inlet to the rotor blade cascade (Sect. 2.1) from the positive direction of $u$ axis, and at the outlet (Sect. 2.2) from the negative direction.

**Shape of blade profiles**. The nature of the energy transformations in the stage is ensured by the choice of the appropriate profiles of the nozzle and rotor blades. In the turbine stages, there are two distinct types of cascades: the cascades in which the expansion of the working fluid is carried out, and the cascades in which the expansion is absent. The first is the nozzle cascades of all types of turbine stages and the rotor blade cascades of the reaction stages. The second is the rotor blade cascades of the impulse turbine stages.

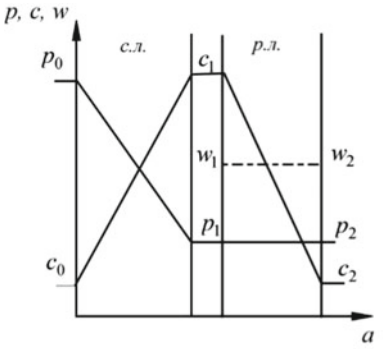


(a) The Impulse Stage

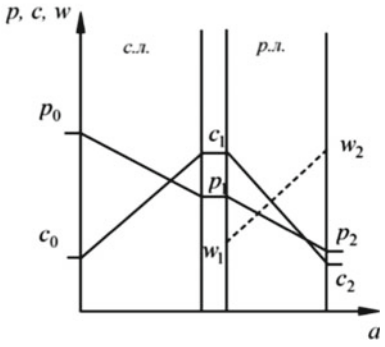


(b) The Reaction Stage

**Fig. 2.6** Graphs of change of flow pressure and velocities

In order to allow the significant expansion of the working fluid in the first group of cascades, the width of the blade channels must be reduced in the outlet direction (with the subsonic flow). Therefore, the blade profiles of these cascades have a pronounced asymmetric shape with the outlet angles much smaller than the inlet angles (Fig. 2.8a). Such cascades are called reaction cascades.

In the impulse cascades where the expansion of the working fluid does not occur, the relative velocity of the flow changes slightly due to energy losses. Therefore, the width of the blade channels should remain approximately the same, which is ensured by the shape of the blade profiles, which is close to symmetrical, with a small difference between the angles of the inlet and the outlet (Fig. 2.8b). These are so-called impulse cascades.

**Impulse stage with reaction**. The impulse stages with reaction are characterized by the features of the reaction stages but to a lesser extent. So, in the graphs of pressure and velocities, the pressure and the velocity curves in the rotor blade cascade are inclined horizontally, as well as in the reaction stage, but at a much smaller

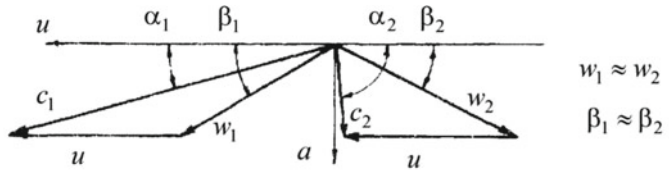


(a) The Impulse Stage

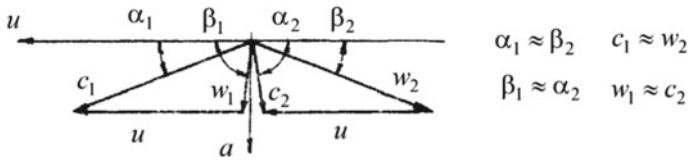


(b) The Reaction Stage

**Fig. 2.7** Typical velocities triangles

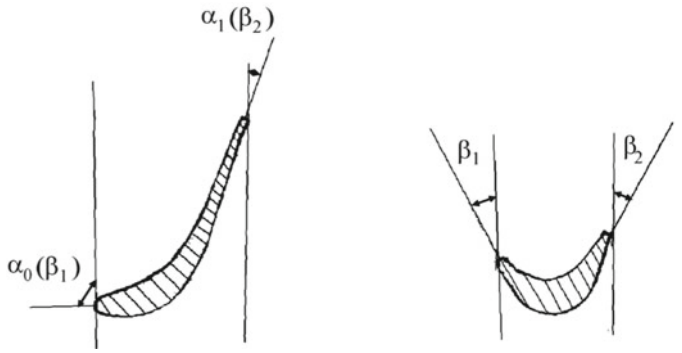


(a) The Reaction Stage (b) The Impulse Stage

**Fig. 2.8** Shape of blade profiles

angle (something mean value between *a* and *b* in Fig. 2.6). The velocity triangles have the intermediate view between *a* and *b* (Fig. 2.7): $c_1 > w_2 > w_1 > c_2$ *i* $\alpha_2 > \beta_1 > \beta_2 > \alpha_1$. The rotor blade profiles have an intermediate shape between *a* and *b* (Fig. 2.8).

## 2.3 Multi-ring Impulse Stages

The operation of the turbine stage can be effective only at a certain ratio of the circumferential velocity $u$ on the average diameter of the rotor blade ring to the velocity at the outlet of the nozzle $c_1$. For the impulse stage, the most favorable ratio of velocities is close to 0.5, and for the reaction stage, it is up to 2.

In order to ensure the most favorable ratio $u/c_1$, it is necessary to increase the circumferential velocity proportionally. In practice, this is achieved by increasing the average diameter of the stage or the rotation frequency. However, it must be taken into account that at the rotating of the rotor the centrifugal forces act on its elements that is the cause of the appearance of the tensile stresses in the rotor details. These tensions with increasing diameter and speed will also increase. Therefore, in terms of strength, the amount of potential energy that is converted to mechanical work in the turbine stage is limited.

If a large amount of the potential energy is processed in the single turbine stage without conservation of the optimum velocity ratio, it will result in a deterioration of the kinetic energy conversion into mechanical work in the rotor blade channels due to the increase in the kinetic energy losses, which will be expressed in the significant absolute velocities of the working fluid behind the stage. As a result, the efficiency of the turbine stage is reduced.

One of the ways to improve the efficiency of the impulse stages, working with a large reserve of the potential energy of the working fluid, is to use multi-ring wheels (with two–three moving rings). The part of the stream kinetic energy leaving the first moving ring is used to obtain the useful work in the second or the third moving ring. To provide the necessary flow direction at the inlet to the second and the subsequent moving rings in front of each of them. It is necessary for the additional fixed intermediate blades install in the casing.

The moving rings are usually mounted on a single disk, and depending on stage number are called respectively two-ring or three-ring, unlike the previously considered stages, which are single-ring. Historically, such stages are known as the Curtis two-or three-wheel turbine (named after the American engineer who first created a similar design in 1900).

A schematic diagram of the Curtis stage impulse turbine, with two rings of the moving blades and one ring of the fixed blades is shown in Fig. 2.9.

The velocity compounded impulse turbine was at first proposed to solve the problem of the single-stage impulse turbine for use of the high pressure and temperature fluid. The rings of the moving blades are separated by the rings of the fixed blades. The moving blades are jointed to the turbine shaft and the fixed blades are fixed to the casing. The high-pressure fluid coming from the boiler is expanded in the nozzle at first. The nozzle converts the pressure energy of the fluid into kinetic energy. The total enthalpy drop and then the pressure drop occurs in the nozzle. Then, the pressure thereafter remains constant.

This high-velocity fluid is directed on to the first set (ring) of the moving blades. As the fluid flows over the blades, due to the shape of the blades, it imparts some of

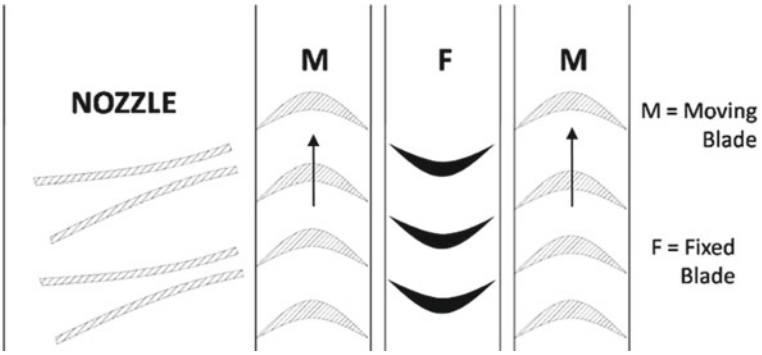


**Fig. 2.9** Schematic diagram of curtis stage impulse turbine

its momenta to the blades and loses some velocity. Only a part of the high kinetic energy is absorbed by these blades. The remainder is exhausted on to the next ring of the fixed blade. The function of the fixed blades is to redirect the fluid leaving from the first ring of the moving blades to the second ring of the moving blades. There is no change in the velocity of the fluid as it passes through the fixed blades. The fluid then enters the next ring of the moving blades; this process is repeated practically when all the energy of the fluid has been absorbed.

The multi-ring stages are impulse or with a little reaction (i.e. the additional expansion of the working fluid) in the rotor and guide channels.

The diagram of the impulse two-ring stage, the profiles of its blades and the graphs of pressure and velocities are shown in Fig. 2.10 [1].

As in the single-ring impulse stage, the expansion of gas occurs only in the nozzle channels 1. In the moving rings 2 and 4, in the fixed ring 3 there is no expansion, so the pressure in the moving and fixed channels remains unchanged, i.e. $p_{11} = p_{21} = p_{12} = p_{22}$, and therefore $w_{21} = w_{11}, w_{22} = w_{12}$ (the second digit of the index corresponds to the ring number of the rotor blades). In the rotor channels, only the flow kinetic energy is converted into mechanical work, and the absolute velocities in the moving blade channels are reduced: $c_{21} < c_{11}, c_{22} < c_{12}$. The inlet and the outlet angles of the corresponding cascades are approximately the same: $\beta_{11} \approx \beta_{21}$, $\alpha_{12} \approx \alpha_{21}, \beta_{22} \approx \beta_{12}$.

The use of the kinetic energy and the reduction of the absolute velocity in the moving rings occurs stepwise, so these stages are also called wheels with the appropriate number of stages of velocity, and in a separate implementation—a turbine with stages of velocity (the velocity compounded turbine).

Since the expansion of the working fluid is negligible or absent at all, the blade profiles of these devices are made similar to the rotor blade profiles (the impulse cascades).

The optimal velocity ratio $u/c_1$ for the two-ring stage is approximately 0.25, and for the three-ring stage is 0.167. This means that, compared to the single-ring impulse stage, the required circumferential velocities (with the same amount of the potential

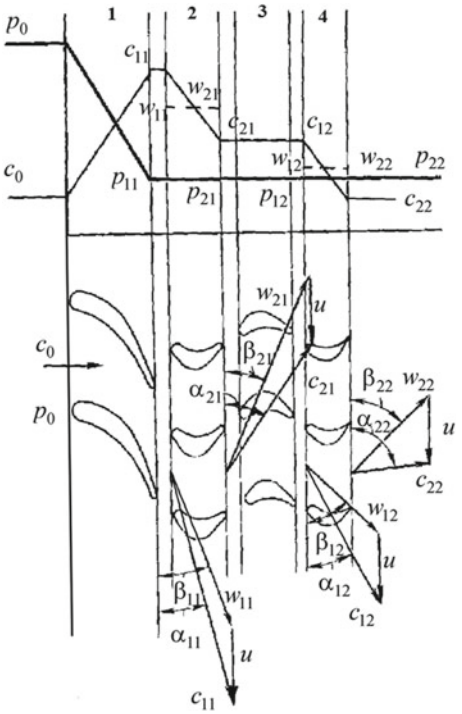


**Fig. 2.10** Pressure and velocity graphs and cascade profiles of the two-ring impulse stage

energy that has been processed and the maximum efficiency) will be less than about 2 and 3 times, respectively.

A design in which a similar two-ring stage turbine process is implemented is the stage with the re-supplying of the working fluid (Fig. 2.11).

This stage consists of the nozzles and one ring of the moving blades (the first velocity stage). After moving blades, the working fluid enters the turned chamber, which acts as an intermediate guide device. From the turned chamber the flow at an angle $\alpha_1'$ directs for the second time to the moving blades and leaves them with velocity $c_2'$, where $w_2 \approx w_1, c_1' \approx c_2, w_2' \approx w_1', c_2' < c_2$. Thus two stages of velocity are realized [1].

## 2.4 Multistage Pressure Compounded Turbines

In such turbines, the total pressure differential is divided into several parts, each of which is processed in its own stage—the stage of pressure. The turbine is a series of one-by-one stages (located on a single shaft in a common casing) through which the

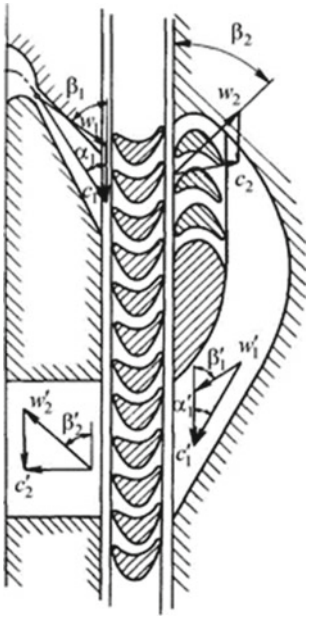


**Fig. 2.11** Diagram of the stage with re-supplying of the working fluid

working fluid passes. The total turbine power is equal to the sum of the power of all its stages.

The potential energy of the working fluid corresponding to one stage is much less than its total reserve in the turbine, so the value of the absolute velocity $c_1$ is numerically smaller compared with the one-stage variant of the turbine. Therefore, the selection of the number of stages can ensure (with the optimum ratio $u/c_1$) the acceptable (in terms of strength) circumferential velocities.

Within each stage, the working process is organized according to any of the principles discussed above.

In the general case, the multi-stage turbine consists of the stages of pressure, which can be: the single-ring impulse (including the impulse stage with reaction), the reaction, two- or three-ring impulse.

The diagram of the multi-stage impulse turbine with the stages of pressure (the pressure compounded impulse turbine), as well as graphs of pressure and velocities, are shown in Fig. 2.12 [1].

The turbine consists of five single-ring stages. The nozzle blades of the first stage are fixed in the turbine casing, and the nozzle blades of the other stages are in the diaphragms. The diaphragms are detachable, their upper joints are mounted in the casing cover and the lower joints are mounted in the turbine casing. The presence of the diaphragms and the disk rotor is a hallmark of the impulse multi-stage turbine. This design allows the loss reduction from the leakage of the working fluid between the nozzle cascades and the rotor by reducing the diameter of the diaphragm seals.

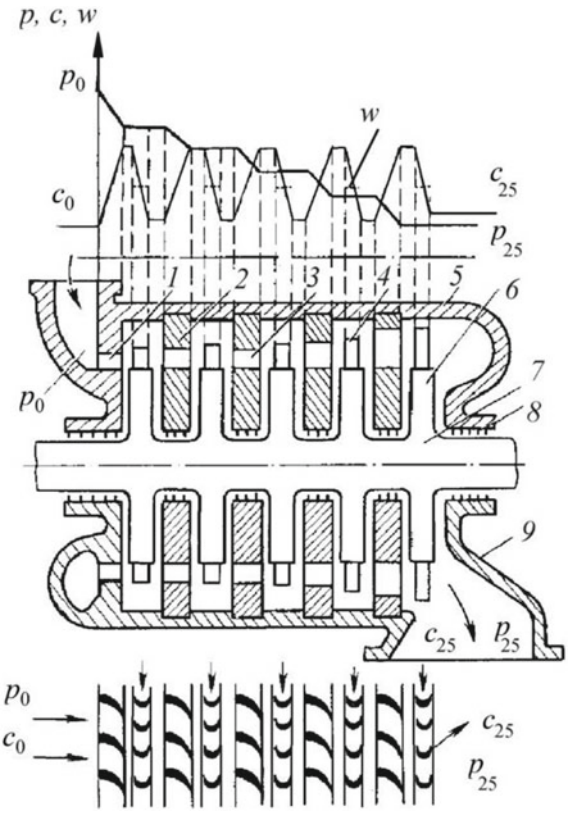


**Fig. 2.12** Diagram of the Multistage Impulse Turbine with stages of pressure. 1, 3—nozzle blades of the first and the third stages, respectively; 2—diaphragm; 4—rotor blades; 5—casing cover; 6—disk; 7—shaft; 8—end seal; 9—turbine casing

The pressure compounded impulse turbine is also called as Rateau turbine (1900) after its inventor. This is used to solve the problem of the high blade velocity in the single-stage impulse turbine. It consists of the alternate rings of the nozzles and the turbine blades. The nozzles are fitted to the casing and the blades are jointed to the turbine shaft.

In this type of compounding the fluid is expanded in a number of stages, instead of just one (nozzle) in the velocity compounding. It is done by the fixed blades which act as nozzles. The fluid expands equally in all rows of the fixed blade. The fluid comes from the boiler and it is fed to the first set of the fixed blades i.e. the nozzle ring. The fluid is partially expanded in the nozzle ring. Then, there is a partial decrease in the pressure of the incoming fluid. This leads to an increase in the velocity of the fluid. Therefore the pressure decreases and the velocity increases partially in the nozzle.

This is then passed over the set of moving blades. As the fluid flows over the moving blades nearly all its velocity is absorbed. However, the pressure remains constant during this process. After this, it is passed into the nozzle ring and it is again partially expanded. Then it is fed into the next set of moving blades, and this process

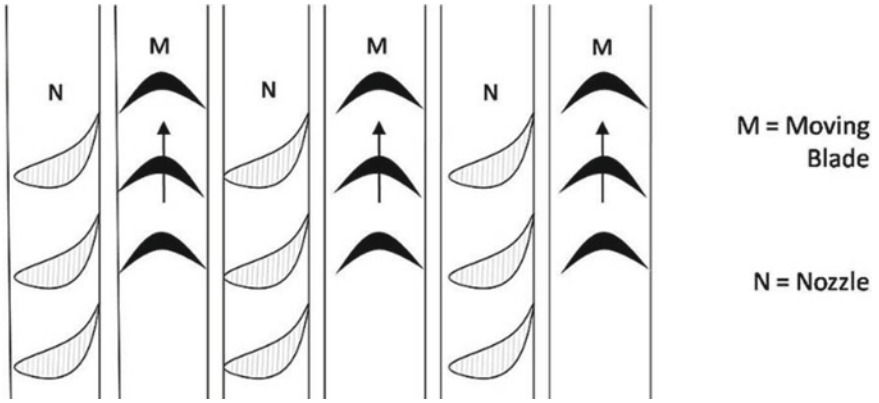


**Fig. 2.13** Schematic diagram of pressure compounded impulse turbine

is repeated until the condenser pressure is reached. This process has been illustrated in Fig. 2.13.

It is a three-stage pressure compounded impulse turbine. Each stage consists of one ring of the fixed blades, which acts as nozzles, and one ring of the moving blades.

The diagram of the multistage reaction turbine with stages of pressure (the pressure compounded reaction turbine) is shown in Fig. 2.14. The pressure and velocity graphs are also presented there. The turbine consists of four reaction stages. The nozzle blades are fixed in the casing, the moving blades are in the rotor. The peculiarity of the reaction turbine is the rotor of the drum type [1].

As explained earlier, a reaction turbine is one in which there is pressure and velocity loss in the moving blades. The moving blades have a converging fluid nozzle. Then fluid passes over the fixed blades, it expands with a decrease in the fluid pressure and an increase in the kinetic energy. This type of turbine has a number of rings of the moving blades which are attached to the rotor and an equal number of the fixed blades which are attached to the casing. In this type of turbine the pressure drops take place in a number of stages.

The fluid passes over a series of alternate fixed and moving blades. The fixed blades act as nozzles i.e. they change the direction of the fluid and also expand it. Then the fluid is passed on to the moving blades, which further expand the fluid and also absorb its velocity. This is explained in Fig. 2.15.

Due to the presence of a pressure differential on the moving blades, a considerable axial force acts on its rotor, which creates a large load on the thrust bearing (it is not shown). To unload the thrust bearing and reduce its size the special unloading device (a dummy piston) in the turbine inlet is provided. It consists of the piston (a part of a larger diameter rotor) and the labyrinth seal between the cylindrical piston surface and the casing. Therefore, the dummy piston is the part of the turbine which serves to balance the axial component of the pressure of the working medium.

The higher pressure acts on the piston from the inlet $p_0$ which is compared with the pressure $p_d$ from the other side. This results in an axial force directed in the direction

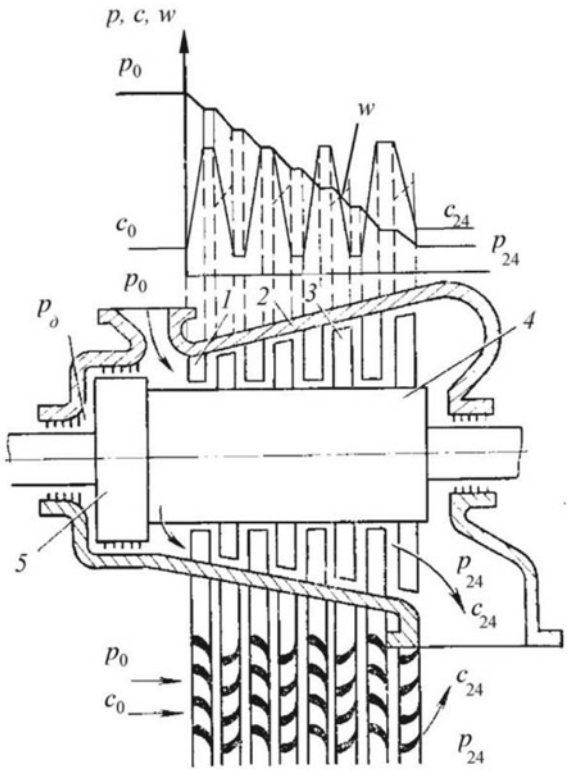


**Fig. 2.14** Diagram of the multistage reaction turbine with stages of pressure: 1—nozzle blades; 2—casing; 3—moving blades; 4—rotor; 5—dummy piston

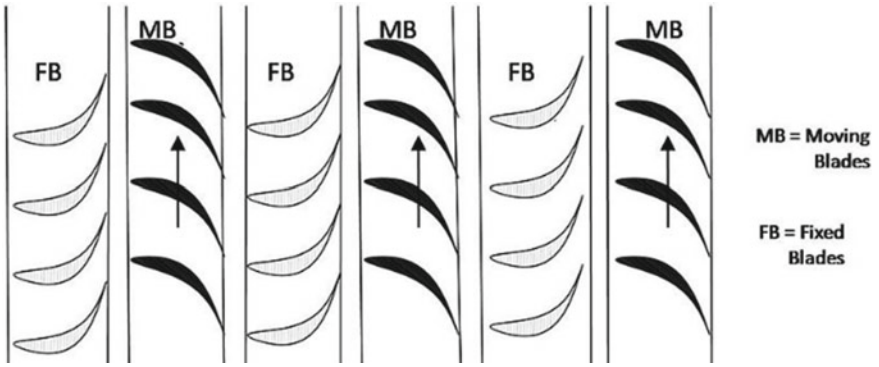


**Fig. 2.15** Schematic diagram of the pressure compounded reaction turbine

opposite to the action of the unbalanced forces caused by pressure differential on the moving blades. The reduced pressure $p_d$ in the dummy chamber is achieved by the fact that the chamber is connected by the pipeline or the drillings in the drum with the turbine outlet part. The labyrinth seal assists to reduce the leakage of the working fluid through the dummy piston.

The design of the reaction multi-stage turbine was proposed at first in 1884 by the English engineer Parsons.

The advantage of turbines with stages of pressure is that they allow the actuation of (any theoretically) large reserves of the potential energy at acceptable circumferential blade velocities and provide high efficiency.

## 2.5 Radial Turbines

In the stages which are discussed above, the flow of the working fluid had a general direction coinciding with the direction of the turbine axis. Therefore, such stages and turbines are generally called **axial** ones.

In the **radial** stages, the working fluid moves mainly along the radius of the turbine. Depending on the direction of the movement (from the periphery to the center or from the center to the periphery), the stages are centripetal (Fig. 2.16a) and centrifugal (Fig. 2.16b).

Among the radial stages, the most important for practice are the centrifugal stages with the axial direction of the flow behind the impeller, which are called the radial-axial (Fig. 2.16c). At this stage, under the process of energy conversion, the working fluid at first moves inside nozzle 1 from the periphery to the center, then it moves into the inter-blade impeller channels 2, gradually changing the direction of the movement to the axial.

The radial-axial stages are single-flowing or double-flowing (Fig. 2.16d), the latter are used at the increased flow rates of the working fluid and the limited impeller diameter. The multistage turbines, consisting of separate radial-axial stages, are made by the sequential connection of the several stages with the assistance of the guide vanes (Fig. 2.16f).

In the birotatory radial stages (Fig. 2.16e) there are two discs with blades (or two wheels) that are rotated in opposite directions (Ljungströmbirotatory turbine).

Figure 2.17 shows the diagrams of the blade cascades of the centripetal, centrifugal and radial-axial stages, as well as their velocity triangles. In the nozzles of radial stages, the expansion of the working fluid obeys the same laws as axial ones. By reducing the pressure $p_0$ from the inlet to the pressure $p_1$ at the cascade outlet, the flow is accelerated from velocity $c_0$ to velocity $c_1$.

The fundamental difference between the working process in the radial stages compared to the axial ones is that the conversion of energy in the moving channels is accompanied by a change in the circumferential velocity from the inlet $u_1$ to the outlet $u_2$ of the cascade. The relative velocity $w$ changes both due to the expansion of the working fluid in the impeller and under the action of the inertial (Coriolis) forces.

(a) Centripetal Stage

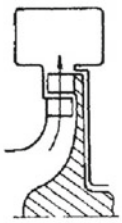

(b) Centrifugal Stage

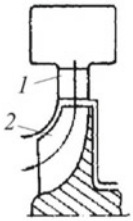


(c) Radial-Axial Stage

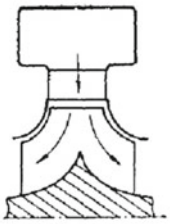

(d) Two-Flowing Radial-Axial Stage

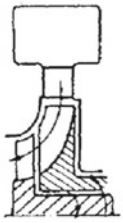

(e) Birotatory Ljungström Stage

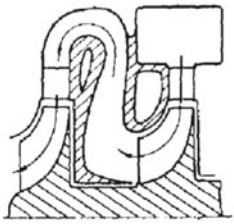

(f) Fragment Of Two-Stage Centrifugal Turbine

**Fig. 2.16** Types of the radial stages

In the centripetal turbines, these forces slow down the flow inside the inter-blade channels, and in the centrifugal turbines, accelerate the flow.

The centrifugal turbines are distributed to a much less extent than the centripetal turbines because of their lower efficiency. The centrifugal multistage turbines have become widespread due to the fact that, with a significant increase in the specific fluid volume, the required cross-sectional area of the channels can only be provided when flowing from the center to the periphery.

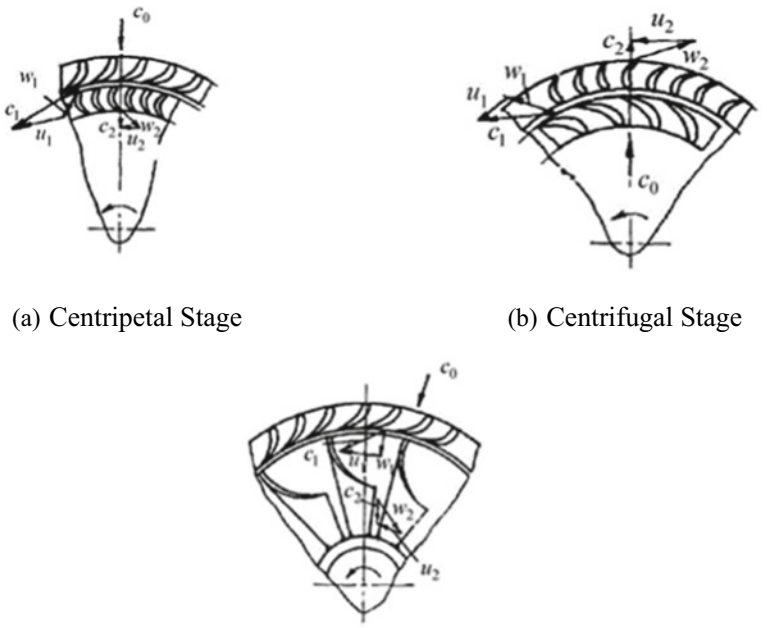


(a) Centripetal Stage

(b) Centrifugal Stage

(c) Radial-Axial Stage

**Fig. 2.17** Diagram of the radial stage blades

## Reference

1. Romanovsky GF, Ipatenko OY, Patlaychuk VM (2002) Theory and calculation of steam and gas turbines. Publisher USMTU, Mykolaiv, 292 p. (in Ukrainian)

# Chapter 3
# Thermodynamic Basics of the Turbine Theory


## 3.1 Basic Equations for the Steady-State One-Dimensional Gas Flow

The flow in the turbine channels has a complex spatial 3D structure. In the turbine theory, many issues can be solved, based on the laws of the simplest, one-dimensional, steady-state gas flow. In a one-dimensional flow, all working fluid and motion parameters depend on only one spatial coordinate which is counted in the flow direction. The change of the parameters in the other two directions is neglectedly considered insignificant. Thus, the flow patterns for a one-dimensional gas flow are a relationship only between the working fluid and the current parameters and do not contain the spatial coordinates.

One-dimensional flow is the ideal flow model. However, in some cases, the one-dimensional gas flow can be applied to a real flow with an uneven distribution of the parameters across sections. We consider the basic equations of the working fluid concerning the one-dimensional gas flow [1].

**Equation of thermodynamic state of the working fluid**. The relationship between the physical parameters of the gas is as follows:

$$\mathrm{pv} = \mathrm{RT} \text{ or } p = \rho \mathrm{RT} \tag{3.1}$$

where $p$ is the absolute pressure, Pa; $v$ is the specific volume, $m^3/kg$; $R$ is the gas constant, J/(kg K); $T$ is the absolute temperature, K; $\rho = 1/v$ is the gas density, $kg/m^3$.

The Eq. (3.1) was obtained for ideal (thermodynamically) gases in which the gas becomes dependent only on their nature, but nevertheless, they are widely used in gas turbine calculations for real gases, providing an acceptable result.

The gas constant can be determined by the formula:

$$R = R_\mu / \mu,$$



K. Liu et al. (eds.), *Gas Turbines Structural Properties, Operation Principles and Design Features*, https://doi.org/10.1007/978-981-99-0977-3_3

where $R_\mu = 8314$ J/(kmol K) is the universal gas constant; $\mu$ is the molar mass of gas, kg/kmol.

For air, the gas constant is $R = 287.1$ J/(kg K). For gas (mixture of combustion products with the excess air) which is the working fluid in gas turbines, it ranges from 277.6 to 284.5 J/(kg K) depending on the air excess coefficient.

For the calculation of the steam turbines, Eq. (3.1) is not applicable because the gas vapor of water vapor is essentially dependent on the pressure and the temperature. In practice, the steam parameters are calculated by use of the water vapor tables and the *h-s* diagram.

The turbine theory often uses the relationship between the gas constant *R*, the gas heat capacity $c_p$, and the isentropy (adiabat) index *k*:

$$R = \frac{k-1}{k} c_p. \tag{3.2}$$

The isobaric mass heat capacity determines the amount of the heat that must be supplied to 1 kg of the working fluid in order to increase its temperature by 1 K in the process at constant pressure. The heat capacity of the real gases depends on their temperature and pressure. The pressure dependence is usually neglected as being very weak.

When $p = \text{const}$ and $t = 0$ °C the air heat capacity $c_p = 1004$ J/(kg K). The heat capacity of the gas obtained from the fuel combustion used in the gas turbine units is (within the same conditions) within the range of 1007–1017 J/(kg K). The smaller values correspond to the air excess coefficient $\alpha = 5$, larger to $\alpha = 2.7$.

**The continuity equation**. The continuity stream condition has been executed if for any of its sections

$$\frac{Fw}{v} = G = \text{const}, \tag{3.3}$$

where *F* is the cross-sectional area of the channel perpendicular to the velocity vector *w*, $m^2$; *G* is the mass flow rate of the working fluid, kg/s.

Thus, the mass flow of the working fluid for all channel sections is constant. We obtain the continuity equation in the differential form:

$$\frac{dF}{F} + \frac{dw}{w} - \frac{dv}{v} = 0$$

to find the logarithm and then differentiating Eq. (3.3).

For a fixed channel, for example, a nozzle $\boldsymbol{w} = c$, and then the initial Eq. (3.3) has the following form:

$$\frac{Fc}{v} = G = \text{const}. \tag{3.4}$$

**Equation of the thermodynamic process**. During the flow in the turbine channel of the working fluid, its parameters are changed. The relationship between the parameters in different sections is described, in the general case, by the polytropic equation:

$$\mathrm{pv}^n = \text{const}. \tag{3.5}$$

The polytropic index $n$ for each case is a constant value and depends on the nature of the process (the presence of the heat exchange, friction, etc.). For example, for an isoentropic process ($s = \text{const}$) it is equal to the isoentropic index $n = k$, for an isobaric ($p = \text{const}$) process $n = 0$, and for an isothermal ($T = \text{const}$) $n = 1$.

The process equation can also be represented as a relation between the gas temperature and the specific volume by replacing of pressure in (3.5) with its value from the ideal gas Eq. (3.1):

$$\frac{\mathrm{RT}}{v} v^n = \text{const},$$

where

$$\mathrm{Tv}^{n-1} = \text{const}. \tag{3.6}$$

Finally, expressing in a similar way the specific volume, we find the relationship between pressure and temperature:

$$p\left(\frac{\mathrm{RT}}{p}\right)^n = \text{const},$$

where

$$\frac{T^n}{p^{n-1}} = \text{const}. \tag{3.7}$$

**Energy equation**. Let in that some channel (Fig. 3.1) the one-dimensional gas flow is realized. The channel itself moves progressively relative to some ab-solute coordinate system with the constant relative velocity ($u = \text{const}$).

We separated at some moment inside the stream the elementary mass of gas using two infinitely close cross-sections. Due to the proximity of the cross-sections, all gas and flow parameters will be considered constant in the allocated mass.

During a period, $d\tau$ the allocated mass of gas will move along the stream. The gas and flow parameters are subject to change depending on the flow conditions.

Applying the law of conservation and conversion of energy to the considered mass of gas, in the general case of flow with heat exchange, friction and the implementation of the work we can write [1]

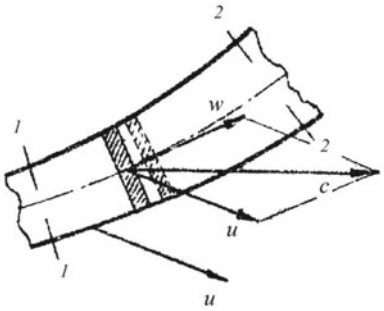


**Fig. 3.1** To the energy equation determination

$$dq + dq_r = dU + d\left(\frac{c^2}{2}\right) + d(pv) + dl_T + dl_r, \tag{3.8}$$

where $dq$ is the heat transmitted to the gas from outside due to heat exchange with the environment; $dq_r$ is the friction heat (the equivalent to friction work); $dU$ is the change of the internal thermal energy; $d(c^2/2)$ is the change in the kinetic energy; $d(pv)$ is the change in the internal mechanical energy; $dl_T$ is the external or technical work; $dl_r$ is the friction work (the work against forces which are acting on the channel walls, tangentially to them).

Due to the low gas density, the work of the gravity forces in the energy equation has been omitted. All terms in Eq. (3.8) are related to 1 kg of gas and expressed in J/kg.

Since $dq_r$ and $dl_r$ are numerically equal, the energy equation has been reduced to the expression:

$$dq = dU + d\left(\frac{c^2}{2}\right) + d(pv) + dl_T. \tag{3.9}$$

But as we know from thermodynamics:

$$dU + d(pv) = dh,$$

where $h$ is the working fluid enthalpy, J/kg. The enthalpy as the sum of internal heat and mechanical energies represents the total internal (potential) energy of the working body.

Therefore, we obtain from Eq. (3.9), the following:

$$dq = dh + d\left(\frac{c^2}{2}\right) + dl_T. \tag{3.10}$$

The form of the Eqs. (3.9) and (3.10) does not depend on whether there is friction (and energy loss) at flow or not. This does not mean that the friction does not affect

the flow. This indicates only that the total flow energy at the given amounts of the heat exterior and the external work are determined explicitly. The presence of friction leads only to the redistribution of the energy between its individual components. The presence of friction also has an effect on the gas entropy $s$, which at the end of the process in the presence of friction is always greater than it would have been in the absence of friction.

Integrating Eq. (3.10) for a limited flow Sect. 5.1–5.2 (Fig. 3.1), after some transformations, we will have:

$$\pm q \pm l_T = c_p(T_2 - T_1) + \frac{c_2^2 - c_1^2}{2}. \tag{3.11}$$

There is here, on the left side, the sign "+" is taken when consuming heat or the technical work outside, and "−" in case of heat removal or the execution of the work by gas.

The equations discussed above are written in an absolute coordinate system.

Let's put the beginning of some new coordinate system (moving together with the selected element) in its center of gravity. Then, considering the element as stationary relative to this coordinate system, we write the energy equation as the first law of thermodynamics for the process of the gas state change:

$$dq + dq_r = dU + pdv = dh - vdp. \tag{3.12}$$

Comparing the Eqs. (3.10) and (3.12), after substituting $dq_r$ for $dl_r$ and some transformations, we obtain:

$$vdp + d\left(\frac{c^2}{2}\right) + dl_T + dl_r = 0. \tag{3.13}$$

The so-called *generalized Bernoulli equation* is the equation of the conservation of energy in the mechanical form. This equation does not involve explicitly the process of heat.

In the case of the energy-insulated flow, the Eqs. (3.10) and (3.13) have the following form:

$$dh + d\left(\frac{c^2}{2}\right) = 0, \tag{3.14}$$

$$vdp + d\left(\frac{c^2}{2}\right) + dl_r = 0. \tag{3.15}$$

We integrate Eqs. (3.14) and (3.15) for the flow part between Sects. 5.1 and 5.2.

From Eq. (3.14) we obtain

$$h_2 + \frac{c_2^2}{2} = h_1 + \frac{c_1^2}{2}. \tag{3.16}$$

For gas (with the equation of state pv = RT)

$$h = c_p T = \frac{c_p}{R}\mathrm{pv} = \frac{k}{k-1}\mathrm{pv},$$

we will have finally the following:

$$\frac{k}{k-1}p_2 v_2 + \frac{c_2^2}{2} = \frac{k}{k-1}p_1 v_1 + \frac{c_1^2}{2}. \tag{3.17}$$

It is from the Eq. (3.15)

$$\int_1^2 v dp + \frac{c_2^2 - c_1^2}{2} + l_r = 0. \tag{3.18}$$

In the energy-insulated friction process, the gas parameters are related by the polytropic equation $\mathrm{pv}^n = \mathrm{const}$, therefore

$$\int_1^2 v dp = (\mathrm{const})^{\frac{1}{n}} \int_1^2 p^{-\frac{1}{n}} dp = (\mathrm{const})^{\frac{1}{n}} \frac{n}{n-1}\left(p_2^{\frac{n-1}{n}} - p_1^{\frac{n-1}{n}}\right).$$

After opening the brackets, taking into account the following ratio:

$$p_1 v_1^n = p_2 v_2^n = \mathrm{const}$$

after substitution in (3.18) and the terms grouping we obtain finally the following:

$$\frac{n}{n-1}p_1 v_1 + \frac{c_1^2}{2} = \frac{n}{n-1}p_2 v_2 + \frac{c_2^2}{2} + l_r. \tag{3.19}$$

The Eqs. (3.17) and (3.19) are obtained for the same case, i.e.—an energy-insulated friction flow.

The Eq. (3.17), as well as (3.16), is similar in appearance to the flow with friction and without friction. In the presence of friction, there are only the values of the terms of the right-hand side change, without changing their sum.

On the basis of (3.17) and (3.19), it is easy to find the expression for friction work (in the absence of the heat exchange)

$$l_r = \left(\frac{n}{n-1} - \frac{k}{k-1}\right)(p_1 v_1 - p_2 v_2) = \left(\frac{n}{n-1} - \frac{k}{k-1}\right)R(T_1 - T_2). \tag{3.20}$$

The flow energy equations can also be written in the relative coordinate system associated with the moving channel. In this case, instead of the absolute velocity $c$, it is necessary to enter the relative velocity $w$ and to have the technical work which is equal to zero, because in this system the channel is stationary. Thus, in the absence of the heat exchange ($dq = 0$) and the translational motion of the channel, the energy equation in the relative coordinate system is as the following:

$$dh + d\left(\frac{w^2}{2}\right) = 0. \tag{3.21}$$

The Eq. (3.21) is suitable for the moving (rotor) channels of the axial turbine stages.

At the same time, the Eq. (3.10) in the absolute coordinate system corresponds to the following relation:

$$dh + d\left(\frac{c^2}{2}\right) + dl_T = 0. \tag{3.22}$$

Comparing (3.21) and (3.22), we obtain the formula for technical work:

$$dl_T = d\left(\frac{w^2}{2}\right) - d\left(\frac{c^2}{2}\right)$$

or for the restricted area 1–2:

$$l_T = \frac{c_1^2 - c_2^2}{2} + \frac{w_2^2 - w_1^2}{2}. \tag{3.23}$$

If the transport velocity for the different points of the channel is different ($u \neq$ const), for example in the radial stages (Fig. 3.2), instead of (3.21) it should be as the following:

$$dh + d\left(\frac{w^2}{2}\right) = d\left(\frac{u^2}{2}\right),$$

and then it will be as the following:

$$l_T = \frac{c_1^2 - c_2^2}{2} + \frac{w_2^2 - w_1^2}{2} + \frac{u_1^2 - u_2^2}{2}. \tag{3.24}$$

The third term on the right side is the work obtained by the action of the additional inertial Coriolis forces.

The above gas flow energy equations are applied to stage channels under certain conditions. For some cases, these equations are summarized in Table 3.1 [1].

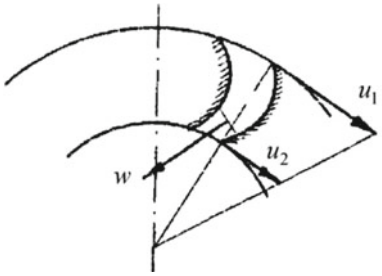


**Fig. 3.2** The diagram of the channel in the radial turbine

**Table 3.1** Energy equations for the turbine stage elements

| Stage element | | In the absolute coordinate system | In the relative coordinate system | |
|---|---|---|---|---|
| | | | $u = \text{const}$ (the axial stages) | $u \neq \text{const}$ (the radial and radial-axial stages) |
| The stages of the cooled turbines ($dq \neq 0$) | Fixed nozzle and guide channels | $(dl_T = 0)$ $dq = dh + d\left(\frac{c^2}{2}\right) vdp + d\left(\frac{c^2}{2}\right) + dl_r = 0$ | – | – |
| | Moving blade channels | $dq = dh + d\left(\frac{c^2}{2}\right) + dl_T$ $vdp + d\left(\frac{c^2}{2}\right) + dl_T + dl_r = 0$ | $(dl_T = 0)$ $dq = dh + d\left(\frac{w^2}{2}\right) vdp + d\left(\frac{w^2}{2}\right) + dl_r = 0$ | $(dl_T = 0)$ $dq = dh + d\left(\frac{w^2}{2}\right) - d\left(\frac{u^2}{2}\right) vdp + d\left(\frac{w^2}{2}\right) - d\left(\frac{u^2}{2}\right) + dl_r = 0$ |
| The stages of the uncooled turbines ($dq = 0$) | Fixed nozzle and guide channels | $(dl_T = 0)$ $dh + d\left(\frac{c^2}{2}\right) = 0$ $vdp + d\left(\frac{c^2}{2}\right) + dl_r = 0$ | – | – |
| | Moving blade channels | $dh + d\left(\frac{c^2}{2}\right) + dl_T = 0$ $vdp + d\left(\frac{c^2}{2}\right) + dl_T + dl_r = 0$ | $(dl_T = 0)$ $dh + d\left(\frac{w^2}{2}\right) = 0$ $vdp + d\left(\frac{w^2}{2}\right) + dl_r = 0$ | $(dl_T = 0)$ $dh + d\left(\frac{w^2}{2}\right) = d\left(\frac{u^2}{2}\right)$ $vdp + d\left(\frac{w^2}{2}\right) - d\left(\frac{u^2}{2}\right) + dl_r = 0$ |

## 3.2 Stagnation Parameters in the Absolute and Relative Motion

It is necessary to distinguish between static and total parameters of the working fluid in the flow. The static parameters are the parameters that characterize the thermodynamic state of the working fluid which moves with a certain velocity. In order to measure accurately the static parameters, the measuring instruments must move with the flow at the same speed [1].

If the flow is slowed down to zero velocity, the kinetic energy will be converted into the potential energy according to the law of the conservation of energy, and the parameters of the working fluid will change.

The flow parameters stagnated hypothetically in the energy-insulated ($dq = 0$; $dl_T = 0$) process to zero velocity are called the *total parameters*, or the *stagnation parameters*. The total parameters are usually denoted by the asterisk (*), namely: $h^*$, $T^*$, $p^*$, etc.

For any arbitrary section, the total enthalpy, as the total energy of the working fluid, is the sum of the potential and kinetic energy, that is the following:

$$h^* = h + \frac{c^2}{2}, \tag{3.25}$$

where $h$ and $c$ are the static enthalpies and the flow velocity.

Let us transform (3.25), taking into account that:

$$h^* = h\left(1 + \frac{c^2}{2h}\right) = h\left(1 + \frac{c^2}{2c_pT}\right),$$

and replacing $c_p$ from (3.2) we have the following:

$$h^* = h\left(1 + \frac{c^2}{2\frac{k}{k-1}\mathrm{RT}}\right) = h\left(1 + \frac{k-1}{2} \cdot \frac{c^2}{a^2}\right),$$

where $a = \sqrt{k\mathrm{RT}}$ is the local speed of sound.

Keeping in mind that $\frac{c}{a} = M$ is the Mach number in the absolute motion, for the total enthalpy we write down finally:

$$h^* = h\left(1 + \frac{k-1}{2}M^2\right), \tag{3.26}$$

and dividing both parts of the equation by $c_p$ we will get the total temperature:

$$T^* = T\left(1 + \frac{k-1}{2}M^2\right). \tag{3.27}$$

From (3.26) and (3.27), it is understood that the enthalpy and the stagnation temperature do not depend on the nature of the stagnation.

In the isoentropic stagnation $\left(\mathrm{pv}^k = \mathrm{const}\right)$

$$\frac{p^*}{p} = \left(\frac{T^*}{T}\right)^{\frac{k}{k-1}}, \frac{\rho^*}{\rho} = \left(\frac{p^*}{p}\right)^{\frac{1}{k}},$$

and therefore the total pressure and the total density of the stagnated flow can be determined as the following:

$$p^* = p\left(\frac{T^*}{T}\right)^{\frac{k}{k-1}} = p\left(1 + \frac{k-1}{2}M^2\right)^{\frac{k}{k-1}},$$

$$\rho^* = \rho\left(\frac{p^*}{p}\right)^{\frac{1}{k}} = \rho\left(1 + \frac{k-1}{2}M^2\right)^{\frac{1}{k-1}}.$$

The process of the isoentropic stagnation and the stagnation parameters on the *h-s* diagram are shown in Fig. 3.3.

In the case of the other nature of the stagnation, on the right side of the last formulas, the polytropic exponent *n*, instead of the exponent *k*, should be included.

In case, in the energy-insulated flow, integrating (3.14), we obtain for an arbitrary cross-section:

$$h + \frac{c^2}{2} = \mathrm{const} = h_0^*,$$

where $h_0^*$ is the total enthalpy in the initial channel section.

Thus, the enthalpy in the energy-insulated stream, and therefore the stagnation temperature, remain constant along the stream.

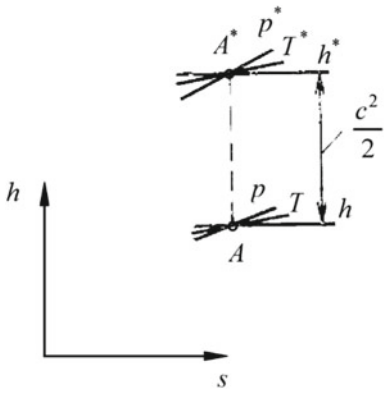


**Fig. 3.3** Total working fluid parameters (A–A* is the stagnated process)

In the energy-insulated frictionless (isoentropic) flow, the other stagnation parameters remain unchanged along the flow length. In the energy-insulated friction stream parameters $p^*$, $\rho^*$ and $v^*$ change, however

$$\frac{p^*}{\rho^*} = \text{const and } p^* v^* = \text{const.} \tag{3.28}$$

In the presence of the heat exchange or the technical work in the flow, in general, all the stagnation parameters, including the enthalpy and the temperature, are changed.

Thus, from the Eq. (3.22), during the work execution (Fig. 3.1), we will have the following:

$$h_1 + \frac{c_1^2}{2} = h_2 + \frac{c_2^2}{2} + l_T,$$

or

$$h_1^* = h_2^* + l_T. \tag{3.29}$$

From (3.29), the stagnation enthalpy (and the temperature) decreases during the technical work execution by gas. If the work supplies outside (in the compressor channels) i.e. the stagnation enthalpy and the temperature increase. The heat exchange with the environment is similarly affected.

It follows the formula (3.29)

$$l_T = h_1^* - h_2^*.$$

The latter ratio is of great importance in the turbine theory. Responding to it, the work of 1 kg of the working fluid in the turbine or in the separate stage (in the absence of cooling) can be found as the difference in the stagnation enthalpy at the beginning and at the end of the expansion process. The formula is true for both: the ideal turbine and the real one, in which the workflow is accompanied by internal losses (such as friction).

The stagnation parameters can also be found in the relative motion:

$$h_w^* = h + \frac{w^2}{2}, T_w^* = T + \frac{w^2}{2c_p}.$$

With isoentropic stagnation

$$h_w^* = h\left(1 + \frac{k-1}{2} M_w^2\right), T_w^* = T\left(1 + \frac{k-1}{2} M_w^2\right),$$
$$p_w^* = p\left(1 + \frac{k-1}{2} M_w^2\right)^{\frac{k}{k-1}}, \rho_w^* = \rho\left(1 + \frac{k-1}{2} M_w^2\right)^{\frac{1}{k-1}}.$$

Here $M_w = \frac{w}{a}$ is the Mach number in the relative motion.

In the absence of the heat exchange, the stagnation enthalpy and the temperature remain constant in the relative motion, although they are changed in the absolute motion. The stagnation pressure and the density in the relative motion in the presence of losses are decreased, but their relation $p_w^*/p_w^*$ remains constant.

The stagnation parameters are conditional (non-existent) parameters that are used as a tool to simplify the analysis and the calculation.

## 3.3 Isoentropic Flow of the Working Fluid in the Nozzle Channels

We consider the gas flow in a fixed frictionless nozzle (the theoretical or gas-dynamically ideal process) and the absence of the heat exchange between gas and the environment (the adiabatic process).

According to the definition of gas entropy, we have the following:

$$ds = \frac{dQ}{T},$$

where $dQ$ is the total amount of the heat which has been received by the gas in the elementary process.

Because in the gas stream, we have the following:

$$dQ = dq + dq_r$$

then in the case of the adiabatic flow without friction ($dq = 0$; $dq_r = 0$) $dQ = 0$ and then $ds = 0$, and $s = \text{const}$.

Thus the adiabatic frictionless process is isoentropic and is described by the equation $pv^k = \text{const}$ or $p/\rho^k = \text{const}$.

Let the gas parameters before the nozzle: $p_0$, $T_0$, $v_0$; the velocity $c_0$; the nozzle pressure $p_1$ (Fig. 3.4). We will assume that the expansion of gas from $p_0$ to $p_1$ occurs completely within the nozzle [1].

Integrating the gas flow energy Eq. (3.14) for this case between sections 0 and 1, we obtain the following:

$$h_{1t} - h_0 + \frac{c_{1t}^2}{2} - \frac{c_0^2}{2} = 0, \tag{3.30}$$

where the index "$t$" indicates that the theoretical process has been considered.

**The theoretical velocity of the nozzle outflow** according to (3.30) will be the following:

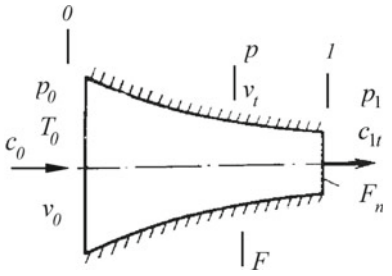


**Fig. 3.4** The diagram of the nozzle channel

$$c_{1t} = \sqrt{2\left[(h_0 - h_{1t}) + \frac{c_0^2}{2}\right]} = \sqrt{2(h_0^* - h_{1t})}. \tag{3.31}$$

In Fig. 3.5 in the coordinates *h*-*s* (diagram *h*-*s*), the line $0–1_t$ depicts the isoentropic process of the working fluid expansion in the nozzle from the initial parameters $p_0$, $T_0$ to the final pressure $p_1$. The point $0^*$ is the state of the stagnated flow before the nozzle; $0–0^*$ is the isoentropic stagnation process [1].

The diagram shows that: $h_0 - h_{1t} = \Delta h_{\text{an}}$, i.e. it is the isoentropic heat drop in the nozzle; $h_0^* - h_{1t} = \Delta h_{\text{an}} + \frac{c_0^2}{2} = \Delta h_{\text{an}}^*$ is the total available heat drop in the nozzle.

The isoentropic heat drop is the amount of the potential energy that transfers into the kinetic energy during the expansion in the nozzle channel.

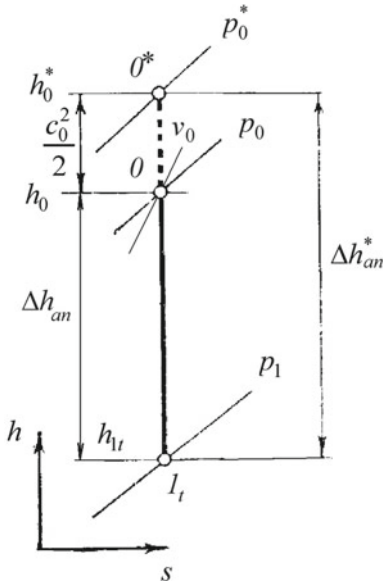


**Fig. 3.5** Isoentropic process in the nozzle channels

It is based on the following notation:

$$c_{1t} = \sqrt{2\left(\Delta h_{\text{an}} + \frac{c_0^2}{2}\right)} = \sqrt{2\Delta h_{\text{an}}^*}. \tag{3.32}$$

It is convenient to use this equation when there is an *h-s* diagram for the working fluid.

For gases, where such diagrams are not available, heat drops can be determined through some parameters. For this, in Eq. (3.31) for enthalpies, we need to use the substitution: $h_0 = \frac{k}{k-1} p_0 v_0$, $h_0^* = \frac{k}{k-1} p_0^* v_0^*$ and $h_{1t} = \frac{k}{k-1} p_1 v_{1t}$. Then for the theoretical velocity of the nozzle outflow, we will have

$$c_{1t} = \sqrt{2\frac{k}{k-1} p_0 v_0 \left[1 - \left(\frac{p_1}{p_0}\right)^{\frac{k-1}{k}}\right] + c_0^2}, \tag{3.33}$$

or

$$c_{1t} = \sqrt{2\frac{k}{k-1} p_0^* v_0^* \left[1 - \left(\frac{p_1}{p_0^*}\right)^{\frac{k-1}{k}}\right]}. \tag{3.34}$$

These formulas can also be used to determine the velocity $c_t$ in any arbitrary section.

From the continuity Eq. (3.4) for the outlet section will be the following:

$$G_t = \frac{F_c c_{1t}}{v_{1t}},$$

or after substituting $c_{1t}$ from (3.35) taking into account that in the isentropic process will be the following:

$$v_{1t} = v_0^* \left(\frac{p_0^*}{p_1}\right)^{\frac{1}{k}},$$

after some transformations will be the following:

$$G_t = F_c \sqrt{\frac{2k}{k-1} \cdot \frac{p_0^*}{v_0^*} \left[\left(\frac{p_1}{p_0^*}\right)^{\frac{2}{k}} - \left(\frac{p_1}{p_0^*}\right)^{\frac{k+1}{k}}\right]}. \tag{3.35}$$

## 3.4 Actual Flow Process in the Nozzle Channels

The actual process of the working fluid flow is accompanied by energy losses due to friction, eddy formation, and others. The marked losses lead to the fact that some of the kinetic energy in the expensing process is converted into heat, which is accepted by the working fluid itself ($dq_r > 0$). As a result, its enthalpy at the end of the actual expansion process is greater than at the end of the isoentropic one, and the actual flow velocity at the nozzle outlet is less than the theoretical flow velocity [1].

For the energy-insulated flow in the nozzle in the presence of friction ($dl_T = 0$; $dq = 0$; $dq_r > 0$) by analogy with (3.30), since the energy equation of the gas stream has the same appearance as in the absence of friction,

$$h_1 - h_0 + \frac{c_1^2}{2} - \frac{c_0^2}{2} = 0, \tag{3.36}$$

where $h_1$ and $c_1$ are the parameters in the actual process, and in comparison with the Eq. (3.30): $h_1 > h_{1t}$ and $c_1 < c_{1t}$. Due to the enthalpy change, the temperature at the end of the actual process is higher than at the end of the isoentropic process ($T_1 > T_{1t}$). The flow process is some polytropic process ($pv^n = \text{const}$), which goes with the increase in the entropy, because $ds = \frac{dq_r}{T} > 0$.

In the *h-s* diagram, the actual process of the gas expansion in the nozzle channels is represented by the line 0–1 (Fig. 3.6).

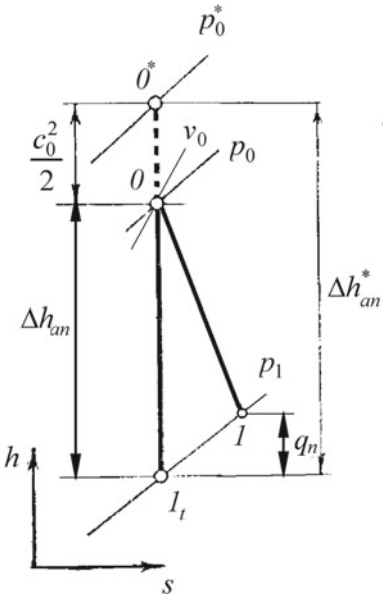


**Fig. 3.6** The actual process of the gas expansion in the nozzle channels

Since the kinetic energy which has been obtained by the working fluid in the turbine stage nozzles is subject to the conversion into the mechanical energy within moving blades, the reduction of the flow kinetic energy in the actual process in comparison with isentropic will be the following:

$$q_n = \frac{c_{1t}^2}{2} - \frac{c_1^2}{2} \tag{3.37}$$

It represents the energy loss in the nozzle channels.

Comparing (3.36) with (3.30), we obtain the following:

$$q_n = h_1 - h_{1t}. \tag{3.38}$$

In the actual process, the velocity in the nozzle cross-sections is not uniform for all points: the maximum is in the flow core, and in the boundary layer it decreases to zero in the wall. Therefore, in formulas (3.36) and (3.37), you should understand $c_1$ as some average velocity.

**The actual velocity of the nozzle outflow** is connected with the theoretical one as the following:

$$c_1 = \varphi c_{1t}, \tag{3.39}$$

where $\varphi$ is the nozzle velocity coefficient, which depends on the nozzle shape, the surface condition, the flow mode, and other factors. It is usually determined experimentally ($\varphi < 1.0$).

Using the formulas of the isoentropic expansion process and introducing the coefficient $\varphi$ into them, we obtain the following formulas for the actual velocity:

$$c_1 = \varphi\sqrt{2\Delta h_{\text{an}} + c_0^2} = \varphi\sqrt{2\Delta h_{\text{an}}^*};$$
$$c_1 = \varphi\sqrt{\tfrac{2k}{k-1} p_0 v_0\left[1 - \left(p_1/p_0\right)^{\frac{k-1}{k}}\right] + c_0^2} = \varphi\sqrt{\tfrac{2k}{k-1} p_0^* v_0^*\left[1 - \left(p_1/p_0^*\right)^{\frac{k-1}{k}}\right]}.$$

After substituting $c_1$ from (3.39) into (3.37) will be the following:

$$q_n = (1-\varphi^2)\frac{c_{1t}^2}{2} = (1-\varphi^2)\Delta h_{\text{an}}^* = (1-\varphi^2)\left(\Delta h_{\text{an}} + \frac{c_0^2}{2}\right). \tag{3.40}$$

Since from (3.38) we have the following:

$$h_1 = h_{1t} + q_n,$$

then to plot the actual nozzle expansion process in the diagram *h-s*, it is required from the point $1_t$ (the end of the isoentropic expansion process) put up to the nozzle

losses $q_n$ and find the point *1* of the enthalpy $h_1$ intersection with the isobar $p_1$. Line 0–1 will represent conditionally the polytropic expansion in the nozzle channel.

The ratio of the kinetic energy losses to the total heat drop in the nozzle is called the loss nozzle coefficient:

$$\zeta_c = \frac{q_c}{\Delta h^*_{\text{an}}} = 1 - \varphi^2. \tag{3.41}$$

## 3.5 Flow in the Moving Blade Channels

As it can be seen from Table 3.1, the energy equation of the gas stream in the channels moves progressively ($u = \text{const}$) in the relative coordinate system associated with the channels and has the same form as the equation in the absolute system for fixed channels ($dl_T = 0$). This means that the flow which is relative to the channel walls behaves as if they were stationary. And if the initial gas flow equations are similar, then all the dependencies and the formulas that follow from them must be similar.

Thus, for the moving channels (the rotor blade channels of the axial stages) all the formulas and the ratios obtained for the fixed nozzle channels can be applied if considering the flow in relative motion. It is enough in the following cases:

- everywhere, instead of the absolute velocity $c$ substitute the relative velocity $w$;
- determine the stagnation flow parameters in the relative motion, as indicated by the index "$w$" near the parameter;
- instead of indices 0 and 1 at the channel inlet and outlet, take 1 and 2, respectively;
- replace the index "$n$" with "$r$" near the heat drops, the flow rates, and the losses;
- instead of $\varphi$ denote by $\psi$ the velocity coefficient for the rotor channel.

As an example, here are some formulas written as follows:

- the theoretical velocity of the gas outflow from the moving channel, by the analogy with (3.34):

$$w_{2t} = \sqrt{\frac{2k}{k-1} p^*_{1w} v^*_{1w} \left[1 - \left(\frac{p_2}{p^*_{1w}}\right)^{\frac{k-1}{k}}\right]};$$

- the actual outflow velocity—by the analogy with (3.39)

$$w_2 = \psi w_{2t};$$

- the energy losses in the rotor channel according to (3.40)

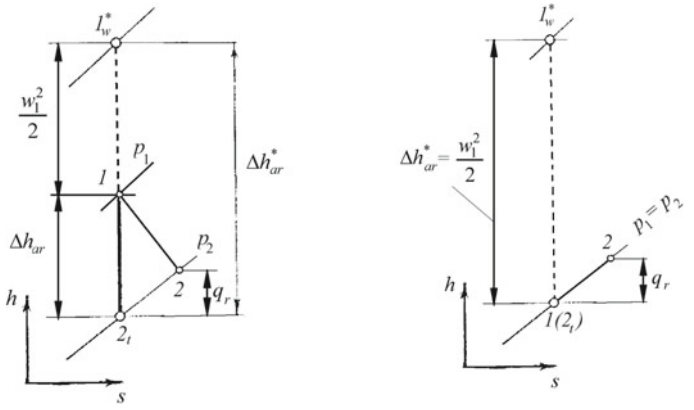


(a) The Reaction Stage (b) The Impulse Stage

**Fig. 3.7** Process of the gas expansion in the moving channel (1–$2_t$-the theoretical process; 1–2-the actual process)

$$q_r = (1-\psi^2)\frac{w_{2t}^2}{2} = (1-\psi^2)\Delta h_{\text{ar}}^* = (1-\psi^2)\left(\Delta h_{\text{ar}} + \frac{w_1^2}{2}\right),$$

where $\Delta h_{\text{ar}}$ is the isentropic heat drop in the rotor channel; $\Delta h_{\text{ar}}^*$ is the total available heat drop in the rotor channel.

Figure 3.7 shows the process in the moving channel on the *h*-*s* diagram for two cases: (a) with the significant expansion of the working fluid in the channel and (b) in the absence of expansion. In the first case, the process is not fundamentally different from the process in the nozzle channel (Fig. 3.6). In the second case $\Delta h_{\text{ar}} = 0$, since this is the potential energy that is converted into the kinetic, and in the absence of the gas expansion, there is no such transformation. As a result, points 1 and $2_t$ coincide and the process is represented by the segment of the isobars 1–3.

While in the nozzle channels the potential energy converted to the kinetic significantly exceeds the kinetic energy at the inlet ($\Delta h_{\text{an}} \gg c_0^2/2$), in the moving channels the ratio $\Delta h_{\text{ar}}/\frac{w_1^2}{2}$ can vary widely, from the values characteristic of the nozzle channels to zero, as it takes place in the process in Fig. 3.7b.

## Reference

1. Romanovsky GF, Ipatenko OY, Patlaychuk VM (2002) Theory and calculation of steam and gas turbines. Publisher USMTU, Mykolaiv, 292 p. (in Ukrainian)

# Chapter 4
# Flow in the Plane Turbine Channels


## 4.1 Geometric Characteristics of the Axial Turbine Cascades

In the axial stages, the nozzle and rotor blades are located within the ring which has been formed by the inner and outer cylindrical or slightly conical limiting surfaces, and the blade axes approximately coincide with the radii. Therefore, such cascades are called ring cascades.

The sweeping of the blade cylindrical cross-sections into the plane gives the nozzle and rotor blade cascade profiles. Figure 4.1 shows the longitudinal and cross-sections of the ring cascade, as well as the cascade profiles at one of the diameters [1].

The main geometrical characteristics of the stage and the cascade are:

- the blade length (the height of the cascade) $l$ is the distance along the radius between the root blade section and its apex near the outlet edge (tip);
- the average (medium) diameter of the ring cascade $D_m$ is the diameter of the circle passing through the middle of the blades;
- the middle profile line is the geometric position of the circle centers which have been inscribed in the profile;
- the blade chord $b$ is the distance between the endpoints of the profile, which is measured in the direction of the joint tangent to the inlet and outlet edges of the concave surface (blade pressure surface);
- the lifting height (deflection) of the middle profile line $h$ is the distance between the joint tangent to the inlet and outlet edges of the concave surface and the tangent to the middle profile line;
- the profile thickness $\delta_{max}$ is the maximum diameter of the circle that fits into the profile;
- the thickness of the inlet $s_{in}$ and the outlet $s_{out}$ edges are the circle diameters which are forming the inlet and outlet profile edges, respectively;



K. Liu et al. (eds.), *Gas Turbines Structural Properties, Operation Principles and Design Features*, https://doi.org/10.1007/978-981-99-0977-3_4

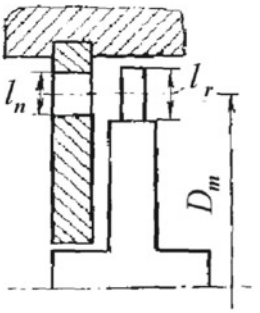


(a) Longitudinal Section

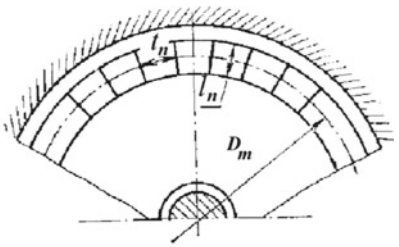


(b) Cross-Section Of The Nozzle Blade Cascade

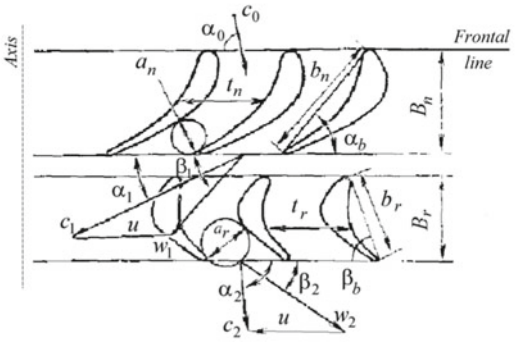


(c) Plane Cascade Of Nozzles And Rotor Blades

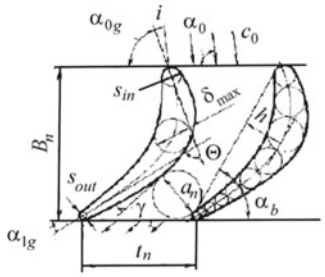


(d) Nozzle Blade Profile

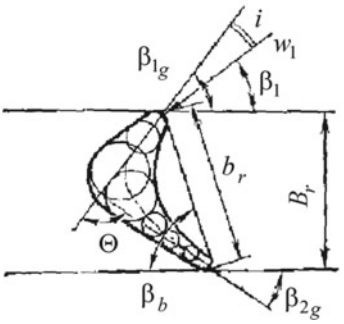


(e) Rotor Blade Profile

**Fig. 4.1** Geometrical characteristics of the turbine stage

- the back (the suction face) bend angle $\gamma$ is the angle between the tangent to the profile back (the suction face) in the minimum channel cross-section and the tangent to the outlet edge;
- the frontal line is a line which has been drawn through similar profile points;
- the cascade axis is a line which is perpendicular to the frontal line;
- the blade angle $\alpha_b(\beta_b)$ is the angle between the joint tangent to the inlet and outlet profile edges from the concave surface and the frontal line;
- the profile width $B$ is the distance between the end profile points which has been measured in the cascade axis direction (the axial size of the blade profile);
- the blade pitch $t$ is the distance between the similar points of the adjacent profiles which have been measured in the frontal line direction;
- the width of the outlet channel cross-section $a$ is the smallest distance from the outlet edge to the convex surface (the suction face) of the adjacent blade;
- the geometrical inlet $\alpha_{0g}$ and outlet $\alpha_{1g}$ profile angles for the nozzle cascade and $\beta_{1g}$, $\beta_{2g}$ are for the rotor cascade;
- the profile bending angle $\Theta$ is the angle between the tangents to the midline at its extreme points:

$$\Theta_n = 180^\circ - (\alpha_{0g} + \alpha_{1g}) \quad \text{and} \quad \Theta_r = 180^\circ - (\beta_{1g} + \beta_{2g}).$$

The inlet and outlet angles can be constant or variable along the length of the blades. In the first case, the blades are called cylindrical. In the second case, the blades are called screws or twisted. In stages with the cylindrical blades, the cascade pitch and the channel width in the outlet section are increased from the root to the top in proportion to the section diameter. In the case of the screw blades, the channel width changes in height according to a more complex law, taking into account the configuration change of the profile.

The actual cascade angles of the inlet and the outlet are slightly different from the geometrical ones. The actual inlet angles $\alpha_0$ and $\beta_1$ are determined by the conditions of the flow formation in front of the cascade, namely, the conditions of the exit from the previous stage and the nozzles of this stage, respectively. In general, the actual inlet angle does not match the geometrical one. The concept of the attack angle $i$ is introduced to evaluate the flow conditions on the blades. The angle of attack is the difference between the geometrical inlet blade angle and the stream inlet angle, i.e. $i_n = \alpha_{0g} - \alpha_0$ (or $i_r = \beta_{1g} - \beta_1$). If $i > 0$, then the angle of attack is positive; if $i < 0$—the attack angle is negative. At $i = 0$, the inlet to the cascade channel is conditionally called non-impact (shock-free). With this flow, the energy losses in the cascade channel are minimal.

The actual outlet flow angles from the nozzle $\alpha_1$ and the rotor $\beta_2$ cascades are quite close in value to the so-called effective outlet angles $\alpha_{1\text{ef}}$ and $\beta_{2\text{ef}}$, which are determined by the formulas:

$$\alpha_{1\text{ef}} = \arcsin \frac{a_n}{t_n} \quad \text{and} \quad \beta_{2\text{ef}} = \arcsin \frac{a_r}{t_r}.$$

Given the small difference between actual and effective angles, we can assume that $\alpha_1 \approx \alpha_{1ef}$ and $\beta_2 \approx \beta_{2ef}$.

The geometrical turbine stage characteristics, in addition to the absolute ones, also include the relative characteristics. Thus, for ring cascades, the ratio of the average diameter to the blade length is often used

$$\lambda = \frac{D_m}{l}.$$

The most commonly used:

– the relative cascade pitch

$$\bar{t} = \frac{t}{b} \quad \text{or} \quad \bar{t}_B = \frac{t}{B},$$

– the relative blade length

$$\bar{l} = \frac{l}{b} \quad \text{or} \quad \bar{l}_a = \frac{l}{a},$$

and the relative lifting height (deflection) of the profile midline $h/b$.

The relative cascade dimensions are the criteria for the geometric cascade similarity.

## 4.2 Plane Cascades of the Turbine Blades

The flow of the working fluid in the turbine channels has a complex spatial structure. The theoretical solution to the problem of the spatial viscous compressible fluid flow in the blade cascades is a very difficult task. Therefore, simplified models of the actual process are usually explored, which preserve the most important flow features, with the subsequent analysis and the consideration of the influence of the minor factors.

For example, the flow problem is considerably simplified in the case of the infinite plane cascade, that is, in which all the parameters along the blade length remain constant and the number of blades and their length is infinitely large.

In plane cascade, the flow is regarded as a plane. In this case, it is sufficient to study the flow only in one section, which is perpendicular to the axial axis of the blades.

The transition from the ring cascade to the plane cascade can be carried out on the basis of the hypothesis of plane sections which has been proposed by Zhukovsky in 1890. According to the main provisions of this hypothesis, the flow of the working fluid is considered as a movement by concentric layers, and the flow in each layer does not affect the adjacent layers. Thus, if we bring two coaxial cylindrical sections of the ring cascade on the diameters $D$ and $D + \Delta D$ (where $\Delta D$ is very small), and

then unroll the obtained ring cascade to the plane, then we obtain the plane cascade of the small height. Increasing the number of blades and their length to infinity, we obtain the plane cascade corresponding to the profile cascade with the diameter $D$.

The flow of the working fluid on any diameter $D$ of the ring cascade can be considered as the flow in the corresponding plane cascade. This does not extend to the areas of flow close to the root and the periphery of the blades, where the flow is affected by the limiting wall channels.

The plane hypothesis requires the correction in the case where the blade cascades are characterized by a small ratio ($\lambda = D_m/l < 10 \sim 12$), i.e. for the stages with relatively long blades. There is a significant change in the tangential velocity along the blades and the influence of the centrifugal forces which are acting on the working fluid particles.

### 4.2.1 Forces in the Plane Cascade

In the steady flow of the plane cascade which moves at a constant velocity $u$ in the direction of the similar axis, we distinguish some volume (Fig. 4.2) which is limited by [1]:

(a) the surfaces $ad$ and $bc$ at the distance of the step $t$ from each other;

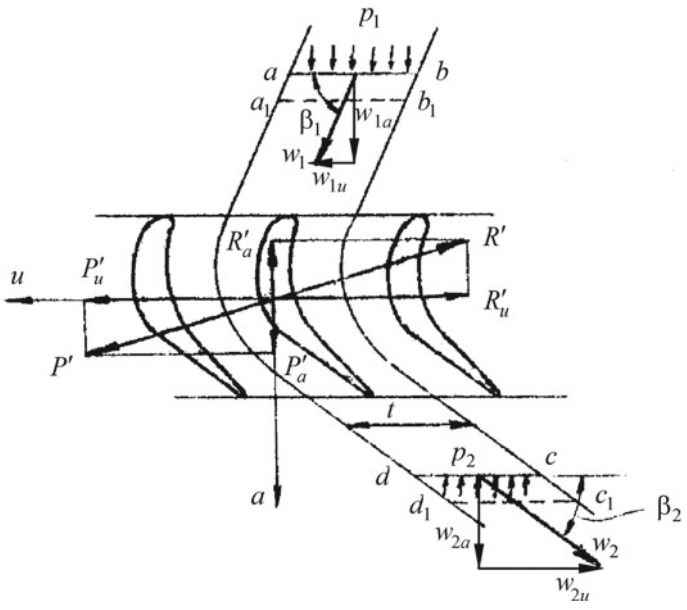


**Fig. 4.2** The forces acting in the plane cascade

(b) two frontal surfaces *ab* and *dc* at such distance from the cascade at which all the parameters along these surfaces can be considered constant;
(c) two areas that are paralleled to the plane of the drawing, the distance between which is equal to the blade length *l*.

During a period $d\tau$ the mass of gas which is placed initially in the dedicated volume will move to a position which is limited by the figure $a_1b_1c_1d_1$.

The change in the momentum of the considered mass of gas during the period $d\tau$

$$d\overrightarrow{K} = \overrightarrow{K}_{a_1b_1c_1d_1} - \overrightarrow{K}_{abcd} = \overrightarrow{K}_{cdd_1c_1} - \overrightarrow{K}_{abb_1a_1}.$$

Because

$$\overrightarrow{K}_{cdd_1c_1} = \vec{w}_2 dm_2,$$
$$\overrightarrow{K}_{abb_1a_1} = \vec{w}_1 dm_1,$$

due to the continuity of the flow $dm_1 = dm_2 = dm$, we have the following:

$$d\overrightarrow{K} = dm\,(\vec{w}_2 - \vec{w}_1), \tag{4.1}$$

where $\vec{w}_1$ and $\vec{w}_2$ are the flow velocities before and after the cascade.

The momentum equation in vector form is the following:

$$d\overrightarrow{K} = (\vec{p}_1 tl + \vec{p}_2 tl + \overrightarrow{R}')\,d\tau. \tag{4.2}$$

The right side of the Eq. (4.2) is the momentum of the main vector of the external forces which are acting on the considered mass of gas. There is here: $p_1$ and $p_2$ are the pressure in the cross-sections *ab* and *cd*; $\overrightarrow{R}'$ is the resultant blade action force on the stream. The forces which are caused by the pressures on the surfaces *ad* and *bc* did not enter into the equation because their result is equal to zero. The Eq. (4.2) does not take into account the mass forces (gravity and centrifugal forces) due to the low gas density.

After substituting $d\overrightarrow{K}$ from (4.1), assuming that

$$\frac{dm}{d\tau} = G',$$

where $G'$ is the mass gas flow rate through the cascade within at height *l*, we obtain the following:

$$G'(\vec{w}_2 - \vec{w}_1) = \vec{p}_1 tl + \vec{p}_2 tl + \overrightarrow{R}'. \tag{4.3}$$

The projecting Eq. (4.3) to mutually perpendicular directions *u* and *a*:

$$R'_u = G'(\overline{w}_{2u} - \overline{w}_{1u}),$$
$$R'_a = G'(\overline{w}_{2a} - \overline{w}_{1a}) - (p_1 - p_2)t\,l.$$

In these formulas, the strokes above the velocity projections indicate that the actions in brackets should be performed algebraically, taking into account the signs of the projections.

The power $\overrightarrow{R}'$ is the blade action on the stream. The flow acts on the blade with equal magnitude but with the opposite force $\overrightarrow{P}'$. Then

$$P'_u = G'(\overline{w}_{1u} - \overline{w}_{2u}), \tag{4.4}$$

$$P'_a = G'(\overline{w}_{1a} - \overline{w}_{2a}) + (p_1 - p_2)t\,l. \tag{4.5}$$

For the entire cascade of the finite dimensions, if the flow through it is $G$, kg/s, and the number of blades $z$ at their length $l$, we have the following:

$$P_u = G\,(\overline{w}_{1u} - \overline{w}_{2u}), \tag{4.6}$$

$$P_a = G\,(\overline{w}_{1a} - \overline{w}_{2a}) + (p_1 - p_2)t\,l\,z. \tag{4.7}$$

From the inlet and outlet velocity triangles and at the outlet (Fig. 4.3) we have the following:

$$\overline{w}_{1u} - \overline{w}_{2u} = \overline{c}_{1u} - \overline{c}_{2u},$$
$$\overline{w}_{1a} - \overline{w}_{2a} = \overline{c}_{1a} - \overline{c}_{2a}$$

in the first case, due to $\overline{w}_{1u} = \overline{c}_{1u} - \overline{u}$ and $\overline{w}_{2u} = \overline{c}_{2u} - \overline{u}$, in the second case, due to $\overline{w}_{1a} = \overline{c}_{1a}$ and $\overline{w}_{2a} = \overline{c}_{2a}$.

Therefore, the Eqs. (4.6) and (4.7) can be rewritten as the following:

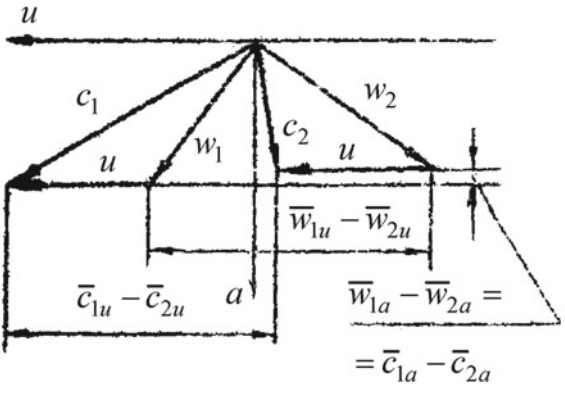


**Fig. 4.3** Turbine stage velocity triangles

$$P_u = G\,(\overline{c}_{1u} - \overline{c}_{2u}), \tag{4.8}$$

$$P_a = G\,(\overline{c}_{1a} - \overline{c}_{2a}) + (p_1 - p_2)\,t\,l\,z. \tag{4.9}$$

In the case of the fixed cascade $w = c$, both formulas for $P_u$ and $P_a$ are obtained directly in the form (4.8) to (4.9) at the corresponding indices at the velocities and the inlet and outlet pressures.

The formulas (4.4)–(4.9) for the flow force components were the first which have been obtained by Leonard Euler in 1754 for the hydraulic turbine wheel and are known by the name Euler equations.

The Euler equations are valid for both the ideal (theoretical) and actual cases of flow. However, using them involves the determination of the flow velocities before and after the cascade. The actual velocities can only be found on the basis of the detailed analysis of the gas flow in the cascade and energy losses due to the process's irreversibility. This task is identical to finding the velocity coefficients $\varphi$ and $\psi$.

### 4.2.2 *Working Fluid Flow Rate Through Cascades and Flow Coefficients*

For the working flow rates we will have:

– for the theoretical flow through the nozzle and the moving (rotor) cascades with narrowed channels (at subsonic flow):

$$G_{nt} = F_n c_{1t} \rho_{1t}; \quad G_{rt} = F_r w_{2t} \rho_{2t}; \tag{4.10}$$

– for actual flow:

$$G_n = F_n c_1 \rho_1; \quad G_r = F_r w_2 \rho_2. \tag{4.11}$$

where $F_n$ and $F_r$ are the area of the outlet sections which is perpendicular to the flow direction. At full inlet we have the following:

$$F_n = \pi D_m l_n \sin\alpha_1; \quad F_r = \pi D_m l_r \sin\beta_2.$$

The actual flow rates which are calculated by the formula (4.11) are slightly different from the actual flow rates which are obtained experimentally. The reasons for this are the uneven velocity fields and other parameters in the outlet section; the inaccuracy in the determination of the losses which affect the polytropic index; the physical properties of the working fluid, etc.

Therefore, in the calculations to determine the actual flow rates should be used the so-called *flow coefficients*:

$$\mu_n = \frac{G_n}{G_{nt}}; \quad \mu_r = \frac{G_r}{G_{rt}}.$$

They are found experimentally.
Then we have the following:

$$G_n = \mu_n G_{nt}; \quad G_r = \mu_r G_{rt}.$$

The value of the cascade flow coefficient μ depends on the working flow condition, the profile geometric characteristics, the relative blade dimensions, and other factors. According to the experimental data, the nozzle flow coefficient is 0.96–0.97, and in the moving cascades—0.92 to 0.96 depending on the profile bending and the relative blade length (the smaller values refer to the impulse stages, the larger values refer to the reaction stages).

## Reference

1. Romanovsky GF, Ipatenko OY, Patlaychuk VM (2002) Theory and calculation of steam and gas turbines. Publisher USMTU, Mykolaiv, 292 p. (in Ukrainian)

# Chapter 5
# Features of the Actual Profile Flow. Cascade Loss Classification

When the real working fluid flows through the cascades, the overall flow pattern may differ significantly from the ideal one. Due to the viscosity of the working fluid, the boundary layer with significant transverse velocity gradients is formed on the profile surfaces, in which energy losses from friction are concentrated.

In general, the flow in plane cascades with infinitely long blades can be conditionally divided into two zones (Fig. 5.1): the *flow core*, where the flow can be considered as potential, and the *boundary layer* during passing along the cascade into the aerodynamic wake. The thickness of the boundary layer does not usually exceed 0.1 of the blade pitch (i.e. 1–3 mm), but it is the reason for the kinetic energy losses due to the viscosity of the working fluid [1].

In the ring cascades with finite blade length, there is the third flow zone—the zone in which the influence of the walls limiting the channel at the blade ends appears. There are also additional energy losses in this area.

In view of the above, the energy losses in the ring cascades can be divided into two groups:

(a) the *profile losses* are those that occur during the flow around the profile blade part;
(b) *end losses* are those that occur during the flow around the external and internal butt (end) surfaces of the turbine channels.

The profile losses include:

(a) the friction losses;
(b) the edge losses;
(c) the losses due to flow separation from the profile surface;
(d) the wave losses.

In all cases, the friction and edge losses are mandatory, while the flow separation and the wave losses occur only under certain conditions.

The end losses are determined by the finite length of the blades:

(a) the friction in the boundary layer on the end channel surfaces;



K. Liu et al. (eds.), *Gas Turbines Structural Properties, Operation Principles and Design Features*, https://doi.org/10.1007/978-981-99-0977-3_5

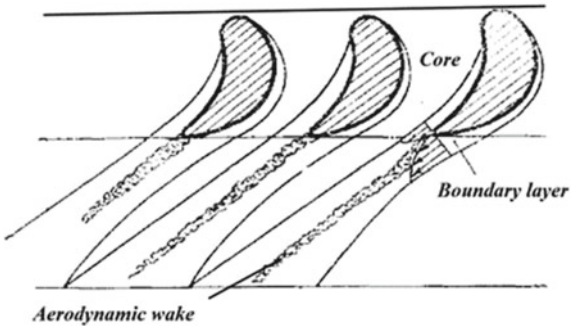


**Fig. 5.1** Flow structure in the turbine channels

(b) the formation of the secondary or induced flows in the channel between the blades caused by the uneven pressure distribution along the channel section (from the twin vortex);
(c) the gas flow—from the concave blade side to the convex side through the peripheral edge (in the presence of the gap between the blade and the channel boundary surface).

The above losses are inherent in both fixed and moving cascades. In the latter in addition, there are losses:

– from the radial gas flow;
– from the unsteady flow of the incoming stream.

Each of the cascade loss components can be estimated by the corresponding loss coefficient

$$\zeta_i = \frac{q_i}{\Delta h^*_{ai}},$$

where $q_i$ is the absolute value of the energy losses; $\Delta h^*_{ai}$ ($\Delta h^*_{an}$ або $\Delta h^*_{ar}$) is the total available heat drop in the cascades (nozzle or moving).

The total loss coefficient in the cascade is the following:

$$\zeta = \zeta_{\text{pr}} + \zeta_{\text{en}}. \tag{5.1}$$

In the formula (5.1), $\zeta_{\text{pr}}$ is the coefficient of the profile losses; $\zeta_{\text{en}}$ is the coefficient of the end losses.

Therefore

$$\zeta_{\text{pr}} = \zeta_{\text{fr}} + \zeta_{\text{ed}} + \zeta_{\text{se}} + \zeta_{\text{wa}}$$

and

$$\zeta_{en} = \zeta_{fr} + \zeta_{sf} + \zeta_{fo},$$

where $\zeta_{fr}$, $\zeta_{ed}$, $\zeta_{se}$, $\zeta_{wa}$, $\zeta_{sf}$ $i$ $\zeta_{fo}$ are the corresponding loss coefficients.

If the profile losses consist only of the friction and the edge losses, then (4.1) will be as the following:

$$\zeta = \zeta_{fr} + \zeta_{ed} + \zeta_{en}. \tag{5.2}$$

The cascade efficiency is as the following:

$$\eta = 1 - \zeta. \tag{5.3}$$

The velocity coefficient of the nozzle cascade is as the following:

$$\varphi = \sqrt{1 - \zeta_n} = \sqrt{\eta_n}.$$

The moving blade:

$$\psi = \sqrt{1 - \zeta_r} = \sqrt{\eta_r},$$

where the total loss coefficients and the efficiency of the corresponding cascades are determined from (5.2) to (5.3).

## 5.1 Stage with Relatively Short Blades Degree of Reaction

The stages with relatively short blades are the stages in which $\lambda = D_m / l \geq 10 \ldots 12$, when the blade length is relatively small in comparison with the average stage diameter. If the blades have a constant profile, then the change of the cascade parameters and the flow in radius can be neglected. The nozzle and rotor profile flow is considered as a plane flow with parameters which are corresponding to the average stage diameter and the limited blade length. The stage parameters calculation is simplified because it is conducted only for the average diameter cross-section. The velocity coefficients are defined as the average along the blade length, taking into account the profile and the end losses.

We consider the process of the working fluid expansion in the turbine stage (Fig. 5.2). For the control of the surfaces, we will accept the sections 0—in the front of the nozzles; 1—in the gap between the nozzles of the rotor blades; 2—behind the stage [1].

The working fluid condition in front of the stage can be determined by the parameters $p_0$, $v_0$, the initial working fluid velocity $c_0$; the pressures in Sects. 5.1 and 5.2 are $p_1$ and $p_2$, respectively; the circumferential (rotary) velocity $u$ at the average diameter. The cascade characteristics ($\alpha_1$, $\beta_2$, $\varphi$ and $\psi$) will be known.

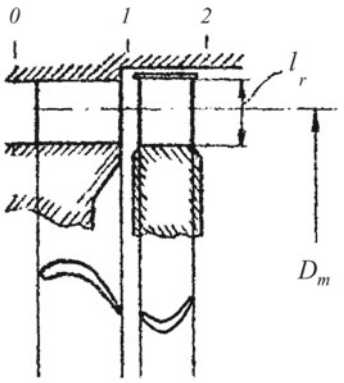


(a)

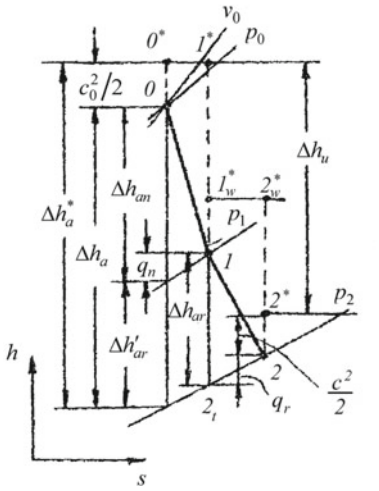


(b)

**Fig. 5.2** The turbine stage scheme (**a**) and the process of the working fluid expansion in the *h-s* diagram (**b**)

In Fig. 5.2, *b* point 0 is the condition of the working fluid before the stage, $0^*$ is the condition of the stagnated flow in the same place; the line $0–1_t$ is isentropic, and the line 0–1 is the actual process of the working fluid expansion in the nozzle.

In this case, $\Delta h_{\text{an}}$ is the isoentropic heat drop in the nozzle cascade; $\Delta h^*_{\text{an}} = \Delta h_{\text{an}} + \frac{c_0^2}{2}$ is the total available nozzle heat drop; $q_n$ is the nozzle energy loss.

The actual working fluid velocity from the nozzle is as the following:

$$c_1 = \varphi c_{1t} = \varphi\sqrt{2(h_0^* - h_{1t})} = \varphi\sqrt{2\Delta h_{\text{an}}^*}.$$

The energy loss in the nozzle is as the following:

$$q_n = (1 - \varphi^2)\Delta h_{\text{an}}^* = (1 - \varphi^2)\frac{c_{1t}^2}{2}.$$

There are known $c_1$, $u$ and $\alpha_1$, you can build the inlet velocity triangle, from which the relative flow velocity $w_1$ and its direction $\beta_1$ are determined.

The parameters $w_1$ and $\beta_1$ can be found without building the inlet velocity triangle by use of the following formula:

$$\text{tg}\beta_1 = \frac{c_1 \sin\alpha_1}{c_1 \cos\alpha_1 - u}, w_1 = \frac{c_1 \cos\alpha_1 - u}{\cos\beta_1}.$$

Point 1 in the *h-s* diagram determines the static working fluid parameters behind the nozzle that is at the inlet to the rotor cascade. The working fluid has the absolute velocity $c_1$ and the relative velocity $w_1$. The stagnated flow condition in absolute and relative motion for Sect. 5.1 will be shown, respectively, by the points $1^*$ and $1_w^*$. Then $h_1^* = h_1 + \frac{c_1^2}{2}$; $h_{1w}^* = h_1 + \frac{w_1^2}{2}$.

In the presence of the working fluid expansion in the rotor cascade is $p_2 < p_1$. The conditional flow expansion process is represented by line 1–2.

In this case, $\Delta h_{\text{ar}}$ is the isoentropic heat drop in the rotor cascade; $w_1^2/2$ is the flow of kinetic energy at the inlet to the rotor cascade in the relative motion; $\Delta h_{\text{ar}}^* = \Delta h_{\text{ar}} + \frac{w_1^2}{2}$ is the total available heat drop in the rotor cascade.

The actual outlet relative velocity of the working fluid from the rotor cascade is as the following:

$$w_2 = \psi w_{2t} = \psi\sqrt{2(h_{1w}^* - h_{2t})} = \psi\sqrt{2\Delta h_{\text{ar}}^*} = \psi\sqrt{2\left(\Delta h_{\text{ar}} + \frac{w_1^2}{2}\right)}.$$

The energy losses in the rotor cascade are as the following:

$$q_r = (1 - \psi^2)\Delta h_{\text{ar}}^* = (1 - \psi^2)\frac{w_{2t}^2}{2}.$$

Or due to, $w_{2t} = \frac{w_2}{\psi}$,

$$q_r = \frac{1 - \psi^2}{\psi^2} \cdot \frac{w_2^2}{2}.$$

There are known $w_2$, $u$ and $\beta_2$, you can build the outlet velocity triangle, from which the absolute flow velocity $c_2$ and its direction $\alpha_2$ are determined.

It is obvious that

$$\mathrm{tg}\alpha_2 = \frac{w_2 \sin\beta_2}{w_2 \cos\beta_2 - u}, c_2 = \frac{w_2 \cos\beta_2 - u}{\cos\alpha_2}.$$

On the *h-s* diagram, the working fluid condition at the stage outlet is represented by point 2, the stagnated flow condition in relative and absolute motion, respectively, by points $2_w^*$ and $2^*$, for which $h_{2w}^* = h_2 + \frac{w_2^2}{2}$ and $h_2^* = h_2 + \frac{c_2^2}{2}$. In general, we accept $\Delta h_a$ is the isoentropic stage heat drop and $\Delta h_a^* = \Delta h_a + \frac{c_0^2}{2}$ the total available stage heat drop.

The process of the energy transformation in the turbine stage can be characterized by the so-called *degree of reaction* (reaction ratio)

$$\rho = \frac{\Delta h_{\mathrm{ar}}}{\Delta h_a^*},$$

that is, the ratio of the isoentropic rotor heat drop to the total available stage heat drop.

Taking into account that, $\Delta h_{\mathrm{ar}} \approx \Delta h'_{\mathrm{ar}}$ (see Fig. 5.2b)

$$\Delta h_{\mathrm{ar}} = \rho\, \Delta h_a^* = \rho\, (\Delta h_{\mathrm{an}}^* + \Delta h_{\mathrm{ar}}),$$

$$\Delta h_{\mathrm{an}}^* = (1 - \rho)\, \Delta h_a^*,$$

where,

$$\Delta h_{\mathrm{ar}} = \frac{\rho}{1-\rho} \Delta h_{\mathrm{an}}^* = \frac{\rho}{1-\rho} \cdot \frac{c_{1t}^2}{2} = \frac{\rho}{1-\rho} \cdot \frac{c_1^2}{2\varphi^2},$$

$$\Delta h_a^* = \frac{1}{1-\rho} \cdot \frac{c_{1t}^2}{2} = \frac{1}{1-\rho} \cdot \frac{c_1^2}{2\varphi^2}.$$

Due to,

$$\Delta h_{\mathrm{ar}} = \frac{1}{2}\left(\frac{w_2^2}{\psi^2} - w_1^2\right) \text{ and } \Delta h_a^* = \Delta h_{\mathrm{an}}^* + \Delta h_{\mathrm{ar}} = \frac{c_1^2}{2\varphi^2} + \frac{1}{2}\left(\frac{w_2^2}{\psi^2} - w_1^2\right),$$

then

$$\rho = \frac{\frac{w_2^2}{\psi^2} - w_1^2}{\frac{c_1^2}{\varphi^2} + \frac{w_2^2}{\psi^2} - w_1^2}.$$

The latter formula makes it possible to determine the stage degree of the reaction from the velocity triangles by estimating the velocity coefficients $\varphi$ and $\psi$. It means that the stages with similar velocity triangles at equal $\varphi$ and $\psi$ have the same degree of the reaction and vice versa.

If $\rho = 0$ the turbine stage is called *impulse.* When $0 < \rho \leq 0.3$ the stage is an *impulse with the reaction.* If $\rho > 0.3$ the stage is called *reactive.*

It should be noted that stages with $\rho > 0.5$ are rarely used.

## 5.2 Circumferential Stage Work

For the axial turbine stage, the rotary moment is defined as the product of the circumferential aerodynamic force component by half of the average stage diameter (the shoulder force application):

$$M = P_u \frac{D_m}{2}.$$

Knowing the rotational force and the angular rotational speed $\omega$, we can find the work of the circumferential force per one second (power) equal to the energy of the wheel rotation

$$L_u = M\,\omega = P_u \frac{D_m}{2}\omega = P_u\,u.$$

This is the work that is done in 1 s by the entire mass of the working fluid flowing through the cascade.

Taking into account Euler equations,

$$L_u = G\,u\,(\overline{w}_{1u} - \overline{w}_{2u}) = G\,u\,(\overline{c}_{1u} - \overline{c}_{2u}).$$

The specific rotor blades work, which is carried out of 1 kg of the working fluid which is passed through the cascade, was called circumferential *(rotor)* stage work.

$$l_u = \frac{L_u}{G} = P_u \frac{u}{G} = u\,(\overline{w}_{1u} - \overline{w}_{2u}) = u\,(\overline{c}_{1u} - \overline{c}_{2u}) = u\,(c_1 \cos\alpha_1 + c_2 \cos\alpha_2), \tag{5.4}$$

where $G$ is the mass flow rate of the working fluid.

From the velocity triangles of the turbine stage by the cosine theorem we have the following:

$$w_1^2 = c_1^2 + u^2 - 2u c_1 \cos\alpha_1;$$

$$w_2^2 = c_2^2 + u^2 - 2u\,c_2 \cos(180^\circ - \alpha_2) = c_2^2 + u^2 + 2u\,c_2 \cos\alpha_2,$$

where

$$u\,c_1 \cos\alpha_1 = \frac{1}{2}(c_1^2 + u^2 - w_1^2)$$

and

$$u\,c_2 \cos\alpha_2 = \frac{1}{2}(w_2^2 - c_2^2 - u^2).$$

After substituting these equations in formula (4.4) we obtain the following:

$$l_u = \frac{c_1^2 - c_2^2}{2} + \frac{w_2^2 - w_1^2}{2}. \tag{5.5}$$

The formula (5.5) which is obtained for the circumferential work coincides with the expression for the technical work, derived from the general energy equation for the gas stream.

You can also determine the rotor work by using the formula for technical work in the moving channel:

$$l_T = h_1^* - h_2^*.$$

Since the absence of the heat exchange in the nozzle $h_1^* = h_0^*$, this equation can be rewritten in the following form:

$$l_u = h_0^* - h_2^* = \Delta h_u. \tag{5.6}$$

The value $\Delta h_u$ which is called circumferential (rotor) heat drop can be obtained directly from the *h-s* diagram (Fig. 5.2b).

From formula (5.6), it follows that the value of the outlet energy of the working fluid will be the following:

$$q_{\text{out}} = \frac{c_2^2}{2}.$$

This energy is not used in the single turbine stage and is a loss for it.

It is easy to see from the process which is shown in the *h-s* diagram that

$$\Delta h_u \approx \Delta h_a^* - q_n - q_r - q_{\text{out}}. \tag{5.7}$$

## 5.3 Circumferential Efficiency

The efficiency of the stage converting energy is usual and to be estimated by the *circumferential efficiency*, which represents the ratio of the circumferential work to

the available stage work (the available work is equivalent to the available heat drop):

$$\eta_u = \frac{l_u}{\Delta h_a^*} = \frac{\Delta h_u}{\Delta h_a^*}. \tag{5.8}$$

From formula (4.7) for circumferential heat drop:

$$\begin{aligned}\eta_u = \frac{\Delta h_u}{\Delta h_a^*} &\approx \frac{\Delta h_a^* - q_n - q_r - q_{\text{out}}}{\Delta h_a^*} = 1 - \frac{q_n + q_r + q_{\text{out}}}{\Delta h_a^*} \\ &= 1 - \xi_n - \xi_r - \xi_{\text{out}},\end{aligned} \tag{5.9}$$

where $\xi_n$, $\xi_r$ and $\xi_{\text{out}}$ are the relative losses.

From the above formulas, it follows that the circumferential stage efficiency takes into account:

- the loss of the kinetic energy in the nozzle $q_n$;
- the losses in the rotor cascade $q_r$;
- the energy loss with the outlet velocity $q_{\text{out}}$.

These losses are the turbine stage *circumferential losses.*

We substitute into the formula for the circumferential efficiency (5.8) the value of the circumferential work from (5.5).

Considering that available stage heat drop:

$$\Delta h_a^* = \frac{\Delta h_{\text{ac}}^*}{(1-\rho)} = \frac{c_{1t}^2}{2\,(1-\rho)},$$

We have the following:

$$\eta_u = \frac{c_1^2 - c_2^2 + w_2^2 - w_1^2}{c_{1t}^2}(1-\rho). \tag{5.10}$$

From the outlet velocity triangle by the cosine theorem

$$c_2^2 = w_2^2 + u^2 - 2w_2 u\cos\beta_2.$$

We substitute the found dependencies for $c_2^2$ and $w_1^2$ into the formula (5.10). After simplification we will have the following:

$$\eta_u = 2\,(1-\rho)\frac{u\,(c_1\cos\alpha_1 - u + w_2\cos\beta_2)}{c_{1t}^2}.$$

Due to,

$$w_2 = \psi w_{2t} = \psi\sqrt{2(\Delta h_{ap} + w_1^2/2)}$$

$$= \psi\sqrt{\frac{2\rho}{1-\rho}\Delta h_{ac}^{*} + w_1^2} = \psi\sqrt{\frac{\rho}{1-\rho}c_{1t}^2 + w_1^2}$$
$$= \psi\sqrt{\frac{\rho}{1-\rho}c_{1t}^2 + c_1^2 + u^2 - 2c_1 u\cos\alpha_1}$$

then

$$\eta_u = 2\varphi^2(1-\rho)\frac{u\left(c_1\cos\alpha_1 - u + \psi\cos\beta_2\sqrt{\frac{\rho}{1-\rho}c_{1t}^2 + c_1^2 + u^2 - 2c_1 u\cos\alpha_1}\right)}{c_1^2}.$$

Then, we mark

$$\nu_1 = \frac{u}{c_1}, \tag{5.11}$$

And finally, we will have:

$$\eta_u = 2\varphi^2\nu_1(1-\rho)\left(\cos\alpha_1 - \nu_1 + \psi\cos\beta_2\sqrt{\frac{\rho}{(1-\rho)\varphi^2} + 1 + \nu_1^2 - 2\nu_1\cos\alpha_1}\right). \tag{5.12}$$

Thus, the circumferential efficiency of the stage is a function of the dimensionless quantities number, the circumferential geometric, aerodynamic and mode parameters, i.e.

$$\eta_u = f(\alpha_1, \beta_2, \varphi, \psi, \rho, \nu_1)$$

The velocity coefficients of the modern cascades $\varphi$ and $\psi$, as well as the angle $\alpha_1$, are usually varied at small intervals: $\varphi = 0.95\ldots0.98$, $\psi = 0.94\ldots0.98$, $\alpha_1 = 8\ldots30^{\circ}$ ($\cos\alpha_1 = 0,87\ldots0,99$). The angle $\beta_2$ corresponds to the selected rotor cascade. Therefore, the impact of these parameters on efficiency cannot be determined.

The most interesting is the study of the influence of the parameters $\rho$ and $\nu_1$ mode on the stage efficiency.

It is easy to determine that:

- at fixed values $\rho$ the circumferential efficiency is significantly dependent on $\nu_1$;
- the parametric curves $\eta_u = f(\nu_1)$ have the parabolic character with the maximum efficiency at a certain value of $\nu_1 = \nu_{1\text{opt}}$;
- with increasing $\rho$, the maximum efficiency shifts toward a larger value of $\nu_1$, that is, the increase in value $\nu_{1\text{opt}}$.

The value $\nu_1 = u/c_1$ is called the *velocity characteristic* of the stage and is one of the important parameters that determine the efficiency of the turbine stage.

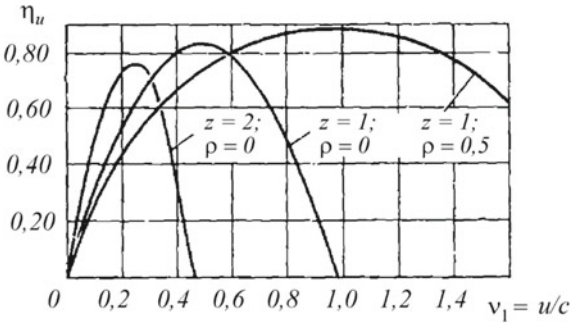


**Fig. 5.3** Dependences of the circumferential efficiency of different type stages on velocity characteristic

In the theory of turbines in addition to the velocity characteristic $\nu_1 = u/c_1$ other forms are used, namely:

- $\nu = u/c_{1t}$ is the ratio of the circumferential velocity to the theoretical outlet gas velocity from the nozzle, as well
- $\nu_a = u/c_a$, where $c_a$ is the conditional outflow velocity calculated at the available stage heat drop in the theoretical process, i.e. $c_a = \sqrt{2\Delta h_a^*}$.

All three characteristics are uniquely linked:

$$\nu = \frac{u}{c_{1t}} = \frac{u}{c_1/\varphi} = \varphi\nu_1;$$

$$\nu_{a\partial} = \frac{u}{\sqrt{2\Delta h_a^*}} = \frac{u}{\sqrt{\frac{2\Delta h_{ac}^*}{1-\rho}}} = \frac{u\sqrt{1-\rho}}{c_{1t}} = \nu\sqrt{1-\rho} = \varphi\nu_1\sqrt{1-\rho}\,.$$

Figure 5.3 presents the generalized dependences of the circumferential efficiency on the velocity characteristic for the different type stages (with some average values of $\alpha_{11}$, $\varphi$ and $\psi$), the single-ring ($z = 1$) impulse and the reaction stages, as well as two-ring ($z = 2$) impulse stage [1].

## 5.4 Internal Stage Losses

*The internal losses* are called losses that affect the condition of the working fluid. The internal loss is the difference between the ideal stage work (without losses) and the

work which is done by the actual stage. Since the internal losses affect the condition of the working fluid, they must be reflected on the *h-s* diagram.

The internal turbine stage losses are combined into two main groups:

- the circumferential losses, which include losses in the nozzle and the moving cascades $q_n$, $q_r$, as well as losses with the outlet velocity $q_{\text{out}}$;
- the additional internal losses, often referred to as *chamber* losses; these losses occur as a result of the design stage features or the operating conditions.

The chamber losses include such losses as the following:

- from leaks through the diaphragm seals;
- from leaks through the peripheral gaps;
- from gas friction of disks and the bandage;
- from the inlet incompleteness;
- from the fluid humidity (in the steam turbines);
- from the cooling of the hot stage details (in gas turbines);
- other losses (which are caused by various structural, technological or operational deviations from the stage design scheme).

While circumferential losses always occur at any stage, the chamber losses occur depending on the particular stage operating conditions and the constructive design and they are optional.

The chamber losses are estimated using the loss coefficients:

$$\xi_i = \frac{q_i}{\Delta h_a^*},$$

where $q_i$ is the absolute value of the corresponding chamber loss in J/kg.

## 5.5 Internal Efficiency and Stage Power

Figure 5.4 shows the process of the stage working fluid state change taking into account all internal losses. $\sum q_{i\,\text{cham}}$ is the sum of all the chamber losses (the internal losses that are not taken into account by the circumferential efficiency).

The chamber losses increase the working fluid enthalpy and entropy, and they are shown in the *h-s* diagram on the top of the moving cascade loss. The loss of the kinetic energy with the outlet velocity $q_{\text{out}}$ is usually shown last, because in the general case, the output kinetic energy may not be converted into heat (for example, when it is used as the next energy input).

The useful work which is done by 1 kg of the turbine stage working fluid, taking into account all internal losses, is called *internal work* $l_i$. The internal work is numerically equal to the internal enthalpy drop (heat drop) $\Delta h_i$, which is determined by the *h-s* diagram, and it is equal to the enthalpy drop (difference) of the stagnated

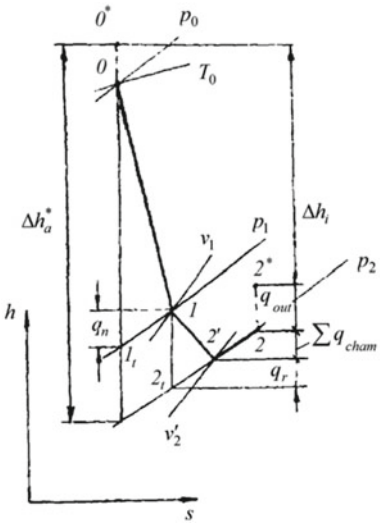


**Fig. 5.4** The working fluid flow process in the turbine stage taking into account all internal losses

flow before and after the stage taking into account all internal losses, i.e., it is as the following:

$$l_i = \Delta h_i = h_0^* - h_2^* = \Delta h_u - \sum q_{i\,\text{cham}},$$

or as the following:

$$l_i = l_u - \sum q_{i\,\text{cham}}, \tag{5.13}$$

where $\Delta h_u$ is the stage circumferential heat drop.

The turbine stage internal efficiency is the ratio of the internal work to the available work, or the ratio of the internal stage heat drop to the available stage heat drop, i.e. it is as the following:

$$\eta_i = \frac{l_i}{\Delta h_a^*} = \frac{\Delta h_i}{\Delta h_a^*}.$$

With the formula (5.4)

$$\eta_i = \frac{l_u - \sum q_{i\,\text{cham}}}{\Delta h_a^*} = \eta_u - \sum \xi_{i\,\text{cham}}, \tag{5.14}$$

where $\eta_u$ is the circumferential stage efficiency; $\sum \xi_{i\,\text{cham}}$ is the sum of the chamber losses coefficients.

If the internal stage efficiency is determined empirically by measured pressures and temperatures at the beginning and the end of the expansion process, then the necessary value of the internal and available heat drops can be determined by the following formulas:

$$\Delta h_i = c_p\,(T_0^* - T_2^*) = \frac{k}{k-1} R\,(T_0^* - T_2^*)$$

and

$$\Delta h_a^* = \frac{k}{k-1} R\,T_0^* \left[1 - \left(\frac{p_2}{p_0^*}\right)^{\frac{k-1}{k}}\right].$$

That is the following: $\eta_i = \frac{T_0^* - T_2^*}{T_0^*\left[1-\left(\frac{p_2}{p_0^*}\right)^{\frac{k-1}{k}}\right]}$.

Denote the mass flow rate of the working fluid through the stage as $G$, kg/s, then the turbine stage executes the internal power:

$$N_i = G\,\Delta h_i = G\,\Delta h_a^* \eta_i.$$

The internal efficiency takes into account the circumferential and the chamber internal losses. The circumferential losses amount is approximately 80 ~ 95% of all internal stage losses.

For the circumferential stage efficiency, the velocity characteristic $u/c_a$ or $u/c_1$ is crucial. The dependencies of $\eta_u$ and $\sum q_{i\,\text{cham}}$ on the velocity characteristic are shown in Fig. 5.5. There is also a graph of the function $\eta_i = f(u/c_a)$.

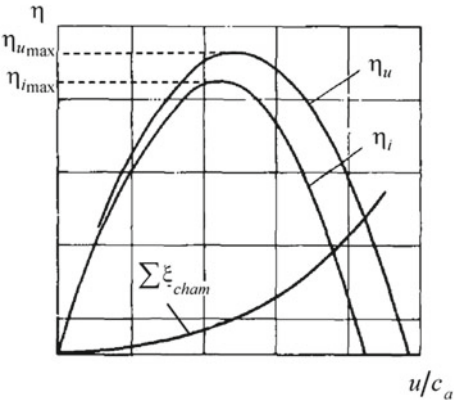


**Fig. 5.5** The dependences of the circumferential and internal stage efficiency and the chamber losses on the velocity characteristic

Since most of the chamber losses increase with increasing characteristics $u/c_a$, the maximum of the function $\eta_i = f(u/c_a)$ shifts to the left relative to the maximum of the function [In].

This shift for the stage with full admission (intake) is small, so the optimal characteristic of such stage can be determined by the maximum of the function $\eta_u = f(u/c_a)$. At the partial inlet, the value of the optimal characteristic (which is determined by the circumferential efficiency) should be reduced by 8 ~ 10%.

## Reference

1. Romanovsky GF, Ipatenko OY, Patlaychuk VM (2022) Theory and calculation of steam and gas turbines. Publisher USMTU, Mykolaiv, 292 p. (in Ukrainian)

# Chapter 6
# Gas Turbine Engine Classification


According to the scope of the application in various fields of technology, the gas turbine engines (GTE) can be classified as follows:

– the aircraft gas turbine engines;
– the marine and ship GTE;
– the power and driving GTE;
– the transport GTE.

The gas turbine units (GTUs), which include GTEs, can be created by use of the simple or complex thermal schemes that implement various thermodynamic cycles. We will consider the gas turbine engines of the simple and complex schemes which are based on the so-called Brighton cycle, in which the process of the fuel combustion occurs at the constant pressure ($p = \text{const}$).

The modern aircraft gas turbine engines are classified by the method of the thrust creation, which ensures the movement of the aircraft, as the following:

– the turbojet engine;
– the turbofan engine;
– the turboprop engine.

## 6.1 The Turbojet Engine

The turbojet is the airbreathing jet engine, which is typically used in the aircraft. It consists of the gas turbine with the propelling nozzle.

Let's consider in detail the **turbojet engine** (Figs. 6.1, 6.2 and 6.3), which consists of the following main functional elements: the input device, the compressor, the combustion chambers, the compressor drive turbine, and the exhaust system.

The intake device of the turbojet engine serves to increase previously the air pressure under the action of its dynamic velocity pressure (dynamic head) and organize the air feed to the compressor. It is designed with as low hydraulic losses as possible



K. Liu et al. (eds.), *Gas Turbines Structural Properties, Operation Principles and Design Features*, https://doi.org/10.1007/978-981-99-0977-3_6

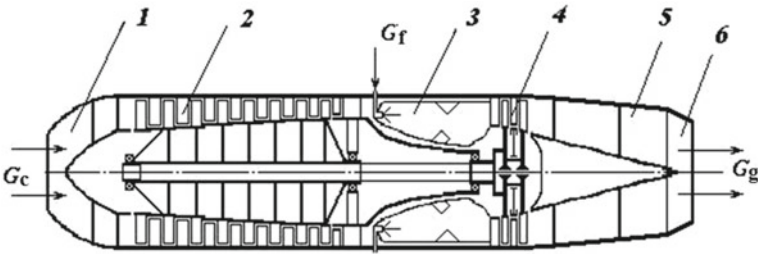


**Fig. 6.1** Scheme of a turbojet engine 1—intake device; 2—compressor; 3—combustion chamber; 4—compressor turbine; 5—transition camera; 6—jet (propelling) nozzle

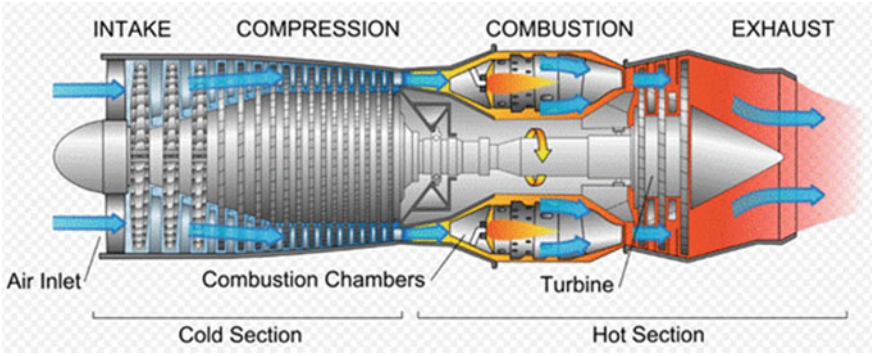


**Fig. 6.2** Diagram of a typical gas turbine jet engine

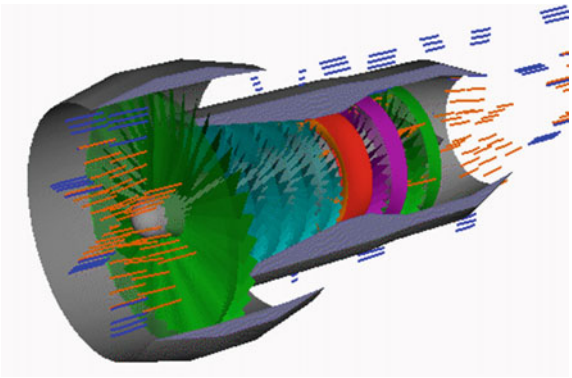

**Fig. 6.3** Turbojet animation

so that a uniform velocity field of the incoming air takes place at the inlet of the gas turbine compressor [1].

A compressor increases the pressure of the air which is entering the gas turbine engine to the calculated value. This process is accompanied by a significant increase in air temperature.

In the combustion chamber (CC), the process of heat generation occurs as a result of the chemical reaction of the fuel combustion. The combustion products which are obtained in CC acquire a high temperature and pressure and represent a working fluid with high energy potential.

In the compressor drive turbine, this high-potential gaseous working fluid expands to certain design pressure. In the turbine stages, the potential energy of the gas is converted into kinetic energy and then the mechanical energy on the shaft of this turbine. It should be emphasized that in the case of turbojet engines, all turbine power is consumed by the compressor drive.

The exhaust system of the turbojet engine consists of the transition chamber and the jet (propelling) nozzle. The transition chamber serves to provide the gas supply with minimal losses to the jet nozzle. In the jet nozzle, there is a further process of expansion of the gaseous working fluid to the level of atmospheric pressure. In this case, the gas flow velocity is increased to a value of 550 –650 m/s at the exit section of the jet nozzle. Thus, the gas-air flow through the turbojet engine receives acceleration, which leads to the occurrence of the reaction force at the jet nozzle exit. This force is perceived by the power elements of the engine structure and it is called thrust.

The formula for estimating the internal thrust of a turbojet engine provided that the gas in the jet nozzle is completely expanded to the atmospheric pressure is written as the following:

$$R_{\text{TJE}} = G_g \cdot \varphi \cdot W_R - G_c \cdot W_\infty, \tag{6.1}$$

where $G_g$ and $G_c$ are accordingly the mass flow rates of gas through the turbines and air through the turbojet compressor; $\varphi$ is the jet nozzle velocity coefficient, taking into account the energy loss in the nozzle; $W_\infty$ is the velocity of the turbojet engine; $W_R$ is the theoretical nozzle outflow gas velocity at full expansion from the parameters behind the compressor turbine to the atmospheric pressure.

Thus, the foregoing allows us to argue that the turbojet engine is both the engine and the driver (propulsion device). The thrust is created by relatively small masses of gas which is exiting at high speed from the jet nozzle.

## 6.2 The Turbofan Engine

**In the turbofan engine**, the internal circuit consists of the same elements as the turbojet engine (Figs. 6.4, 6.5 and 6.6). However, its turbine drives both the turbojet engine compressor and, optionally, the external circuit fan [1].

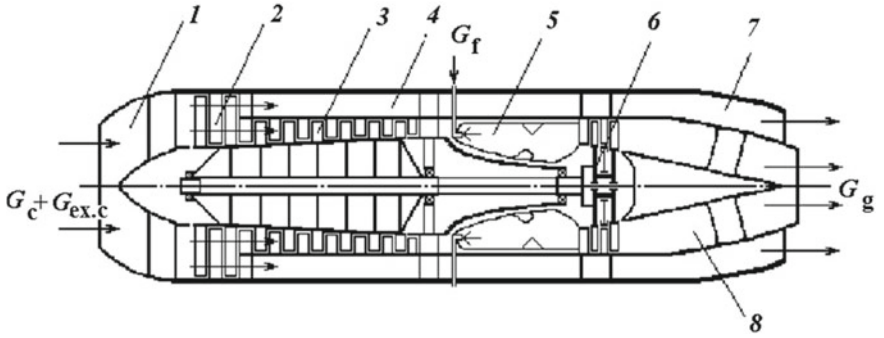


**Fig. 6.4** Diagram of a turbofan engine 1—intake device; 2—external circuit fan (ducted fan); 3—compressor; 4—duct channel of the external circuit; 5—combustion chamber; 6—compressor turbine; 7—exhaust system of the external circuit; 8—exhaust system of the internal circuit turbojet engine

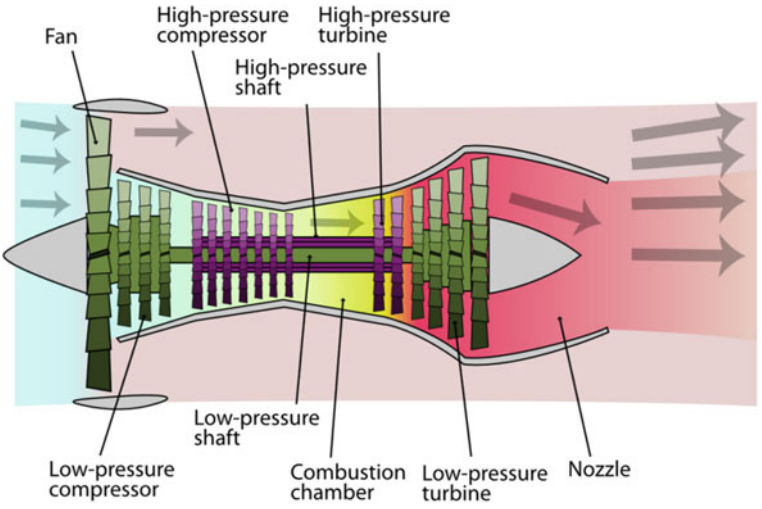


**Fig. 6.5** Schematic diagram of the high-bypass turbofan engine

The word "turbofan" is a portmanteau of "turbine" and "fan": the turbo portion refers to the gas turbine engine which achieves the mechanical energy from the combustion, and the fan, the ducted fan that uses the mechanical energy from the gas turbine to accelerate the air rearwards. Thus, whereas all air which is taken by the turbojet, passes through the turbine (through the combustion chamber), in the turbofan, some of that air bypasses the turbine. A turbofan thus can be thought of as a turbojet that has been used to drive a ducted fan, with both of these for the contribution to the thrust.

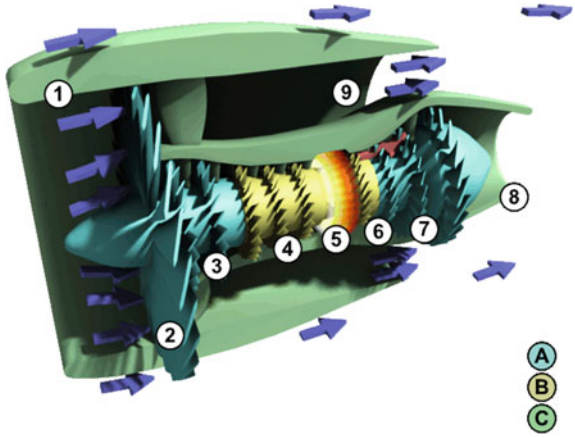


**Fig. 6.6** Animation of two-spool, high-bypass turbofan A—Low-pressure spool; B—High-pressure spool; C—Stationary components; 1—Nacelle; 2—Fan; 3—Low-pressure compressor; 4—High-pressure compressor; 5—Combustion chamber; 6—High-pressure turbine; 7—Low-pressure turbine; 8—Core nozzle; 9—Fan nozzle

Air through the intake device enters the external circuit fan. The fan increases the air pressure to a predetermined value and feeds it into the annular duct through which air is supplied to the exhaust nozzle of the external circuit. The fan supplies part of the air to the turbojet engine of the internal circuit. The action of the fan in the turbofan engine (in the sense of thrust creating) is similar to the action of a multi-blade propeller which is rotating in an annular duct. Such a "fan-driven propeller," in comparison with a conventional propeller, has higher values of efficiency at significant speeds, but it has lower values of efficiency at low speeds. It also has a smaller mass, and dimensions and does not require the reduced rotor speeds to drive, which allows it to be connected directly to a power turbine, it is abandoning the gearbox.

The thrust which is created by the turbofan engine consists of the thrust of the external circuit fan and the thrust of the internal circuit turbojet engine,

$$R_{\text{TFE}} = R_{\text{TJE}} + R_{\text{ex.c}}, \tag{6.2}$$

where $R_{\text{TGE}}$ is the thrust of the internal circuit turbojet engine; $R_{\text{ex.c}}$ is the external circuit thrust.

If we neglect the difference between the airflow through the compressor and gas through the turbine of the turbojet engine, then formula (6.1) can be represented as the following:

$$R_{\text{TJE}} = G_c \cdot (\varphi \cdot W_R - W_\infty). \tag{6.3}$$

Considering the external circuit thrust can be determined by the following formula:

$$R_{\text{ex.c}} = G_{\text{ex.c}} \cdot \varphi \cdot W_{\text{ex.c}} - G_{\text{ec.c}} \cdot W_\infty, \tag{6.4}$$

then, substituting (6.3) and (6.4) in (6.2), we can write the expression for determining the turbofan engine thrust in the following form:

$$R_{\text{TFE}} = G_c \cdot (\varphi \cdot W_R - W_\infty) + G_{\text{ex.c}} \cdot \varphi \cdot W_{\text{ex.c}} - G_{\text{ex.c}} \cdot W_\infty, \tag{6.5}$$

where $G_{\text{ex.c}}$ is the airflow through the external circuit; $W_{\text{ex.c}}$ is the theoretical velocity of the airflow from the external circuit jet nozzle when it is fully expanded to the atmospheric pressure.

Let's introduce the concept of the bypass ratio of the turbofan engine $m = \frac{G_{\text{ex.c}}}{G_c}$, which is the ratio between the air mass flow through the external circuit to the air mass flow through the internal circuit turbojet engine (core). We perform the substitution $G_{\text{ex.c}} = m \cdot G_c$ in (6.5) and we get the following:

$$R_{\text{TFE}} = G_c \cdot \varphi \cdot W_R - G_c \cdot W_\infty + m \cdot G_c \cdot \varphi \cdot W_{\text{ex.c}} - m \cdot G_c \cdot W_\infty.$$

After carrying out the necessary transformations, we have finally the following:

$$R_{\text{TFE}} = G_c \cdot [\varphi \cdot (W_R + m \cdot W_{\text{ex.c}}) - (1 + m) \cdot W_\infty]. \tag{6.6}$$

We know that for the well-known turbofan engine designs, the value of the bypass ratio $m = 0.5$ –6.0 and more. The external circuit can be up to 20–70% of the entire turbofan thrust. Thus, the turbofan engine is both the engine and the driver (propulsion device).

## 6.3 The Turboprop Engine

The turboprop engine, which is shown in Figs. 6.7 and 6.8, consists of the following main elements: the propeller, the gearbox, the air supply device, the compressor, the combustion chamber, the turbine, and the exhaust channel [1].

In the turboprop engine under consideration, the processes in the compressor and combustion chamber proceed exactly like in the turbojet engine which has been considered above. The distinction is in the process of expansion. There is the energy of a high-potential gaseous working fluid which is generated in a combustion chamber and is fully activated in the turbine when expanded to the atmospheric pressure. This turbine rotates the compressor, and the excess of the generated power through the gearbox transfers to the propeller that creates the thrust.

In the aircraft design, the overall propulsive efficiency $\eta$ is the efficiency with the energy which has been contained in a vehicle's propellant, is converted into kinetic energy of the vehicle, to accelerate it, or to replace losses due to aerodynamic drag or gravity. It can also be described as the proportion of the mechanical energy actually used to propel the aircraft. It is always less than one because the conservation of momentum requires that the exhaust has some of the kinetic energy, and the propulsive mechanism (whether a propeller, a jet exhaust, or the ducted fan) is never perfectly efficient. The overall propulsive efficiency is greatly dependent on air density and airspeed (Fig. 6.9).

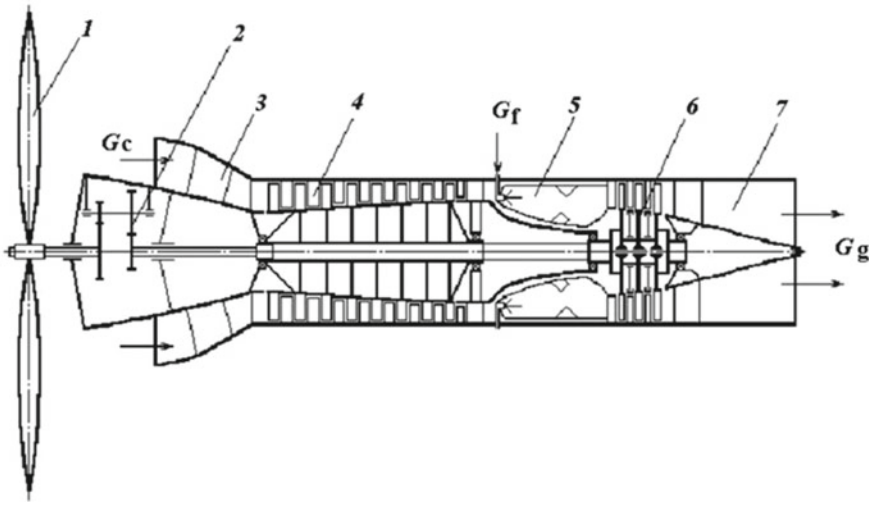


**Fig. 6.7** Diagram of the turboprop engine 1—propeller; 2—gearbox; 3—intake device; 4—compressor; 5—combustion chamber; 6—turbine; 7—exhaust channel (propelling nozzle)

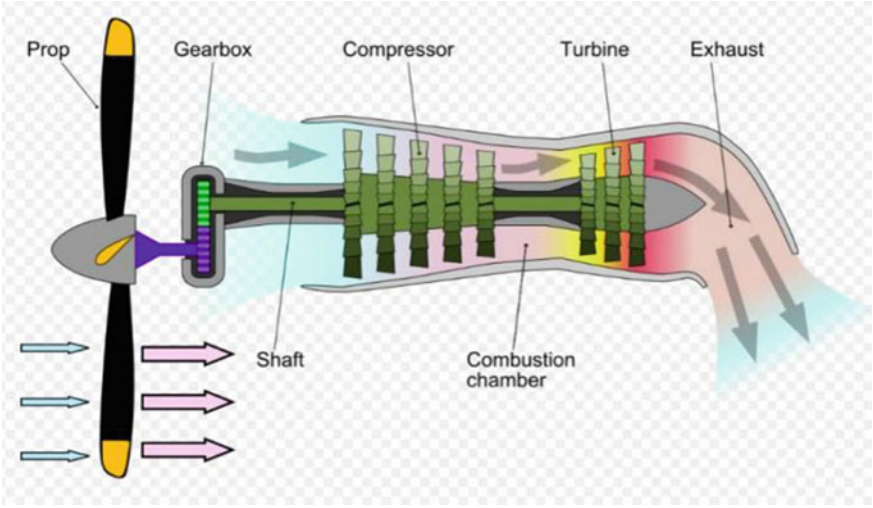


**Fig. 6.8** Schematic diagram showing the operation of the turboprop engine

**A marine or ship gas turbine engine**, which is shown in Fig. 6.10 [1], consists of the following main elements: the air supply device which is placed in front of the compressor, the compressor, the combustion chambers, the compressor turbine, the free propulsion turbine, the referred commonly to propeller turbine, the gas exhaust device, and the gearbox and the propeller (screw).

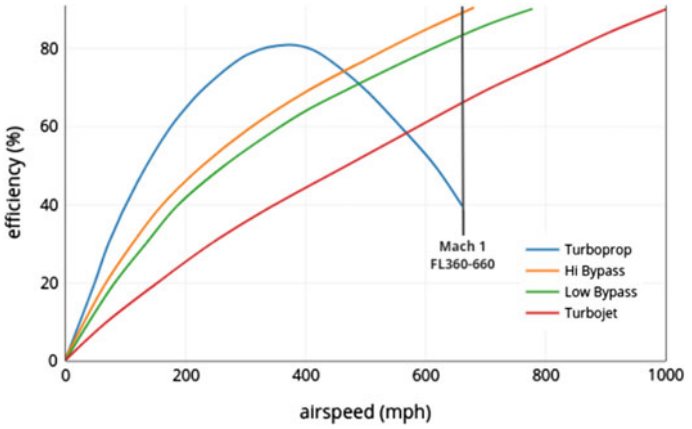


**Fig. 6.9** Propulsive efficiency comparison for various gas turbine engine configurations

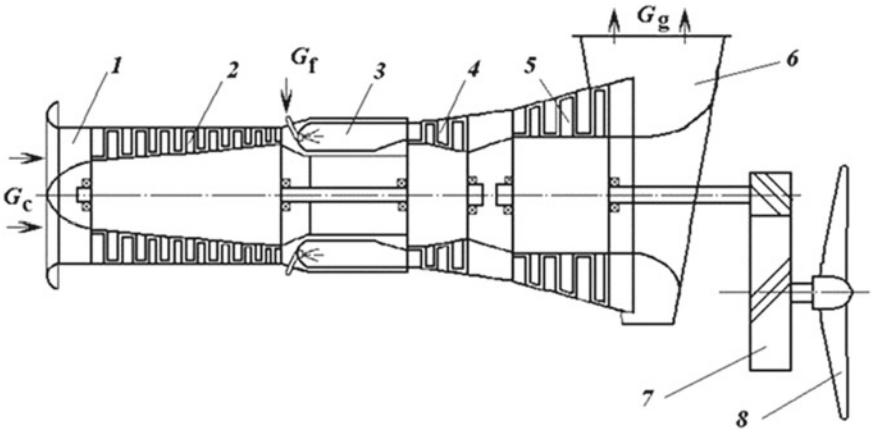


**Fig. 6.10** Ship gas turbine engine 1—air supply device; 2—compressor; 3—combustion chamber; 4—compressor turbine; 5—propeller turbine; 6—gas exhaust device; 7—gearbox; 8—propeller

In the turboprop engine under consideration, all the processes in the compressor and the combustion chamber do not differ from the aircraft turboprop engine which has been considered above. The difference is in the expansion process. There is the energy of a high-potential gaseous working fluid which is generated in the combustion chamber and transmitted sequentially in the compressor turbine, and then in the propeller (free) turbine. This free turbine through the gearbox transmits the generated power to the propulsion unit, i.e. to the propeller which is creating the thrust.

The power of a marine or ship gas turbine engine which is transmitted through the gearbox to the propeller can be determined by the following formula:

$$N_{\text{TPE}} = G_{\text{PT}} \cdot c_{p_g} \cdot \Delta T_{\text{PT}} \cdot \eta_m \cdot \eta_g \tag{6.7}$$

where $G_{\text{PT}}$ is the gas flow through the propeller turbine; $c_{p_g}$ is the average mass isobaric heat capacity of the gas for the actual expansion process in the propeller turbine; $\Delta T_{\text{PT}}$ is the actual temperature difference in the propeller turbine; $\eta_m$, $\eta_g$ are, respectively, the mechanical efficiency of the propeller turbine and the gearbox.

A turboprop propeller creates thrust by use of large masses of water or air discarding at relatively low speeds.

**Power and drive gas turbine** engines have the following features. Power GTE has the simplest kinematic scheme (Fig. 6.11). It consists of the air supply device, a single rotor compressor, the combustion chamber, and the turbine rotates both the compressor and the electric generator, which is the consumer of GTE energy. The rotor is located only on two bearing supports which are in the zone of relatively low temperatures. The gas exhaust diffuser is placed behind the last stage of the turbine to reduce energy losses with an output speed [1].

This scheme creates power engines with a capacity of 100 –150 MW or more, which are designed for installation at stationary power plants. For mobile, floating and modular power plants, engines from 2.5 to 25 MW are used, which are designed according to more complex kinematic schemes. Such engines usually have a free propulsive (free) turbine, which drives the generator through a gearbox. The compressor of these engines can be performed in two spools (rotors), with a separate drive of each compressor by its own turbine.

If we neglect the return of cooling air along the gas-air path of the gas turbine engine, then the engine power taken from its outlet flange can be determined by the following formula:

$$N_{\text{GTE}} = \left(G_T \cdot c_{p_g} \cdot \Delta T_T - G_c \cdot c_{p_c} \cdot \Delta T_c\right) \cdot \eta_m \tag{6.8}$$

where $G_T$ is the mass gas flow through the turbine; $G_c$ is the mass airflow through the compressor; $c_{p_c}$, $c_{p_g}$ are the average mass isobar heat capacities of air and gas

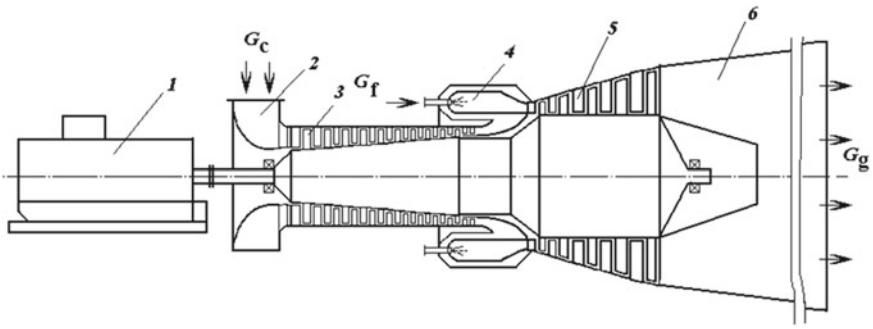


**Fig. 6.11** Power GTE 1—electric generator; 2—air supply device; 3—compressor; 4—combustion chamber; 5—turbine; 6—gas exhaust diffuser

for processes in the compressor and the turbine, respectively; $\Delta T_c$ is the actual air heating in the compressor; $\Delta T_c$ is the actual temperature difference in the turbine; $\eta_m$ is the mechanical engine efficiency.

**Driving gas turbine engines** are used in the natural gas transport system to drive the centrifugal compressors, i.e. the gas blowers. GTEs which are created on the basis of either ship or aircraft GTE, are used here.

In terms of design and construction, the driving gas turbine engines do not differ from the gas turbine engines, i.e. the prototypes on the basis of which they were developed. The level of the thermodynamic parameters is usually lower, based on the requirements for achieving a longer operational life of such gas turbine engines.

**Transport gas turbine engines** are designed and built for the wheeled and tracked vehicles for various purposes: automobiles (including cars), wheeled and tracked tractors, heavy-duty dump trucks, trunk buses, tractors, and tanks.

It should be noted that the features of the use of the transport gas turbine engines in automobile transport require the careful selection of its kinematic scheme, and the use of various mechanical gears allows you to expand significantly this choice.

Currently, the most famous serial transport gas turbine engines with a capacity of 700 –1,000 kW are installed on American as well as Russian tanks.

## 6.4 Justification for the Choice of a Gas Turbine Engine

When choosing a gas turbine engine as the main engine for a sea vessel, the maximum speed of the object, its structural capabilities and features, its purpose, the intended type of propulsion, and the necessary power for movement are taken into account. The studies that have been executed show the reasons for the economy, for all types of gas turbine engines which are considered above. There are ranges of ship speeds in which it is preferable to use one or another type of turbine engine.

As you know, the power of the thrust which is created by the propulsion device will be as the following:

$$N_P = P \cdot v_\infty, \left[\frac{N \cdot \mathrm{m}}{\mathrm{s}}\right], \text{ [W]} \tag{6.9}$$

where $P$ is the thrust, N; $v_\infty$ is the speed of a movement, m/s.

The thrust power is associated with the effective power of the GTU, i.e. the power which is removed from the output shaft of its gearbox will be as the following:

$$N_P = N_e \cdot \eta_p, \tag{6.10}$$

where $N_e$ is the effective power of the GTU; $\eta_p$ is the efficiency of the propulsion device.

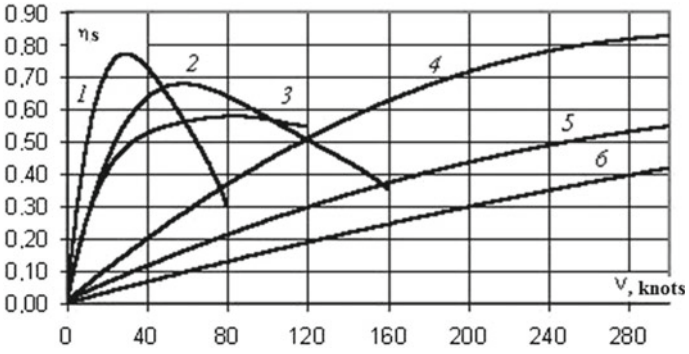


**Fig. 6.12** The dependence of the propulsive efficiency on the speed of movement 1—propellers; 2—supercavitating propellers; 3—water cannons; 4—airscrews; 5—fan screw—turbofan engine; 6—thrust efficiency of the turbojet engine

Thus, at a constant value of the gas turbine engine power, the value of the thrust power, which is generated by GTU, depends on the efficiency of the used propulsion device.

The effectiveness of the propulsion device of various types depends on the speed of the object, where it is mounted. Using the different author's data we will present the averaged dependences of the propulsive efficiency on the object speed (Fig. 6.12) [1].

We can draw the following conclusions. For displacement vessels and hydrofoil vessels in the range of speeds 0 –40 knots (1 knot = 1 mile per hour = 1.85 km/h), a turboprop engine with a conventional cavitating propeller has the best efficiency. This is explained by the fact that, up to a vessel speed of 40 knots, the efficiency of the cavitating propeller is 0.70 –0.78 and is always higher than it of other types of propulsion devices. Therefore, all of the Navy displacement ships have main power plants with gas turbine engines which are operating with a cavitating propeller, usually of a fixed pitch. The same can be said of merchant ships, where quite widely, similarly variable-pitch propellers have been used recently.

In the range of speeds from 40 to 100 knots, typical for high-speed ferries—catamarans, torpedo boats, and hydrofoils, the best results are obtained with the use of a gas turbine engine which is operating on a supercavitating propeller or on water-jet propulsion. At these speeds, the supercavitating propeller has an efficiency of 0.55 –0.68 which is better than that of other types of propulsion systems under consideration, and a water cannon has a number of indisputable operational advantages. It is a propulsion device, and it has the properties of steering and reversing devices.

The supercavitating propeller is a variant of a propeller for propulsion in water, where a supercavitation is actively used to have an increased speed by reducing friction. They are used for military purposes and for high performance of racing boats as well as model racing boats.

The supercavitating propeller operates submerged with the entire diameter of the blade below the water line. Its blades are wedge-shaped to force cavitation at

the leading edge and to avoid water skin friction along the whole forward face. As the cavity collapses well behind the blade, the supercavitating propeller avoids the damage due to cavitation which is a problem with conventional propellers.

At speeds of more than 100 knots, which can have some hovercraft, as well as winged surface effect vehicles (ekranoplanes), GTE with an airscrew will have maximum efficiency. Moreover, the efficiency of the air screw is very high (0.80–0.85) at speeds up to 300 knots.

If the use of an airscrew for any reason is unacceptable, then for such vessels as hovercraft and winged surface effect vehicles, at speeds of more than 150–200 knots, it is more expedient to use the turbofan engine. Note that, as a rule, it is necessary to abandon the propeller for reasons of the power plant arranging, or, if necessary, to use a gas turbine engine of high power. The fact is that when the gas turbine engine power grows, the designer is also forced to increase the diameter of the air screw. So, for example, for a power of 22,000 kW, an air screw with a diameter of about 15 m is required. The existing technologies make it possible to create propellers with a diameter of up to 8 m. There are also serious problems of erosion of the propeller blades when the condensed moisture is on them. Therefore, for example, the winged surface effect vehicle “Lun” (MD-160) which has been created in the USSR, had a maximum flight speed of about 270 knots, and it was equipped with eight turbofans.

In the entire conceivable range of the motion speeds inherent in marine navy and merchant ships, turbojet engines are much less economical. Consequently, the use of turbojet engines in shipbuilding seems inappropriate.

## Reference

1. Romanovsky GF, Washchilenko NV, Serbin SI (2003) Theoretical basics of ship gas turbine designing. Publisher USMTU, Mykolaiv, 304 p. (in Ukrainian)

# Chapter 7
# Simple Cycle Gas Turbine Units


## 7.1 The Structure and Operation of a Simple Thermodynamic Cycle Gas Turbine Unit

A distinctive feature of the gas turbine units is the presence in their structure, as the main source of mechanical energy, a turbine which is operating on a gaseous (with the exception of steam[1]) working fluid. In the overwhelming majority of cases, the working fluid is the product of hydrocarbon fuel combustion. But in the closed thermodynamic cycle gas turbine units inert gases (helium, argon), nitrogen, carbon dioxide and other substances can also be used.

The structure of the simplest **gas turbine unit (GTU)** is shown in Fig. 7.1. The first element of a gas turbine unit at the movement of a working fluid is a **compressor**. The function of the compressor in the GTU is to increase the pressure of the working fluid (atmospheric air).[2] In modern units, the air pressure at the exit of the compressor exceeds the atmospheric pressure by 7–35 times.

After the compressor, air enters the second main element of the GTU, i.e. the **combustion chamber**. The function of the combustion chamber as part of the GTU is to heat the working fluid. Typically, this process is carried out by burning hydrocarbon (liquid or gaseous) fuel directly in the flow of the air moving through the combustion chamber at a practically constant pressure. The temperature of the gas which is formed in the modern gas turbine units is 1400–1800 K.

After the combustion chamber, the working fluid, which at this moment has a certain potential energy reserve (increased pressure and temperature), enters the **turbine**. The function of the turbine is to produce the mechanical energy of rotation.

A part of the power which is produced by the turbine is spent on the rotation of the compressor, and the remaining part (**useful power**) is given to the **consumer**. The power which is consumed by the compressor is relatively large and in simple

[1] For turbines that operate on water steam, the name of **steam turbines** has been established.

[2] It is possible to create a gas turbine unit without a compressor.



K. Liu et al. (eds.), *Gas Turbines Structural Properties, Operation Principles and Design Features*, https://doi.org/10.1007/978-981-99-0977-3_7

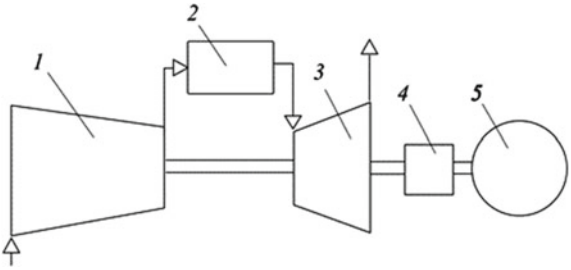


**Fig. 7.1** The structure of the simple cycle gas turbine unit 1—compressor; 2—combustion chamber; 3—turbine; 4—gear; 5—consumer (load)

schemes at a moderate temperature of the working fluid, it can be 1.5–2.0 times higher than the useful power of the unit.

After the turbine, the gas is exhausted into the environment (into the atmosphere). The gas temperature at the turbine exhaust in modern GTUs is 650–900 K.

We will use the term **gas turbine engine (GTE)** to denote the combination of a compressor, a combustion chamber and a turbine. The combination of a gas turbine engine and the complete set of systems, devices, mechanisms and machines which are serving, will be designated as a **gas turbine plant (GTP)**.

The speed of a turbine rotor is several thousand revolutions per minute, therefore, the transfer of the useful power to the consumer sometimes can be executed through a reduction device—a **gear**.

Figures 7.2 and 7.3 show a 3 MW UGT 3000 gas turbine engine that has been produced by "Zorya-Mashproekt" (Ukraine) [1].

For the normal operation of a gas turbine unit, a set of systems is required. **The main systems which are serving the GTU** are:

- the starting system;
- the fuel system;
- the oil system;
- the venting and unloading system;
- the cooling system;
- the compressed air system;
- the air intake and the exhaust systems.

**The starting system**. The gas turbine can work if there is compressed air received from the compressor which is driven by the same turbine. Therefore, it is obvious that the start of the gas turbine should be executed from the external source of energy, i.e. the **starting engine** (starter). With the assistance of the starter, the compressor rotates until the gas of certain parameters begins to flow and rotate the turbine. The launch of the marine GTUs is usually 80–100 s.

The starting engine is connected to the compressor rotor of the gas turbine unit. When starting a GTU with a two-spool compressor, at first the starter can rotate only one rotor or both rotors at the same time. As a rule, they try to execute the rotation of the lightest rotor, because this will require less starting engine power.

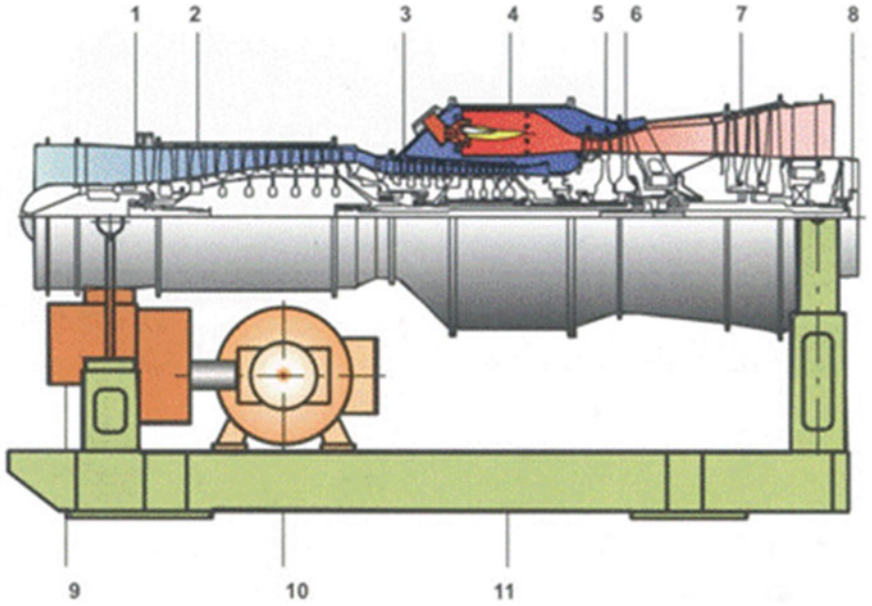


**Fig. 7.2** The layout of the UGT 3000 1—inlet guide vanes; 2—low pressure compressor; 3—high pressure compressor; 4—combustion chamber; 5—high pressure turbine; 6—low pressure turbine; 7—power turbine; 8—power take-off flange; 9—drive box; 10—electric starter; 11—frame

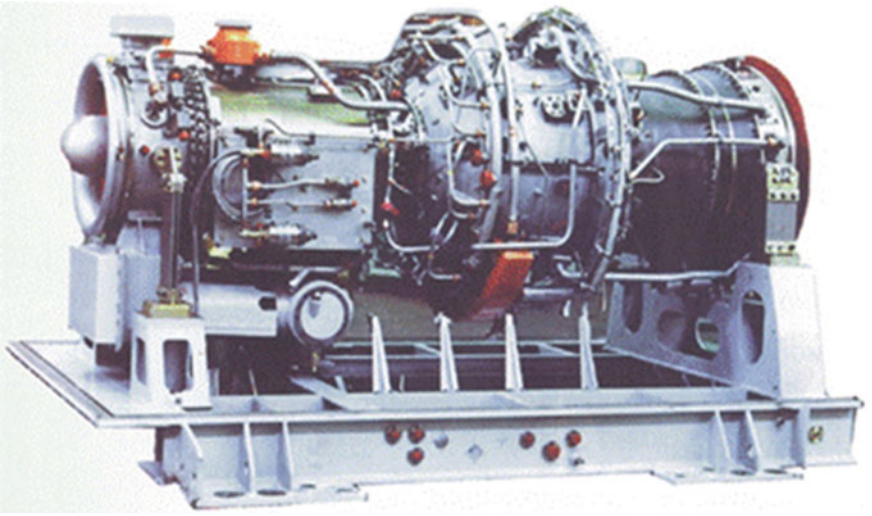

**Fig. 7.3** UGT 3000

As starting engines, the electric motors of direct and alternating current, the gas turbine engines of lower power and different turbo starters (gas, air, powder, etc.) are used.

**The fuel system** is designed to store, prepare and supply fuel to the combustion chamber of a gas turbine unit.

**The oil system** is used to store, prepare and supply oil for lubrication and cooling of friction surfaces of the engine and the gearbox. Oil is also used as a working fluid in some mechanisms of the GTU control system and the gearbox.

In the GTUs, the oil cavities are separated from the flow part by several rows of labyrinth seals. To ensure the normal operation of these seals, as well as the GTU oil system as a whole, the engine oil cavities communicate with the atmosphere. **The venting system** connects the oil cavities of the engine with the atmosphere in order to reduce the pressure in them, prevent the exit of oil into the flow part through the gaps in the labyrinth seals and also ensure the separation of oil from the air.

The venting system is often considered as one with the unloading system, which ensures the maintenance of the required pressure in some air cavities of the GTU, thereby achieving a reduction in axial loads on the engine mounts.

The venting system is often combined with an **unloading system** that maintains the required pressure in some GTU air cavities, thereby reducing the axial loads on the engine thrust bearings.

The high level of gas temperatures before the turbine in modern GTUs necessitates the use of special **cooling systems** in them. In most existing designs, the cooling of nozzles, blades, disks and turbine casings is executed by use of air which is taken from the compressor of the same GTU. After cooling the parts, this air enters the flow part of the turbine, where it is mixed with the main gas flow (open-air cooling system).

In gas turbine plants, a **compressed air system** is used to control the gearbox and reverse devices, for the emergency engine shutdown, the operation of pneumatic and uncoupling friction clutches, the engine cleaning, etc. In addition, on ships, compressed air is used to start the diesel generators and for the needs of the engine room and a ship.

The compressed air systems include typically electric piston compressors, air storage tanks, fittings, instruments, pipelines, etc.

The axial compressors and turbines are very sensitive to the quality of the air which is entering them. The air purification before supplying it to the GTU is executed by the **air intake system**.

The gas exhaust system is used to exhaust gas from the GTU to the atmosphere.

## 7.2 Ideal and Actual Thermodynamic Cycles of the Simplest Gas Turbine Unit

### Ideal Thermodynamic Cycle

The ideal cycle of a GTU does not consider the energy losses in its parts. All processes in the cycle are reversible.

The ideal thermodynamic cycle which is corresponding to the simplest GTU in the thermal diagram is shown in Fig. 7.4.

**The process between points 1 and 2** takes place in the compressor. Under ideal conditions (i.e., without considering losses during compression), it occurs at a constant value of entropy, i.e. **isentropic**, and is displayed as a vertical line in the thermal diagram.

The process is characterized by the **compressor pressure ratio**:

$$\pi_c = \frac{p_2}{p_1},$$

where $p$ is the pressure, Pa.

For isentropic process, it can be written as:

$$\frac{T_2}{T_1} = \left(\frac{p_2}{p_1}\right)^{\frac{k-1}{k}},$$

where $T$ is the temperature, K; $k$ is the specific heat ratio.

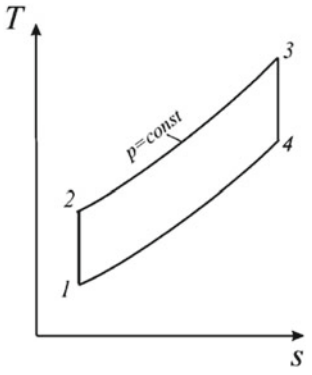


**Fig. 7.4** The ideal cycle in the thermal diagram

Then

$$T_1 = \frac{T_2}{\left(\frac{p_2}{p_1}\right)^{\frac{k-1}{k}}} = \frac{T_2}{\pi_c^{\frac{k-1}{k}}} = \frac{T_2}{\pi_c^m} = T_2 \cdot \pi_c^{-m}, \tag{7.1}$$

where $m = \frac{k-1}{k}$.

**The process between points 2 and 3** takes place in the combustion chamber. For the vast majority of the modern gas turbine units, it is implemented in the combustion chambers that are constantly open to a moving air stream, which means that the pressure in them is kept almost unchanged (under ideal conditions absolutely unchanged). Such a process is called **isobaric**.

For the isobaric process, it can be written as:

$$\frac{T_3}{T_2} = \frac{v_3}{v_2},$$

where $v$ is the specific volume, $m^3/kg$.

Then

$$T_3 = T_2 \cdot \frac{v_3}{v_2}. \tag{7.2}$$

**The expansion in the turbine (process 3–4)** in an ideal cycle is also represented as a vertical line, i.e. **isentropic**.

The process is characterized by the **turbine pressure ratio**:

$$\pi_t = \frac{p_3}{p_4}.$$

For isentropic process, it can be written as:

$$\frac{T_3}{T_4} = \left(\frac{p_3}{p_4}\right)^{\frac{k-1}{k}}.$$

Then

$$T_4 = \frac{T_3}{\left(\frac{p_3}{p_4}\right)^m} = \frac{T_3}{\pi_t^m} = T_3 \cdot \pi_t^{-m} = T_2 \cdot \frac{v_3}{v_2} \cdot \pi_t^{-m}. \tag{7.3}$$

**The process between points 4 and 1** is called **the cooling process**, closing the cycle. From the thermodynamic point of view, after the turbine, the working fluid must be cooled and only after that is directed again to the compressor inlet. However, in most modern GTUs, this cooling process is executed by mass transfer with the environment, i.e. after the turbine the hot gas exhausts into the atmosphere, and cold air enters the compressor from the atmosphere at the same time.

The thermodynamic cycle of a GTU with heat supply at constant pressure is called the **Brayton cycle**. The automobile piston engine which is worked on this cycle was patented and built-in 1872 by engineer George Brayton (Boston, USA).

The ideal cycle is usually characterized by **thermal efficiency**:

$$\eta_t = \frac{Q_{\text{use}}}{Q_{\text{in}}} = \frac{Q_t - Q_c}{Q_{\text{in}}} = \frac{(h_3 - h_4) - (h_2 - h_1)}{h_3 - h_2},$$

where $Q_{\text{use}}$ is the useful mechanical work of the cycle, kJ/kg; $Q_{\text{in}}$ is the heat which is supplied to the cycle in the combustion chamber, kJ/kg; $Q_t$ is the mechanical work which is generated by the turbine, kJ/kg; $Q_c$ is the mechanical work which is consumed by the compressor, kJ/kg; $h$ is the enthalpy, kJ/kg.

From the course of thermodynamics, we know that:

$$h_2 - h_1 = c_p(T_2 - T_1),$$

where $c_p$ is the specific heat of the working fluid, kJ/kg/K.

Because in the ideal cycle, the specific heat is constant and does not depend on temperature, we can write the following:

$$\eta_t = \frac{c_p(T_3 - T_4) - c_p(T_2 - T_1)}{c_p(T_3 - T_2)} = \frac{(T_3 - T_4) - (T_2 - T_1)}{T_3 - T_2}.$$

In the ideal cycle $\pi_c = \pi_t$. Using formulas (7.1), (7.2) and (7.3) we have the following:

$$\eta_t = \frac{(T_3 - T_4) - (T_2 - T_1)}{T_3 - T_2} = \frac{\left(T_2 \cdot \frac{v_3}{v_2} - T_2 \cdot \frac{v_3}{v_2} \cdot \pi_c^{-m}\right) - \left(2 - T_2 \cdot \pi_c^{-m}\right)}{T_2 \cdot \frac{v_3}{v_2} - 2} =$$

$$= \frac{\frac{v_3}{v_2}(1 - \pi_c^{-m}) - (1 - \pi_c^{-m})}{\frac{v_3}{v_2} - 1} = \frac{\left(\frac{v_3}{v_2} - 1\right)(1 - \pi_c^{-m})}{\frac{v_3}{v_2} - 1} = 1 - \pi_c^{-m}.$$

From this formula, it is understood that the **thermal efficiency of the ideal cycle of GTU depends on the compressor pressure ratio**, because of the parameter $m = \frac{k-1}{k} = \text{const}$.

The dependence of the thermal efficiency on the compressor pressure ratio is shown in Fig. 7.5. An increase in the compressor pressure ratio leads to an increase in the thermal efficiency.

**Actual Thermodynamic Cycle**

In real conditions, all processes in gas turbine units are irreversible. The irreversibility of the processes which are caused by the following:

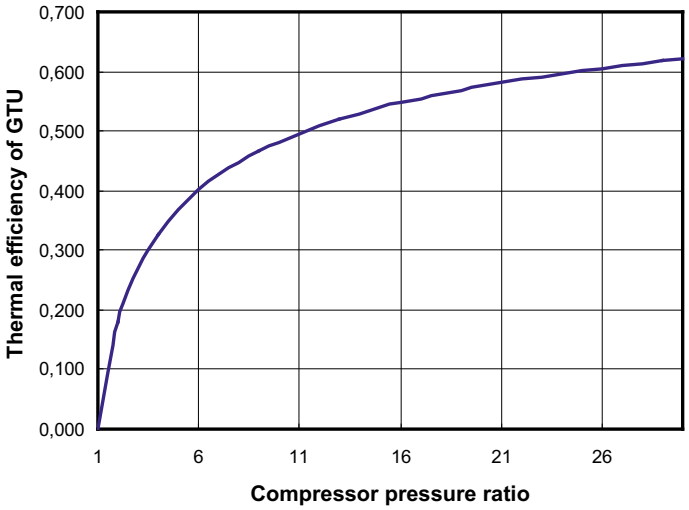


**Fig. 7.5** The dependence of thermal efficiency on the compressor pressure ratio

– the energy conversion losses in the compressor, the combustion chamber, the turbine and the gear;
– the pressure losses in the transitional parts of GTU (we have the friction of the air or gas flow at the walls of the parts).

The irreversibility of the processes has a great influence on the parameters of GTU. For this reason, the use of data which is taken from the ideal cycle can lead to serious errors.

The actual cycle is usually characterized by the actual (real) efficiency:

$$\eta_e = \frac{Q_{r.\text{use}}}{Q_{r.\text{in}}} \eta_m \eta_g,$$

where $Q_{r.\text{use}}$ is the real useful mechanical work of the cycle, kJ/kg; $Q_{r.\text{in}}$ is the real heat which is supplied to the cycle in a combustion chamber, kJ/kg; $\eta_m$ is the mechanical coefficient (considers the friction losses in bearings and the power consumption for driving of some mechanisms); $\eta_g$ is the gear efficiency.

In modern marine gas turbine units the mechanical coefficient $\eta_m = 0.99$–$0.995$ (for roller and ball bearings) and $\eta_m = 0.97$–$0.98$ (for plain bearings).

For marine gears, the gear efficiency $\eta_g = 0.97$–$0.98$.

The losses change the Brayton cycle (Fig. 7.6).

**The process between points 1 and 2** that takes place in the compressor is not isentropic. During this process, entropy increases, and $s_1 < s_2$.

**The process between points 2 and 3** that takes place in the combustion chamber is not isobaric. During this process, the pressure decreases, and $p_2 > p_3$ .

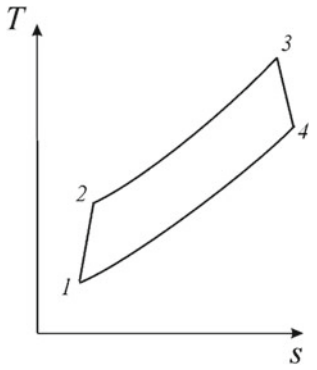


**Fig. 7.6** The actual cycle of the GTU in the thermal diagram

**The expansion in the turbine (process 3–4)** in an actual cycle is not isentropic. During this process, entropy increases, and $s_3 < s_4$.

In addition to the efficiency, the actual cycle of GTU can be estimated by **specific fuel consumption** and **specific power**.

The specific fuel consumption, kg/(kW h),

$$g_e = \frac{G_f}{N_e},$$

where $G_f$ is the fuel consumption, kg/h; $N_e$ is the effective (useful) power of GTU, kW.

Specific power, kW s/kg,

$$N_{\text{sp}} = \frac{N_e}{G_c},$$

where $G_c$ is the air flow rate through the compressor, kg/s.

The efficiency and the specific fuel consumption estimate the economic efficiency of GTU. The higher the efficiency and the lower the fuel consumption, the better for the gas turbine unit.

The specific power estimates the weight and size of GTU. The higher the specific power, the smaller the weight and the size of the GTU.

**The efficiency of the gas turbine unit depends on**:

(1) The compressor pressure ratio $\pi_c$.

The dependence is not so simple (Fig. 7.7), unlike the ideal cycle. The increase of that parameter is the first cause of the efficiency increase, and the second is the efficiency decrease. There is an optimum for the compressor pressure ratio, at which the efficiency takes the maximum value.

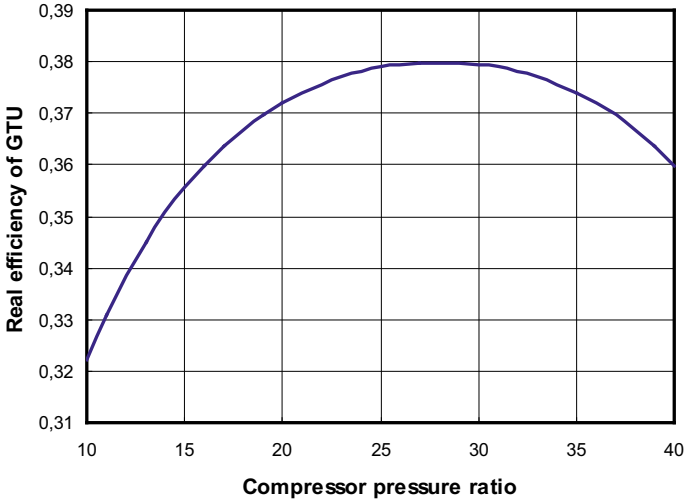


**Fig. 7.7** The dependence of efficiency on the compressor pressure ratio

(2) The gas temperature after the combustion chamber $T_3$.

It can be seen from Fig. 7.8 that the increase of the gas temperature $T_3$ causes an increase in efficiency. It is also seen that with increasing gas temperature $T_3$ the optimum of the compressor pressure ratio also increases.

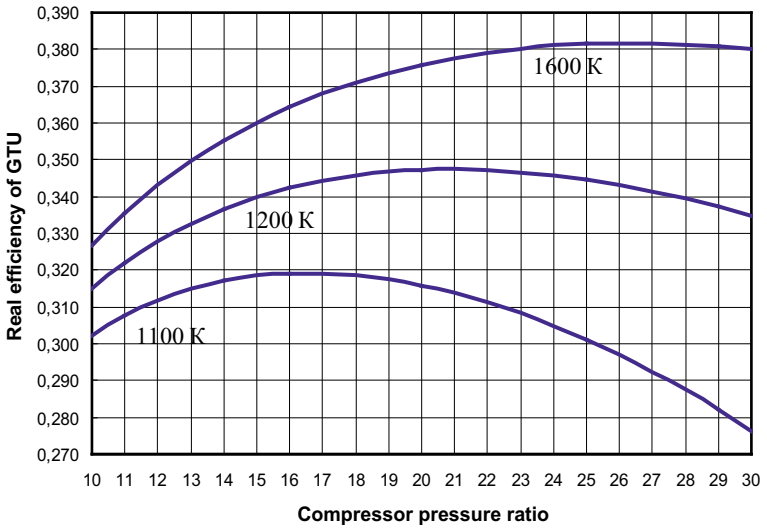


**Fig. 7.8** The dependence of efficiency on the compressor pressure ratio and temperature $T_3$

(3) The efficiency of the compressor $\eta_c$, combustion chamber $\eta_{c.c}$ and turbine $\eta_t$.

The increase in the efficiency of the compressor, the combustion chamber and the turbine leads to an increase in the efficiency of the entire gas turbine unit. If the efficiency of the compressor and the turbine does not exceed 0.60 (60%), then the efficiency of the GTU is equal to zero.

(4) The mechanical coefficient $\eta_m$ and the gear efficiency $\eta_g$.

The increase in these coefficients leads to an increase in the efficiency of GTU.

(5) The pressure losses in the transitional parts of GTU.

The decreasing in the pressure losses leads to an increase in GTU efficiency.

The pressure losses depend on gas or air velocity and the length of the transitional parts. These parameters are smaller, the pressure losses are lower.

Now the efficiency of the simple cycle gas turbine units is 0.28–0.42. The power of GTU is higher, its efficiency is better.

## Reference

1. Romanovsky GF, Washchilenko NV, Serbin SI (2003) Theoretical basics of ship gas turbine designing. Publisher USMTU, Mykolaiv, 304 p. (in Ukrainian)

# Chapter 8
# The Features of GTU Thermal Calculation


## 8.1 Structural Schemes of the Marine Gas Turbine Units

For use on ships, two structural schemes of GTU have become the most popular (Fig. 8.1).

**The first structural scheme**, which has been realized in such marine GTUs, is the following:

- LM500, LM1500, LM2500, LM2500+ and LM2500G4 of "General Electric Co.";
- TF40 and TF50 of "Vericor Power Systems Inc.".

**The second structural scheme**, which has been realized in such marine GTUs is the following:

- "Olympus", "Tyne", "Spey" and MT30 of "Rolls-Royce plc";
- UGT3000, UGT6000, UGT15000, UGT16000 and UGT25000 of "Zorya-Mashproekt".

For further consideration, **we choose the second structural scheme**.

For this structural scheme, we will use some indexes: $c_1$—a low-pressure compressor; $c_2$—a high-pressure compressor; $t_1$—a high-pressure turbine; $t_2$—a low-pressure turbine; $t_3$—a power turbine.

The cycle in the thermal diagram that corresponds to this structural scheme is shown in Fig. 8.2 [1].

The main processes in the gas turbine cycle are:

- the process (1–2.1)—in LPC;
- the process (2.1–1.2)—in the intersection between LPC and HPC;
- the process (1.2–2)—in HPC;
- the process (2–3)—in CC;
- the process (3–4.1)—in HPT;
- the process (4.1–3.2)—in the intersection between HPT and LPT;
- the process (3.2–4.2)—in LPT;
- the process (4.2–3.3)—in the intersection between LPT and PT;



K. Liu et al. (eds.), *Gas Turbines Structural Properties, Operation Principles and Design Features*, https://doi.org/10.1007/978-981-99-0977-3_8

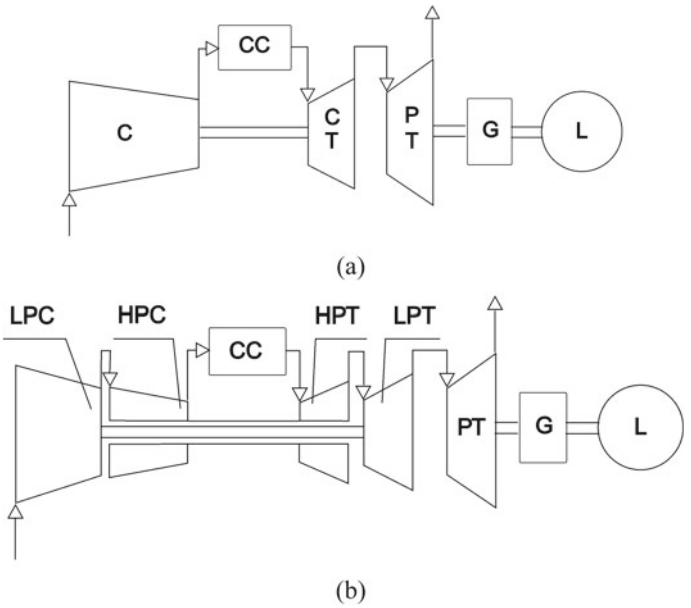


**Fig. 8.1** The structural schemes of marine GTU. C—compressor; CC—combustion chamber; CT—compressor turbine; PT—power turbine; G—reduction gear; L—load (consumer); LPC—low-pressure compressor; HPC—high-pressure compressor; HPT—high-pressure turbine; LPT—low-pressure turbine

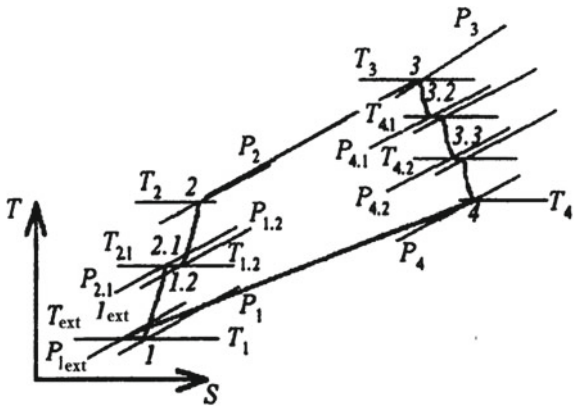


**Fig. 8.2** Cycle of GTU with two-spool compressor and free power turbine

– the process (3.3–4)—in PT;
– the process (4–$1_{amb}$)—so-called "cooling process".

## 8.2 Determination of Air and Gas Pressure in GTU

We will determine the pressure in different parts of the GTU by use of the **pressure coefficients**. These coefficients consider the pressure losses due to friction in the transitional parts of the GTU [1].

The pressure coefficient is generally defined as the following:

$$\nu = \frac{p_{\text{out}}}{p_{\text{in}}}.$$

**Pressure calculation example**

(1) We have the ambient pressure $p_{\text{amb}}$ (for example, $p_{\text{amb}} = 0.101$ MPa).

(2) Pressure at point 1 (before LPC)

$$p_1 = p_{\text{amb}} \cdot \nu_{\text{in}l},$$

where $\nu_{\text{in}l}$ is the inlet casing pressure coefficient (0.98 ~ 0.99).

(3) Pressure at point 2.1 (after LPC)

$$p_{2.1} = p_1 \cdot \pi_{c1} = p_{\text{amb}} \cdot \nu_{\text{in}l} \cdot \pi_{c1},$$

where $\pi_{c1}$ is the LPC pressure ratio.

(4) Pressure at point 1.2 (before HPC)

$$p_{1.2} = p_{2.1} \cdot \nu_c = p_{\text{amb}} \cdot \nu_{\text{in}l} \cdot \nu_c \cdot \pi_{c1},$$

where $\nu_c$ is the compressor intersection pressure coefficient (0.99–1.00).

(5) Pressure at point 2 (after HPC)

$$p_2 = p_{1.2} \cdot \pi_{c2} = p_{\text{amb}} \cdot \nu_{\text{in}l} \cdot \nu_c \cdot \pi_{c1} \cdot \pi_{c2},$$

where $\pi_{c2}$ is the HPC pressure ratio.

(6) Pressure at point 3 (after CC)

$$p_3 = p_2 \cdot \nu_{cc} = p_{\text{amb}} \cdot \nu_{\text{in}l} \cdot \nu_c \cdot \nu_{cc} \cdot \pi_{c1} \cdot \pi_{c2}$$

where $\nu_{cc}$ is the combustion chamber pressure coefficient (0.95–0.97).

(7) Pressure at point 4.1 (after HPT)

$$p_{4.1} = \frac{p_3}{\pi_{t1}} = p_{\text{amb}} \cdot \nu_{\text{in}l} \cdot \nu_c \cdot \nu \cdot \frac{\pi_{c1} \cdot \pi_{c2}}{\pi_{t1}},$$

where $\pi_{t1}$ is the HPT pressure ratio.

(8) Pressure at point 3.2 (before LPT)

$$p_{3.2} = p_{4.1} \cdot \nu_{t1} = p_{\text{amb}} \cdot \nu_{\text{in}l} \cdot \nu_c \cdot \nu \cdot \nu_{t1} \cdot \frac{\pi_{c1} \cdot \pi_{c2}}{\pi_{t1}},$$

where $\nu_{t1}$ and $\nu_{t2}$ are the turbine intersection pressure coefficients (0.99–1.00).

(9) Pressure at point 4.2 (after LPT)

$$p_{4.2} = \frac{p_{3.2}}{\pi_{\ell 2}} = p_{\text{amb}} \cdot \nu_{\text{in}l} \cdot \nu_c \cdot \nu \cdot \nu_{t1} \cdot \frac{\pi_{c1} \cdot \pi_{c2}}{\pi_{t1} \cdot \pi_{t2}},$$

where $\pi_{t2}$ is the LPT pressure ratio.

(10) Pressure at point 3.3 (before PT)

$$p_{3.3} = p_{4.2} \cdot \nu_{R2} = p_{\text{amb}} \cdot \nu_{\text{in}l} \cdot \nu_c \cdot \nu \cdot \nu_{t1} \cdot \nu_{t2} \cdot \frac{\pi_{c1} \cdot \pi_{c2}}{\pi_{t1} \cdot \pi_{R2}}.$$

(11) Pressure at point 4 (after PT)

$$p_4 = \frac{p_{3.3}}{\pi_{t3}} = p_{\text{amb}} \cdot \nu_{\text{in}l} \cdot \nu_c \cdot \nu \cdot \nu_{t1} \cdot \nu_{t2} \cdot \frac{\pi_{c1} \cdot \pi_{c2}}{\pi_{t1} \cdot \pi_{t2} \cdot \pi_{t3}}$$

or

$$p_4 = \frac{p_{amb}}{\nu_{exh}},$$

where $\pi_{t3}$ is the PT pressure ratio; $\nu_{\text{ex}h}$ is the exhaust casing pressure coefficient (0.98–0.99).

From the last equations, it follows that:

$$p_{\text{amb}} \cdot \nu_{\text{in}l} \cdot \nu_c \cdot \nu_{\text{cc}} \cdot \nu_{t1} \cdot \nu_{t2} \cdot \frac{\pi_{c1} \cdot \pi_{c2}}{\pi_{t1} \cdot \pi_{t2} \cdot \pi_{t3}} = \frac{p_{\text{amb}}}{\nu_{\text{ex}h}}$$

and

$$\nu_{\text{in}1} \cdot \nu_c \cdot \nu_{\text{cc}} \cdot \nu_{t1} \cdot \nu_{t2} \cdot \nu_{\text{ex}h} \cdot \pi_{c1} \cdot \pi_{c2} = \pi_{t1} \cdot \pi_{t2} \cdot \pi_{t3}.$$

## 8.3 Determination of the Compressor and Turbine Efficiency

If the number of axial compressor stages $z_c$ is more than 5, the efficiency of the compressor can be estimated by the following formula:

$$\eta_c = \frac{\pi_c^m - 1}{\pi_c^{\frac{m}{\eta_{\text{st}.c}}} - 1},$$

where $m = \frac{k-1}{k}$; $k$ is the specific heat ratio; $\eta_{st.c}$ is the efficiency of the single compressor stage (Fig. 8.3).

The efficiency of the single axial compressor stage is 0.89–0.91.

If the number of axial turbine stages is more than 5, the efficiency of the turbine can be estimated by the following formula:

$$\eta_t = \frac{1 - \pi_t^{-m\eta_{st.t}}}{1 - \pi_t^{-m}},$$

where $m = \frac{k-1}{k}$; $k$ is the specific heat ratio; $\eta_{st.t}$ is the efficiency of the single turbine stage (Fig. 8.4).

The efficiency of the single axial turbine stage is usually 0.86–0.90.

In real conditions, the turbines of the GTUs have a number of stages from 1 to 3 and the previous formula cannot be used.

During the thermal calculation of GTU you must take such values of the efficiency of the turbine:

for HPT $\eta_{t1} = 0.86 \sim 0.89$;

for LPT $\eta_{t2} = 0.88 \sim 0.90$;

for PT $\eta_{t3} = 0.90 \sim 0.92$.

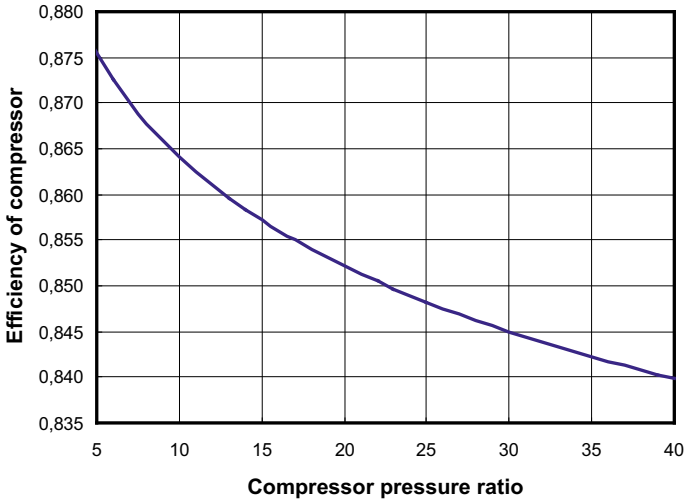


**Fig. 8.3** The dependence of compressor efficiency on the compressor pressure ratio ($\eta_{st.c} = 0.90$; $k = 1.40$)

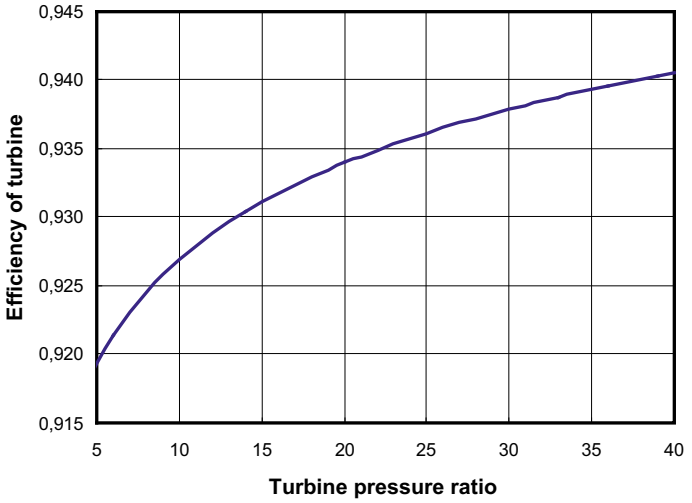


**Fig. 8.4** The dependence of the turbine efficiency on the turbine pressure ratio ($\eta_{st.t} = 0.90$; $k = 1.40$)

## 8.4 Determination of Specific Heat

The working fluid in the GTU compressor is air, in the GTU turbine, it is gas.

**Determination of specific heat for air**

During the thermal calculation of GTU we need to determine the specific heat of air.

Specific heat depends on temperature. During the calculation, we will use the parameter $c_{pa}|_{T_{in}}^{T_{out}} = f(T_m)$. That is the specific heat of air for the process that goes from temperature $T_{in}$ to temperature $T_{out}$. The specific heat is determined for a medium temperature of this process:

$$T_m = \frac{T_{in} + T_{out}}{2}.$$

The next determination of specific heat can be done in several ways.

**The 1st way: by** Table 8.1. You need to interpolate the values of that table.

In Table 8.1 $\alpha$ is the air excess coefficient.

**The 2nd way: by use of the graph**

Using the data from Table 8.1, we can draw the graph of specific heat (Fig. 8.5). Using the graph, we determine the specific heat $c_{pa}|_{T_{in}}^{T_{out}} = f(T_m)$.

**Table 8.1** Specific heat of air and gas (by use of the liquid fuel)

| $T_m$, K | Air | Combustion products | | |
|---|---|---|---|---|
| | | $\alpha = 1$ | $\alpha = 3$ | $\alpha = 5$ |
| | $c_{pa}$, kJ/kg/K | $c_{pg}$, kJ/kg/K | $c_{pg}$, kJ/kg/K | $c_{pg}$, kJ/kg/K |
| 273 | 1.0035 | 1.055 | 1.0215 | 1.0173 |
| 373 | 1.0102 | 1.0801 | 1.0383 | 1.0299 |
| 473 | 1.0245 | 1.1095 | 1.0550 | 1.0467 |
| 573 | 1.0446 | 1.1388 | 1.0801 | 1.0718 |
| 673 | 1.0684 | 1.1723 | 1.1053 | 1.0969 |
| 773 | 1.0923 | 1.1974 | 1.1304 | 1.1220 |
| 873 | 1.1149 | 1.2309 | 1.1597 | 1.1471 |
| 973 | 1.1354 | 1.2560 | 1.1806 | 1.1681 |
| 1073 | 1.1538 | 1.2853 | 1.2057 | 1.1890 |
| 1173 | 1.1702 | 1.3062 | 1.2225 | 1.2057 |
| 1273 | 1.1844 | 1.3272 | 1.2351 | 1.2225 |
| 1373 | 1.1970 | 1.3439 | 1.2518 | 1.2351 |
| 1473 | 1.2083 | 1.3607 | 1.2644 | 1.2476 |
| 1573 | 1.2179 | 1.3732 | 1.2769 | 1.2560 |
| 1673 | 1.2267 | 1.3855 | 1.2853 | 1.2644 |
| 1773 | 1.2346 | 1.3983 | 1.2937 | 1.2769 |

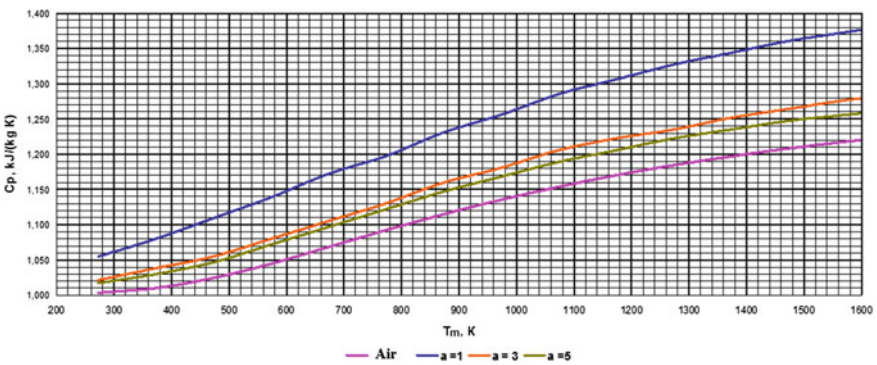


**Fig. 8.5** The dependence of air and gas-specific heat on the temperature

### The 3rd way: by use of the approximating formula

Using the data from Table 8.1, we can have the approximating formula. Using the formula, we determine the specific heat for air:

$$c_{p\,a}\Big|_{T_{\text{in}}}^{T_{\text{out}}} = f(T_m) = 0.917747497558594 + 0.000268046831479296 * T_m -$$
$$-4.88794533737291 * 10^{-8} * T_m * T_m.$$

**Determination of specific heat for gas**

The marine gas turbine units operate by use of liquid fuel (diesel fuel, etc.). Gas for GTU turbine is the product of that fuel combustion.

The specific heat of that gas depends on the **air excess coefficient in the combustion chamber** α. Therefore, for gas we have the following:

$$c_{p\,g}\Big|_{T_{\text{in}}}^{T_{\text{out}}} = f(T_m, \alpha).$$

The next steps of the specific heat determination are similar to the previous one.

Approximating formula for the specific heat of gas:

$$c_{p\,g}\Big|_{T_{\text{in}}}^{T_{\text{out}}} = f(T_m, \alpha) = 1.00549757480621 + 0.000384173501515761 * T_m -$$
$$-0.0556742288172245 * \alpha - 6.81171030691985 * 10^{-8} * T_m * T_m +$$
$$+0.00784802157431841 * \alpha^{*}\alpha - 0.0000133457979245577 * T_m * \alpha$$

**Determination of gas constant**

Gas constant **for air**:

$$R_{\text{air}} = 0.287\text{kJ/kg/K}.$$

Gas constant **for turbine gas** $R_{\text{gas}} = 0.288 \sim 0.290$ kJ/kg/K and depends on the air excess coefficient α. Approximating formula for it:

$$R = f(\alpha) = 0.291471034288406 - 0.00253063812851906 * \alpha +$$
$$+0.000602589745540172 * \alpha * \alpha - 0.000049502617912367 * \alpha * \alpha * \alpha.$$

**Determination of specific heat ratio**

Specific heat ratio both for air and gas has been determined as:

$$k = \frac{c_p}{c_p - R}.$$

## 8.5 Determination of Cooling Air Flow Rate

To increase the service life, the blades and disks of the modern GTU turbines are air-cooled. Cooling air is taken from the compressor of the same GTU and is supplied to the turbine through special channels and tubes. For cooling, the turbine blades have internal cavities. After cooling the blades, the air enters the flow part and mixes with the gas stream [1].

Without cooling, the turbine blades can withstand the maximum temperature:

$$T_{\text{perm}} = 1073 \sim 1123\text{K}.$$

If the gas temperature before the turbine is less than permissible ($T_3 \leq T_{\text{perm}}$), then the blades do not need to be cooled.

If $T_3 > T_{\text{perm}}$, then the number of the turbine blades cooled rows

$$n_{\text{cool}} = \frac{2 \lg \frac{T_{\text{perm}}}{T_3}}{\lg[1 - (0.11...0.15)]}.$$

The number of the turbine blades cooled rows $n_{cool}$ cannot be bigger than the total number of the turbine blade rows. HPT and LPT of many GTU (UGT6000, UGT10000, UGT15000, UGT25000) have a single stage, then the total number of the blade rows in that turbine is 2 (one row of the stationary nozzles and one row of the rotating blades) [2].

The specific cooling of the airflow rate can be estimated by the following formula:

$$g_{\text{cool}} = \frac{G_{\text{cool}}}{G_c} = a\, k_b\, g_m\, \beta_t \frac{(n_{\text{cool}} + 1)}{2} \cdot \frac{(T_3 - T_{\text{perm}})}{(T_{\text{perm}} - T_{\text{cool}})} \cdot \left(\frac{T_3}{T_{\text{cool}}}\right)^{0,25},$$

where $G_{\text{cool}}$ is the cooling air flow rate, kg/s; $G_c$ is the air flow rate through the compressor, kg/s; $T_3$ is the temperature before the turbine, K; $T_{\text{perm}}$ is the permissible blade metal temperature, K; $T_{\text{cool}}$ is the cooling air temperature (consider equal to the air temperature after the compressor $T_2$ ), K; $a$ is the coefficient (if $T_3 - T_{\text{perm}} \leq 100$, then $a = 1.7$; if $T_3 - T_{\text{perm}} > 100$, then $a = 1.4 \sim 1.3$); $k_b = 1.05 \sim 1.10$ is the heat transfer coefficient at the ends of the blades; $g_m = 0.020 \sim 0.025$ is the model of the airflow rate; $\beta_t = \frac{G_t}{G_c}$ is the turbine flow rate coefficient; $G_t$ is the gas flow rate through the turbine, kg/s.

## References

1. Romanovsky GF, Washchilenko NV, Serbin SI (2003) Theoretical basics of ship gas turbine designing. Publisher USMTU, Mykolaiv, 304 p. (in Ukrainian)
2. Romanovsky GF, Serbin SI, Patlaychuk VM (2005) Modern gas turbine units. Volume 1. Production units of Ukraine and Russia. Publisher NUS, Mykolaiv, 344 p. (in Ukrainian)

# Chapter 9
# Thermal Calculation of the Simple Cycle Gas Turbine Unit


The calculation is carried out according to the method described in [1].

## 9.1 Calculation of GTU Compressors

(1) Choose the ambient parameters. For standard conditions:
The ambient pressure $p_{amb} = 0.101$ MPa.
The ambient temperature $T_{amb} = 288$ K.

(2) Pressure at point 1 (before LPC)

$$p_1 = p_{amb} \cdot \nu_{inl},$$

where $\nu_{inl}$ is the inlet casing pressure coefficient (0.98–0.99).
The temperature at point 1 (before LPC)

$$T_1 = T_{amb}.$$

(3) We **accept with the next clarification** the value of the total compressor pressure ratio:

$$\pi_{c\,\Sigma}.$$

(4) Choose the HPC pressure ratio:

$$\pi_{c2} = \sqrt{\pi_{c\,\Sigma}}, \quad \text{but} \quad \pi_{c2} \leq 4.4 \sim 4.6.$$

(5) LPC pressure ratio:



K. Liu et al. (eds.), *Gas Turbines Structural Properties, Operation Principles and Design Features*, https://doi.org/10.1007/978-981-99-0977-3_9

$$\pi_{c1} = \frac{\pi_{c\,\Sigma}}{\pi_{c1}}.$$

(6) We **accept the next clarification of** the value of the specific heat ratio for the process in LPC:

$$k'_{a1} = 1.40.$$

(7) The parameter:

$$m_{a1} = \frac{k'_{a1} - 1}{k'_{a1}}.$$

(8) The efficiency of LPC:

$$\eta_{c1} = \frac{\pi_{c1}^{m_{a1}} - 1}{\pi_{c1}^{\frac{m_{a1}}{\eta_{st.c}}} - 1},$$

where $\eta_{st.c}$ is the efficiency of the single compressor stage (0.89–0.91).

(9) The increasing temperature in LPC:

$$\Delta T_{c1} = T_1\left(\pi_{c1}^{m_{a1}} - 1\right)\frac{1}{\eta_{c1}}.$$

(10) Temperature at point 2.1 (after LPC):

$$T_{2.1} = T_1 + \Delta T_{c1}.$$

(11) The medium temperature in LPC:

$$T_{m1} = \frac{1}{2}(T_1 + T_{2.1}).$$

(12) The calculation of the specific heat of the air in LPC:

$$C_{p\,a1} = f(T_{m1}).$$

and the specific heat ratio for the process in LPC:

$$k_{a1} = \frac{c_{pa1}}{c_{p\,a1} - R_{\text{air}}},$$

where $R_{\text{air}} = 0.287\,\text{kJ/kg/K}$ is the gas constant for air.

After this, we **repeat the calculation from point 7 to point 12**.

(13) Pressure at point 2.1 (after LPC):

$$p_{2.1} = p_1 \cdot \pi_{c1}.$$

(14) Pressure at point 1.2 (before HPC)

$$p_{1.2} = p_{2.1} \cdot \nu_c,$$

where $\nu_c$ is the compressor intersection pressure coefficient (0.99–1.00).

The temperature at point 1.2 (before HPC)

$$T_{1.2} = T_{2.1}.$$

(15) We **accept the next clarification of** the value of the specific heat ratio for the process in HPC:

$$k'_{a2} = k_{a1}.$$

(16) The parameter:

$$m_{a2} = \frac{k'_{a2} - 1}{k'_{a2}}.$$

(17) The efficiency of HPC:

$$\eta_{c2} = \frac{\pi_{c2}^{m_{a2}} - 1}{\pi_{c2}^{\frac{m_{a2}}{\eta_{st.c}}} - 1}.$$

(18) The increasing temperature in HPC:

$$\Delta T_{c2} = T_{1.2}\left(\pi_{c2}^{m_{a2}} - 1\right)\frac{1}{\eta_{c2}}.$$

(19) Temperature at point 2 (after HPC):

$$T_2 = T_{1.2} + \Delta T_{c2}.$$

(20) The medium temperature in HPC:

$$T_{m2} = \frac{1}{2}(T_{1.2} + T_2).$$

(21) The calculation of the specific heat of the air in HPC:

$$c_{p\,a2} = f(T_{m2})$$

and the specific heat ratio for the process in HPC:

$$k_{a2} = \frac{c_{pa2}}{c_{pa2} - R_{\text{air}}}.$$

After this, we **repeat the calculation from point 16 to point 21**.

(22) Pressure at point 2 (after HPC):

$$p_2 = p_{1.2} \cdot \pi_{c2}.$$

## 9.2 Calculation of GTU Combustion Chamber

(23) Pressure at point 3 (after CC):

$$p_3 = p_2 \cdot \nu_{cc},$$

where $\nu_{cc}$ is the combustion chamber pressure coefficient (0.96–0.98).

(24) The calculation of the specific heat of air:

$$c_{pa}\Big|_{293}^{T_2} = f(T_m) \quad \text{and} \quad c_{pa}\Big|_{293}^{T_3} = f(T_m),$$

where $T_3$ is the temperature in front of the combustion chamber (input data for work).

(25) The calculation of the specific heat of "pure" gas:

$$c_{pg}\Big|_{293}^{T_3} = f(T_m, \alpha = 1).$$

(26) To choose the fuel parameters: the calorific value of fuel $Q_f$ and the stoichiometric coefficient $L_0$.

For the standard liquid fuel $Q_f = 42915\,\text{kJ/kg}$ and $L_0 = 14.78\,\text{kg/kg}$; for natural gas $Q_f = 50032\,\text{kJ/kg}$ and $L_0 = 17.18\,\text{kg/kg}$.

(27) The relative fuel consumption:

$$g_f = \frac{c_{pa}\Big|_{293}^{T_3}(T_3 - 293) - c_{pa}\Big|_{293}^{T_2}(T_2 - 293)}{Q_f \eta_{cc} - \left[c_{pg}\Big|_{293}^{T_3}(L_0 + 1) - c_{pa}\Big|_{293}^{T_3} L_0\right](T_3 - 293)},$$

where $\eta_{cc}$ is the combustion chamber efficiency (0.985–0.995).

(28) The excess air coefficient in the combustion chamber:

$$\alpha = \frac{1}{g_f L_0}.$$

## 9.3 Calculation of GTU Turbines

(29) The specific cooling air consumption for HPT:

$$g_{\text{cool.1}} = a\, k_b\, g_m\, \beta'_{t1} \frac{(n_{\text{cool.1}} + 1)}{2} \cdot \frac{\left(T_3 - T_{\text{perm}}\right)}{\left(T_{\text{perm}} - T_{\text{cool}}\right)} \cdot \left(\frac{T_3}{T_{\text{cool}}}\right)^{0,25},$$

where $T_{\text{perm}} = 1073 \sim 1123$ K is the permissible blade metal temperature for HPT; $T_{\text{cool}} = T_2$ is the cooling air temperature, K; $a$ is the coefficient (if $T_3 - T_{\text{perm}} \leq 100$, then $a = 1.7$; if 0, then $a = 1.4 \sim 1.3$); $k_b = 1.05 \sim 1.10$ is the heat transfer coefficient at the ends of the blades; $g_m = 0.020 \sim 0.025$ is the model air flow rate; $\beta'_{t1} = \frac{G_{t1}}{G_{c2}} \approx 0.90$ is the simplified value of HPT flow tare coefficient; the number of the cooled blade rows for HPT:

$$n_{\text{cool.1}} = \frac{2 \lg \frac{T_{\text{perm}}}{T_3}}{\lg[1 - (0.11 \ldots 0.15)]}.$$

You must remember that:

- the maximum value of the single-stage HPT is 2;
- if $T_3 \leq T_{\text{perm}}$, then HPT blades do not need to be cooled. Then $n_{\text{cool.1}} = 0$ and $g_{\text{cool.1}} = 0$.

(30) The simplified gas temperature before LPT:

$$T'_{3.2} \approx T_3 - 0,9 \cdot \frac{\Delta T_{c2}}{2}.$$

(31) The specific cooling air consumption for LPT:

$$g_{\text{cool.2}} = a\, k_b\, g_m\, \beta'_{t2} \frac{(n_{\text{cool.2}} + 1)}{2} \cdot \frac{\left(T'_{3.2} - T_{\text{perm}}\right)}{\left(T_{\text{perm}} - T_{\text{cool}}\right)} \cdot \left(\frac{T'_{3.2}}{T_{\text{cool}}}\right)^{0,25},$$

where $T_{\text{perm}} = 1073 \sim 1123$ K is the permissible blade metal temperature for LPT; $T_{\text{cool}} = T_2$ is the cooling air temperature, K; $a$ is the coefficient (if $T'_{3.2} - T_{\text{perm}} \leq 100$, then $a = 1.7$; if $T'_{3.2} - T_{\text{perm}} > 100$, then $a = 1.4 \sim 1.3$); $k_b = 1.05 \sim 1.10$ is the heat transfer coefficient at the ends of the blades; $g_m = 0.020 \sim 0.025$ is the model air flow rate; $\beta_{t2} = \frac{G_{t2}}{G_{c1}} \approx 0.98$ is the simplified value of LPT flow rate coefficient; the number of the cooled blade rows for LPT:

$$n_{\text{cool.2}} = \frac{2 \lg \frac{T_{\text{perm}}}{T'_{3.2}}}{\lg[1 - (0.11 \ldots 0.15)]}.$$

You must remember that:

– the maximum value of $n_{\text{cool.2}}$ for single-stage LPT is 2;
– if $T'_{3.2} \leq T_{\text{perm}}$, then LPT blades do not need to be cooled. Then $n_{\text{cool.2}} = 0$ and $g_{\text{cool.2}} = 0$.

(32) The combustion chamber flow rate coefficient:

$$\alpha_{cc} = \frac{G_{cc}}{G_{c1}} = \alpha_{c2} - g_{\text{cool.1}} - g_{\text{cool.2}} - 0.011,$$

where $\alpha c_{k2} = \frac{G_{c2}}{G_{c1}} \approx 0.9 \sim 1.0$ is the HPC flow rate coefficient.

(33) HPT flow rate coefficient:

$$\beta_{t1} = \frac{(1 + g_f) \cdot \alpha_{cc}}{\alpha_{c2}}.$$

(34) LPT flow rate coefficient:

$$\beta_{t2} = \beta_{t1} \cdot \alpha_{c2} + g_{\text{cool.1}} + 0.006.$$

(35) PT flow rate coefficient:

$$\beta_{t3} = \beta_{t2} + g_{\text{cool.2}} + 0.004.$$

(36) Exhaust casing flow rate coefficient:

$$\beta_{\text{ex}h} = \beta_{t3} + 0.004.$$

(37) The medium gas temperature in HPT:

$$T_{m1} = T_3 - 0.9 \cdot \frac{\Delta T_{c2}}{2 \cdot \eta_{t1}},$$

where $\eta_{t1} = 0.86 \sim 0.89$ is the HPT efficiency.

(38) The calculation of the specific heat of gas for the process in HPT:

$$c_{p\,g1} = f(T_{m1}, \alpha).$$

(39) The specific heat ratio of gas for the process in HPT:

$$k_{g1} = \frac{c_{p\,g1}}{c_{p\,g1} - R_{\text{gas}}}.$$

where $R_{\text{gas}} = 0.288 \sim 0.290\,\text{kJ/kg/K}$ is the gas constant for the turbine gas.

(40) The power balance ratio for HPC and HPT:

$$C_2 = \frac{c_{p\,a2}}{\beta_{t1} \cdot c_{p\,g1} \cdot \eta_{m1}},$$

where $\eta_{m1} = 0.99 \sim 0.995$ is the mechanical coefficient for HPT.

(41) Reducing of temperature in HPT:

$$\Delta T_{t1} = C_2 \cdot \Delta T_{c2}.$$

(42) The simplified gas temperature after HPT:

$$T'_{4.1} = T_3 - \Delta T_{t1}.$$

(43) The calculation of the specific heat of gas for the process of the cooling air mixing with the gas flow in HPT:

$$c_{p\,gm1} = f(T'_{4.1}, \alpha).$$

(44) The calculation of the specific heat of air for the process of the cooling air mixing with the gas flow in HPT:

$$c_{p\,am1} = f(T'_{4.1}).$$

(45) The gas temperature after HPT (it considers reducing the gas temperature during mixing with cooling air)

$$T_{4.1} = \frac{\alpha_{c2} \cdot \beta_{t1}}{(\alpha_{c2} \cdot \beta_{t1} + g_{\text{cool.1}})} \cdot T'_{4.1} + \frac{c_{p\,am1} \cdot g_{\text{cool.1}}}{c_{p\,gm1} \cdot (\alpha_{c2} \cdot \beta_{t1} + g_{\text{cool.1}})} \cdot T_{\text{cool}}.$$

(46) HPT pressure ratio:

$$\pi_{t1} = \left( \frac{T_3 \cdot \eta_{t1}}{T_3 \cdot \eta_{t1} - \Delta T_{t1}} \right)^{\frac{k_{\text{g1}}}{k_{\text{g1}}-1}}.$$

(47) Pressure at point 4.1 (after HPT):

$$p_{4.1} = \frac{p_3}{\pi_{t1}}.$$

(48) Temperature and pressure at point 3.2 (before LPT):

$$T_{3.2} = T_{4.1} \quad \text{and} \quad p_{3.2} = p_{4.1}.$$

(49) The medium gas temperature in LPT:

$$T_{m2} = T_{3.2} - 0.9 \cdot \frac{\Delta T_{c1}}{2 \cdot \eta_{t2}},$$

where $\eta_{t2} = 0.88 \sim 0.90$ is the LPT efficiency.

(50) The calculation of the specific heat of gas for the process in LPT:

$$c_{p\,g2} = f(T_{m2}, \alpha).$$

(51) The specific heat ratio of gas for the process in LPT:

$$k_{g2} = \frac{c_{p\,g2}}{c_{p\,g2} - R_{\text{gas}}}.$$

(52) The power balance ratio for LPC and LPT:

$$C_1 = \frac{c_{p\,a1}}{\beta_{t2} \cdot c_{p\,g2} \cdot \eta_{m2}},$$

where $\eta_{m2} = 0.99 \sim 0.995$ is the mechanical coefficient for LPT.

(53) The reducing of temperature in LPT:

$$\Delta T_{t2} = C_1 \cdot \Delta T_{c1}.$$

(54) The simplified gas temperature after LPT:

$$T'_{4.2} = T_{3.2} - \Delta T_{t2}.$$

(55) The calculation of the specific heat of gas for the process of the cooling air mixing with the gas flow in LPT:

$$c_{p\,gm2} = f(T'_{4.2}, \alpha).$$

(56) The calculation of the specific heat of air for the process of the cooling air mixing with the gas flow in LPT:

$$c_{p\,am2} = f(T'_{4.2}).$$

(57) The gas temperature after LPT (it considers the reducing of the gas temperature during mixing with cooling air):

$$T_{4.2} = \frac{\beta_{t2}}{(\beta_{t2} + g_{\text{cool.2}})} \cdot T'_{4.2} + \frac{c_{p\,am2} \cdot g_{\text{cool.2}}}{c_{p\,gm2} \cdot (\beta_{t2} + g_{\text{cool.2}})} \cdot T_{\text{cool}}.$$

(58) LPT pressure ratio:

$$\pi_{t2} = \left( \frac{T_{3.2} \cdot \eta_{t2}}{T_{3.2} \cdot \eta_{t2} - \Delta T_{t2}} \right)^{\frac{k_{g2}}{k_{g2-1}}}.$$

(59) Pressure at point 4.2 (after LPT):

$$p_{4.2} = \frac{p_{3.2}}{\pi_{t2}}.$$

(60) Temperature and pressure at point 3.3 (before PT):

$$T_{3.3} = T_{4.2} \quad \text{and} \quad p_{3.3} = p_{4.2} \cdot \nu_t,$$

where $\nu_t$ is the turbine intersection pressure coefficient (0.99–0.995).

(61) Pressure at point 4 (after PT):

$$p_4 = \frac{p_{\text{amb}}}{\nu_{\text{ex}h}},$$

where $\nu_{\text{ex}h}$ is the exhaust casing pressure coefficient (0.98–0.99).

(62) PT pressure ratio:

$$\pi_{t3} = \frac{p_{3.3}}{p_4}.$$

(63) The simplified medium gas temperature in PT:

$$T'_{m3} = T_{3.3} - \frac{\Delta T_{c1} + \Delta T_{c2}}{4}.$$

(64) The calculation of the specific heat of gas for the process in PT:

$$c_{p\,g3} = f(T'_{m3}, \alpha).$$

(65) The specific heat ratio of gas for the process in PT:

$$k_{g3} = \frac{c_{p\,g3}}{c_{p\,g3} - R_{gas}}.$$

(66) The reducing of temperature in PT:

$$\Delta T_{t3} = T_{3.3} \left( 1 - \frac{1}{\pi_{t3}^{\frac{k_{g3-1}}{k_{g3}}}} \right) \cdot \eta_{t3},$$

where $\eta_{t3} = 0.90 \sim 0.91$ is the PT efficiency.

(67) Temperature at point 4 (after PT):

$$T_4 = T_{3.3} - \Delta T_{t3}.$$

(68) The medium gas temperature in PT:

$$T_{m3} = T_{3.3} - \frac{\Delta T_{t3}}{2\,\eta_{t3}}.$$

## 9.4 Calculation of GTU Efficiency

(69) Specific power:

$$N_{\text{sp}} = c_{p\,g3} \cdot \Delta T_{t3} \cdot \beta_{t3} \cdot \nu_{\text{in}l} \cdot \eta_{m3},$$

where $\eta_{m3} = 0.99 \sim 0.995$ is the mechanical coefficient for PT.

(70) The specific air flow rate through LPC:

$$G_{c1.\text{sp}} = \frac{N_e}{N_{\text{sp}} \cdot \eta_g},$$

where $\eta_g = 0.97 \sim 0.98$ is the gear efficiency; $N_e$ is the effective (useful) power of GTU (input data for work), kW.

(71) The air flow rate through LPC:

$$G_{c1} = G_{c1.\text{sp}} \cdot \nu_{\text{in}l}.$$

(72) The air flow rate through HPC:

$$G_{c2} = G_{c1} \cdot \alpha_{c2}.$$

(73) The air flow rate through the combustion chamber:

$$G_{cc} = G_{c1} \cdot \alpha_{cc}.$$

(74) The fuel consumption:

$$G_f = 3600 \cdot G_{cc} \cdot g_f.$$

(75) The gas flow rate through HPT:

$$G_{t1} = G_{c2} \cdot \beta_{t1}.$$

(76) The cooling air flow rate through HPT:

$$G_{\text{cool.1}} = G_{c1} \cdot g_{\text{cool.1}}.$$

(77) The gas flow rate through LPT:

$$G_{t2} = G_{k1} \cdot \beta_{t2}.$$

(78) The cooling air flow rate through LPT:

$$G_{\text{cool.2}} = G_{c1} \cdot g_{\text{cool.2}}.$$

(79) Gas flow rate through PT:

$$G_{t3} = G_{c1} \cdot \beta_{t3}.$$

(80) Gas flow rate through exhaust casing:

$$G_{\text{ex}h} = G_{c1} \cdot \beta_{\text{ex}h}.$$

(81) Specific fuel consumption:

$$g_e = \frac{G_f}{N_e}.$$

(82) Actual GTU efficiency:

$$\eta_e = \frac{3600}{g_e \cdot Q_f}.$$

## 9.5 Optimization of GTU Thermodynamic Cycle Parameters

We know that the actual efficiency of the gas turbine units depends on:

- the compressor pressure ratio $\pi_c$;
- the gas temperature after the combustion chamber $T_3$;
- the efficiency of the compressor $\eta_c$, the combustion chamber $\eta_{c.c}$ and the turbine $\eta_t$;
- the mechanical coefficient $\eta_m$ and the gear efficiency $\eta_g$;
- the pressure losses in the transitional parts of GTU.

The dependence of the actual efficiency on most parameters is simple. If we want to increase the actual efficiency **we must increase**:

- the gas temperature after the combustion chamber $T_3$,

– the efficiency of the compressor $\eta_c$, the combustion chamber $\eta_{c.c}$ and the turbine $\eta_t$,
– the mechanical coefficient $\eta_m$ and the gear efficiency $\eta_g$ and **we must reduce** the pressure losses in the transitional parts of GTU.

But the dependence of the actual efficiency on the compressor pressure ratio is not so simple (Fig. 9.1). The increase in that parameter is the first cause of the actual efficiency increasing, and then it is the cause of the efficiency decreasing. There is the optimum for the compressor pressure ratio $\pi_c^{opt}$, at which the efficiency has the maximum value $\eta_e^{max}$.

We know that the compressor pressure ratio is the input data for the calculation. Therefore, if at the beginning of the calculation we accept the value of the compressor pressure ratio which is closely located to its optimal value, then at the end we get the value of the actual efficiency which is maximum. On the contrary, if we accept the value of the compressor pressure ratio which is located far from its optimal value, then we get the value of the actual efficiency which is very small.

This is the reason for optimizing the parameters of the GTU cycle. During this optimization, we must fulfill several thermal calculations of GTU with different values of the compressor pressure ratio. Based on the calculation results, a graph of the actual efficiency versus the compressor pressure ratio is drawn. Using this graph, the optimum value of the compressor pressure ratio $\pi_k^{opt}$ is determined.

Near the optimum value, the graph is very gentle and small deviations from the optimum do not lead to a large decrease in efficiency. For this reason, for the further calculation of GTU, the value of the compressor pressure ratio $\pi_{c\,\Sigma}$ is taken slightly less than optimal.

The smaller values of the compressor pressure ratio reduce the number of compressor stages and therefore reduce its complexity, size and weight. Also increases the reliability of the compressor.

But the equation

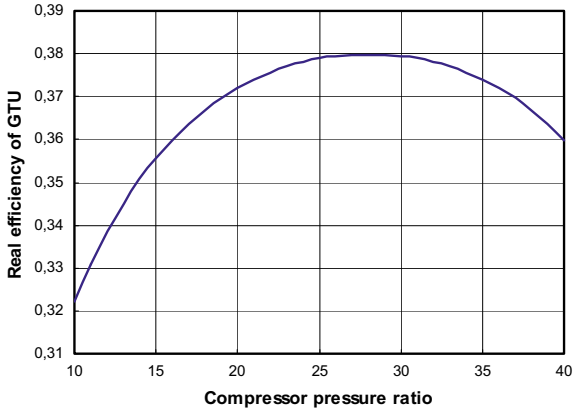


**Fig. 9.1** The dependence of the actual efficiency on the compressor pressure ratio

$$\eta_e^{\max} \quad > \quad \eta_e = f(\pi_{c\,\Sigma}) \quad > \quad \eta_e^{\max} - 0.005$$

must be fulfilled. The efficiency of the reduction doesn't exceed 0.005.

## Reference

1. Romanovsky GF, Washchilenko NV, Serbin SI (2003) Theoretical basics of ship gas turbine designing. Publisher USMTU, Mykolaiv, 304 p. (in Ukrainian)

# Part II
# Design Features

# Chapter 10
# Advantages and Disadvantages of the Power Plants with Gas Turbine Units


Power plants with gas turbine units have some advantages and disadvantages in comparison with other types of power plants. Let us discuss them for the gas turbine units of a simple thermodynamic cycle [1].

## 10.1 Advantages of the Power Plants with Gas Turbine Units

1. **Small weight and dimensions**

We will compare the various types of power plants for marine applications. As a weight indicator, we will take the specific power plant weight $m_e$ which is the ratio of the dry plant weight (the weight of all its elements without water, oil and fuel) to the effective (useful) power of the power plant. The approximate values of this indicator for the main types of marine power plants are shown in Table 10.1.
For displacement ships with the same power, **the weight of the power plant with a simple cycle GTU is 10–16 times less than the weight of a diesel power plant with LSE** (now the dominant type of power plant for a commercial fleet).

Then, we will compare the main types of marine power plants in dimensions. As the indicator, we use the energy saturation of the engine room area $n_F$ that is the ratio of the power plant's total power to the area of the engine room (Table 10.2).

It follows from Fig. 10.1 that for the same useful power, **a power plant with a simple cycle GTU occupies an area approximately 12 times smaller than a power plant with a diesel LSE**.

What does explain the small weight and size of the power plants with GTU? In comparison with a steam turbine power plant, it does not include several elements with significant dimensions and weight. First of all, there is no steam generator (boiler), i.e. a structure that has a big height and requires a separate room for installation. If in the GTU combustion chamber the fuel combustion process is carried out



K. Liu et al. (eds.), *Gas Turbines Structural Properties, Operation Principles and Design Features*, https://doi.org/10.1007/978-981-99-0977-3_10

**Table 10.1** Specific marine power plant weight comparison [1]

| Marine power plant | $m_e$, kg/kW |
|---|---|
| Diesel power plant with a low-speed engine (LSE) and a direct (without gear) power transmission to the screw[1] | 80–100 |
| Diesel power plant with a medium-speed engine (MSE) and a reduction gear | 60–70 |
| Diesel power plant with electric power transmission per screw | 90–110 |
| Steam turbine power plant of the transport ships | 50–60 |
| Gas turbine plant of displacement ships with simple cycle GTU | 5–10 |
| Gas turbine plant of hovercrafts with simple cycle GTU | 2–3 |
| Gas turbine plant of hydrofoil ships with simple cycle GTU | 1.2–1.5 |

**Table 10.2** Energy saturation indicators

| Marine power plant | $n_F$, kW/m$^2$ |
|---|---|
| Diesel power plant with a low-speed engine (LSE) and a direct (without gear) power transmission to the screw | 15–30 |
| Steam turbine power plant of the transport ships | 22–37 |
| Gas turbine plant of displacement ships with a simple cycle GTU | 185–370 |

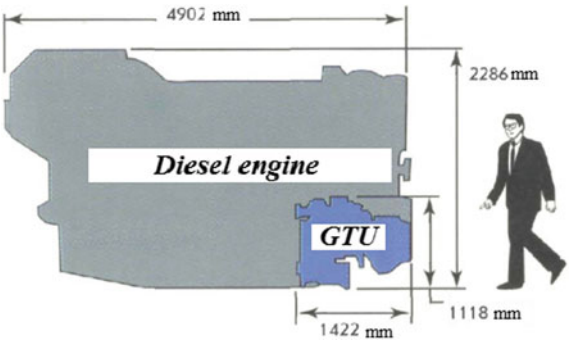


**Fig. 10.1** Dimensions of 3 MW diesel LSE and 3 MW gas turbine engine

at a pressure of 0.7–3.5 MPa, while combustion in the boiler occurs at atmospheric pressure and, therefore, the volume of the generated hot gases is 7–35 times more.

The steam turbine power plant also contains a condenser with several pumps, a regeneration system with 3–11 ha (lower values for ship power plants, large—for stationary ones), turbine pumps (from one to three), and a deaerator. As a result, if a simple cycle gas turbine power plant can be installed in the ship's engine room (machine room of a power station, etc.), then a steam turbine plant requires, as a rule, a frame foundation of the considerable height (it is 9–16 m for stationary power

[1] According to the rotational speed of the crankshaft ($n$, rpm), marine diesels are classified as low-speed engines (LSE) $50 \leq n < 250$, medium-speed engines (MSE) $250 \leq n < 750$ and high-speed engines (HSE) $750 \leq n < 2500$.

plants) with the installation of a steam turbine on the upper foundation plate and the auxiliary equipment in the lower condensation room.

It should also be considered that in the GTU the gas expansion process takes place in a turbine which is consisting of only 3–7 stages, while a steam turbine of the same power contains 20–35 stages. As a result, even considering the length of the compressor and the combustion chamber, the total length of the gas turbine unit is significantly less than the length of a steam turbine of the same power (for a 150 MW power plant it is approximately less in 1.5 times).

The significant dimensions and weight of the power plants with diesel engines are explained by the influence of the engine parameters (LSE or MSE). Due to the specifics of the energy conversion, a decrease in the rotational speed of the crankshaft of these engines is accompanied by a significant increase in their size and weight.

It should be noted that the above information is typical for power plants with simple cycle GTUs. The complication of the GTU cycle which is carried out in order to increase efficiency leads to a significant increase in its size and weight.

2. **High maneuverability**

Power plant maneuverability is the ability to perform various maneuvers during operation. The power plant maneuverability indicators are:

– time of the preparation for the start;
– time from start to full power;
– time of the transition from one operating mode to another;
– the ranges of the possible operating modes;
– time of the reverse.

It is clear that maneuverability has value mainly for the transport power plants.

**Time of the preparation for the start** is mainly determined by the time which is necessary for the heating of the engines (units), and for the steam turbine plants, also by the time for the rising of the steam pressure in the boilers. It also includes time for turning off the mechanisms, preparing systems for operation, etc.

The time of preparation for the start of the marine steam turbine plants is at least 4 h. Warming up before starting a heavy diesel LSE requires 2.0–2.5 h. The start of a simple cycle GTU is performed without preliminary heating. In this case, the preparation time for start-up is 5–10 min.

It should be noted that GTU starting at low air temperature practically does not differ from normal temperature, because there are no friction parts in the unit (like in diesel engines) and there is no need to heat oil.

The required for gaining full power from idle time is approximately 1.0–1.5 h for steam turbine plants and LSE, about 30 min for MSE, 3–5 min for simple cycle GTU and HSE.

The need for preliminary warming up of some engines, as well as the further power gain, is caused by the desire to avoid the significant thermal stresses and deformations of parts, which can cause their destruction. The bigger weight and thermal inertia of the engine, the longer it takes to warm up the worse it is for the

power plant maneuverability. In this case, the high maneuverability of the gas turbine units is explained by their small size and weight.

It should be noted that although the time from start to full power for GTU is allowed to be very small, nevertheless, the process itself is inevitably accompanied by a rapid and significant change in the temperature of its elements that negatively affects the stress state of many parts. According to the harmful effects on the metal, each start is equivalent to 5–25 h of GTU operation.

3. **Low installation and maintenance costs**

The compactness and low weight of a simple cycle GTU allow them to execute their assembly and testing at the turbine factory with the next delivery as a single module to their destination by rail, road, or air. So, in particular, GTU is transported with built-in combustion chambers. When transporting gas turbine units with remote chambers, the latter are transported separately but are easily and quickly connected via flanges to the compressor-gas turbine module.

The steam turbine is supplied with numerous units and parts, the installation of both itself and the numerous auxiliary equipment and the connections between them takes several times longer than the GTU.

The installation of a power plant with a simple cycle GTU is usually carried out on a simple foundation at the zero mark of the ship engine room or the power station engine room. A steam turbine plant, in most cases, requires a frame foundation of a considerable height with equipment which is placed on different levels.

An advantage from the installation point of view is the power plant with GTU compared with heavy diesel LSE and MSE. The cost of installing a marine power plant with GTU is five times less than the cost of installing a diesel plant.

The maintenance of the gas turbine units is much simpler than the piston engines and especially steam turbine plants. In a power plant with GTU, there are not many systems that require constant monitoring. Some elements (for example, fuel equipment, nozzles, controls, etc.), are more complicated and they require less maintenance.

**Gas turbine units are well adapted for remote control**. Consumers want to reduce operating costs by use of automation equipment. Many power plants are developed for remote control, without the presence of the maintenance personnel at the station. The operation of the GTU is well controlled automatically, their service systems are not complicated, water cooling is not required (oil can be cooled with air), starting engines do not consume much power and they are reliable in performance.

In this case, the personnel makes some initial settings of the equipment, after which the gas turbine unit works without inspections until the remote monitoring shows the deviation of the parameters from the set values. Arriving at operation place, a team of workers replaces the engine (or only its gas generator). An engine (gas generator) that has been displaced is sent for repair to the manufacturer. The process of replacing an aircraft-type GTU gas generator with a free power turbine is about eight hours.

4. **Low lubrication costs (compared to piston engines)**

**Table 10.3** Specific oil consumption for marine engines

| Marine engine | Specific oil consumption, g/(kW h) |
|---|---|
| Diesel LSE | 0.4–1.1 |
| Diesel MSE | 1–2.5 |
| Diesel HSE | 3–5 |
| Steam turbine | 0.06 |
| Gas turbine engine | 0.14–0.16 |

In heat engine lubrication systems, as a rule, made from petroleum mineral oils are used. During operation, under the influence of high temperatures the light fractions evaporate from oils, as a result, their physical properties are worsening. In particular, an increase in viscosity leads to an increase in resistance in the oil layer in the friction elements.

Oil pollution worsens viscosity and lubricity in the future too. The permissible loads in friction elements are reduced, and the oxidative processes are intensified. A decrease in viscosity by 20–25% compared with the initial value is considered to be the limit. In this case, oil in the system must be replaced.

The oil consumption in gas turbine units is several times less than in any piston engine. This is explained by the fact that in the GTU there are fewer bearings, there are no friction elements and the direct contact between oil and hot combustion gas is excluded. Thanks to the latter, oil does not oxidize or contaminate during operation.

For various types of marine engines, the specific oil consumption[2] is presented in Table 10.3.

As can be seen from Table 10.3, with the same power and operating time, **the lubricant costs in a gas turbine unit are 3–7 less than in a diesel low-speed engine, and 20–30 times less than in a diesel high-speed engine**.

It is also obvious that the oil consumption in GTUs is more than in steam turbines.

5. **Low content of harmful substances in the exhaust gas**

The working process of the heat engines is based on the hydrocarbon fuels burning. The formation as a result of the combustion gas is released into the atmosphere. It includes a large number of substances that are harmful to humans and the ambient. These include the following: carbon monoxide CO, sulfur oxides $SO_2$ and $SO_3$, unburned hydrocarbons $C_xH_y$, nitrogen oxides NO and $NO_2$, soot and ash particles, aldehydes, formaldehyde, benz-α-pyrene, etc.

Compared with other types of power plants, the content of the harmful substances in the gas turbine exhaust gases is significantly lower. This is due to the following factors:

**Firstly**, the concentration of harmful substances in the combustion products depends on the type of used fuel. The heavier the grade of the liquid fuel which is used the more these substances in the gas exhaust. The most environmentally friendly type of hydrocarbon fuel, from this point of view, is natural gas, the least is

[2] This parameter takes into account oil losses due to leaks, evaporation and during the separation.

the solid fuels (coal, peat, etc.). The gas turbine units use either natural gas (stationary units), kerosene (aviation gas turbine engines), or light grades of diesel fuel (marine gas turbine engines). All of these fuels are among the least polluting.

It should be noted that most piston engines operate on light or heavy grades of hydrocarbon fuel. The steam turbine plants, as a rule, use heavy fuels.

**Secondly**, the working process in the combustion chambers of the modern gas turbine units is continuous in time: the working fluid continuously goes through the flame tubes, fuel continuously enters this flow, etc. The piston engines, on the contrary, are characterized by the discrete processes which are occurring in the working cylinders, which negatively affect the environmental cleanliness.

**Thirdly**, a feature of the gas turbine units is that several times more air is pumped through them (2.5–4.0) than is required for the fuel burning. As a result, the exhaust gas is highly diluted and, therefore, the specific content of the harmful substances in them is proportionally reduced. For comparison, the air excess coefficient in boilers only slightly exceeds 1.0 (for main ship boilers it is 1.03–1.08); the air excess coefficient for marine LSE is 1.8–2.2, for MSE is 1.6–2.0, for HSE is 1.5–1.8.

A large amount of air and consequently, of oxygen in the GTU is useful for a number of other reasons:

(1) The smokeless exhaust. In the piston engines which are operating with air excess coefficients close to optimal, especially in engines that have been in the operation for a long time, it is difficult to avoid smokeless and sometimes corrosive exhaust.
(2) In comparison with the diesel engines, the exhaust gas of GTU does not contain poisonous carbon monoxide in large quantities.

### 6. Generation of the large power in the single unit

This advantage is largely due to the small weight and dimensions of the gas turbine units. Many researchers note that the power in a single GTU can be raised to almost any value which is necessary for the transport power plants with quite acceptable dimensions and weights. At the same time, the GTU is assembled as a single module, which facilitates its transportation and installation.

Now the useful power of the stationary simple cycle GTU has exceeded 340 MW. The gas turbine units for the mechanical drive (used to drive various mechanisms: compressors, pumps, etc.) have reached 50 MW. The marine gas turbine units have power from 0.5 to 40 MW.

As an advantage, it should also be noted the increase in GTU power with a decrease in the temperature of the atmospheric air, which positively affects the operation of the power plant in the cold season.

### 7. Low vibration (compared to piston engines)

The modern gas turbine units are characterized by the constant combustion mode in time; they do not have the reciprocating moving elements. It ensures the smooth operation of the GTU at any speed.

The rotor of a GTU can be very accurately balanced both statically and dynamically by using the modern balancing methods. However, in piston engines, the changes in the torque due to the variable loads and the influence of the inertia forces lead to the appearance of torsional vibrations, which become especially significant at certain resonant speeds. With the exception of some 8-, 12- and 16-cylinder engines, it is impossible to ensure the smooth operation of the piston engine in the entire speed range.

## 10.2 Disadvantages of the Power Plants with Gas Turbine Units [1]

1. **Low efficiency, especially at the partial operation modes**

The main disadvantage of a simple cycle gas turbine unit is a lower efficiency compared to other types of power plants, or, in other words, a higher specific fuel consumption. So, for example, the actual efficiency of the modern gas turbine units with a power of 3 MW or more is 28–42%, the diesel power plants with LSE and MSE is 46–54%, and the steam turbine power plants are 30–43%.

The low efficiency of a simple cycle GTU is due to the thermodynamic cycle imperfection (Brayton cycle) as a result of which the exhaust gas leaves the GTU with a high temperature—650 to 900 K. For example, the temperature of the exhaust gas of the modern marine diesel LSE is 530–650 K.

In addition, in the modern gas turbine engines, the maximum pressure of the working fluid is 0.7–3.5 MPa, which is much less than in the piston engine cycles (in diesel LSE and MSE it reached 14–18 MPa). The consequence of this is the lower thermal efficiency of the gas turbine units.

In the GTU, the processes of the air pressure increasing, its heating, and producing the mechanical energy occur in three different parts (a compressor, a combustion chamber, and a turbine), each of them with some losses. However, in piston engines, these processes occur in one place (in the working cylinders), therefore, the total losses of these processes are much smaller.

The complication of the GTU thermodynamic cycle, in particular by the use of the heat recovery steam generators, can increase its efficiency (up to 50–60%), but at the same time it increases its cost, size, weight, worsens the maneuverability, complicates the operation, i.e. eliminates largely the positive qualities of the GTU, which we discussed earlier.

A serious disadvantage of the gas turbine units of a simple cycle is the lower efficiency than other types of heat engines during the operation at the partial power modes (at partial loads). Any engine is designed (calculated) for one operating mode. In this mode, which is called **nominal**, the engine generates 100% of the planned power. All other operating modes for it are **off-design**. However, during operation, the power plants are often operated at partial power modes, i.e. generate power less than 100%. The operation of such "off-design" modes for all types of the heat engines

is accompanied by a deterioration in efficiency compared to the nominal "design" mode. An unpleasant feature of the simple cycle GTU is that the deterioration in efficiency for them manifests itself most intensively.

The dependence of the actual efficiency of the gas turbine engines which have been produced by "Zorya-Mashproekt" on the load is shown in Fig. 10.2. Obviously, for a GTU with a free power turbine (graphs 2, 3, 4, and 5), the efficiency at 20% power mode is worse than the efficiency in the nominal mode by 1.5–2.0 times. For a single-shaft UGT 2500, the decrease is even greater—by 2.8 times.

Figure 10.3 shows the dependences of the relative specific fuel consumption on the load, compiled for three types of engines: a diesel engine, a petrol engine and a simple cycle gas turbine engine have the same rated power of 375 kW (500 hp). This power is typical, for example, for driving a large truck. The gas temperature after the GTU combustion chamber is 1350 K, the compressor pressure ratio is 12. The parameters of the piston engines are assumed to be typical for this power.

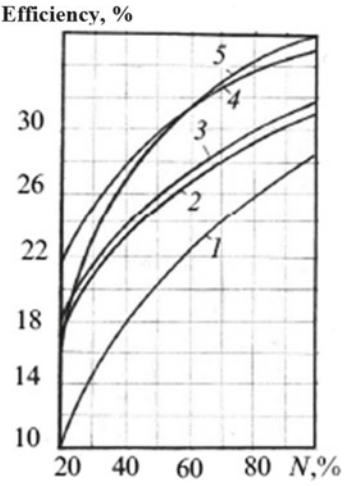


**Fig. 10.2** Actual efficiency of marine gas turbine engines produced by "Zorya-Mashproekt" versus the load: 1—UGT 2500; 2—UGT 3000; 3—UGT 6000; 4—UGT 15,000; 5—UGT 25,000

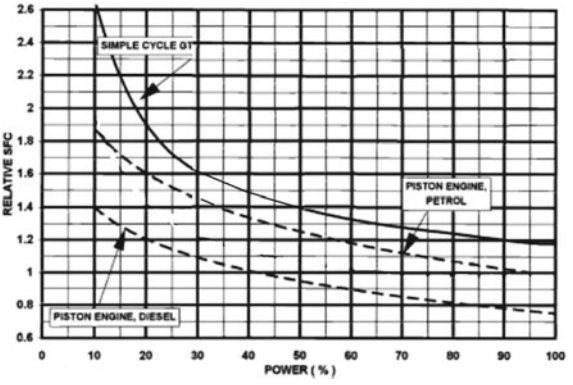


**Fig. 10.3** Relative specific fuel consumption compiled for engines which have a rated power of 375 kW (500 hp) versus the load. 1—piston engine (diesel fuel); 2—piston engine (petrol fuel); 3—simple cycle gas turbine engine

The main reason for reducing the actual efficiency of the gas turbine units at partial modes is that the generated power is reduced by decreasing the amount of the supplied to the combustion chamber fuel, as a result of which the working fluid temperature in the turbine inlet decreases and the thermal efficiency of the cycle decreases (**reason No. 1**). The working fluid flow rate through the GTU with decreasing load (i.e. with a reduction in the rotor speed) is decreased. The turbine inlet gas temperature is also decreased.

In addition, in the partial operation mode, the compressor and turbine efficiencies are worsening. That is a consequence of the flow violation around the blade airfoils at the compressor and the turbine (**reason No. 2**). It should be remembered that the airfoils for the compressor and turbine blades are also selected for one "calculated" mode of operation. The deviation from this mode distorts the velocity triangles and causes losses due to the separation of the boundary layer.

For the gas turbine units operation for a long time at nominal or close to its modes (for example, driving of a generator), the discussed disadvantage is not particularly relevant. However, for cases where the GTU must operate in a wide range of loads, such as transport, this feature can seriously affect the consumer's choice.

The use of the additional heat exchangers, the variable turbine nozzles, the schemes with a free power turbine, the production of new high-quality heat-resistant material, cooling systems, etc., leads to the increase in the efficiency of the gas turbine units at partial modes.

2. **High structural complexity**

A feature of the gas turbine units is a **high rotor speed**. This parameter is much higher than the rotational speed of the crankshaft of petrol engines and the diesel engines. GTUs operate at speeds from 3,000 rpm for the largest stationary power plants to 60,000 rpm for the smallest engines.

The high revolutions increase demands on the design of the rotor elements (rotor blades, disks, shafts, etc.), which are subjected to significant centrifugal forces during operation, causing tensile stresses and, in some cases, torsion.

The high speeds require a detailed development of the bearings of a gas turbine unit. The lubrication and sealing systems are especially complicated. A special set of measures should be provided if the rotor is operated at revolutions which are exceeding critical (the so-called **flexible rotor**).

The high revolutions necessitate careful rotor balancing, as well as the use in some cases of the reduction gears with the big gear ratios.

The gas turbine units are characterized by a **high temperature of gas** which is moving through the combustion chamber and the turbine. Before the turbine the temperature is 1300–1800 K, at the exhaust it is 650–900 K. Directly in the combustion zone the temperature reaches 2,000–2,200 K and more.

In addition to the difficulties with the reliable operation of the combustion chamber elements, the high temperature worsens the strength of the materials which are operating under load. It relates primarily to the first turbine stage blades. The temperature for them is the highest, and the rotor speed, consequently, the centrifugal loads are

usually also the highest. A special task of GTU design is the creation of new heat-resistant materials and the development of more efficient cooling systems for the combustion chamber and the turbine elements.

The gas turbine units, as already noted, are characterized by the increased airflow. This parameter exceeds significantly the similar indicators of other types of power plants. The consequence of this is **the increased complexity of the air intake and the exhaust gas devices**.

The GTU exhaust is significantly complicated by the high gas temperature, which is much higher than that of the piston engines and steam turbine plants. The high temperatures, in turn, are the causes of the even greater increase in exhaust gas volume.

It should be noted that the complexity of the air intake devices is also explained by the increased sensitivity of the GTU elements to the quality of the air passing through them (especially for the axial compressor vanes). Therefore, very often the air intake devices are equipped with additional elements that clean the incoming air from moisture and dust.

It should be noted that the power plants with gas turbine units, in comparison with other types of power plants, also have the same design simplifications. So, for example, the number of the working elements of a twin-shaft gas turbine engine is 4–6 times less than that of a 6-cylinder petrol engine (may be proportional to the number of the cylinders). The combustion mode in the GTUs is unchanged, the pressure is relatively low; there is no complex crank mechanism and valve system like piston engines; there is no need for so many different elements and service systems as in the steam turbine plants.

3. **Shorter service life**

One of the main disadvantages of gas turbine units is the shorter service life, which is certainly the result of the high structural complexity. The high rotational speeds, and therefore the high centrifugal loads, together with the high temperature, lead to the accelerated destruction of the turbine blades, the rolling bearings, the elements of the combustion chamber and the fuel equipment, etc.

It should be noted that the continuous improvement of the gas turbine units over the past decades has led to a significant increase in this indicator. If the first aviation gas turbine engines (German and English engines have been produced during World War II) had a resource before the overhaul of only 20–50 h, now it is already several thousand hours for this field of application. At the same time, the parameters of the working fluid (pressure, temperature) and the acting loads are also sharply increased.

The modern marine gas turbine units have a resource until the overhaul of 5,000–20,000 h.

So, for example, LM2500 engines which are widely used on the ships of the US Navy have a value of this parameter of 8,000 h; the new ETF40B engine has 2,000 h; the main marine UK engines Spey SM1A and Spey SM1C have 7,500 and 5,000 h; the resource of the MT30 is 12,000 h.

For comparison, the marine diesel MSE has a resource until the overhaul of 45–60 thousand hours; when working on the high-viscosity fuel, it decreases to 35–40

thousand hours. The resource of the low-speed diesel engines is up to 70–90 thousand hours. The estimated time of the operation under load for the steam turbine blades is 100,000 h.

The service life of the stationary gas turbine units is much higher. The period between the preventive repairs for them is 20–50 thousand hours. For example, the "Alstom S.A." during the operation of its GTU conducts a number of inspections. The most complex is the inspection of the category "C". It is the inspection which consists of the opening of the GTU casing and the execution of the preventive repair and troubleshooting. That inspection is carried out every 24,000 h of the operation. American "General Electric Co." executes the inspection of the hot part of its industrial engines after 25,000 h of operation, it executes the main inspection after 50,000 h.

4. **High requirements for fuel quality**

In theory, in the gas turbine units, any type of fuel can be used: solid, liquid, or gaseous. However, if the natural gas and the light grades of diesel fuel are burned in them without special difficulties, then the viscous heavy fuels require special preparation and restrictions on such elements as sulfur, vanadium, calcium, sodium, silicon, and lead. Sulfur and vanadium oxides can be laid on the turbine surfaces and can be a cause of their corrosion.

The operation of the main GTU parts: the fuel system, the combustion chamber, and the turbine, as well as their resource and reliability, depends significantly on the quality of the used fuel. The quality of the fuel also affects the maneuverability of the gas turbine unit, the convenience, and the ease of maintenance.

Natural gas should be considered as the ideal fuel for gas turbine units because it does not contain harmful impurities and does not pollute the GTU ducts during combustion. From this point of view, it is also the best type of fuel for the environment.

The use of liquid fuels in gas turbine units depends largely on their physicochemical properties.

**The heavy grades of the liquid fuel**:

– it contains more carbon, aromatic and unsaturated hydrocarbons, sulfur, tarry substances, and mechanical impurities;
– it has a higher viscosity, density, luminometric number, surface tension, and tendency to sedimentation;
– it has more asphaltenes, carbenes, carbides, sulfur, nitrogen, and acid compounds.

A consequence of the foregoing is that the use of the high-viscosity liquid fuels in a GTU is impossible without the inclusion of the complex, cumbersome, and expensive fuel preparation system that does not, however, provide the ideal result.

Compared to the gas turbine units, the diesel engines and, especially, the steam turbine plants are less demanding on fuel quality. The use of highly viscous fuels for them is a traditional technical solution.

## 10.3 Application of the Gas Turbine Units

The advantages and the disadvantages of the gas turbine units are determined by the features of their application in fields such as the electric power generation, industry, and transport [1].

**Electric power generation**

The first gas turbine unit for electric power generation was produced in Neuchatel (Switzerland) by "Brown, Boveri & Cie" in 1939. It was a standby unit with a power of 4,000 kW, and has been made according to a simple cycle. The initial gas parameters in the turbine inlet were: the pressure is 400 kPa, the temperature is 823 K; the rotor speed is 3,000 rpm. The actual efficiency which is determined during the tests was 17.4%.

Now the gas turbine plants are one of the main players in the electricity generation market, and have annual supply orders for a total power of up to 30,000 MW. This success is largely due to the presence in the world of large reserves of the natural gas, which, firstly, is a relatively cheap type of fuel, and secondly, having a high hydrogen content, it provides less carbon dioxide emissions into the atmosphere compared to the liquid and the solid fuels. Another factor which is contributing to the growth of GTU's popularity in the energy sector is the high (up to 60%) efficiency of the **combined cycle gas turbine (CCGT) plants** which are created on their basis. Another advantage is the wide power range of the produced gas turbine units, i.e. up to 340 MW for simple cycle GTUs and up to 500 MW in the combined cycle plants.

Now about 27% (in value cost) of all gas turbine engines which have been produced in the world are intended for driving electric generators.

Table 10.4 shows the main fields of GTU application for the electric power generation. For comparison, the power of the steam turbine power station which is operated by use of coal is 200–800 MW, the nuclear fuel is 800–2,000 MW; their actual efficiency is 34–40 and 29–34%.

(1) **Standby power stations** are used for the emergency power supply of the hospitals, the office blocks, and other buildings when the main power is cut off. The generated electricity in this case is consumed locally and the units are not connected to the grid.

In this field, the most popular drive is a diesel engine, it is largely due to the wide variety of the produced automobile and marine models and, therefore, a low cost. GTUs have an advantage where weight and size come first (for example, if a standby power station is located on the roof of a building).

(2) **In small-sized combined heat and power (CHP) stations** the heat from the exhaust gas is used for industrial processes. Hot gas can be sent directly to the drying of something, or, passing through a heat recovery steam generator (HRSG), give their heat to boil the water and generate the steam, which is then used in industry.

Most of these power stations operate on natural gas. The generated electricity is often used only locally and it is not sent to the grid.

**Table 10.4** Main field of the gas turbine application for the electric generation

| Type of power station | Application examples | Power, MW | Plant efficiency,[3] % | Average operating time per year, h |
|---|---|---|---|---|
| Standby power stations with microturbines | Warehouses, small office blocks, restaurants | 0.04–0.25 | <15 | 0–500 |
| Standby power stations with simple cycle GTU | Office blocks, hospitals | 0.25–1.5 | 15–20 | 0–500 |
| Small-sized combined heat and power stations with GTU | Hospitals, small factories | 0.5–10 | 78–85 | 6,000–8,700 |
| Large combined heat and power stations with GTU | Electricity and heat supply to towns with a population of up to 25,000 people; large factories; export of electricity | 10–60 | 78–85 | 6,000–8,700 |
| Peak lopping power stations with simple cycle GTU | Supply to grid | 20–60 | 25–33 | 500–2,000 |
| Mid-merit power stations with simple cycle GTU | Supply to grid | 30–60 | 34–41 | 2,000–6,000 |
| Base load power stations with CCGT plants | Supply to grid | 50–450 | 51–59 | 6,000–8,700 |

The gas turbine units are the most suitable for this field. The stable market position has also the diesel engines, which are mainly used where a low-temperature level of thermal energy is acceptable or high values of the drive efficiency are required.

(3) **In large combined heat and power (CHP) stations** the exhaust gas heat is used to produce steam, which is sent then for the industrial needs (pulp and paper mills, etc.) or for heating of the buildings. The generated electricity can be consumed both locally and it can be supplied to the grid.

The gas turbine units are only used in this field. The diesel engines of such power have huge dimensions and weight, and are also not able to provide the required temperature level of the resulting steam.

(4) **Power stations that supply electricity to the grid** are divided into three categories:

[3] For combined heat and power (CHP) plants, this parameter also takes into account the use of heat.

- the peak lopping power stations,
- the mid-merit power stations,
- the base load power stations.

**Peak lopping power stations** are designed to meet the peak power demand of the system (for example, in the evening); the annual utilization rate is usually less than 10%.

**Mid-merit power stations** typically have a 30–50% utilization. They cover the seasonal increase in the electricity demand (for example, in winter).

**Base load power stations** are almost used 100% a year and they are used for the continuous and stable production of the electric energy.

For the base load, the GTU is used as part of the combined cycle plants in order to achieve the maximum efficiency. In this field, in recent decades they have competed successfully with the steam turbine plants by use of organic and nuclear fuels. They are currently considered the most effective and environmentally friendly source of the electrical energy.

**Industrial mechanical drive application**

There is the GTU which is used to drive a pump or a compressor. The most prolific example is the gas and oil industry which orders typically 1GW per year of the new engines. The majority of GTUs are installed onshore, although there is an offshore sector where engines are located on the platforms.

Now about 1.5% (in value cost) of all gas turbine engines which have been produced in the world are used in the industry.

**Transport**

**Air transport**

The study of the used gas turbine engines in aviation began in the late 1920s. In 1935, the German engineer **Hans Joachim Pabst von Ohain** patented, and in 1936, with the assistance of Max Khan, he designed and tested the experimental model of the turbojet gas turbine engine. Working for Ernst Heinkel's company, they created a **HeS 3b** engine with a thrust of 4.4 kN, which on August 27, 1939, took the aircraft He 178 into the air (the world's first flight of the aircraft with a gas turbine engine).

In 1929, the English engineer **Frank Whittle** was invited for the design of the turbojet engines. At first, **W.U**. experimental engine was tested by him in April 1937. Subsequently, with the participation of specialists from "Rover Co., Ltd." the turbojet engine **W.1** was created with the thrust of 3.8 kN, which on May 15, 1941, has been taken into the air by the E.28/39 "Pioneer" aircraft. Since January 1943, the development of F. Whittle engines was carried out by "Rolls-Royce Ltd".

The post-war period was marked by the rapid development of the military and civil aviation GTUs. This period was greatly facilitated by the achievements of English and German engineers, which were intensively used by engine manufacturers in the USA, the Soviet Union, France, Sweden, and some other countries to establish their own GTU production.

Now the gas turbine engine due to its excellent weight and size characteristics completely displaced the piston engine in most types of aircraft. The exception is small aircraft with a flight speed of up to 0.3 M.

It should be noted that at present about 70% (in value cost) of all gas turbine engines which are produced in the world are intended for aviation.

**Land transport**

One of the promising fields of GTU application is a **railway transport**. The first projects to equip locomotives with this drive appeared in the 1920s.

In 1939, immediately after the successful completion of work on its first industrial gas turbine unit, "Brown, Boveri & Cie" (Switzerland) began to develop the world's first locomotive with GTU. At the end of 1941, **the locomotive "1101"** was put into operation on the Swiss railways. The GTU had a power of 1.7 MW, its efficiency was 15.5%.

The country in which GTU locomotives were widespread the most is the USA. This fact is explained by the insufficient number of electrified railways in the USA in the first half of the twentieth century. In the late 40s, "General Electric Co." on the basis of the aircraft engines TG100 and TG180 which have been created 3.4 and 6.3 MW gas turbine units which are working with an electric generator. In total, 55 units of GTU locomotives in the USA were built.

It should be noted that the energy crises of the 70s and 80s, which caused a significant increase in oil prices, led to a sharp decline in the interest in gas turbine trains. Many of them were decommissioned during this period as uneconomical. Now the use of gas turbine engines in railway transport is mainly experimental. Among the latest research in this field, mention should be made of the design of the "**JetTrain**" turbotrain of the Canadian company "Bombardier Inc.". The train's drive is a 4 MW ST40 gas turbine engine of the Canadian branch of "Pratt & Whitney Corp.".

In the late 40s and early 50s, several European and American companies began to develop special **gas turbine engines for cars**. In 1948, English firms "Centrax Ltd." and "Rover Co., Ltd." examined the first experimental samples, and in 1950 the first car, which has been driven by a gas turbine engine, was successfully tested on a track near Birmingham (England). It was "Rover Car Co." **"Jet 1"**. A gas turbine engine with a power of 150 kW provided a speed of up to 180 km/h for a two-seater roadster. In the 50–60 s, "Rover Co., Ltd." created several more successful designs that were mainly used on racing cars.

The research in the field of car GTU in the second half of the twentieth century was conducted by "General Motors Corp.", "AB Volvo", "Turbomeca SA", "Boeing Co.", "General Electric Co.", "C. A. Parsons & Co.", "Kawasaki Heavy Industries, Ltd.", and many other companies. It should be noted that the gas turbine engine, despite its excellent size and environmental characteristics, could not be widely used in the car industry. Their main disadvantages in comparison with traditionally used high-speed piston engines are the worst throttle response (when you press the fuel pedal, the increase in power and the increase in the number of revolutions of the gas turbine engine are delayed for several seconds relative to the position of the specified pedal) and efficiency. The latter is especially pronounced when working

in partial modes, which prevail for cars. The cost of manufacturing a gas turbine engine, which is explained by the lack of established large-scale production is also significantly higher.

More successful is the use of the **gas turbine engines for tanks**. In 1954, the experimental 485 kW gas turbine engine PU2979 of "C. A. Parsons & Co." was tested on one of the "Conqueror" tanks (England). In the 60s, several Swedish "Strv 103" (as part of a combined diesel and gas turbine plant) were equipped with experimental engines of this type.

Two states in the world produced GTU tanks: the Soviet Union and the USA.

In 1976, the large-scale production of the main **Soviet battle tank T-80**, equipped with the GTD-1000 T gas turbine engine has been started. In 1990, the T-80U tank with a new GTD-1250 engine was adopted by the Soviet army. However, in 1992, the production of tanks with gas turbine plants in Russia was canceled.

T-80s and their modifications are currently in service with the armies of Russia, Belarus, Cyprus, South Korea, and Kazakhstan. In total, from 1976, more than 6500 such tanks were produced.

AGT1500 engine is installed at **M1 "Abrams"** which is the main battle tank of the US ground forces and naval corps. From 1979 to 2006, about 9,000 such tanks were manufactured. With a weight of 62 tons, the maximum speed is 67 km/h. The gas turbine engine provides the tank acceleration to a speed of 30 km/h in 6 s. M1 "Abrams" is also used by the armies of Australia, Egypt, Saudi Arabia, and Kuwait.

The gas turbine engine is also used in tanks as an auxiliary power unit. An example is GTU "Oredon IV" of "Turbomeca S.A." (France), used on the tanks of the French, American, and Korean armies, as well as the army of Saudi Arabia.

### Marine transport

After the end of World War II, many manufacturers of aircraft gas turbine engines began to work on the creation of marine gas turbine units. For this purpose, the commercially available designs of the turboprop and the turbojet engines were used as initial ones, which were subjected to special conversion.

The world's **first navy ship** which is equipped with a GTU power plant was the gun boat ("Motor Gun Boat") MGB 2009 (Great Britain), on which in 1947 it was successfully tested the engine G.1 "Gatric" with power of 1.86 MW of "Metropolitan-Vickers Electrical Co. Ltd.".

Now the gas turbine engine is used at power plants of many navy ships (patrol and missile boats, patrol and anti-submarine ships, frigates, corvettes, destroyers, cruisers, light aircraft carriers, hydrofoils, and hovercrafts), successfully competing in this field with the diesel engines. The gas turbine engines are used in the navies of 40 countries in Europe, Asia, and America. At present, more than 500 ships (including more than 300 displacement ships) with GTU are in operation.

In the 1950s, the **first gas turbine units appeared on commercial ships**.

The test operation of the "Auris" tanker of the English company "Anglo-Saxon Petroleum Co. Ltd." which is equipped with a 955 kW gas turbine generator has been executed from October 1951 to 1960.

In 1956, in connection with the campaign which is conducted by the US Maritime Administration to select the most suitable type of energy drive for transport ships, “General Electric Co.” placed on board the vessel “John Sargeant” (one of four vessels of the type “Liberty” which is allocated for this purpose) the gas turbine unit with a power of 4.4 MW.

The relatively large construction of the gas turbine ships was observed in the first half of the 70s. According to 1978 data, 24 commercial vessels with a GTU were in operation. The marine gas turbine units for tankers, gas carriers, container ships, ferries, and ore carriers were produced during this period by “Zorya-Mashproekt”, “General Electric Co.”, “Pratt & Whitney Corp.”, “General Motors Corp.” (“Allison Division”), and others.

However, in the 80s, after a significant increase in oil prices, the using of GTU (as less economical compared to low-speed engine diesel) on commercial ships decreased significantly. Now GTUs are installed mainly on the high-speed freight and passenger ferries, as well as cruise liners. The scheme of a combined diesel and gas turbine unit with electric power transmission from both engines to propellers, “Integrated Electric Propulsion” (“IEP”), is becoming very popular.

The leading position in the field of marine gas turbine unit production is currently held by “General Electric Co.” (USA), “Rolls-Royce plc” (Great Britain), and “Zorya-Mashproekt” (Ukraine). The marine engines which are produced by “Vericor Power Systems Inc.” and “Pratt & Whitney Corp.” also find some use.

## Reference

1. Romanovsky GF, Serbin SI, Patlaychuk VM (2016) Gas turbine plants. Part 1.General structure and classification. Publisher NUS, Mykolaiv, 216 p. (in Ukrainian)

# Chapter 11
# Combined Marine Power Plants with Gas Turbine Engines


Now gas turbine engines are widely used in the power plants of navy ships for various purposes, i.e. patrol and missile boats, guard and anti-submarine ships, frigates, corvettes, destroyers, cruisers, light aircraft carriers, hydrofoil and hovercraft ships.

The operation with **maximum speed** is usually very short for all types of navy ships. The most of time ships move at **cruising speed**, which is significantly less than the maximum speed. If the power plant will consist of only a single engine, this engine most of the time will work at partial operating modes.

One of the main disadvantages of gas turbine engines is the low efficiency in partial operation modes. Therefore, if we use only a single GTU, the most of time its efficiency will be very low.

For this reason, the power plants for navy ships are combined. They contain two parts—**the marching part**, which is designed to provide a cruising speed, and **the accelerator part**, designed together with the marching part (or instead of it) to provide the full (maximum) speed of the ship.

As marching engines, diesel engines are often used; gas turbine engines are used less often. There are examples of applications as a march part of a steam turbine plant.

As accelerator engines, the gas turbine units of a simple thermodynamic cycle are widely used.

We consider the main types of combined marine power plants with gas turbine engines [1].

## 11.1 Combined Diesel or Gas (CODOG)

The combined diesel and the gas turbine plant, in which diesel engines are used as marching engines, and the gas turbine engines are used as accelerator ones. The maximum speed is provided only by gas turbine engines (Fig. 11.1).



K. Liu et al. (eds.), *Gas Turbines Structural Properties, Operation Principles and Design Features*, https://doi.org/10.1007/978-981-99-0977-3_11

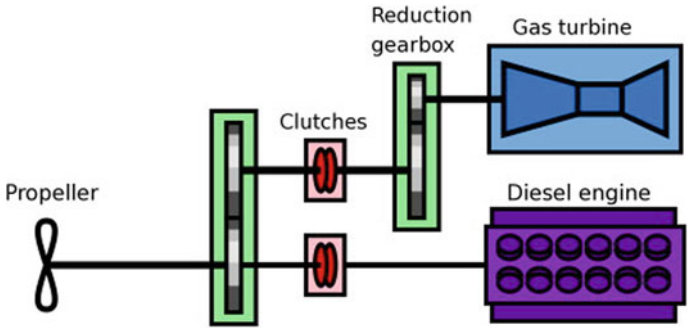


**Fig. 11.1** CODOG type marine power plant

For each propeller, as a rule, one diesel engine and one gas turbine engine are provided. Both of them are connected to the shaft by use of the special clutches, which ensure their alternate inclusion in the work.

The advantage of the CODOG type (compared to the CODAG type) is the simpler design of the gearboxes of the power plant, the disadvantages are:

- the need for more powerful accelerator engines to provide the required maximum speed;
- the higher specific fuel consumption of the power plant at full speed. The diesel is more economical than the gas turbine engines. Even if they generate only part of the total power, the total fuel consumption will be less.
- 7 frigates of "Georges Leygues" class (France, 1979–1990);
- destroyer "Ishikari" (Japan, 1981);
- 8 frigates of "Bremen" class (Germany, 1982–1990);
- 24 "Pohang" class corvettes (South Korea, 1984–1993);
- 3 frigates of "Vasco da Gama" class (Portugal, 1991–1992);
- 12 frigates of "Halifax" class (Canada, 1992–1996);
- 6 corvettes of "Gepard" 1166.1 (Russia, Vietnam, 1993–2016);
- 4 frigates of "Brandenburg" class (Germany, 1994–1996);
- 10 frigates of "Anzac" class (Australia and New Zealand, 1996–2006);
- 5 "Visby" class corvettes (Sweden, 2000–2009);
- 4 frigates of "De Zeven Provinciën" class (Netherlands, 2002–2005);
- 3 frigates of "Shivalik" class (India, 2010–2012).

## 11.2 Combined Diesel and Gas (CODAG)

The combined diesel and gas turbine plant, in which diesel engines are used as the marching engines, and the gas turbine engines are used as accelerator ones. The maximum speed is ensured by the joint operation of diesel and gas turbine engines (Fig. 11.2).

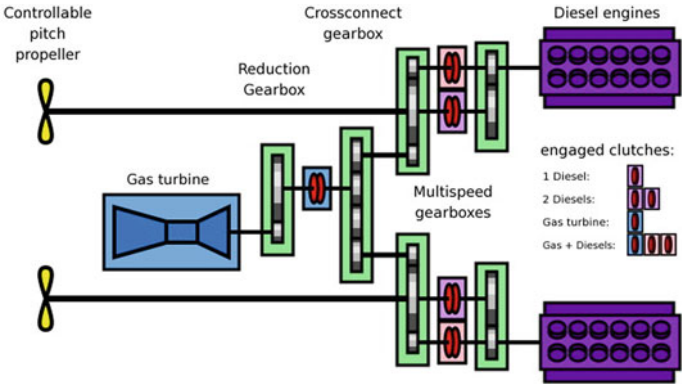


**Fig. 11.2** CODAG type marine power plant

A feature of these plants is the use of two-speed gearboxes (at different modes they provide different speeds of rotation of the output shaft), which allow for the operation of the diesel engines in both modes without reducing efficiency.[1]

Compared to purely diesel power plants, the CODAG type has significantly smaller dimensions and weight with a high total efficiency of the plant, from which mainly diesel engines are operated (moreover, at the nominal operating mode).

The typical cruising speed of ships with CODAG is about 20 knots, the maximum speed is about 30 knots.

In some cases, the diesel and gas turbine engines can operate each on their own output shaft and their propeller. This arrangement avoids the use of the complex multi-speed gearboxes; however, it has the following disadvantages:

– the propellers are not working in this mode causes which is braking the ship;
– due to the number of propellers in such power plants should be increased, their diameter is smaller, and therefore, their efficiency decreases.

**Examples of CODAG type used at the Navy**:

– 25 torpedo boats of 183TK type (Soviet Union, 1955–1957);
– 63 small anti-submarine ships of 204 type (Soviet Union, Bulgaria, Romania, 1960–1969);
– 54 frigates of 159 types (Soviet Union, Ethiopia, India, Syria, Vietnam, Azerbaijan, 1961–1978);
– 6 frigates of “Köln” class (Germany, 1961–1964);
– 18 frigates of 35 types Soviet Union, 1965–1967);
– 2 gun boats of the “Turunmaa” class (Finland, 1969);

[1] An increase in the power transmitted to the fixed-pitch propeller when the accelerator engine is connected will cause the propeller to switch from the optimal operating mode to the “hydrodynamically light” mode, in which the supplied power will not be fully used. To avoid this, the output shaft speed must be increased. In variable pitch propellers, the same effect can be achieved by switching the position of the propeller blades.

– 92 frigates of 1124, 1124M, 1124P, 1124R "Albatross" type (Soviet Union, Russia, Ukraine, Lithuania, 1970–2005);
– 67 missile boats of 1241.1, 1241.7, 1241RE and 1241.8 "Molniya" type (Soviet Union, Russia, Bulgaria, Poland, Romania, Germany, India, Ukraine, Yemen, Vietnam, 1981–2012);
– 2 small missile hovercrafts of 1239 "Sivuch" type (Soviet Union, Russia, 1989–2000);
– 8 frigates of "Karel Doorman" class (Netherlands, 1991–1995).

## 11.3 Combined Diesel-Electric and Gas (CODLAG)

The combined diesel and gas turbine plant, in which diesel engines are used as the marching engines, and the gas turbine engines are used as accelerator ones. The maximum speed is ensured by the joint operation of the diesel and gas turbine engines. It differs from the CODAG type in that the transfer of power from diesel engines to the propellers is not applied mechanical (as in the previous case), but electric (Fig. 11.3). Diesel generators produce electricity, which is transmitted to propeller motors. At full speed, with the help of special clutches, gas turbine engines are connected to the propeller shafts.

In such plants, the same diesel engines are used to move the ship and to provide it with electric energy, which reduces significantly the cost of the shipboard electric power station, as it reduces the number of the used drive engines, mechanisms and devices. In addition, the electric motors can operate in a wide range of rotational speeds and can be directly connected to the propeller shafts, which in turn leads to a significant simplification of the design of the gearboxes (i.e. there is no need for two-speed gearboxes).

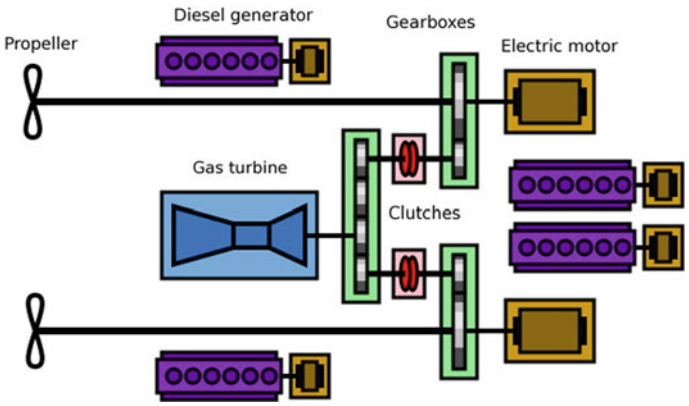


**Fig. 11.3** CODLAG type marine power plant

Another advantage of CODLAG type is that the diesel generators are not mechanically connected to other equipment and they can be placed separately in well-sound proofed rooms, which will reduce the overall noise of the power plant. This quality is especially valuable for anti-submarine ships.

The CODLAG type has found application on the following ships:

– 16 frigates of "Duke" class (Great Britain, Chile, 1990–2002).

## 11.4 Integrated Electric Propulsion (IEP)

The combined diesel and gas turbine plant, in which diesel engines are used as marching engines, and gas turbine engines are used as accelerator ones. The maximum speed is ensured by the joint operation of the diesel and gas turbine engines. Its difference from the CODAG and CODLAG types is that the transmission of power to the propeller shafts from all engines is electric.

This type of plant is also often named as Integrated Full Electric Propulsion (IFEP).

The IEP type was implemented on six destroyers of the "Daring" class (Great Britain, 2009–2014) (Fig. 11.4) and on the transatlantic ocean liner "Queen Mary 2" (2004). In the latter case, the power plant consists of four 17 MW "Wärtsilä" 16V46C-CR diesel engines and two 30 MW LM2500 gas turbine engines.

The IEP power plant is also implemented on four "Zumwalt" class destroyers (USA).

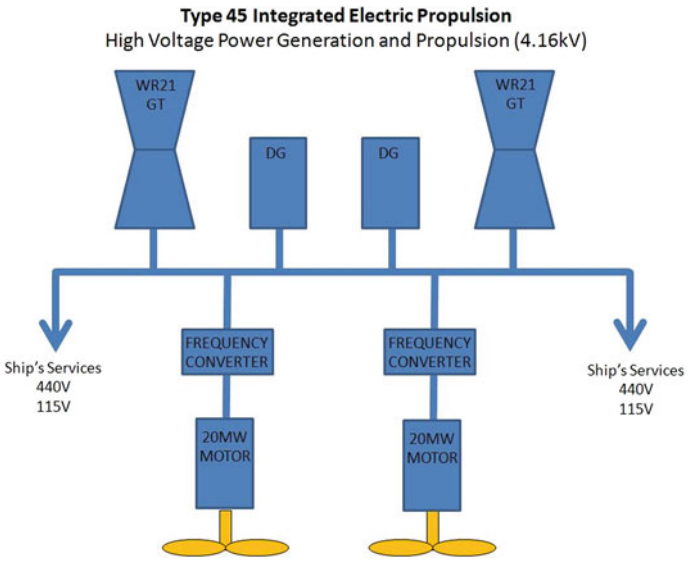


**Fig. 11.4** IEP power plant for English "Daring" class destroyers

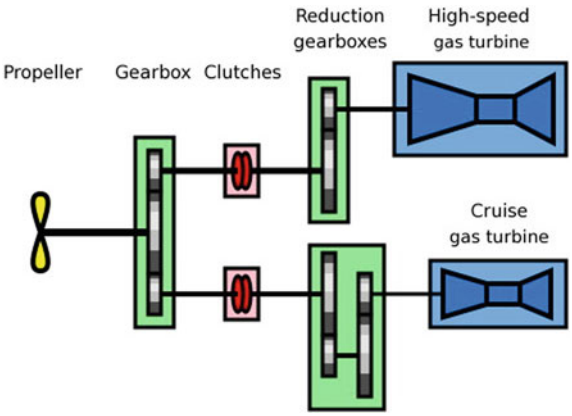


**Fig. 11.5** COGOG type marine power plant

## 11.5 Combined Gas or Gas (COGOG)

The combined gas and gas turbine plant, in which the gas turbine engines are used both as marching and accelerating engines. The maximum speed is provided only by accelerator engines (Fig. 11.5).

The efficiency of a combined gas and gas turbine plant is higher than the efficiency of a non-combined gas turbine plant because in this case all engines are operated at the nominal operating mode (100% power mode), which corresponds to their highest efficiency.

As a rule, gas turbine engines of high efficiency and relatively low power are used as marching engines, and high-power engines are used as accelerator engines (they have a short period of operation, and there are no special requirements for efficiency).

Because the joint operation of marching and accelerating engines is not provided, there is no need to use complex, expensive and potentially unreliable two- or three-speed gearboxes.

**Examples of using the COGOG type at the Navy**:

- frigate "Exmouth" (Great Britain, 1957);
- 8 frigates of "Amazon" class (Great Britain, Pakistan, 1974–1978);
- 16 destroyers of the "Sheffield" class (Great Britain, Argentina, 1975–1985);
- 10 frigates of "Broadsword" and "Boxer" classes (Great Britain, Brazil, Romania, Chile, 1979–1988).

## 11.6 Combined Gas and Gas (COGAG)

The combined gas and gas turbine plant, in which the gas turbine engines are used both as the marching and accelerating engines. The maximum speed is ensured by the joint operation of the marching and accelerating engines (Fig. 11.6).

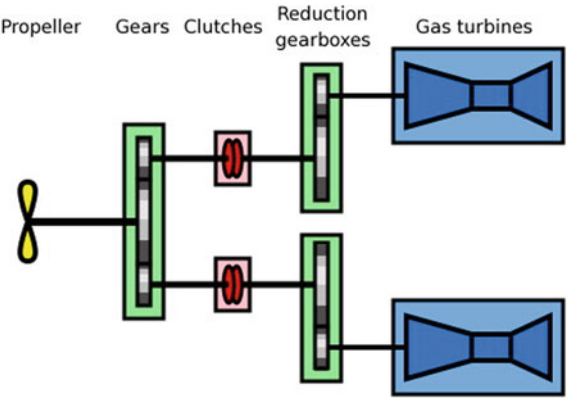


**Fig. 11.6** COGAG type marine power plant

The gearboxes and the clutches of such plants allow both types of gas turbine engines to transfer their power to the propeller shaft both individually (with the other engine switched off) and together (if necessary, the COGAG type can be converted to the COGOG type).

Application of combined plant allows all operating modes to operate gas turbine engines with the highest efficiency.

Compared to CODAG and CODOG types, COGAG has less weight and takes up significantly less engine room. Its disadvantage is the worst efficiency at cruising speed, and in comparison with CODAG type also at full speed.

**Examples of COGAG types used in the Navy**:

- 25 frigates of 61 types (Soviet Union, Russia, Poland, India, 1962–1988);
- 44 frigates of 1135 "Burevestnik" type (20 units), 1135 M "Burevestnik M" (11 units), 1135.1 "Nereus" (8 units), 1135.6 "Talwar" (5 units) (Soviet Union, Russia, Ukraine, India, 1970–2012);
- 7 cruisers of 1134B "Berkut-B" type (Soviet Union, Russia, 1971–1975);
- 31 destroyers of the "Spruance" class (USA, 1975–1983);
- 71 frigates of "Oliver Hazard Perry" class (USA, Spain, Australia, Taiwan, Pakistan, Bahrain, Egypt, Poland, Turkey, 1977–2004);
- 13 missile boats of 1241.1 "Molniya" type (Soviet Union, Russia, 1979–1984);
- 3 light aircraft carriers of "Invincible" class (United Kingdom, 1980–1985);
- 13 frigates of 1155 "Frigate" type (Soviet Union, Russia, 1980–1999);
- 4 destroyers of the "Kidd" class (USA, Taiwan, 1981–1985);
- 27 cruisers of the "Ticonderoga" class (USA, 1983–1994);
- 4 frigates of "Cornwall" class (Great Britain, 1988–1990);
- 62 destroyers of "Arleigh Burke" class (USA, 1991–2012);
- 2 frigates of 1154 "Yastreb" type (Russia, 1993–2009);
- 9 destroyers of the "Murasame" class (Japan, 1996–2002);
- 3 destroyers of the "Delhi" class (India, 1997–2001);
- 2 destroyers of the "Hyūga" class (Japan, 2009–2011).

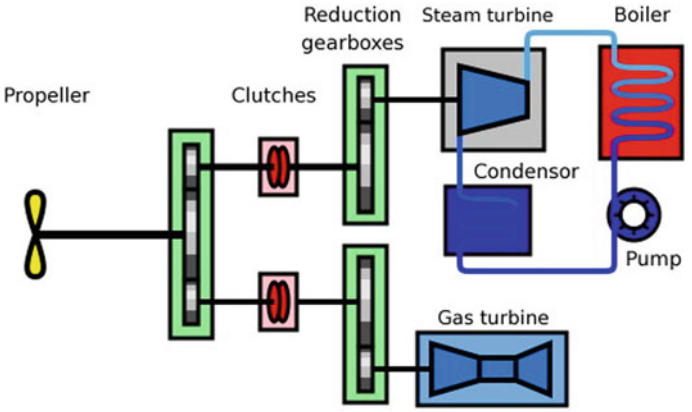


**Fig. 11.7** "COSAG" type marine power plant

## 11.7 Combined Steam and Gas (COSAG)

The combined steam and gas turbine plant, in which the steam turbine plant is used as the marching plant, and the gas turbine engines are used as the accelerator plant. The maximum speed is ensured by the joint operation of the steam turbine plant and the gas turbine engines (Fig. 11.7).

The gearboxes and the clutches allow both types of plants to transmit their power to the propeller shaft both individually (with the other plant disconnected), and together.

COSAG type combines the good efficiency and reliability of a steam turbine plant at cruising speed with the ability to start-up quickly and gain the power from the gas turbine engines at full speed.

The COSAG type got some application on the first ships which are equipped with gas turbine engines. Now they are rarely used.

**Examples of COSAG type used at the Navy**:

- 8 destroyers of the "County" class (Great Britain, Chile, Pakistan, 1962–1970);
- 7 frigates of "Tribal" class (Great Britain, Indonesia, 1961–1964);
  - a light aircraft carrier of "Dédalo" (Spain, 1976).

## Reference

1. Romanovsky GF, Serbin SI, Patlaychuk VM (2016) Gas turbine plants. Part 1.General structure and classification. Publisher NUS, Mykolaiv, 216 p. (in Ukrainian)

# Chapter 12
# Design and Operation of the Gas Turbine Parts. Inlet Casings of the Gas Turbine Unit


The inlet casing is designed for a smooth and uniform circumferential supply of atmospheric air to the compressor. The circular unevenness of the velocity at the entrance can lead to the appearance of vibration of the first stage blades and their possible breakdown.

The most favorable is the application of the **axial-type inlet** to the compressor. In this case, the circumferential symmetry of the entrance can only be violated by the radial struts connecting the outer casing to the bearing casing. However, with a sufficient distance of the struts from the blades of the first stage and with their corresponding profile, the influence of the struts on the velocity can be minimized.

Figure 12.1 shows the axial-type inlet casing of the D050 marine gas turbine engine. It consists of outer and inner surfaces. The annular channel between them serves as the beginning of the engine flow path [1].

The outer surface 1 is made welded and consists of the flanges “b”, “d” and the walls “a”, “c”. Using the flange “d”, the surface is attached to the front casing. On the flange “b”, there are holes for connection to the air intake room.

The inner surface is also made welded, and consists of the flange “e”, the wall “f”, and the flange “g”. Using the flange “g”, it is attached to the front casing. The flange “e” has a hole for mounting of the inner surface, which is closed by the inner surface cover 3.

Figures 12.2 and 12.3 show the gas turbine engines with axial-type inlet casings [2, 3].

The axial-type inlet casings are widely used in aircraft gas turbine engines and the engines which are converted from the aircraft.

The axial inlet to the compressor often uses the intake air from a special room, separated from the engine room by a partition. An example of such a design is shown in Fig. 12.4 [3].

With the obvious advantages of the axial air supply to the compressor, its use in stationary and transport gas turbine units is limited, due to the axial supply:

– it is necessary to use a special room for the intake air,
– the consumer (load) cannot be located on the compressor side,



K. Liu et al. (eds.), *Gas Turbines Structural Properties, Operation Principles and Design Features*, https://doi.org/10.1007/978-981-99-0977-3_12

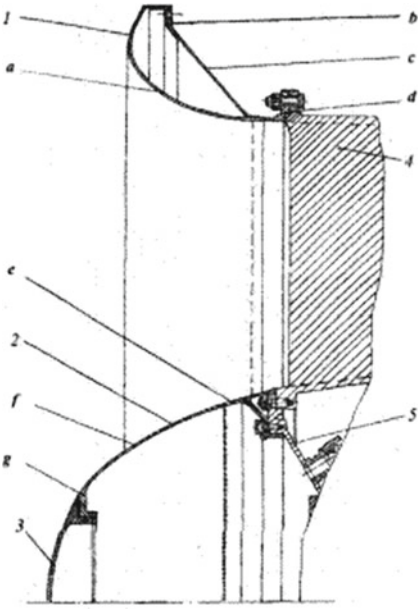


**Fig. 12.1** Inlet casing of D050 engine: *a*, *c*—walls; *b*, *d*—flanges; *e*, *g*—flanges; *f*—wall; 1—outer surface; 2—inner surface; 3—inner surface cover; 4—front casing; 5—wall

**Fig. 12.2** UGT 16,000 with axial-type inlet casing

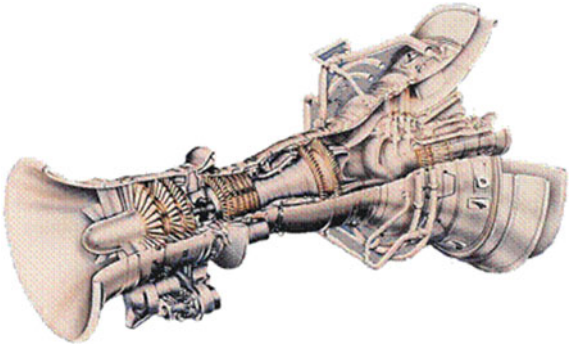

**Fig. 12.3** LM1600 "General Electric Co." with axial-type inlet casing

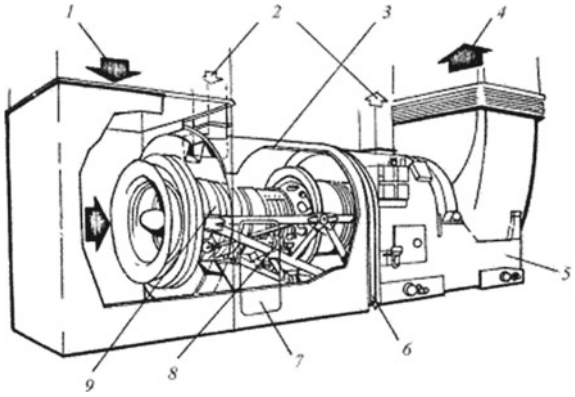


**Fig. 12.4** Marine engine "Olympus TM3B" in special box: 1—air intake; 2—engine casing cooling air; 3—special engine box; 4—gas exhaust; 5—power turbine frame; 6—flexible connection; 7—inspection hatch; 8—engine frame; 9—engine

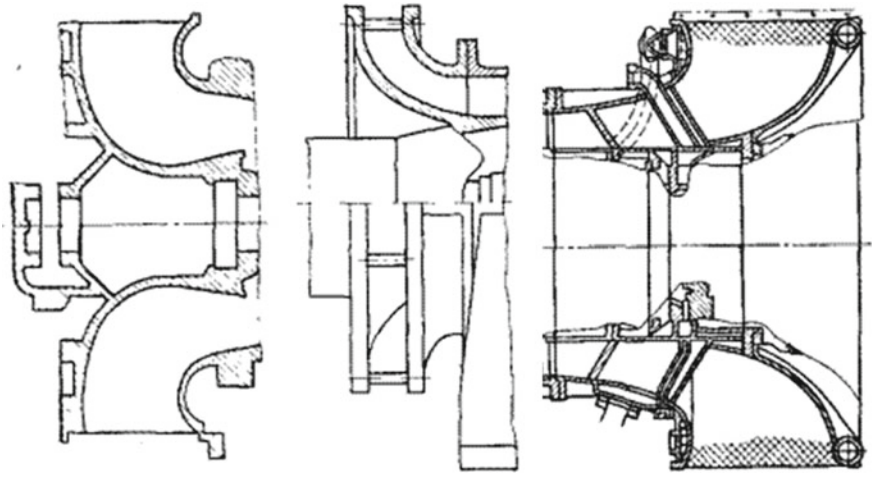

**Fig. 12.5** Ring-type inlet casings

– the access to the compressor front bearing and its disassembly is difficult because the inlet casings of this type are often executed without horizontal connectors.

The application in the gas turbine units gave the **ring-type air supply** to the compressor. The air flow enters the ring-type inlet casing in the radial direction from the periphery to the center, and then inside it rotates in the axial direction to the compressor inlet (Figs. 12.5 and 12.6) [2, 3].

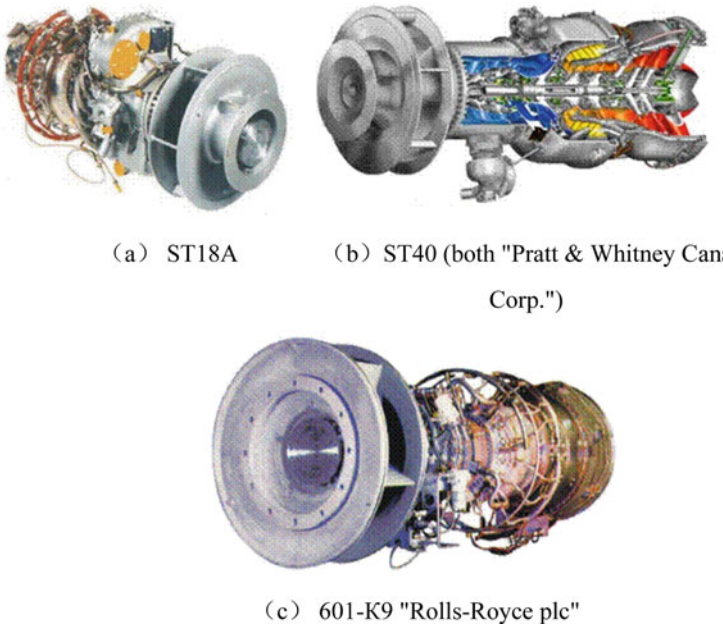


**Fig. 12.6** Gas turbine engines with ring-type inlet casings

Such casing usually uses the intake air directly from the engine room, therefore it can be used either for the low-power plants or for the stationary and transport high-power plants which are placed in separate boxes, the access to which is excluded during the operation of the GTU.

The advantage of the ring-type inlet casings is the free assembling of the auxiliary mechanisms and the access to the front compressor bearing. The struts that connect the bearing casing to the outer compressor casing can be made more rigid and durable than the hollow radial struts in the compressor with the axial inlet. In addition, these struts can be placed at a much greater distance from the compressor blades.

The widespread application in the gas turbine units gave the **inlet casings with one-sided radial input**. The intake air to such casings usually flows through the rectangular or circular air ducts from the intake air rooms, where it is filtered and the suction noise is damped. However, it is also possible to use intake air directly from the engine room.

In the inlet casings of the radial type, two zones can be distinguished: in the first zone the rotation and uniform distribution of the flow to the annular channel is carried out; in the second zone the flow accelerates in front of the compressor blades.

In the **knee-shaped inlet casings** (Fig. 12.7a, b) both of these zones have a smooth transition. Therefore, the pressure losses in them will be minimal, and the uniformity of the air supply around the circumference will be maximum for the radial-type casings [1, 2].

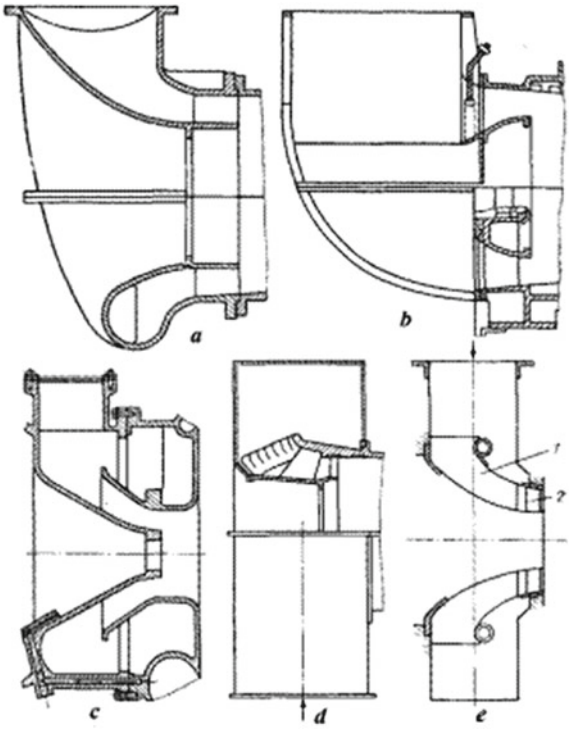


**Fig. 12.7** Radial-type inlet casings: 1—radial ribs; 2—radial blades

However, such inlet casings have relatively large axial dimensions. It complicates the mounting of the compressor front bearing and complicates the access to the bearing.

The knee-shaped inlet casings are mainly molded to create the necessary smooth configuration. The connection of both surfaces of the inlet casings is carried out by radial ribs. In some casings, only the confuser part is molded, and everything else is made of thin-walled sheet steel. So, the inlet casing of a marine gas turbine engine, shown in Fig. 12.7b, is welded from thin sheet steel to reduce the weight. Because the rigidity of the casing is insufficient to absorb the load from the rotor, an aperture is made in its lower part, inside of which is located the front bearing and the drive of the auxiliary mechanisms.

The example of the engine with a knee-shaped inlet casing is shown in (Fig. 12.8).

The complexity of the front bearing mounting and the difficult access to it led to the fact that, despite the most favorable forms from the point of view of aerodynamics, these inlet casings were not widely used.

The application in all stationary and transport gas turbine units gave the **snail-type inlet casings**, which partially cover the compressor casing (Fig. 12.7c–e). These casings are characterized by the fact that due to the large free space above the compressor casing, a uniform air supply to the annular section of the confuser is

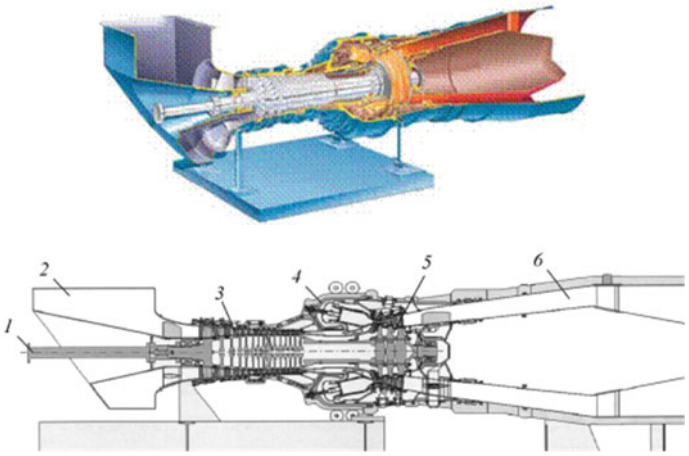


**Fig. 12.8** SGT-800 "Siemens AG" with a knee-shaped inlet casing [2]. 1—output shaft; 2—inlet casing; 3—compressor; 4—combustion chamber; 5—turbine; 6—exhaust casing

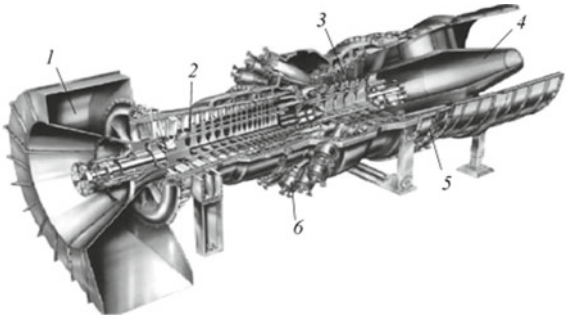


**Fig. 12.9** SGT6-6000G "Siemens AG" with snail-type inlet casing: 1—inlet casing; 2—compressor; 3—turbine; 4—exhaust casing; 5—turbine casing; 6—combustion chamber

achieved with relatively small pressure losses. As a result, the length of the inlet casing is reduced and the access to the front bearing is freed.

The snail-type inlet casings are mainly used due to their small axial size. In most cases, the confuser is curved with a minimum turning radius. In some casings, the annular guide ribs are provided (Fig. 12.7e).

Figures 12.9, 12.10 and 12.11 show the gas turbine engines with snail-type inlet casings [2, 3].

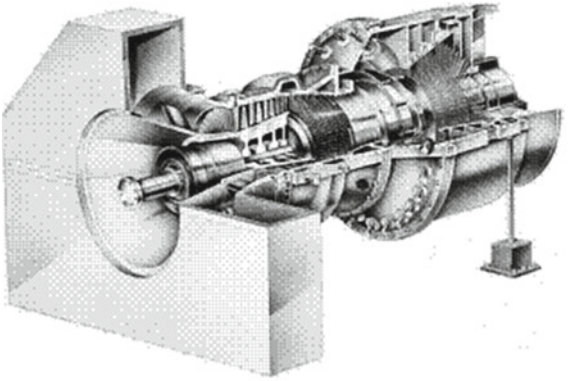

**Fig. 12.10** SGT5-3000E "Siemens AG"

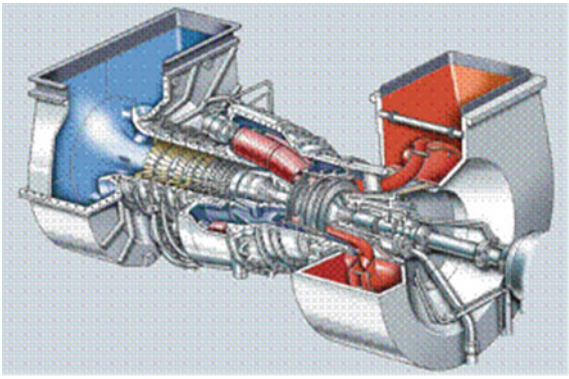

**Fig. 12.11** SGT-100-2S "Siemens AG"

## References

1. Romanovsky GF, Serbin SI, Patlaychuk VM (2005) Modern gas turbine units. Volume 1. Production units of Ukraine and Russia. Publisher NUS, Mykolaiv, 344 p. (in Ukrainian)
2. Romanovsky GF, Serbin SI, Patlaychuk VM (2016) Gas turbine plants. Part 1.General structure and classification. Publisher NUS, Mykolaiv, 216 p. (in Ukrainian)
3. Romanovsky GF, Serbin SI, Patlaychuk VM (2008) Modern gas turbine units. Volume 2. Production units of Western European countries. Publisher NUS, America and Asia, Mykolaiv, 420 p. (in Ukrainian)

# Chapter 13
# Compressor Part of the Gas Turbine Unit


The function of the GTU compressor part is to increase the pressure of the working fluid (atmospheric air). The compressor is driven by the power from the turbine of the same GTU.

The compressors of the volume type (the piston, screw and gear compressors) due to low efficiency and productivity in the GTU are not used.

The gas turbine units use vane compressors of the following types:

- axial-type;
- centrifugal-type;
- axial-centrifugal-type.

Currently, the dominant type of GTU compressor is an axial compressor. The use of the remaining types is limited only by some narrow fields of application in which the use of the axial compressor is undesirable for one reason or another [1–3].

## 13.1 The Structure and Operation of the Axial Compressor

The multi-stage axial compressor of the gas turbine engine is shown in Fig. 13.1 [4]. Its main parts are the inlet casing 1; the front casing 2; the inlet guide vanes 3; the rotor 6 with moving blades 4; the main casing 7, to which the guide vanes 5 of the individual stages are attached; the rotor bearings 11 and 14; the exit (outlet) guide vanes 9; the rear (exit) casing 10.

The air in the compressor passes through the following elements: the inlet casing, the inlet guide vanes, several stages, the exit guide vanes and the rear casing. We consider the function of these elements.

**The inlet casing** is designed for uniformly circumferential air supply from the atmosphere to the compressor blades. The type of the inlet casing is selected from the layout conditions. If the axial size of the compressor is not limited, we accept the



K. Liu et al. (eds.), *Gas Turbines Structural Properties, Operation Principles and Design Features*, https://doi.org/10.1007/978-981-99-0977-3_13

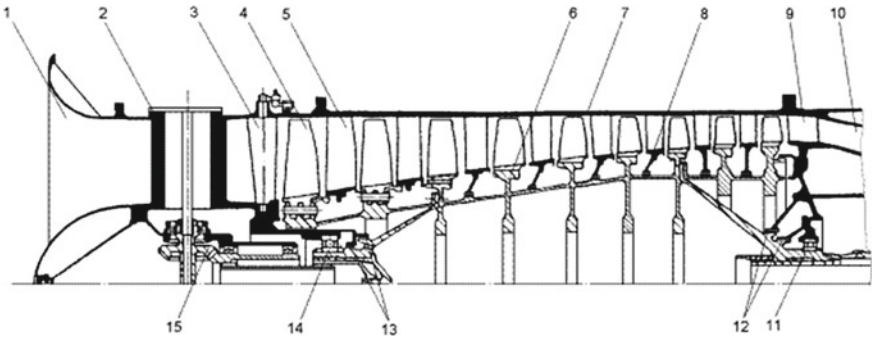


**Fig. 13.1** Multistage axial compressor of gas turbine engine. 1—inlet casing; 2—front casing; 3—inlet guide vanes; 4—blades; 5—guide vanes; 6—compressor rotor; 7—main casing of the compressor; 8—interstage radial seal; 9—exit (outlet) guide vanes; 10—rear (exit) casing; 11—rear bearing; 12—seals of the oil cavity of the rear bearing; 13—seals of the oil cavity of the front bearing; 14—front bearing; 15—drive of the front gearbox

axial-type inlet casing (as the most efficient). In other cases, the acceptance of the ring-type, the snail-type or the knee-shaped-type of the inlet casing.

**The inlet guide vanes** should give the necessary direction to the flow before entering the first stage (to increase its efficiency). The inlet guide vanes form confuser passages (with a decreasing flow area). During passing through them, as well as earlier through the inlet casing, the velocity increases and the pressure decreases. In order to control the operation of the compressor the inlet guide vanes can be rotary.

The combination of one row of the rotating blades and one row of the stationary guide vanes is called **the compressor stage** (Figs. 13.2 and 13.3). In the compressor stages, the air pressure rises due to the use of the mechanical energy of the rotor [5].

From the last compressor stage, air enters **an exit guide vanes** designed to give an axial direction of air before entering the rear casing.

**The rear (exit) casing** is designed to supply air from the compressor to the combustion chamber or to the next compressor.

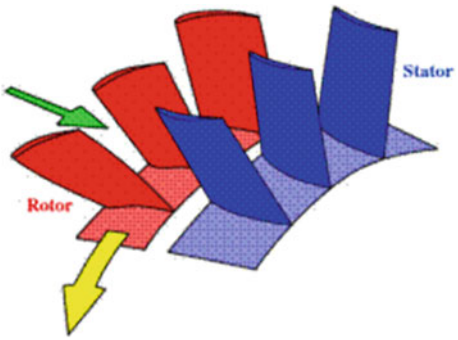


**Fig. 13.2** Axial compressor stage

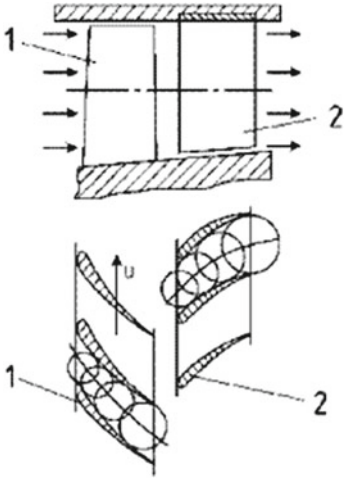


**Fig. 13.3** Axial compressor stage 1—blades; 2—guide vanes

**In the axial compressor stage, there is a double conversion of energy**. At the first step, the mechanical energy of the rotor is converted into kinetic energy of air flow. Compressor blades during rotation by the input edges accelerate air. At the second step, the kinetic energy of the air is converted into potential energy when it is moving through diffuser passages between blades and guide vanes. Air velocity decreases, pressure, temperature and enthalpy increase.

We consider the movement of air through the passages between the blades and the guide vanes.

In Fig. 13.4 we can see the airfoils of several blades and several guide vanes of the compressor stage. To analyze the movement of air, we will use a coordinate system consisting of the axial $a$ and circumferential $u$ directions. The **axial direction** is parallel to the central axis of the rotor. The **circumferential direction** is directed tangentially to the compressor wheel in the side of rotation.

From the previous stage, the air exits with the velocity $c_1$ and at the angle $\alpha_1$. If the passages between the blades would not rotate together with the rotor, the air with the same velocity and at the same angle would enter these passages. But the rotor and the passages move. And if we want to find the velocity $w_1$ and angle $\beta_1$ of entry of air into the passages between blades, then we need to subtract the circumferential velocity vector $u$ from the velocity vector $c_1$:

$$\overline{w}_1 = \overline{c}_1 - \overline{u}.$$

The circumferential velocity is directed in the circumferential direction and may be calculated by the following formula:

$$u = \frac{\pi D_m n_c}{60},$$

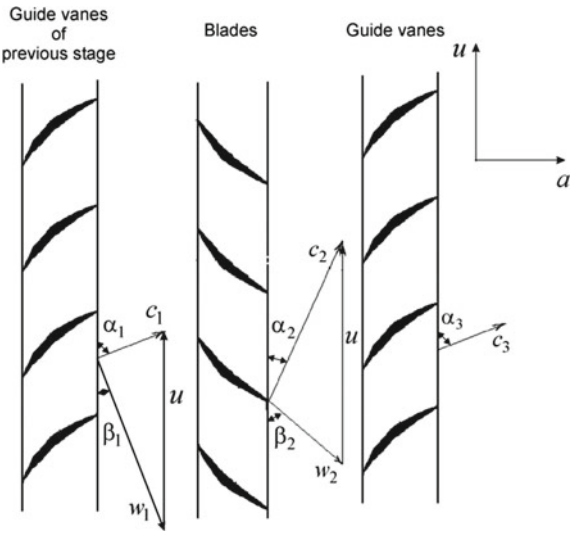


**Fig. 13.4** Velocity triangles for axial compressor stage

where $D_m$ is a medium diameter of the compressor stage, m; $n_c$ is a—rotational compressor speed, rpm.

From the passages between blades, the air exits with the velocity $w_2$ and at the angle $\beta_2$. We straighten hypothetically the single passage along the line of the movement (Fig. 13.5a). This passage has a shape with an increasing flow area; therefore, it is a diffuser. During the movement in such passage, the air velocity will decrease, and the pressure, temperature and enthalpy will increase [3]:

$$w_1 > w_2; \quad p_1 < p_2; \quad T_1 < T_2; \quad h_1 < h_2.$$

Therefore, we have the conversion of the kinetic energy of air into potential energy.

Considering the latter parameters, we are mainly interested in pressure, the increase of which is required from the compressor.

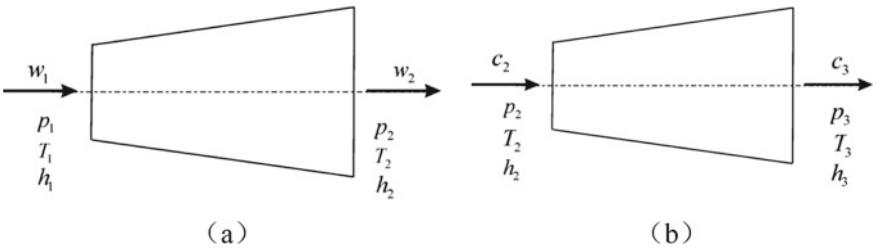


**Fig. 13.5** The passage between compressor blades (**a**) and passage between compressor guide vanes (**b**)

If we want to find the velocity $c_2$ and the angle $\alpha_2$ of entry of air into the passages between stationary guide vanes, we need to add the circumferential velocity vector $u$ to the velocity vector $w_2$:

$$\overline{c}_2 = \overline{w}_2 + \overline{u}.$$

From the passages between guide vanes, the air exits with the velocity $c_3$ and at the angle $\alpha_3$. We straighten hypothetically the single passage along the line of the movement (Fig. 13.5b). This passage has a shape with an increasing flow area, therefore, it is also a diffuser. During the movement in such passage, the air velocity will decrease, and the pressure, temperature and enthalpy will increase:

$$c_2 > c_3; \quad p_2 < p_3; \quad T_2 < T_3; \quad h_2 < h_3.$$

Therefore, we have the conversion of the kinetic energy into the potential energy also in the passages between the guide vanes.

The engineers are trying to design the axial compressor stages in such a way that the velocity and the angle of the air exit from the stage are approximately equal to the velocity and the angle of the entry into the stage:

$$c_3 \approx c_1 \quad \text{and} \quad \alpha_3 \approx \alpha_1.$$

**Advantages of the axial compressors**:

- a high efficiency (for the single stage $\eta_{st.c} = 0.89 \sim 0.91$);
- a high productivity (the modern GTUs had air consumption up to 800 kg/s);
- a simple creation of a multi-stage compressor;
- a small outer diameter (for aircraft engines, this means a small drag);
- the rotor speed is in accordance with the speed of the drive turbine (the gear is not needed).

**Disadvantages of the axial compressors**:

- a small optimal pressure ratio of the single stage (as a rule, $\pi_{st.c} = 1.15 \sim 1.35$);
- a large number of blades and guide vanes (within each row—several tens, sometimes more than a hundred), which complicates the GTU and increases its cost;
- a high sensitivity of blades and guide vanes to air quality (dust and dirt on the surface of the blades increase their roughness and worsen the efficiency of the compressor);
- the blades are easily damaged by the items which are falling into the flow part during operation (GTU, unlike other types of engines, has a large number of small details, and their getting into the flow part is not exceptional case);
- a smaller (compared to the centrifugal compressors) range of the stable operating modes (i.e., it is a higher likelihood of **surging** on the partial operating modes).

**The surge** is the disruption of the operation of the vane compressor, due to a stall in the flow on the blades and guide vanes. This stall can lead to the blocking of the flow part and to the subsequent pulsating movement of air through the compressor. This leads to the following:

- a strong vibration of the compressor blades and their possible breakdown;
- a decrease in air consumption through the gas turbine engine;
- a sharp increase in gas temperature behind the combustion chamber;
- a turbine power drop;
- a fuel unburning in the combustion chamber and the appearance of a smoky trace behind the gas turbine engine (when using the liquid fuel).

## 13.2 Axial Compressor Blades and Guide Vanes

### *13.2.1 Axial Compressor Blades*

The blades of the axial compressor form diffuser passages (i.e., the passages with the increasing flow area), in which the mechanical energy of the rotor is converted into the potential energy of the working fluid (the increasing air pressure).

The compressor blades have a profile part (so-called **airfoil**) 1 and a locking part (**root**) 2 (Fig. 13.6).

Due to the different angles of the flow on the blade airfoil along its length, **the blades are twisted**, i.e., have a different airfoil orientation relative to the incoming flow by length. The spin of the blades increases with their length. For this reason, the blades of the first compressor stages are tightly twisted (as the longest) [5].

The blades withstand significant centrifugal and bending forces and are also under the vibration loads of various natures. The high requirements are imposed on the accuracy of the airfoil processing and the cleanliness of its surface because these factors determine the efficiency of the compressor and the strength of the blades. The blades are polished, any scratches are removed so that they have very smooth

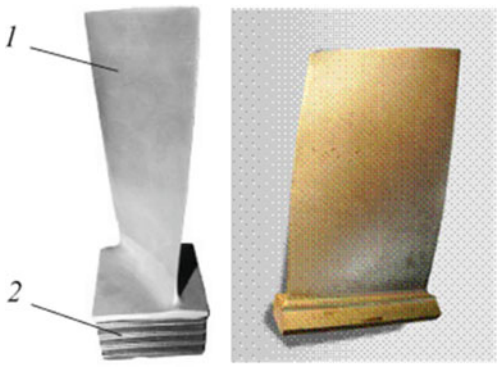


**Fig. 13.6** Axial compressor rotor blades. 1—airfoil; 2—root

transitions. The radius of transition from the airfoil to the root should be as large as possible in order to avoid an increased concentration of stresses.

To reduce the weight of the blades, tensile stresses and loads on the rotor, the blades are performed with decreasing chords and thicknesses, so that the peripheral sectional area can be significantly less than the root sectional area. In this case, the rigidity of the airfoil should be sufficient to maintain the installation angles in the most difficult conditions of the blade.

**The materials for the blades** of the axial compressors are stainless steel, heat-resistant alloys, titanium alloys and aluminum alloys.

Aluminum alloys are strong enough, to lend themselves well to forging, stamping and machining. They find application at temperatures up to 25 °C. To protect against corrosion, aluminum alloy blades are carefully anodized.

At higher temperatures (up to 500 °C), the blades which are made of titanium alloys operate well. The specific strength of such alloys in the temperature range 150–500 °C exceeds the specific strength of aluminum, magnesium alloys and steel.

The density of aluminum and titanium alloys is significantly lower than the density of steel, therefore, the blades at almost the same (in the range of the operating temperatures) strength limits have a lower weight and are under the lower tensile stresses from the centrifugal forces.

The advantage of the steel blades and the blades which are made of heat-resistant alloys is their high mechanical strength, less susceptibility to nicks and roughness when sand and small details get into the compressor, and a good operation at high temperatures.

**The connections of the blades with the rotor** must satisfy the following requirements:

– to have high strength;
– to allow easy mounting and dismounting of the blades;
– to be easy for producing;
– to provide the ability to accommodate the largest number of blades;
– to have a small weight.

In GTUs of both circumferential (in the annular-shaped grooves) and axial (in the individual grooves) mounting of the compressor blades is used.

**Circumferential mounting** is used in some stationary engines having a forged and welded compressor rotor, as well as in the stages of the aircraft engines (Fig. 13.7).

Figure 13.8 shows the **T-shaped mounting method** used by "English Electric Co." for engines EM-27P. Before mounting, each standard blade *1* is turned by 90°, lowered through the lock slot into a deep groove, then turned into a normal position and moved around the circumference of the groove. The last three blades are standard, locking *2* and fitting *3* are mounted in the sequence which is shown in Fig. 13.8. The locking blade has a rectangular root. Between the locking and fitting blades, a gasket *4* is provided to maintain the pitch. In the root of the last blade, plates 5 are installed, the antennae of which are bent to fix the blade [5].

A modification of the T-shaped mounting method is the **groove-type method of mounting**, which is widespread in recent decades in aircraft engines (Fig. 13.9).

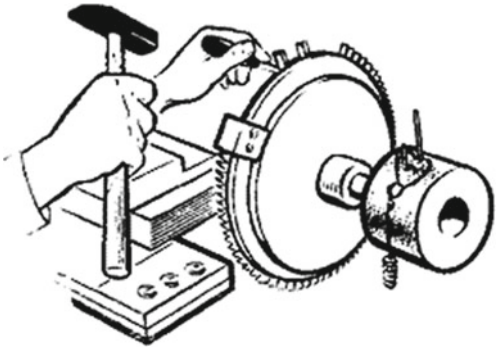

**Fig. 13.7** Circumferential mounting of rotor blades in annular-shaped grooves

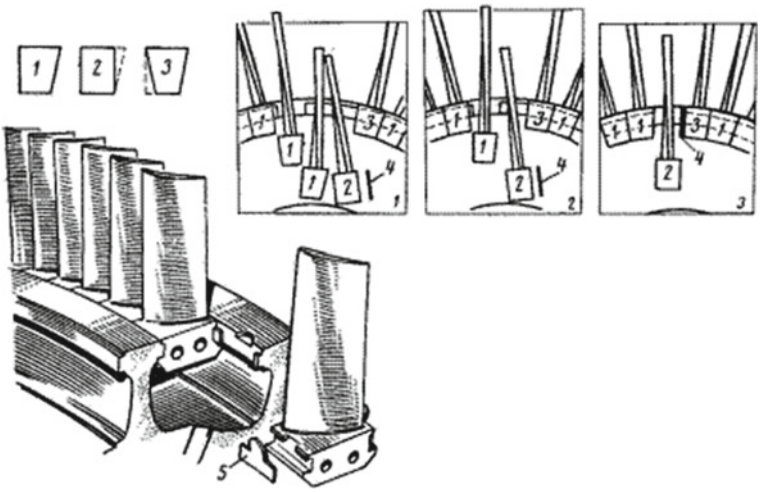


**Fig. 13.8** Circumferential mounting of compressor blades. 1—standard blade; 2—locking blade; 3—fitting blade; 4—gasket; 5—plate

Figure 13.10 shows a **hinge-type method of circumferential mounting**, which is used for the blades of the first (longest) stages of the axial compressors as means of damping vibrations. That method allows mounting the blade so that under the influence of the gas-dynamic and centrifugal forces, the blade, turning on the hinge, will be located at some angle to the radial direction. Under the influence of the variable forces, the blade will sway, transferring the energy of the mechanical vibrations into thermal energy by friction [5].

The disadvantages of this method are the high shear stresses that occur in hinges, as well as a large weight.

**Fig. 13.9** Groove-type method of mounting

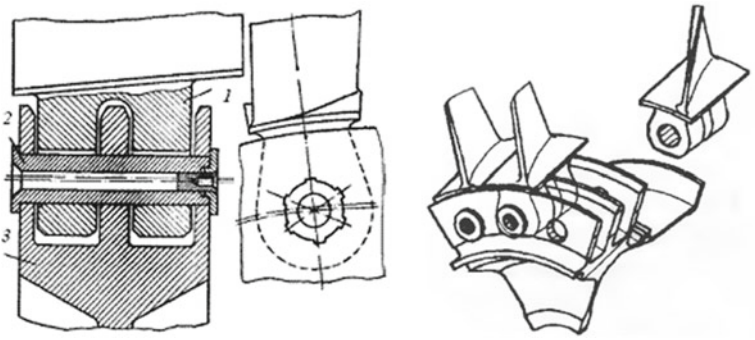


**Fig. 13.10** Hinge-type method of mounting. 1—blade; 2—pin (hinge); 3—disk

**The axial mounting** of the compressor blades has become more widespread than the circumferential mounting. The most popular are the dovetail and fir-type methods of axial mounting.

The **dovetail method of mounting** (Fig. 13.11) meets most of the requirements for the mounting compressor blades. The grooves in the disk are carried out by broaching, and the roots of the blades are executed by milling [5].

The grooves for blades are usually placed at an angle to the axis of the rotor, close to the angle of the mounting of the root sections of the blades. This increases the strength of the connection (by reducing the pressure on the contacting surfaces).

The dovetail connection allows the placement of a large number of blades on the rotor. This connection is simple in design, has a low weight and has sufficient strength.

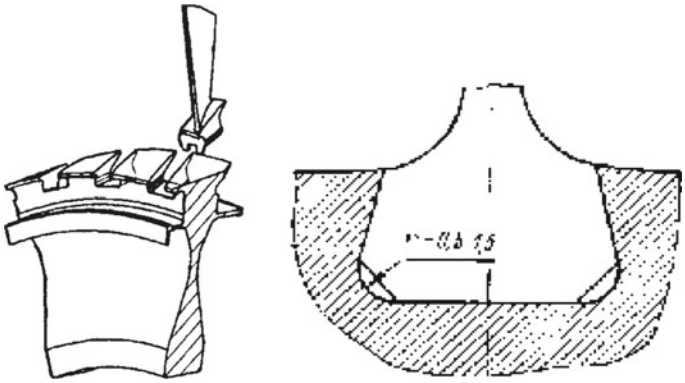

**Fig. 13.11** The dovetail method of mounting

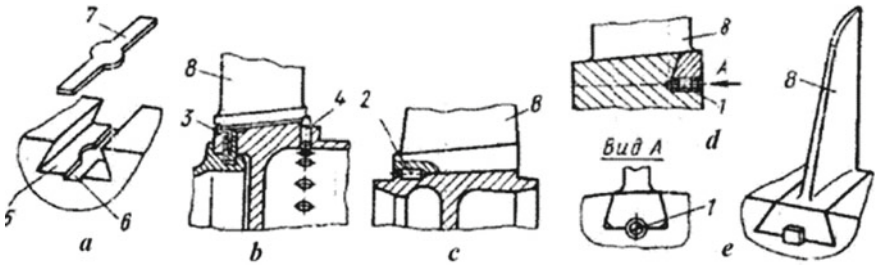


**Fig. 13.12** Fixation of the blades at dovetail method of mounting: *a*—general view of the connection; *b, c, d*—methods of fixing the blades; *e*—fixed blade; 1—threaded rod; 2—axial pin; 3—plate stopper; 4—radial pin; 5—groove for blade; 6—groove for the fixing plate in disk; 7—fixing plate; 8—lade

The mounting of the blades in individual grooves requires fixing them from axial movements. The fixation can be common for all blades or individuals and can be carried out using plates, pins, etc. (Fig. 13.12).

**A fir-type method of mounting** (Fig. 13.13) is widespread in gas turbines. In the axial compressors, it is rarely used, because in the compressors simpler design (for example, dovetail-type) can be used [5].

## *13.2.2 Axial Compressor Guide Vanes*

The guide vanes of the axial compressors form diffuser passages are designed for the following:

– to convert the kinetic energy of the airflow into potential energy;
– to redirect air at the given angle to the passages between blades of the next stage.

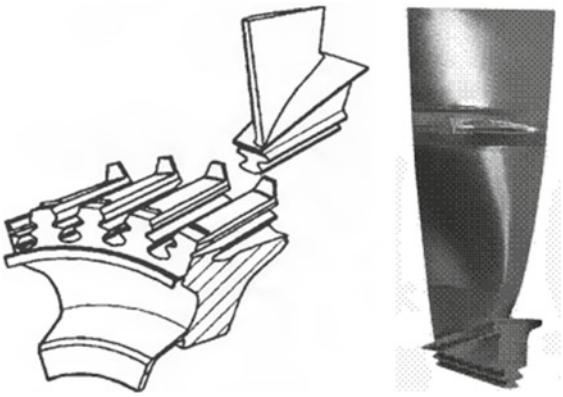

**Fig. 13.13** Fir-type method of mounting

Before the first stage of the compressor, the inlet guide vanes are installed, which ensures the initial air swirl. At the end of the compressor, there are the exit guide vanes straightening the airflow in the axial direction.

**The methods for attaching the guide vanes** to the compressor casing are very different. All methods are divided on single-support mounting and double-support mounting.

The guide vanes can be attached directly to the compressor casing, or in the rings (or the half rings) that form the frame-type **guide devices**.

By design, the frame-type guide devices can be disassembled and non-disassembled (welded, riveted).

**For the single-support mounting** (Fig. 13.14), the cross-sections of the vanes according to the conditions of strength and vibration resistance should be more than for the double-support mounting. The single-support mounting is rarely used because it causes a significant leakage of air through the gap between the end of the vanes and the rotor, which worsens the efficiency of the compressor. Reducing leakage is achieved by reducing the radial clearance. However, a number of factors (rotor runout, etc.) do not allow the reduction of the gap to the acceptable value.

**The double-support mounting** (Fig. 13.15) of the guide vanes allows the achievement of a higher compressor efficiency. The guide devices of this mounting can be of two types:

– with the rigid mounting of the vanes to both rings;
– with the rigid mounting of the vanes to one ring, usually external, and a free mounting, allowing a radial movement of the vanes, to another ring.

The rigid mounting is used in the guide vanes which are made of steel by welding, with relatively short vanes, where the thermal stresses caused by uneven heating of the parts are small.

When the compressor casing is disassembled, the rings are also disassembled and consist of two halves, each of which is independently mounted in the casing, using the radial pins or screws.

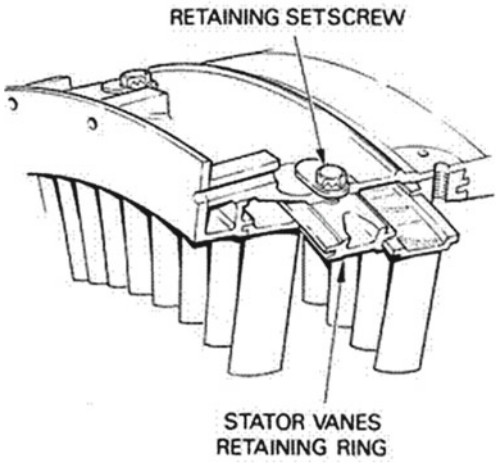


**Fig. 13.14** Single-support mounting of guide vanes

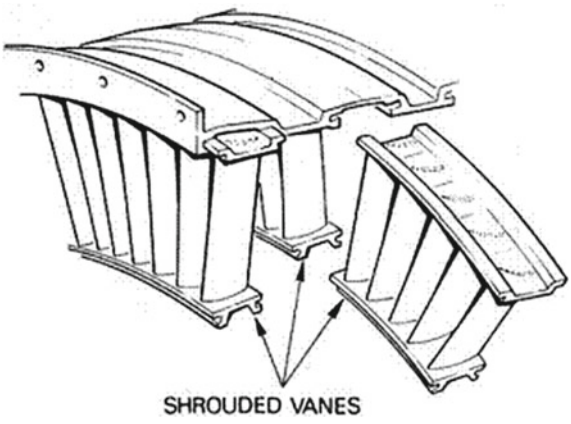


**Fig. 13.15** Double-support mounting of guide vanes

Figure 13.16 shows the low-pressure compressor guide device of DI59 engine from "Zorya-Mashproekt". At one end, vane *2* has a shelf fixing it in a certain position in the outer retaining ring *1*, at the other end there is a cylindrical trunnion for mounting the vane to the inner ring *4*. The grooves are made in the inner ring, into which the copper-graphite inserts *3* are assembled, which, in combination with labyrinths, are made on the rotor disks, form seals that prevent air leakage between the compressor stages. The guide device is mounted inside the casing in the cylindrical grooves with screws [5].

This mounting allows the easy removal and replacement of the vanes. However, as the design of the guide device becomes more complicated, its weight increases.

Figure 13.17 shows the low-pressure compressor guide device of D050 engine from "Zorya-Mashproekt". It consists of the outer *1* and the inner *4* retaining rings and guide vanes *2* which are located between them. The dovetail grooves are made

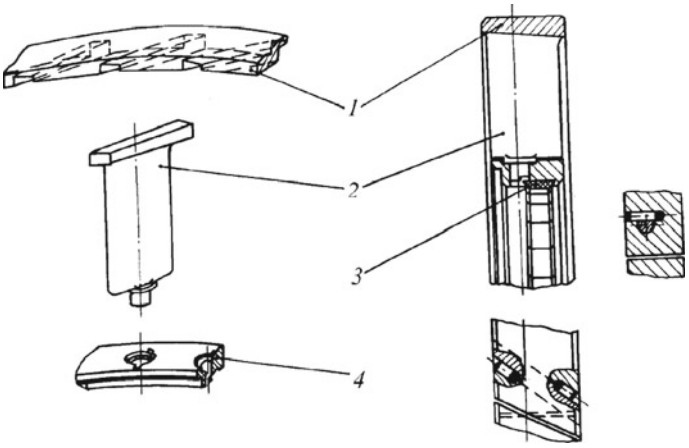


**Fig. 13.16** Low-pressure compressor guide device of DI59 engine from "Zorya-Mashproekt"

in the outer ring, where the guide vanes wind up with their upper shelves. The inner ring has notches, which include the ends of the vanes. The protruding parts of these ends are riveted from the inside of the ring. The annular groove is made in the inner ring, in which copper-graphite inserts *3* are installed. The inserts, in combination with labyrinths made on the rotor disks, form seals of the engine flow part. The guide device is horizontally cut into two parts, each of them is attached to its half of the LPC casing [5].

In order to reduce the losses which are caused by the unfavorable angles of the air flow movement through passages between blades and vanes at partial operating modes (reason No. 1), and to prevent surging of the compressor (reason No. 2) the inlet guide vanes and the guide vanes of the first compressor stages perform the rotary (so-called **variable guide vanes**).

The rotary vanes (Figs. 13.18 and 13.19) are made of stainless steel or aluminum alloy. The cylindrical trunnions of the vanes are placed in the bearings [5].

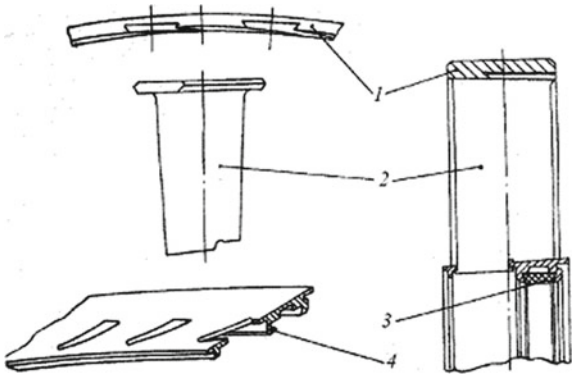


**Fig. 13.17** Low-pressure compressor guide device of D050 engine from "Zorya-Mashproekt":1—outer retaining ring; 2—guide vanes; 3—copper-graphite inserts; 4—inner retaining ring

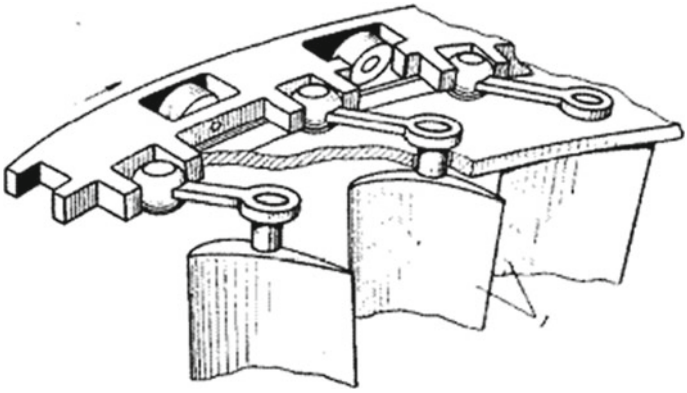

**Fig. 13.18** Variable guide vanes of the compressor

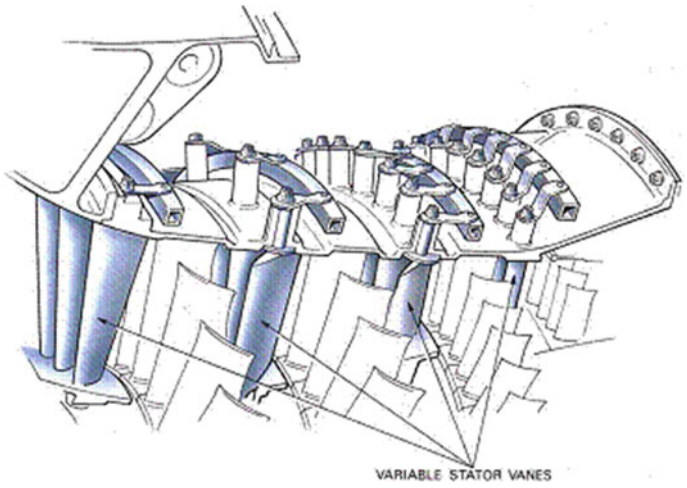


**Fig. 13.19** Aircraft engine compressor with the variable inlet guide vanes and variable guide vanes of the first three stages

The simultaneous rotation of all vanes is carried out either with the assistance of the steel rotary ring which is located outside the casing and with its forks which are connected to levers attached to the upper trunnions of the vanes or with the assistance of a gear wheel connected to the gear sectors mounted on the lower trunnions of the vanes. In both cases, the rotation control of the vanes is carried out by the use of the power cylinders.

# References

1. Giampaolo T (2006) Gas turbine handbook: principles and practices, 3rd edn. The Fairmont Press, 437 p
2. Boyce MP (2006) Gas turbine engineering handbook, 3rd edn. Elsevier Inc., 936 p
3. Saravanamuttoo HIH, Rogers GFC, Cohen H (2013) Gas turbine theory, 5th ed., 491 p
4. Romanovsky GF, Washchilenko NV, Serbin SI (2003) Theoretical basics of ship gas turbine designing, Publisher USMTU, Mykolaiv, 304 p. (in Ukrainian)
5. Romanovsky GF, Serbin SI, Patlaychuk VM (2017) Gas turbine plants. Part 2. Structural elements. Publisher NUS, Mykolaiv, 196 p. (in Ukrainian)

# Chapter 14
# Compression Work and Efficiency of the Compressor Stage


We introduce new several parameters.

**The actual compression work of the compressor stage** is the mechanical energy of the rotor which is spent on the increase in the air pressure in the compressor stage [1, 2]:

$$l_r = h_3 - h_1 =_p (T_3 - T_1) = c_p T_1 \left( \frac{T_3}{T_1} - 1 \right)$$

where $h_1$ and $T_1$ are enthalpy and the temperature of the air before the compressor stage; $h_3$ and $T_3$ are enthalpy and the temperature of the air after the compressor stage.

The actual compression work of the compressor stage may be expressed by the following formula:

$$l_r = \Delta h_{bl} + \Delta h_{g.v},$$

where $\Delta h_{bl}$ is the moving blades compression work; $\Delta h_{g.v}$ is the guide vanes compression work.

Based on the double conversion of the energy in the compressor stage **the moving blade compression work** is equal to kinetic energy which is converted to the potential ones in the passages between the blades:

$$\Delta h_{bl} = h_2 - h_1 = \frac{w_1^2 - w_2^2}{2},$$

where $h_2$ is the enthalpy of air after the blades.

**The guide vanes compression work** is equal to kinetic energy which is converted to the potential ones in the passages between the guide vanes [1, 2]:

$$\Delta h_{g.v} = h_3 - h_2 = \frac{c_2^2 - c_3^2}{2}.$$



K. Liu et al. (eds.), *Gas Turbines Structural Properties, Operation Principles and Design Features*, https://doi.org/10.1007/978-981-99-0977-3_14

Due to $c_3 \approx c_1$ (see above):

$$\Delta h_{g.v} \approx \frac{c_2^2 - c_1^2}{2}$$

We have the following formula:

$$l_r \approx \frac{w_1^2 - w_2^2}{2} + \frac{c_2^2 - c_1^2}{2}.$$

**Reaction degree (reaction rate) of the compressor stage**:

$$\rho_c = \frac{\Delta h_{bl}}{l_r}$$

Where it is 0.5–1.0 in the modern axial compressor. This means that the air compression in the compressor stage by 50–100% occurs in the passages between the moving blades. If the reactivity of the stage is 1.0, then the air compression occurs only on the moving blades. In this case, the guide vanes are only needed to redirect air to the next row of blades.

The actual compression work is connected with losses in the stage by the following formula:

$$l_r = l_t + q_{bl} + q_{g.v},$$

where $l_t$ is the isentropic compression work of the compressor stage; $q_{bl}$ is the energy loss on the blades; $q_{g.v}$ is the energy loss on the guide vanes.

The energy losses on the moving blades and the guide vanes are due to friction of the airflow on the blades and the guide vanes. Due to friction, the kinetic energy of the air is also converted into potential energy.

**The isentropic compression work of the compressor stage** is the mechanical energy of the rotor which is spent on the increase in the air pressure in the compressor stage without losses:

$$l_t = h_{3s} - h_1,$$

where $h_{3s}$ is the enthalpy of air after the compressor stage in the isentropic process (lossless).

The isentropic process occurs with a constant value of entropy. In Fig. 14.1, the actual process in the compressor stage goes from point *1* to point *3*. The isentropic process (lossless) goes from point *1* to point *3*s.

For the isentropic process, we can write:

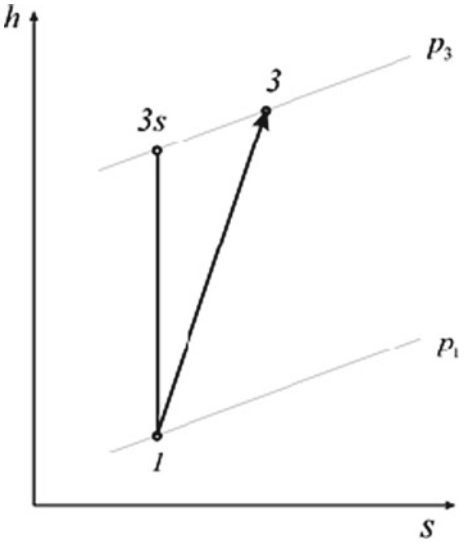


**Fig. 14.1** Compressor stage process

$$l_t = h_{3s} - h_1 =_p (T_{3s} - T_1) = c_p T_1 \left( \frac{T_{3s}}{T_1} - 1 \right) = c_p T_1 \left[ \left( \frac{p_{3s}}{p_1} \right)^{\frac{k-1}{k}} - 1 \right]$$

Due to $p_{3s} = p_3$, we have:

$$l_t = c_p T_1 \left[ \left( \frac{p_3}{p_1} \right)^{\frac{k-1}{k}} - 1 \right] = c_p T_1 \left( \pi_{st.c}^{\frac{k-1}{k}} - 1 \right),$$

where $\pi_{st.c}$ is the pressure ratio of the single compressor stage.

In view of the foregoing actual compression work of the compressor stage:

$$l_r = c_p T_1 \left( \pi_{st.c}^{\frac{k-1}{k}} - 1 \right) + q_{bl} + q_{g.v}.$$

From the above formula we can conclude that mechanical energy which is spent on the increase in the air pressure in the compressor stage depends on:

(1) the pressure ratio of the single compressor stage $\pi_{st.c}$ (an increase in that parameter causes an increase in mechanical energy);
(2) the energy losses on the moving blades $q_{bl}$ and the guide vanes $q_{g.v}$ (an increase in these parameters causes an increase in mechanical energy);
(3) the air temperature before the stage $T_1$ (an increase in that parameter causes an increase in mechanical energy).

The mechanical energy for compressor rotor driving is taken from the turbine rotor. The less of this energy will be taken away, the greater of this energy will be the useful power of the gas turbine unit.

The pressure ratio of the single compressor stage $\pi_{st.c}$ is the initial parameter in the compressor design. Therefore, we can achieve the reduction of mechanical energy for the compressor drive only by reducing the energy losses $q_{bl}$ and $q_{g.v}$ and reducing air temperature $T_1$.

The efficiency of the compressor stage is usually estimated by its isentropic efficiency

$$\eta_{st.c} = \frac{l_t}{l_r} = \frac{c_p T_1 \left[ \left( \frac{p_3}{p_1} \right)^{\frac{k-1}{k}} - 1 \right]}{c_p T_1 \left( \frac{T_3}{T_1} - 1 \right)} = \frac{\left( \frac{p_3}{p_1} \right)^{\frac{k-1}{k}} - 1}{\frac{T_3}{T_1} - 1}.$$

From this formula, we see that the isentropic efficiency of the compressor stage can be calculated from the known parameters (temperature and pressure) of air before and after the stage. Now the isentropic efficiency of the axial compressor stage is 0.89–0.91.

## 14.1 Axial Compressor Stages Layout

When designing an axial multistage compressor, several main types of the layout of its stages are used.

(1) **Layout with a constant outer diameter** $D_{\text{out}} = \text{const}$.

With this layout, the inlet guide vanes and all compressor stages have the same outer diameter (Fig. 14.2) [1]:

$$D_{\text{out.1}} = D_{\text{out.2}}.$$

In the direction from the first stage to the last stage the medium and inner diameters of the stages will increase:

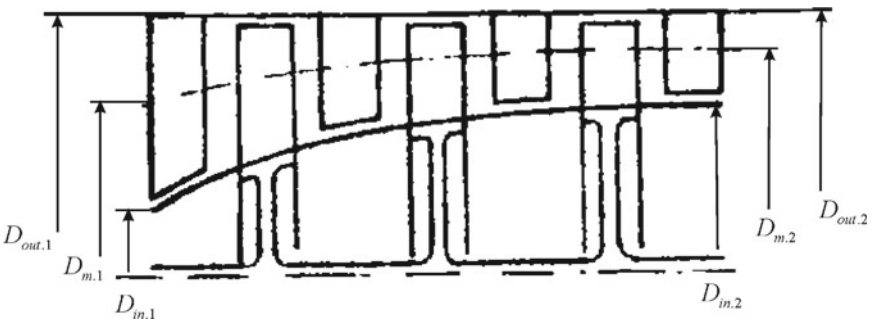


**Fig. 14.2** Layout with a constant outer diameter

$$D_{m.1} < D_{m.2} \quad \text{and} \quad D_{in.1} < D_{in.2}.$$

The layout with a constant outer diameter has such **advantages**:

(A) The total number of compressor stages will be slightly less.

The pressure ratio in every stage $\pi_{st.c}$ at the same rotor speed depends on the medium diameter of the stage. The pressure ratio of each subsequent stage will be larger than the previous one because the medium compressor diameter increases in the direction from the first stage to the last stage.

(B) The unchanging gaps between the blades and the casing with the axial displacements of the rotor.

When GTU is changing the operating mode, there is a slight displacement of the compressor rotor in the axial direction. When gaining power, the rotor is displaced to the inlet casing. With a decrease in GTU power, the rotor is displaced on the opposite side.

Therefore, the gaps between the blades and the casing with the axial rotor displacements may be changed. The reduction of the gaps to zero will cause the rotating blades to touch the casing and will be destroyed. The layout with a constant outer diameter keeps these gaps unchanged.

(C) It's easier to produce a compressor casing.

The compressor casing in this case has the correct cylindrical shape. For this reason, its production is technologically easier.

**Conclusion**: The layout with a constant outer diameter is used in all cases when there are no restrictions on the length of the blades. In two-spool GTU compressors, it is used for a low-pressure compressor.

(2) **Layout with a constant inner diameter** $D_{\text{in}} = \text{const}$.

With this layout, the inlet guide vanes and all compressor stages have the same inner diameter (Fig. 14.3) [1]:

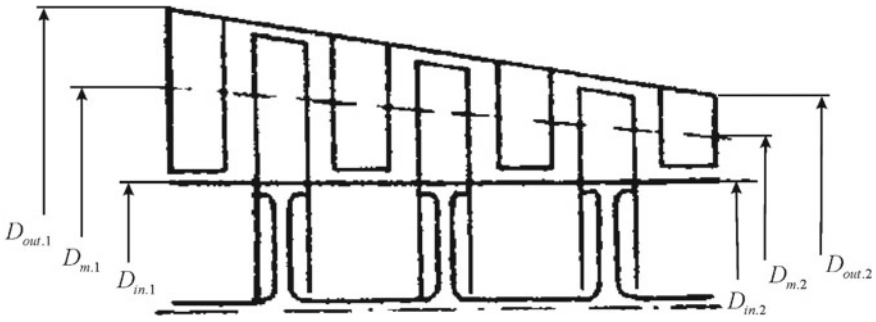


**Fig. 14.3** Layout with a constant inner diameter

$$D_{\text{in.1}} = D_{\text{in.2}}.$$

In the direction from the first stage to the last stage the medium and outer diameters of the stages will decrease:

$$D_{m.1} > D_{m.2} \text{ and } D_{\text{out.1}} > D_{\text{out.2}}.$$

The layout with a constant inner diameter has **only one advantage**: the blades of the last compressor stages are longer.

In the direction from the first stage to the last stage the volume of air decreases. Therefore, in that direction, the required flow area and the length of the blades also decrease. The longest are the blades of the first stages, the shortest are the blades of the last stages. The minimum length of the axial compressor blades is 25–30 mm. If the length of the blades is less, then the efficiency of the compressor stage decreases sharply.

How can the layout of the stages affect the length of the blades? The length of the blades can be calculated by the formula:

$$l_{bl} = \frac{F}{\pi D_m},$$

where $F$ is the required flow area (Fig. 14.4).

At the layout with a constant outer diameter in the direction from the first stage to the last stage, the medium diameter of the stages will increase. Therefore, in that direction, the reduction of the blade length due to the reduction of the required flow area will be summarized with the reduction of the blade length due to the increase in the medium diameter.

On the contrary, at the layout with a constant inner diameter the medium diameter of the stages will decrease. Therefore, the reduction of the blade length due to the reduction of the required flow area will be summarized with the increase of the blade

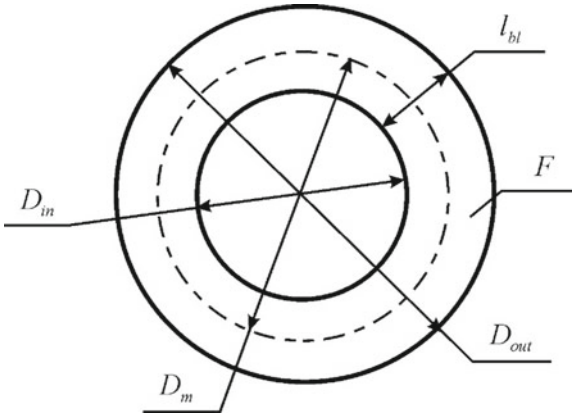


**Fig. 14.4** Axial compressor stage cross-section

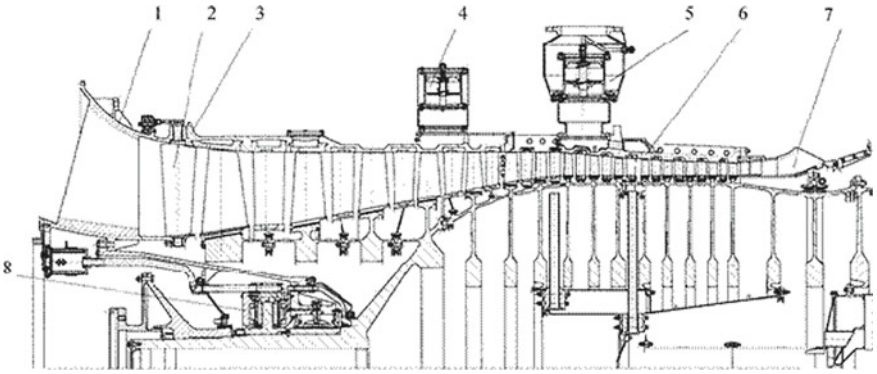


**Fig. 14.5** Compressor of GTD110 engine 1—inlet casing; 2—inlet guide vanes; 3—casing of the 1–5th stages; 4—bypass valve; 5—bypass valve with compensator; 6—casing of the 6–14th stages; 7—exit diffuser; 8—front bearing

length due to the decrease in the medium diameter. For this reason, the blades of the last stages will be longer.

It is easy to see that the layout with a constant inner diameter has **some disadvantages**:

- the total number of compressor stages will be slightly more;
- the gaps between the blades and the casing changes with the axial displacements of the rotor;
- the production of the compressor casing is more complex.

**Conclusion**: The layout with a constant inner diameter is only used to increase the blade length of the last stages. In two-spool GTU compressors, it is used for a high-pressure compressor.

(3) Combined layout.

The combined layout is used to combine the advantages of both of the previously discussed layout types. The first stages of the compressor have a layout with a constant outer diameter; the last stages have a layout with a constant inner diameter (Fig. 14.5) [3].

**Conclusion**: The combined layout is used to increase the blade length of the last stages. Such a layout can be used in single-spool compressors.

## 14.2 Calculation of the GTU Compressor Part

We consider the determination of the main dimensions of the GTU compressor part. First of all, the radial and axial dimensions of low-pressure compressor (LPC) and high-pressure compressor (HPC) will be determined. The number of compressor

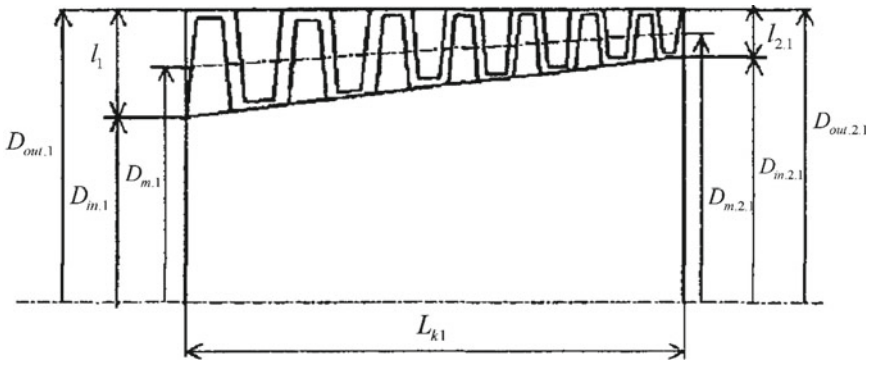


**Fig. 14.6** The scheme of low-pressure compressor

stages and the speed of their rotors will be also estimated. As a result of these calculations, the data will be obtained to design the cross-section of the GTU compressor part.

The dimensions of the GTU compressors are sequentially calculated, starting with LPC. The scheme of low-pressure compressor is shown in Fig. 14.6 [1].

(1) The following parameters were determined during the thermal calculation of GTU at nominal operating mode:

- the air flow rate through LPC $G_{c1}$;
- the temperature at point 1 (before LPC) $T_1$;
- pressure at point 1 (before LPC) $p_1$.

(2) Specific heat of air before LPC

$$c_{pa1} = f(T_1)$$

(3) Specific heat ratio for air before LPC

$$k_{a1} = \frac{c_{pa1}}{c_{pa1} - R_{\text{air}}}$$

where $R_{air} = 0.287$ kJ/kg/K is the gas constant of air.

(4) The circumferential velocity at the outer diameter before LPC is equal to the following:

$$u_{\text{out.1}} = 270{-}340\text{m/s}.$$

If we calculate HPC, then: $u_{\text{out.1.2}} = 240$–$340$ m/s.

(5) The axial velocity before LPC

$$c_{a1} = (0.45...0.55)\ u_{\text{out.1}}.$$

(6) The superficial (reduced) velocity before LPC:

$$\lambda_{c_{a1}} = \frac{c_{a1}}{\sqrt{\frac{2\,k_{a1}}{k_{a1}+1} R_{\text{air}}\, T_1 \cdot 10^3}}.$$

(7) The gas-dynamic flow density function before LPC:

$$q(\lambda_{c_{a1}}) = \lambda_{c_{a1}} \left[ \frac{k_{a1}+1}{2} \left( 1 - \frac{k_{a1}-1}{k_{a1}+1} \lambda_{c_{a1}}^2 \right) \right]^{\frac{1}{k_{a1}-1}}.$$

(8) The required flow area before LPC:

$$F_1 = \frac{G_{c1}\sqrt{T_1}}{\sqrt{\left(\frac{2}{k_{a1}+1}\right)^{\frac{k_{a1}+1}{k_{a1}-1}} \cdot \frac{k_{a1}}{R_{\text{air}} \cdot 10^3}\ p_1\, q(\lambda_{c_{a1}}) \cdot 10^6}}.$$

(9) The diameter ratio for LPC is equal to: $\overline{d}_1 = \frac{D_{\text{in.1}}}{D_{\text{out.1}}} = 0.45 \sim 0.55$.
If we calculate HPC, then $\overline{d}_{1.2} = 0.70 \sim 0.85$.

(10) The outer diameter before LPC:

$$D_{\text{out.1}} = \sqrt{\frac{4\,F_1}{\pi\left(1 - \overline{d}_1^2\right)}}.$$

(11) LPC rotor speed:

$$n_{c1} = \frac{60\,u_{\text{out.1}}}{\pi\, D_{\text{out.1}}}.$$

The relation $n_{c1} < n_{c2}$ must be executed.

(12) The inner diameter before LPC:

$$D_{\text{in.1}} = D_{\text{out.1}} \overline{d}_1.$$

(13) Length of the first stage blades:

$$l_1 = 0.5\,(D_{\text{out.1}} - D_{\text{in.1}}).$$

(14) Medium diameter before LPC:

$$D_{m.1} = 0.5\,(D_{\text{out.1}} + D_{\text{in.1}}).$$

(15) The following parameters were determined during the thermal calculation of GTU at nominal operating mode:

– pressure at point 2.1 (after LPC) $p_{2.1}$;
– the temperature at point 2.1 (after LPC) $T_{2.1}$.

(16) Specific heat of air after LPC:

$$c_{pa2.1} = f(T_{2.1}).$$

(17) The specific heat ratio for air after LPC:

$$k_{d2.1} = \frac{c_{pa2.1}}{c_{pc21} - R_{cdj'}}.$$

(18) The axial velocity after LPC:

$$c_{a2.1} = (0.90...0.95)\, c_{a1}.$$

(19) The superficial (reduced) velocity after LPC:

$$\lambda_{c_{a2.1}} = \frac{c_{a2.1}}{\sqrt{\frac{2k_{a2.1}}{k_{a2.1}+1} R_{\text{air}}\, T_{2.1} \cdot 10^3}}.$$

(20) The gas-dynamic flow density function after LPC:

$$q(\lambda_{c_{a2.1}}) = \lambda_{c_{a2.1}} \left[ \frac{k_{a2.1}+1}{2} \left( 1 - \frac{k_{a2.1}-1}{k_{a2.1}+1} \lambda^2_{c_{a2.1}} \right) \right]^{\frac{1}{k_{a2.1}-1}}.$$

(21) The required flow area after LPC:

$$F_{2.1} = \frac{G_{c1}\sqrt{T_{2.1}}}{\sqrt{\left(\frac{2}{k_{a2.1}+1}\right)^{\frac{k_{a2.1}+1}{k_{a2.1}-1}} \cdot \frac{k_{a2.1}}{R_{air}\cdot 10^3}\; p_{2.1}\, q(\lambda_{c_{a2.1}}) \cdot 10^6}}.$$

(22) The choice of the compressor stages layout. For LPC this is a layout with a constant outer diameter $D_{\text{out}} = \text{const}$. Then the outer diameter after LPC:

$$D_{\text{out.2.1}} = D_{\text{out.1}}.$$

For HPC we choose a layout with a constant inner diameter $D_{\text{in}} = \text{const}$ and the inner diameter after HPC $D_{\text{in.2}} = D_{\text{in.1.2}}$.

(23) The inner diameter after LPC:

$$D_{\text{in.2.1}} = \sqrt{D^2_{\text{out.2.1}} - \frac{4}{\pi} F_{2.1}}.$$

For HPC we calculate the outer diameter after HPC: $D_{\text{out.2}} = \sqrt{D_{\text{in.2}}^2 + \frac{4}{\pi} F_2}$.

(24) Length of the last stage blades:

$$l_{2.1} = 0.5\,(D_{\text{out.2.1}} - D_{\text{in.2.1}}).$$

(25) Medium diameter after LPC:

$$D_{m.2.1} = 0.5\,(D_{\text{out.2.1}} + D_{\text{in.2.1}}).$$

(26) The LPC pressure ratio $\pi_{c1}$ was determined during the thermal calculation of GTU at nominal operating mode.

(27) The pressure ratio of the single LPC stage is equal to:

$$\pi_{st.c} = 1.20 \sim 1.30.$$

For HPC $\pi_{st.c} = 1.15$ –1.20.

(28) Number of LPC stages (round to integer value):

$$z_{c1} = \frac{\lg \pi_{c1}}{\lg \pi_{st.c}}.$$

(29) Medium LPC diameter:

$$D_{\text{mc}} = 0.5\,(D_{m1} + D_{m2.1}).$$

(30) Medium length of LPC blades:

$$l_{\text{mc}} = 0.5\,(l_1 + l_{2.1})$$

(31) Ratio:

$$\lambda_c = \frac{D_{mc}}{l_{mc}}.$$

(32) Coefficient $\bar{\delta}_c = f(\lambda_c)$ is determined by Table 14.1.

(33) The axial dimension of the single LPC stage:

$$b_{st.c} = \bar{\delta}_c l_{\text{mc}}.$$

**Table 14.1** Values of the coefficients $\bar{\delta}_c$

| $\lambda_c$ | 4 | 5 | 6 | 7 | 8 | 9 | 10 | 11 | 12 | 13 | 14 | 15 | 16 | 17 | ≥ 18 |
|---|---|---|---|---|---|---|---|---|---|---|---|---|---|---|---|
| $\bar{\delta}_c$ | 0.91 | 1.02 | 1.12 | 1.21 | 1.29 | 1.37 | 1.47 | 1.54 | 1.60 | 1.65 | 1.71 | 1.75 | 1.81 | 1.85 | 1.88 |

(34) The axial dimension of the LPC main casing (without the length of the inlet casing, a front casing and a rear casing)

$$L_{c1} = z_{c1} b_{st.c}.$$

(35) The axial dimension of the inlet casings for "Zorya-Mashproekt" GTU engines:

$$L_{inl} \approx (0.35...0.40)\, D_{out.1}.$$

(36) The axial dimension of the front casing:

$$L_{fr} \approx (0.30...0.35)\, D_{out.1}.$$

(37) The axial dimension of the intersection between LPC and HPC:

$$L_{int} \approx (0.30...0.35)\, D_{out.2.1}.$$

The calculation of the HPC is carried out according to the same formulas considering the comments which are earlier made.

## 14.3 Application of the Centrifugal Compressor in the Gas Turbine Units

The centrifugal compressor is the type of radial turbomachine in which the air moves in the direction from the center of rotation to the periphery [2, 4]. The centrifugal compressor scheme is shown in Fig. 14.7.

The air enters impeller 3 through the inlet guide vanes 1 and 2, designed to swirl the flow in front of the impeller blades. The stationary guide vanes 1 are the vanes which are rigidly fixed in the casing. The rotating guide vanes 2 are elongated and especially bent front edges of the impeller blades.

To simplify the technology, it is often made separately from the impeller and then connected to it. At the same time, guide vanes 1 and 2 are rarely used in compressors. A rotating guide vane is more popular in designs than a stationary one. There are also compressors in which the guide vanes are absent.

In the impeller, the mechanical energy of rotation is used to increase the velocity of air (to increase the kinetic energy). Passing through the channels between the impeller blades, the kinetic energy of air (its velocity) will decrease, and the potential energy (enthalpy, pressure and temperature) will increase.

After the impeller, air enters diffusers 4 and 5, where there is a further decrease in velocity and increase in pressure. In a vaneless diffuser, the flow area increases in the radial direction. Its use reduces significantly the noise of the compressor. As a rule, both types of the diffuser are simultaneously used. The exit device 6 is designed to further reduce the velocity (increase pressure) and collect the exhaust air.

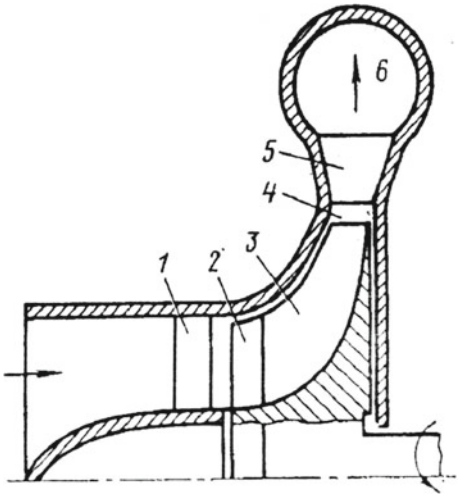


**Fig. 14.7** Diagram and main elements of a centrifugal compressor 1, 2—fixed and rotating inlet guide vanes; 3—impeller; 4—vaneless diffuser; 5—vane diffuser; 6—exit device

According to the design, the impellers of the centrifugal compressors are divided into open, closed and half-open (Fig. 14.8).

The **open impeller** consists of hub 1 and blade 2 which are fixed on it so that the impeller passages from the two end sides are only limited by the walls of the casing which are located at a small distance from the ends of the blades.

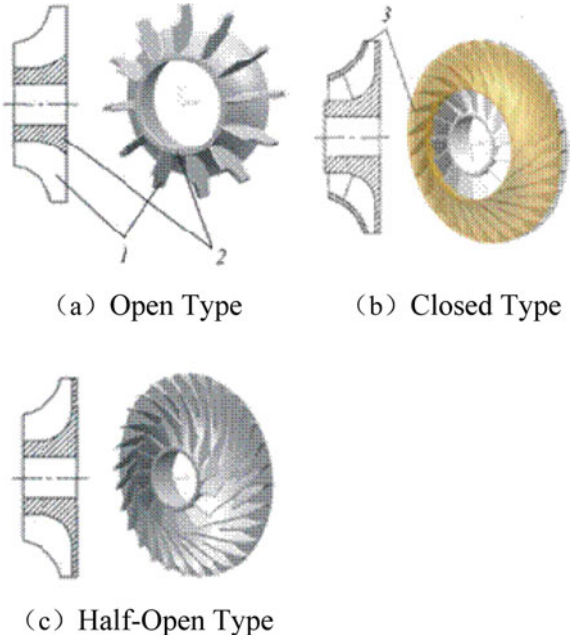


**Fig. 14.8** Types of centrifugal compressor impellers: 1—hub; 2—blades; 3—outer disk

An open impeller is not economical because of the large losses from the leakage of air through the ends of the passages and because of the influence of the fluid in the gap between the impeller and the casing on the movement in the impeller passages. At the same time, this impeller is the lightest of the three which are considered; therefore, it admits the highest rotation speed and provides the highest compressor pressure ratio.

At the closed impeller, the passages from both ends are closed by disks (outer and inner), so that air leakage through them is excluded. The air in the impeller is also isolated from the fluid in the gap between the impeller and the casing. As a result, closed impellers are the most economical and are often used in industrial compressors. However, the addition of metal construction to the rotor leads to a weighting of its structure and increases the loads from the centrifugal forces. The consequence of this is a decrease in the permissible rotor speed and a decrease in the compressor pressure ratio.

For half-open impellers, the passages are closed by the inner disk from one side and open from another. The efficiency and pressure ratio of these impellers are intermediate between open and closed impellers.

According to the shape of the blades, there are impellers with radial blades, with blades bent against rotation (back) and with blades bent on side of rotation (forward) (Fig. 14.9).

**Impellers with blades bent back** (Fig. 14.9a) provide relatively small air velocities at the exit of the impeller. For this reason, more uniform flow forms behind the impeller, which causes the efficient work of the diffusers. At an equal speed of rotation, these impellers provide higher compressor efficiency but have a lower pressure ratio. The impellers of this type are widely used in industrial compressors.

**Impellers with blades bent forward** (Fig. 14.9c) transmit at the same speed of rotation more mechanical energy to the air and have relatively high air velocity at the impeller exit. The increase of pressure in the compressors with such impellers occurs mainly due to the diffusers. This is the reason for the low efficiency of compressors with impellers of this type. Such impellers are often used in fans.

In gas turbine engines, the **impellers with radial blades** are mainly used (Fig. 14.9b). According to the conditions of strength, they allow higher rotation speeds than the impellers with bent blades. In addition, the impellers of this type

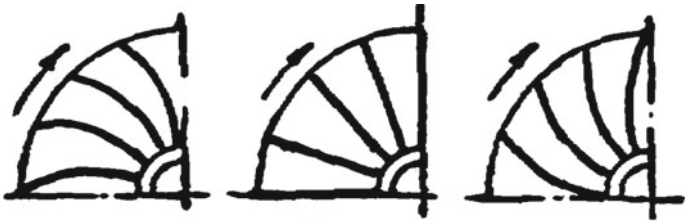


**Fig. 14.9** Impeller with blades bent back (**a**), with radial blades (**b**) and with blades bent forward (**c**)

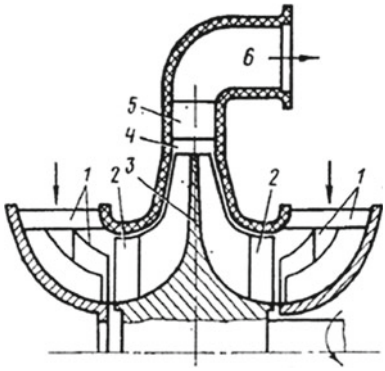


**Fig. 14.10** Centrifugal compressor with double-side inlet 1, 2—fixed and rotating inlet guide vanes; 3—impeller; 4—vaneless diffuser; 5—vane diffuser; 6—exit device

are relatively simple to produce. For efficiency and pressure ratio, they occupy an intermediate position between impellers with the blades bent back and forward.

The centrifugal compressors can be with one-side or double-side inlets (Figs. 14.7 and 14.10).

For a compressor with a **one-side axial inlet**, air enters the impeller through the fixed axial-type guide vanes.

A compressor with a **double-side inlet** is more often used as an annular inlet, and the fixed guide vanes is a special annular device, behind which guide toroidal surfaces are also installed. This rotating guide vane is sometimes performed in conjunction with the impeller—as one part.

The centrifugal compressors with one-side inlets are equipped with single-flow impellers (Fig. 14.11a), and compressors with double-side inlets—with double-flow impellers (Fig. 14.11b). The latter is used to increase the productivity of the compressor or to reduce its radial size.

**Advantages of the centrifugal compressors** (compared to the axial compressors):

– a higher pressure ratio of single stage (as a rule, $\pi_{st.c} = 3.5–7.0$);

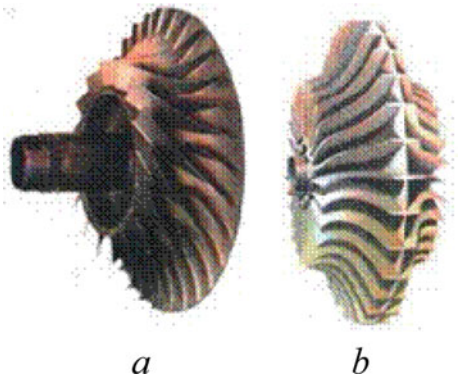


**Fig. 14.11** Single-flow impeller (**a**) and double-flow impeller (**b**)

– the design is more simple, more durable and cheaper to produce (the number of blades is much smaller; the main weight of the rotor is concentrated near the central axis, which means lower centrifugal loads and higher permissible rotational speeds);
– the blades are less sensitive to air quality and less damaged by items falling into the flow part;
– a larger range of stable operating modes.

**Disadvantages of the centrifugal compressors** (compared to the axial compressors):

– a low efficiency (for single stage, as a rule, $\eta_{st.c} = 0.80–0.82$);
– it is more difficult to create a multistage compressor (after leaving the previous stage, air can enter the next stage only with the assistance of a special channel of a complex loop-like shape);
– a large outer diameter.

Because the compressor efficiency determines largely the efficiency, power, size and cost of the gas turbine unit, the centrifugal compressors in GTUs are only used where the use of an axial compressor is undesirable for one reason or another. First of all, they are used in low-power GTUs (approximately up to 300 kW) with low air flow rates. The axial compressors for such units will have a short blade length (less than 25–30 mm), which means they will have low efficiency (it is even worse than the efficiency of the centrifugal compressors).

The centrifugal compressors are also used in various gas turbine units of the emergency services and in special GTUs, the main qualities of which should be simplicity, cheapness, low weight or the ability to work in very dusty air (as a rule, these are also low-power GTUs).

Despite the foregoing, in the practice of GTU construction, there are precedents for the use of centrifugal compressors in gas turbine engines with large air flow rates (i.e. in high-power GTUs). However, this circumstance is rather an exception and can only be explained by orthodoxy and traditions in the design decisions of manufacturers.

**Application of the axial-centrifugal compressor in the gas turbine units**

The axial-centrifugal compressor (Fig. 14.12) is a combined device in which the high efficiency of the axial compressor (the first 5–7 stages) is combined with a high-pressure ratio in the last centrifugal stage. A centrifugal stage is installed instead of several axial stages which have unacceptable small lengths of blades (less than 25–30 mm) [4].

Unlike the axial compressors, the axial-centrifugal compressors with the same pressure ratio have fewer rows of blades, i.e. have a shorter and lighter rotor.

Unlike multistage centrifugal compressors, in the axial-centrifugal compressors the airflow does not have many turns in the flow part: in the axial stages, it moves axially and rotates in the radial direction only within the impeller of the centrifugal stage. This allows using the radial diffuser, which has structural advantages (less

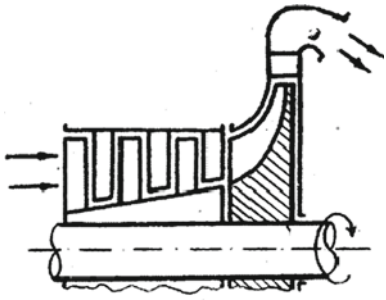

**Fig. 14.12** Scheme of an axial-centrifugal compressor

length of the casing; the simplicity of air transmitting to the combustion chamber; simple access to the rear compressor bearing, etc.).

The axial-centrifugal compressors are used in the gas turbine units with a power of 500–3000 kW. The pressure ratio in them is about 5–7.

## References

1. Romanovsky GF, Washchilenko NV, Serbin SI (2003) Theoretical basics of ship gas turbine designing. Publisher USMTU, Mykolaiv, 304 p. (in Ukrainian)
2. Giampaolo T (2006) Gas turbine handbook: principles and practices, 3rd edn. The Fairmont Press, 437 p
3. Romanovsky GF, Serbin SI, Patlaychuk VM (2005) Modern gas turbine units. Volume 1. Production units of Ukraine and Russia. Publisher NUS, Mykolaiv, 344 p. (in Ukrainian)
4. Romanovsky GF, Serbin SI, Patlaychuk VM (2017) Gas turbine plants. Part 2. Structural elements. Publisher NUS, Mykolaiv, 196 p. (in Ukrainian)

# Chapter 15
# Combustion Chambers of the Gas Turbine Units


The function of GTU combustion chambers is to heat the working fluid by burning hydrocarbon fuel.

In the combustion chambers of the gas turbine units, the burning of fuel (liquid or gaseous) is directly carried out in the airflow which is coming from the compressor. The chemical energy of the fuel is converted into heat and transferred to the working fluid, which then moves to the turbine part of the GTU [1, 2].

## 15.1 Requirements for GTU Combustion Chambers

We will only consider the most important ones of many requirements for combustion chambers [3].

(1) **Maximum fuel combustion completeness**

The completeness of the fuel burning in the combustion chamber will be characterized by the combustion chamber efficiency:

$$\eta_{cc} = \frac{Q_r}{Q_{th}},$$

where $Q_r$ is the real heat generated during the fuel combustion; $Q$th is the theoretically possible heat which is generated during the fuel combustion.

The last parameter can be determined by the following formula:

$$Q_{th} = G_f Q_f,$$

where $G_f$ is the fuel consumption, kg/h; $Q_f$ is the calorific value of the fuel, kJ/kg.

At nominal GTU's operating mode, the combustion chamber efficiency is $\eta_{cc} =$ 0.985–0.995. Smaller values of this parameter occur when using liquid fuel. Higher values of this parameter occur when using natural gas.



K. Liu et al. (eds.), *Gas Turbines Structural Properties, Operation Principles and Design Features*, https://doi.org/10.1007/978-981-99-0977-3_15

The efficiency of the combustion chambers is less than 1.0 due to physical and chemical incompleteness of the combustion.

Now we consider **the stages of the liquid fuel droplet burning** in the combustion chamber.

Stage 1. Gasification (evaporation).
At the first step of combustion, a droplet of liquid fuel should pass into a gaseous form due to the heating process.
Stage 2. Mixing gaseous fuel with air.
The resulting gaseous fuel must be mixed with air. Air contains oxygen, which is an oxidizer of fuel.
Stage 3. Chemical oxidation reaction.
The gaseous fuel reacts chemically with atmospheric oxygen. During this chemical reaction, heat is generated.

The liquid fuel droplet moves in the combustion chamber with air at a certain velocity. Because the length of the combustion zone is limited, the droplet residence time in the combustion zone is also limited.

If the residence time was not enough the ensuring stages 1 and 2, then we have a **physical incompleteness of the fuel combustion**.

If the residence time was not enough for ensuring stage 3 (but stages 1 and 2 are completed), then we have a **chemical incompleteness of the fuel combustion**.

The combustion chamber efficiency depends on temperature and pressure in the combustion zone.

The dependence of the combustion chamber efficiency on the temperature in the combustion zone has an optimum (Fig. 15.1).

**On the one hand**, the higher value of this temperature, the faster value of the liquid fuel is gasified and the chemical reaction passes faster. As a result, the efficiency of the combustion chamber must increase.

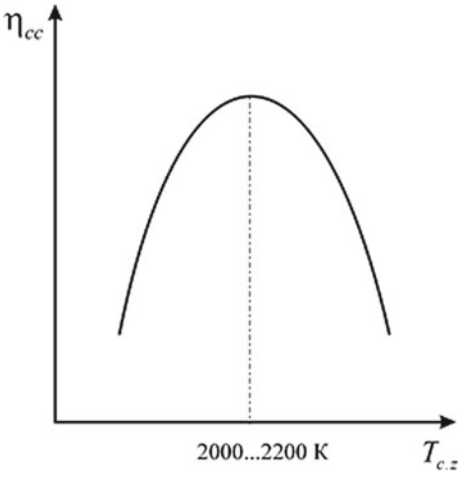


**Fig. 15.1** Combustion chamber efficiency versus temperature in the combustion zone

**On the other hand**, we know that the combustion of hydrocarbon fuels ($C_xH_y$) produces hydrogen and carbon oxides ($H_2O$ and $CO_2$). At high temperatures, these oxides begin to decompose back into components ($H_2O$ into $H_2$ and $O_2$; $CO_2$ into C and $O_2$). The higher value of the temperature in the combustion zone makes the decomposition (dissociation) higher. The decomposition of the oxides takes heat from the combustion products. As a result, the combustion chamber efficiency must decrease.

As a result of the combined action of these two factors, with an increase in temperature, the combustion chamber efficiency increases and then begins to decrease. The maximum efficiency has achieved the range of temperature $T_{c.z} = 2{,}000$–$2{,}200$ K in the combustion zone.

The dependence of the combustion chamber efficiency on the pressure in the combustion zone is becoming simpler (Fig. 15.2). An increase in pressure leads to an increase in efficiency.

(2) **Minimum pressure loss**

Air moves through the combustion chamber with a velocity of tens of meters per second. Due to air friction on the combustion chamber walls, its pressure decreases. The decrease of pressure also occurs due to air turbulence on various details of the combustion chamber (the so-called *local resistances*). The additional factor is that the increased pressure loss is the heating of the air during fuel combustion.

We already know that the higher pressure loss in any part of the gas turbine unit leads to worse efficiency.

The total pressure loss in the combustion chamber:

$$\Delta p_{cc} = p_2 - p_3,$$

where $p_2$ and $p_3$ are pressure before and after the combustion chamber.

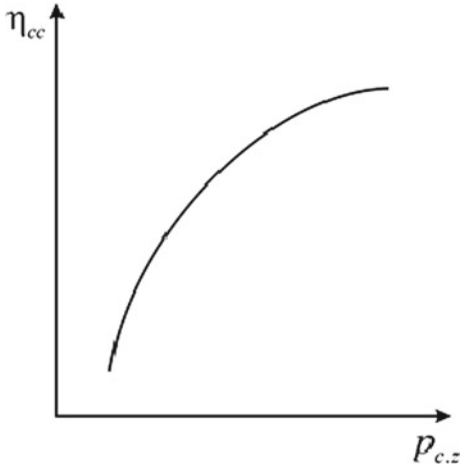


**Fig. 15.2** Combustion chamber efficiency versus pressure in the combustion zone

It is usual to use some dimensionless parameters to characterize the pressure loss in the combustion chamber. For example, the relative pressure loss $\sigma_{cc}$ or the pressure coefficient $\nu_{cc}$.

The relative pressure loss in the combustion chamber:

$$\sigma_{cc} = \frac{\Delta p_{cc}}{p_2}.$$

The combustion chamber pressure coefficient:

$$\nu_{cc} = \frac{p_3}{p_2}.$$

We already know that the combustion chamber pressure coefficient for modern gas turbine units is 0.95–0.97.

The relation between dimensionless parameters is quite simple:

$$\nu_{cc} = \frac{p_3}{p_2} = \frac{p_2 - \Delta p_{cc}}{p_2} = 1 - \sigma_{cc}.$$

And in accordance with it, the relative pressure loss is $\sigma_{cc} = 0.03$–$0.05$.

(3) **High heat intensity of the working volume**

The working volume of the combustion chamber is understood as the internal volume of the flame tubes. The fuel is being burned inside this volume.

The heat intensity of the working volume of the combustion chamber:

$$Q_v = \frac{Q_r}{V_{ft} p_2} = \frac{Q_{th} \eta_{cc}}{V_{ft} p_2} = \frac{G_f Q_f \eta_{cc}}{V_{ft} p_2},$$

where $Q_r$ is the real heat generated during fuel combustion (see above), kJ/h; $V_{ft}$ is the internal volume of the flame tubes, $m^3$.

The influence of heat intensity $Q_v$ on the characteristics of the gas turbine units is not simple.

On the one hand, with the higher value of the heat intensity of the working volume, the dimensions and weight of the combustion chamber are smaller. This is probably good for transport and marine gas turbine units.

On the other hand, the higher value of the heat intensity, the higher thermal stresses in the combustion chamber parts take place.

For this reason, for GTUs of various applications, the different values of the heat intensity $Q_v$ are taken during design. For example, for electric power generation, industry and marine transport it is, $Q_v = 700$–$1100$ kJ/m$^3$/h/Pa. For air transport $Q_v = 4{,}000$–$5{,}000$ kJ/m$^3$/h/Pa. The service life of aviation gas turbine engines is several times shorter than the life of all other gas turbine engines.

(4) **Minimum nonuniformity in the outlet**

For reasons, which we will consider later, the gas temperature at the outlet of the combustion chamber is not the same as at all points (Fig. 15.3). The maximum temperature $T_{max}$ is in the center. The minimum temperature $T_{min}$ is on the combustion chamber walls.

This temperature distribution does not affect the combustion chamber itself. But just behind the combustion chamber are the turbine nozzle vanes and rotor blades (Fig. 15.4). Therefore, the midpoints of the vanes and blades will heat up more; the upper and lower ends of the vanes and blades will heat up less. This temperature variation leads to the appearance of additional thermal stresses in the vanes and rotor blades. The overheating of the middle part of the vanes and blades can lead to their accelerated destruction.

The coefficient of the outlet temperature nonuniformity:

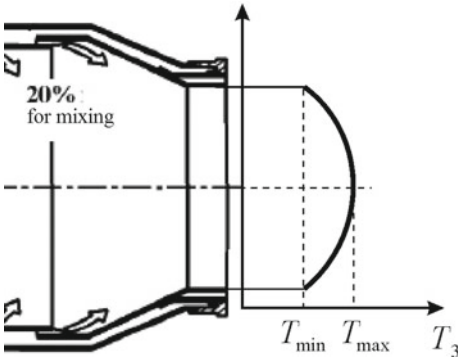


**Fig. 15.3** The distribution of gas temperature in the combustion chamber outlet

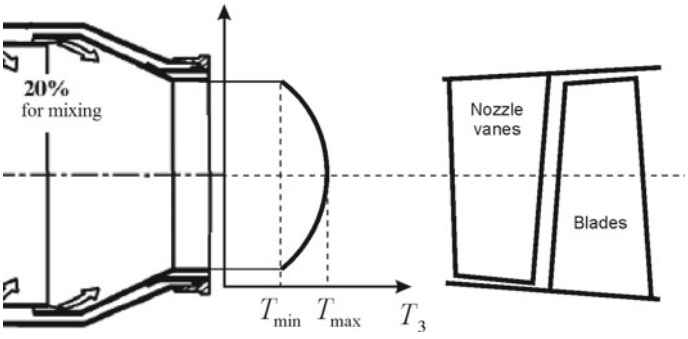


**Fig. 15.4** The effect of temperature on the turbine nozzle vanes and rotor blades

$$\delta = \frac{T_{\max} - T_{\min}}{T_{\text{calc}}},$$

where $T_{\text{calc}}$ is the average calculated gas temperature after the combustion chamber.

The value of this coefficient depends on the heat intensity of the combustion chamber's working volume. If we accept high heat intensity values, then our combustion chamber will be small. For this reason, the gas mixing in it will not be complete and the temperature nonuniformity at the outlet will be high. And vice versa.

The coefficient of the outlet temperature nonuniformity for aviation gas turbine engines is $\delta \geq 0.15$–$0.20$. For electric power generation, industry, and marine transport it is $\delta \leq 0.05$–$0.10$.

(5) **Reliable start-up and stable operation in all modes**

The attempts to improve the environmental cleanliness of the combustion chambers often lead to disruptions in their operation. This is especially evident when the combustion chamber is started and when a change in its operation mode is carried out. A reliable start-up and stable operation in all modes are the important functional requirements for GTU combustion chamber.

(6) **Long service life and simple operation**

Despite the difficult operating conditions, the combustion chamber must have the same service life as the service life of other parts of the gas turbine engine.

The combustion chambers should be easy to operate and maintain. Inspections and repairs should not be complicated and time should not be consumed.

(7) **The minimum content of harmful substances in exhaust gases**

When hydrocarbon fuel is burned, a certain amount of the substances which are hazardous to human health is formed. This is typical for all engines which use fuel combustion, including gas turbine engines.

The main harmful components of exhaust gases are nitrogen oxides NO and $NO_2$, sulfur oxides $SO_2$ and $SO_3$, carbon monoxide CO, unburned fuel, aldehydes, formaldehydes, benzopyrenes, etc.

The inhalation of these substances leads to damage of the lungs and bronchi, and causes heart weakness and nervous disorders. The combination of sulfur ($SO_2$, $SO_3$) and nitrogen ($NO_x$) oxides with water vapor ($H_2O$) leads to the formation of sulfuric ($H_2SO_4$) and nitric ($HNO_3$) acids. The vapors of these acids corrode the lungs and mucous membranes of the human body.

The minimum content of harmful substances in exhaust gases is one of the most important requirements for any engine.

## 15.2 Principles of Fuel Combustion in GTU Combustion Chambers

The scheme and structure of the simplest GTU combustion chamber are shown in Figs. 15.5 and 15.6.

Air from the compressor enters the combustion chamber at high velocity i.e. in modern GTUs it is up to 150 m/s. When heat is supplied to the air which is moving at such a velocity the pressure losses in the combustion chamber would be unacceptable

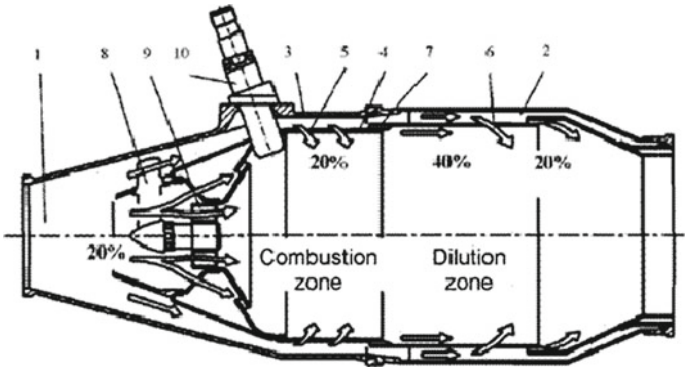


**Fig. 15.5** Scheme of the simplest GTU combustion chamber. 1—diffuser; 2—annular channels; 3—casing of the combustion chamber; 4—flame tube ("General Electric Co." instead of "flame tube" use the name "combustion liner".); 5—holes of the combustion zone; 6—holes of the dilution zone; 7—cooling holes; 8—fuel injector; 9—swirler (swirl vanes); 10—spark plug

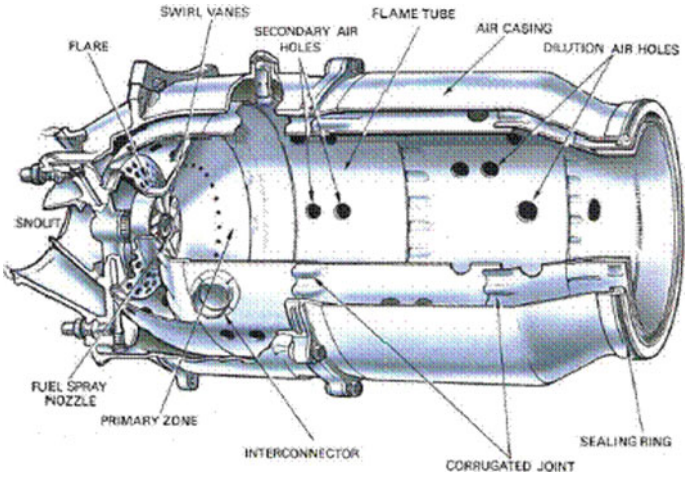


**Fig. 15.6** Structure of the simplest GTU combustion chamber

and would reach a fourth of the compressor pressure ratio. Therefore, to reduce the inlet velocity, a **diffuser** is located in all combustion chambers [1, 2, 4].

We consider the principles of fuel combustion in GTU combustion chambers.

(1) **Parting of the flame tube's internal volume into combustion and dilution zones**

The dilemma arises during the burning of fuel in the GTU combustion chamber. On the one hand, in order to ensure high efficiency of the combustion chamber, we need to burn fuel at a temperature of 2,000–2,200 K. On the other hand, it is impossible to discharge gas at this temperature onto the turbine blades, because this temperature is more than the melting temperature of the blade metal.

To solve this dilemma, the air in the combustion chamber after the diffuser is divided into two flows i.e. for combustion and dilution. The first airflow enters the combustion zone. It is involved in fuel combustion. In this case, combustion occurs at temperatures which are close to the optimal range (2,000–2,200 K).

The second air flow bypasses the combustion zone through the annular channels between the flame tubes and the casing of the combustion chamber. It enters the flame tubes through special holes in the dilution zone and cools the gas to the desired temperature (1300–1800 K).

As a result of such a technical solution, several times more air is pumped through the combustion chamber than is required for fuel burning. To characterize this, we use the **air excess coefficient in the combustion chamber**:

$$\alpha = \frac{G_{cc}}{G_0},$$

where $G_{cc}$ is the air flow rate through the combustion chamber; $G_0$ is the air flow rate which is required for the fuel combustion.

In modern GTUs the air excess coefficient $\alpha \approx 2.2 \sim 4.0$. Because of an increase in the gas temperature in the turbine inlet, it is required to increase the GTU efficiency, therefore for the gas turbine unit's improvement, this coefficient will decrease constantly.

(2) **Step-by-step supply of the combustion air along the combustion zone length**

The combustion air enters the combustion zone gradually, stepwise: it is done partly through the front device (dome) and swirler (primary combustion air), and it is done partly through holes in the flame tube wall (secondary combustion air). This is explained by the need to organize the effective combustion of the atomized fuel droplets of different dispersion (different sizes).

The atomized fuel droplets have different sizes. The small drops evaporate faster and begin to react with atmospheric oxygen in sections closer to the fuel injector. The big droplets evaporate more slowly and begin to react with atmospheric oxygen in sections farther from the fuel injector. If all the combustion air was immediately supplied through the dome to the combustion zone, then the combustion of the first evaporated fuel droplets would occur surrounded by an excess of the cold oxidizing

agent (air). In this case, heating and initiating the fuel-air mixture burning would be difficult and combustion would be slow and incomplete.

For this reason, a small amount of the combustion air is required to burn rapidly using the small droplets evaporating. This combustion air enters through the front device and swirler. Then, as bigger droplets evaporate, the following air portions are entered the combustion zone through holes in the flame tube wall.

It should be noted that the optimal distribution of the combustion air supply along the combustion zone length can be finally established only with the experimental tuning of the combustion chamber at the test site.

(3) **Turbulization of the airflow in the combustion zone**

Fuel will burn faster if it is thoroughly mixed with air. To accelerate the mixing of fuel with air, the airflow in the combustion zone is turbulized (swirled). Turbulization is carried out by installing in the front device the swirl vanes (swirler), perforated plates, and radial air inlet through holes in the flame tube wall.

(4) **Stabilization of the flame in the combustion zone**

Despite the decrease of velocity in the diffuser, the air velocity in the combustion zone remains very high and significantly exceeds the flame propagation velocity. This means that a flame which is ignited by the spark plug will be blown away by airflow. The flame propagation will not be stable and we will constantly need to re-ignite the flame using the spark plug.

To avoid this, additional elements are introduced into the combustion chamber design, which makes it possible to stabilize the flame in the combustion zone. A **swirler** is used for this purpose in most cases.

The change of air velocity in the cross-sections which are located immediately behind the swirler is shown in Fig. 15.7. The passing through the swirler air, under the action of centrifugal forces, is thrown to the flame tube walls. As a result of this, near the walls, the air velocity increases sharply, while in the center of the flame tube, there is a movement of air in the opposite direction (towards the fuel injector).

Part of the combustion zone, which is characterized by reverse air movement, is called the **reverse-flow zone (or recirculation zone)**. In this zone, stable propagation of flame occurs from combustible fuel particles to new particles which are entering the combustion zone.

We must say that the reverse-flow zone exists only in the cross-sections close to the swirler. At a distance from it, this zone disappears (see Fig. 15.7).

(5) **Optimal fuel atomization into the combustion zone**

It is possible to increase the fuel combustion speed by high-quality fuel atomization into the combustion zone. In this case, the fuel droplets should not touch the flame tube walls. Because the combustion temperature of the fuel is higher than the melting temperature of the metal, the burning of the fuel droplets on the flame tube wall will lead to its burnout and failure.

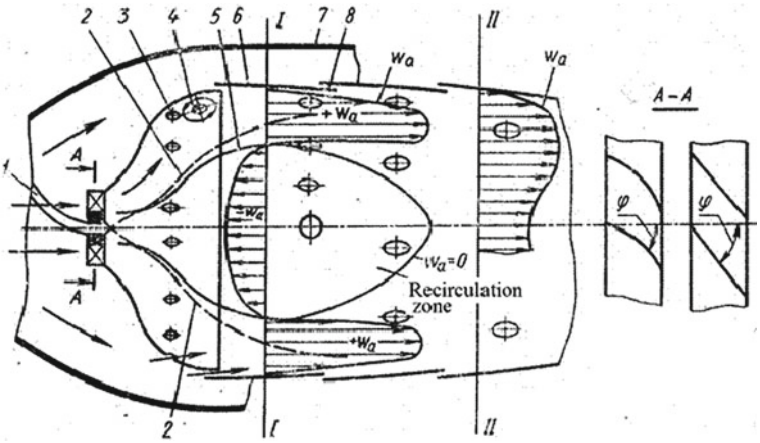


**Fig. 15.7** Diagram of the airflow in the combustion zone: 1—fuel injector; 2—atomized fuel; 3—holes; 4—possible flow separation zone; 5—border of the reverse-flow zone; 6—wall of the flame tube; 7—casing; 8—cooling air holes

The optimal fuel atomization is ensured by special designs of the centrifugal fuel injectors which are spraying fuel in the form of a hollow cone which is consisting of small droplets.

Figure 15.8 shows a schematic of a simple centrifugal injector. The fuel enters the swirling chamber *1* through tangential passages *2*. Then, through outlet nozzle *3*, it is entered the combustion zone in the form of a rotating cone with an angle $\beta_f$. The walls of this cone are consisting of individual fuel drops [4].

The use of **dual-channel centrifugal injectors** provides high-quality fuel atomization in all operating modes of the gas turbine engine.

The need for dual-channel centrifugal injectors is explained by the following: The movement of fuel through the injector is provided by the pressure which is produced

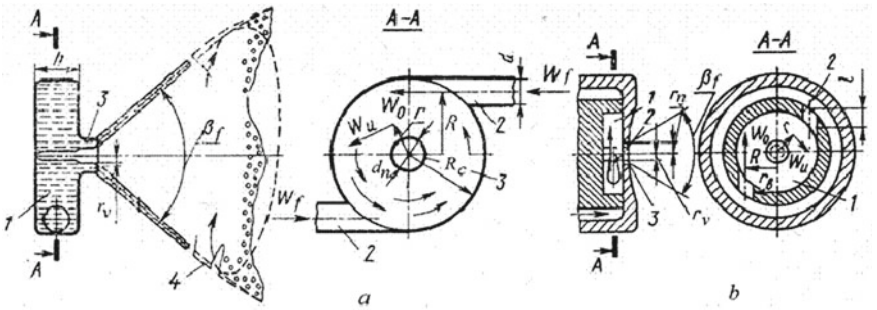


**Fig. 15.8** Diagram of a single-channel centrifugal injector. *a*—scheme of fuel movement; *b*—scheme of the injector; 1—swirling chamber; 2—tangential passages; 3—outlet nozzle; 4—rotating cone of fuel

by the fuel pump. The fuel pump is mounted on the rotor of the GTU compressor, that is, mechanical energy for its rotation is taken from this rotor. In the nominal operating mode (mode of 100% power), the rotor speed of the GTU compressor will be nominal (100%), therefore the rotation speed and pressure of the fuel pump will also be 100%.

When switching to a partial mode of operation, the rotor speed of the GTU compressor will be less than 100%, therefore, the rotation speed of the fuel pump will also be less than 100%. Therefore, the pressure which is produced by the pump will not be enough to atomize the fuel efficiently.

How can a dual-channel injector assist us to solve this problem? Such an injector has two channels (*a* and *b*) for the fuel movement and two output coaxial nozzles (*5* and *6*) (Fig. 15.9). In the nominal operating mode, fuel passes through both channels and is sprayed through both outlet nozzles. In partial operating modes, the pressure which is produced by the pump is not enough to overcome the spring *8* elasticity and open the second channel of the fuel movement. Fuel in this case will pass only through the first channel and will be sprayed through only one nozzle. It will improve fuel atomization greatly [3].

(6) **Cooling the combustion chamber elements**

As already noted, the temperature in the combustion zone is higher than the melting temperature of the metal. For this reason, during the design of the combustion chamber, engineers provide cooling of its more loaded elements.

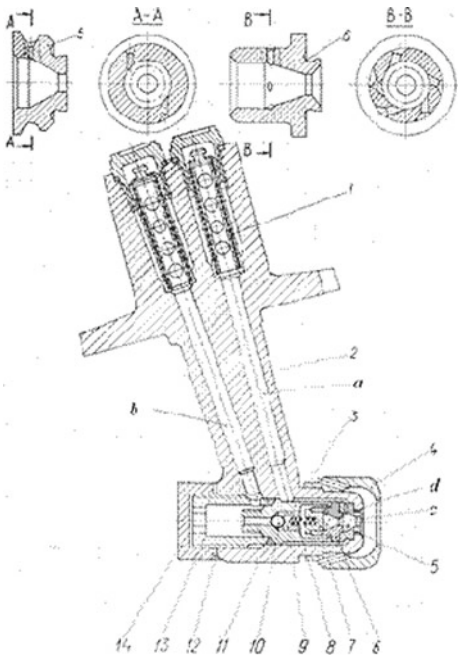


**Fig. 15.9** Dual-channel centrifugal fuel injector of the D050 engine: *a*—the first channel of the injector; *b*—the second channel of the injector; *c*—swirling chamber of the first channel; *d*—swirling chamber of the second channel; 1—filter; 2—casing; 3—tube; 4—cap; 5—nozzle of the first channel; 6—nozzle of the second channel; 7—stub; 8—spring; 9—ball nest; 10—ball; 11—sealing ring; 12—gasket; 13—clip; 14—nut

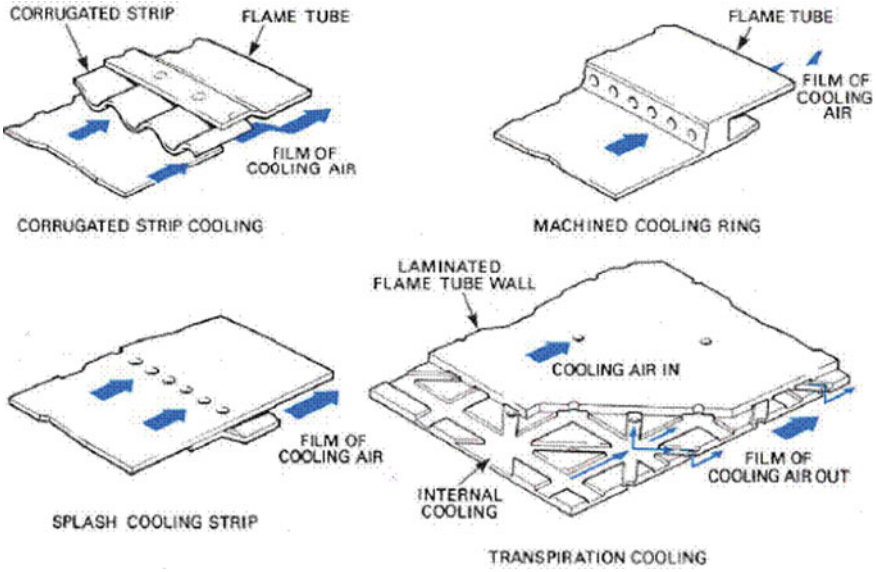


**Fig. 15.10** Methods of film cooling of the flame tube walls

All elements of the combustion chamber are intensively cooled by air.

A stream of air is passed to cool the injector between its body and the swirler in the annular gap. The inside of the injector is cooled by the flow of fuel.

The flame tubes are cooled externally by dilution air, which moves in the annular channels between them and the casing. Moreover, the air supply through the holes to the combustion zone is organized in such a way as to provide an air film on the inner surfaces of the flame tubes (Fig. 15.10). This film prevents the transfer of heat from the combustion zone to the flame tube walls.

## 15.3 Types of GTU Combustion Chambers

Depending on the type of used fuel, and the application and structural scheme of the gas turbine unit, various types and layouts of combustion chambers are used.

(1) **Connection of the combustion chamber with other parts of GTU**

By connecting with other parts of the gas turbine units, the combustion chambers are divided into:

– the external combustion chambers;
– the built-in combustion chambers.

**External combustion chambers** have their own casing, which is often placed on a separate base plate. They are connected to the compressor and turbine of GTU using special air and gas ducts.

163 MW SGT5-2000E engine from "Siemens AG" with such a combustion chamber is shown in Fig. 15.11 [4].

The main advantage of such combustion chambers is the simple maintenance and repair. Access to a similar combustion chamber is easy. For repair work, there is no need to disassemble the main GTU casing and disconnect the other parts of it.

We must say that of all types of combustion chambers, the external combustion chamber has the largest dimensions, weight, and pressure loss.

They are used in some designs of stationary gas turbine units.

**Built-in combustion chambers** are built into the casing of the gas turbine units. At present, there is a vast majority of such combustion chambers and they have their own classification.

Depending on the design, the built-in combustion chambers can be divided into:

– the annular combustion chambers;
– the multi-combustion chambers;

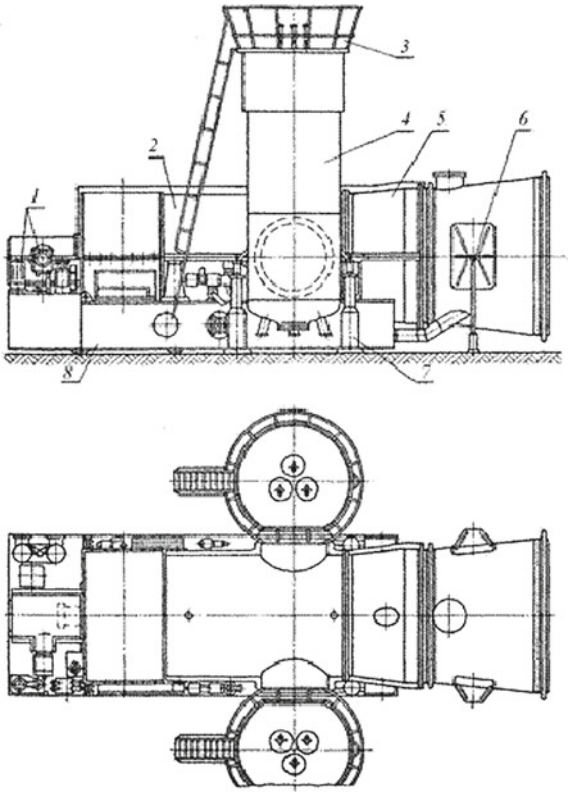


**Fig. 15.11** SGT5-2000E engine from "Siemens AG" with an external combustion chamber. 1—oil pumps; 2—compressor; 3—service platform; 4—combustion chamber; 5—turbine; 6—support; 7—support of the combustion chamber; 8—frame

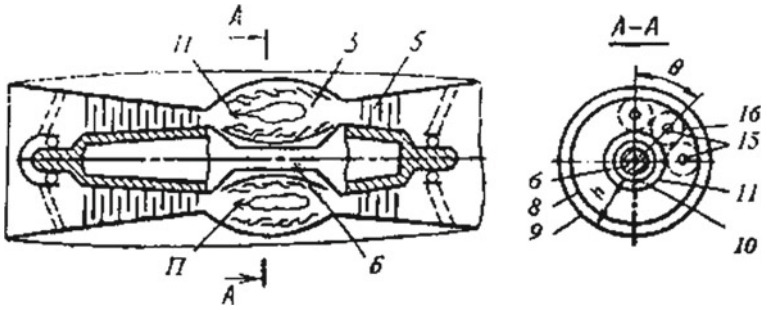


**Fig. 15.12** Design of the annular combustion chamber. 3—combustion chamber; 5—turbine; 6—shaft connecting the compressor rotor to the turbine rotor; 8—outer wall of the annular flame tube; 9—outer casing of the combustion chamber; 10—inner casing of the combustion chamber; 11—inner wall of the annular combustion chamber; 15—fuel injectors; 16—annular space

– the cannular combustion chambers;
– the individual combustion chambers.

The working volume of the **annular combustion chambers**, which are most widely used in aircraft engines, is a continuous annular space between the inner and outer walls of the flame tube (Fig. 15.12).

The annular combustion chamber is lighter and more compact than other types of chambers. When it is installed, the length of the engine is somewhat reduced due to the absence of air-distributing and gas-collecting transition elements in the smooth annular flow part. This chamber is characterized by lower pressure losses at the inlet and outlet, and more uniform gas velocity and temperature at the outlet. Less air is consumed to cool the flame tube [5].

The disadvantages include a large number of fuel injectors (several tens) which are selected by use of the method which is based on the complete filling of the annular space by flame. The experimental debugging of these chambers at the test bench is very complicated due to the need to use the full consumption of air and fuel. The assembly and disassembly of these chambers, and the flame tube removal, as a rule, are associated with complete engine disassembly, because the flame tubes are usually made continuous and circular without connectors. The stiffness of the annular chambers is less than others, therefore, at high pressures deformation of the outer walls is possible.

**The multi-combustion chamber** is the assembly of individual combustors (so-called *cans*). Each combustor (can) has its own flame tube, fuel injector, and casing (Fig. 15.13). All combustors are completely identical, they work independently. The gas flow from each of them goes to its own part of the first stage turbine nozzles [5].

In some cases, the flame tubes are connected by cross-fire tubes for transferring flame. In the presence of the cross-fire tubes, spark plugs (igniters) can be installed in only some cans of the combustion chamber.

The dimensions, weight, and pressure loss in multi-combustion chambers due to the presence of the various transitional and auxiliary elements are more than in

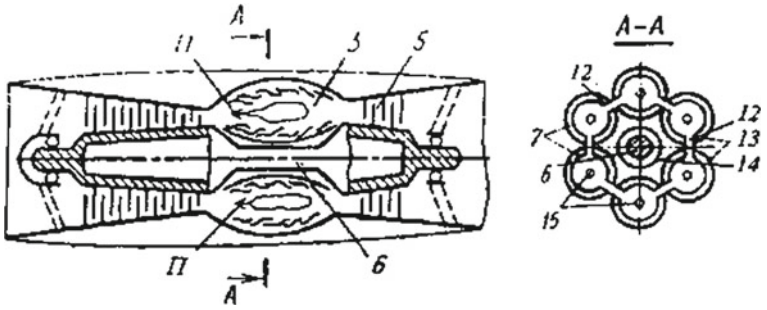


**Fig. 15.13** Scheme of the multi-combustion chamber. 3—combustion chamber; 5—turbine; 6—shaft connecting the compressor rotor to the turbine rotor; 7—flame tubes; 12—cross-fire tubes; 13—cans of the multi-combustion chamber; 14—inner wall of the multi-combustion chamber; 15—fuel injectors

annular ones. However, the cost of such chambers is significantly less; the number of fuel injectors is usually equal to the number of flame tubes; stiffness is much higher; their maintenance and repair are simpler.

**A cannular (can-annular) combustion chamber** combines the features of the annular combustion chamber and a multi-combustion chamber (Fig. 15.14) [2].

The cylindrical flame tubes are located between these casings in the annular space. The gas flows from them are combined in the annular gas collector directly before the first stage turbine nozzles. Like the can-type combustor, the cannular combustors have discrete combustion zones which are contained in separate flame tubes with their own fuel injectors. Unlike the can combustor, all the combustion zones share a common ring (annulus) casing.

The number of flame tubes is selected depending on the layout, GTU sizes, etc. They are often from 6 to 20. Fuel burns in the combustion zones of the flame tubes, interconnected by the cross-fire tubes. Through these cross-fire tubes, when a gas

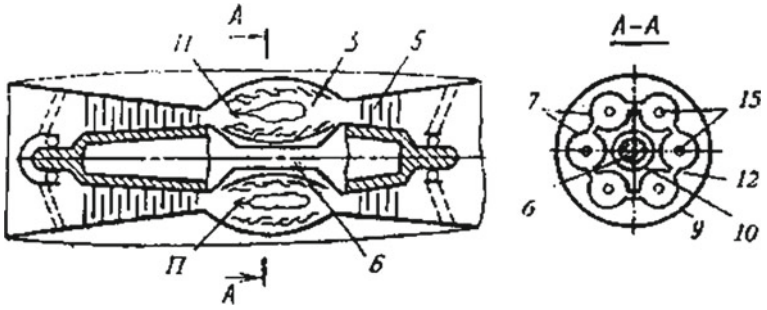


**Fig. 15.14** Design of the cannular combustion chamber. 3—combustion chamber; 5—turbine; 6—shaft connecting the compressor rotor to the turbine rotor; 7—flame tubes; 9—outer casing of the combustion chamber; 10—inner casing of the combustion chamber; 12—cross-fire tubes; 15—fuel injectors

turbine unit starts, fuel is ignited in all flame tubes by transferring flame from a burning torch; because the spark plug (igniter) is installed in two or three flame tubes. Due to the presence of the cross-fire tubes, flame propagation is ensured in case of the accidental failure of the torch in one flame tube. The cross-fire tubes also assist to stabilize the pressure in the flame tubes.

According to their advantages and disadvantages, the cannular combustion chambers occupy an intermediate position between the annular and multiple chambers.

The cannula combustion chambers are widely used in marine gas turbine units. This is the favorite type of combustion chamber of the Ukrainian company "Zorya-Mashproekt".

**Individual combustion chambers** are built into the casing of the gas turbine unit (Figs. 15.15 and 15.16). By design, they are sometimes similar to external combustion chambers. For this reason, many researchers do not distinguish them [5].

The use of individual combustion chambers reduces the distance between the compressor and the turbine and reduces the number of fuel injectors. The latter is especially important for low-power GTUs with low fuel consumption when the use

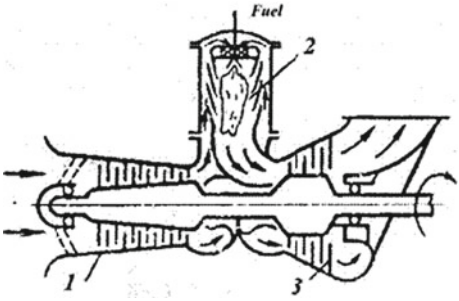


**Fig. 15.15** The layout of a gas turbine engine with an individual combustion chamber. 1—compressor; 2—combustion chamber; 3—turbine

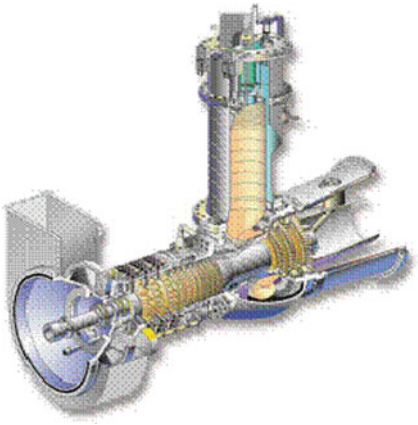

**Fig. 15.16** 11 MW GE10-1 engine from "General Electric Co." with the individual combustion chamber

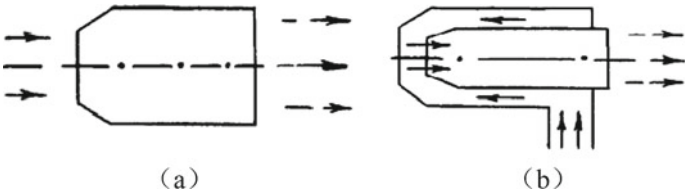


**Fig. 15.17** Straight-flow (**a**) and reversed-flow (**b**) air and gas movement in the combustion chamber

of other combustion chambers with a large number of fuel injectors is undesirable. In this case, the small size of the output nozzles leads to their frequent clogging.

The individual and external combustion chambers are very convenient because their disassembly does not require even partial disassembly of the GTU. However, such combustion chambers have significant dimensions and weight. Their air-distributing and gas-collecting transition elements provide additional pressure losses.

(2) **The movement of the working fluid in the combustion chamber**

According to the working fluid movement (Fig. 15.17), there are:

– straight-flow combustion chambers;
– reversed-flow combustion chambers.

There is the direction of the air movement in the annular channel between the flame tube and the casing coincides with the direction of the outlet gas movement in the **straight-flow combustion chambers**.

In the **reversed-flow combustion chambers**, air and gas flow towards each other. A reversed-flow design can provide significant advantages in the overall layout. The use of the reversed-flow combustion chambers allows reducing the length of the engine due to their location above the compressor or above the turbine. The latter option is often used when using the centrifugal or axial-centrifugal compressor.

We must say that due to the reverse movement of air and gas, the pressure loss in such a combustion chamber will be slightly more than in a straight-flow combustion chamber.

The flame tubes in the reversed-flow combustion chambers in the first GTUs were located horizontally. In recent decades, it is considered rational to place them at a certain angle (15–25°) to the central axis of GTU. With this arrangement, it becomes possible to better cool the combustion chamber details.

## 15.4 Calculation of the Reversed-Flow Cannular Combustion Chamber

We consider the calculation of the reversed-flow cannular combustion chamber.

The calculation of the combustion chamber is performed using the statistics on existing designs of GTU combustion chambers [3].

The diagram of the reversed-flow combustion chamber is shown in Fig. 15.18.

The reversed-flow combustion chamber in a gas turbine unit with an axial compressor is located above the outer casing of the high pressure compressor. After this compressor, air passes through its rear casing. Then it rotates at 180°and enters the annular space between the casings and flame tubes of the combustion chamber. Before entering the combustion chamber front device, there is another turn of the airflow by 180°.

As a result, we have a very strong vortex airflow in the annular space, which provides a uniform distribution of the dilution air between the flame tubes.

(1) The following parameters were determined during the thermal calculation of GTU at nominal operating mode:

- the fuel consumption $G_f$;
- the fuel calorific value $Q_f$;
- the stoichiometric coefficient $L_0$;
- the combustion chamber efficiency $\eta_{cc}$;
- the pressure at point 2 (after HPC) $p_2$;
- the air flow rate through the combustion chamber $G_{cc}$;
- the temperature at point 2 (after HPC) $T_2$.

(2) Heat intensity of the combustion chamber working volume for marine GTUs is equal to:

$$Q_v = 700 \sim 1,000 \text{ kJ/m}^3\text{/h/Pa}.$$

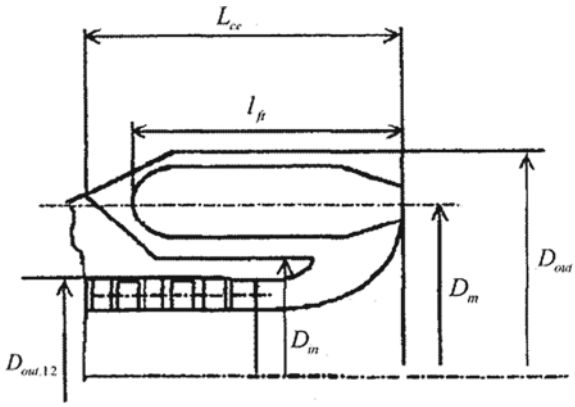


**Fig. 15.18** Diagram of the reversed-flow combustion chamber

(3) The combustion chamber working volume (the internal volume of the flame tubes):

$$V_{ft} = \frac{G_f Q_f \eta_{cc}}{Q_v \, p_2 \cdot 10^6}.$$

(4) Number of the flame tubes is $n_{ft}$ which are accepted with further clarification (in step 18). As a first approximation, it is taken equal to the number of flame tubes of the basic gas turbine unit.

(5) The internal volume of the single flame tube:

$$v_{\text{ft}} = \frac{V_{\text{ft}}}{n_{\text{ft}}}.$$

(6) The coefficient of flame tubes' non-cylindricity:

$$a = 0.70 \sim 0.75.$$

(7) The relative length of flame tubes:

$$\bar{l} = 3 \sim 4.$$

(8) The diameter of the flame tube:

$$d_{\text{ft}} = \sqrt[3]{\frac{4\, v_{\text{ft}}}{\pi \, \bar{l} \, a}}.$$

(9) The flame tube length:

$$l_{\text{ft}} = d_{\text{ft}} \, \bar{l}.$$

(10) The circumferential clearance between flame tubes:

$$\delta = (0.10 \ldots 0.20) \, d_{\text{ft}}.$$

(11) The medium diameter of the flame tubes installation:

$$D_m = \frac{d_{\text{ft}} + \delta}{\sin\left(\frac{180^\circ}{n_{\text{ft}}}\right)}.$$

(12) The primary combustion air excess coefficient:

$$\alpha_{\text{pr}} = 1.2 \sim 1.6.$$

(13) The air flow rate through the front device of all flame tubes:

$$G_{\text{pr}} = \frac{\alpha_{\text{pr}} G_f L_0}{3600}.$$

(14) The air flow rate through the channel between casings and flame tubes:

$$G_{\text{ch}} = G_{\text{cc}} - G_{\text{pr}}.$$

(15) The cross-section area of all flame tubes:

$$F_{\text{ft}} = \frac{\pi}{4} d_{\text{ft}}^2 n_{\text{ft}}.$$

(16) The summary cross-section area of the combustion chamber:

$$F_{\text{cc}} = (2.2 \ldots 2.5)\, F_{\text{ft}}.$$

(17) Diameter of the combustion chamber inner casing

$$D_{\text{in}} = D_m - \frac{F_{\text{cc}}}{\pi D_m}.$$

(18) At this step, we must check the layout of the combustion chamber with the compressor part of GTU. The combustion chamber is reversed-flow and it is located above the high pressure compressor. Therefore, the diameter of the combustion chamber's inner casing must be higher than the outer diameter of this compressor:

$$D_{\text{in}} > D_{\text{out.1.2}}.$$

If this check is not performed, we need to reaccept the number of flame tubes in step 4. An increase in the number of flame tubes leads to an increase in the diameter of the combustion chamber's inner casing.

When we check the layout of the combustion chamber, we must remember that compliance with the condition $D_{\text{in}} \gg D_{\text{out.1.2}}$ is also not desirable. The number of flame tubes should be chosen as the minimum for the correct combustion chamber layout.

(19) The diameter of the combustion chamber outer casing:

$$D_{\text{out}} = D_m + \frac{F_{cc}}{\pi D_m}.$$

(20) The combustion chamber length:

$$L_{cc} = (1.1 \ldots 1.2)\, l_{\text{ft}}.$$

# References

1. Giampaolo T (2006) Gas turbine handbook: principles and practices, 3rd edn. The Fairmont Press, 437 p
2. Boyce MP (2006) Gas turbine engineering handbook, 3rd edn. Elsevier Inc., 936 p
3. Romanovsky GF, Washchilenko NV, Serbin SI (2003) Theoretical basics of ship gas turbine designing. Publisher USMTU, Mykolaiv, 304 p. (in Ukrainian)
4. Romanovsky GF, Serbin SI, Patlaychuk VM (2017) Gas turbine plants. Part 2. Structural elements. Publisher NUS, Mykolaiv, 196 p. (in Ukrainian)
5. Romanovsky GF, Serbin SI, Patlaychuk VM (2016) Gas turbine plants. Part 1. General structure and classification. Publisher NUS, Mykolaiv, 216 p. (in Ukrainian)

# Chapter 16
# Turbine Part of the Gas Turbine Units


The function of the GTU turbine part is to produce the mechanical energy of rotation. The turbine is a heat engine in which the potential energy of the working fluid is converted into the mechanical energy of the rotor. The potential energy spent for this is characterized by enthalpy, which is functionally dependent on the pressure and temperature of the working fluid. The working fluid in gas turbines is the combustion product of the hydrocarbon fuel which is coming from the combustion chamber.

A specific feature of the GTU turbine part is that only 30–40% of its power is transmitted to the consumer, while the rest is used to drive the compressor. In the majority of the gas turbine units, the axial turbines are used; in the low-power GTUs, centripetal radial turbines are used too.

## 16.1 The Structure and Operation of the Axial Turbine

The main elements of the axial turbine are the nozzles, which are formed by the nozzle vanes which are fixed in the casing (Figs. 16.1 and 16.2), and the moving (rotor) blades,[1] mounted on the disk [1, 2]. The disk can be manufactured as a single detail with a shaft or can be performed separately and then connected rigidly to it by welding or fastenings. The shaft, together with all the elements which are installed on it, forms a rotating part of the turbine i.e. **the turbine rotor** (see Fig. 16.2).

The turbine casing serves for supply (inlet) and removal (exhaust) of the gas and withstands overpressure of the working fluid. In places of the shaft exit from the casing, the seals are provided with the internal space of the turbine from the environment for isolating. All stationary parts of the turbine form **the turbine stator**. The power which is produced by the turbine is transmitted to the consumer through the flange or the coupling.

[1] "General Electric Co." instead of "blade" uses the name "bucket".



K. Liu et al. (eds.), *Gas Turbines Structural Properties, Operation Principles and Design Features*, https://doi.org/10.1007/978-981-99-0977-3_16

**Fig. 16.1** Nozzles of an axial turbine from J47 turbojet engine

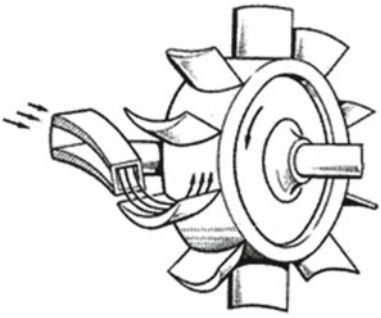

**Fig. 16.2** Single nozzle and rotor of the axial turbine

The combination of one row of the stationary nozzle vanes and one row of the rotating blades is called **the turbine stage** (Figs. 16.3 and 16.4). In the turbine stage, the potential energy of the gas is converted into mechanical energy of rotation.

Figures 16.5 and 16.6 show the high-pressure turbine and the low-pressure turbine of the AI-25 turbojet engine from "Ivchenko-Progress" (a maximum thrust is 17 kN; about 9360 units were produced from 1967 to 2012) [3].

**The choice of the turbine stage number** is one of the main problems in turbine design. In stationary and transport, GTU turbines are used with a small and big number of stages. With an increase in the number of stages, the size and cost of the

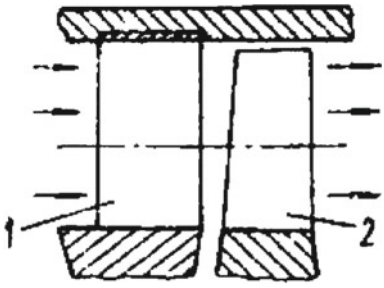


**Fig. 16.3** Scheme of turbine stage: 1—nozzle vanes; 2—rotor blades

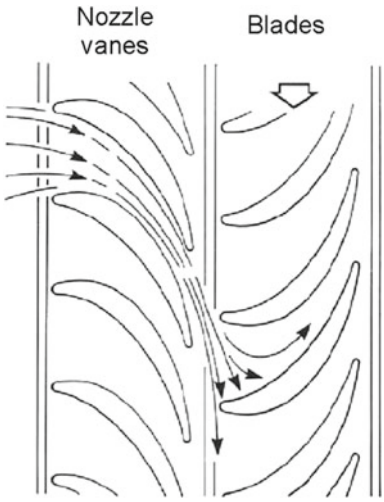


**Fig. 16.4** Airfoils of nozzle vanes and blades

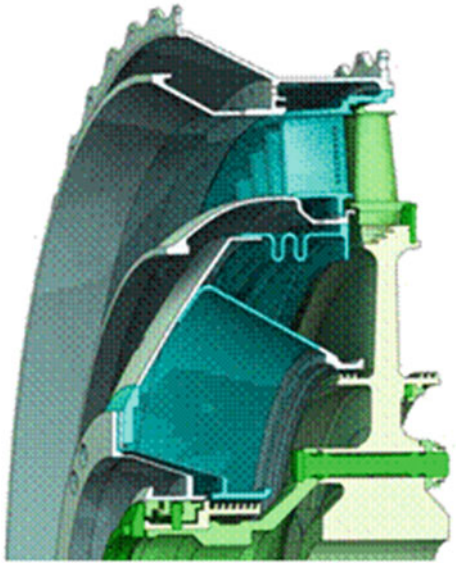

**Fig. 16.5** Single-stage high-pressure turbine of the AI-25 turbojet engine

turbine increase, the design of the elements and the organization of their cooling becomes more complicated, but the efficiency of the turbine increases.

There are many factors that influence the choice of the turbine stage number, and both turbines with a small and big number of stages are quite viable and have a fairly wide application.

The choice of the design scheme is also influenced by the traditions and production capabilities of the manufacturer. The companies that produce compact and light aircraft gas turbines, in stationary GTUs, use a small number of stages and cantilever

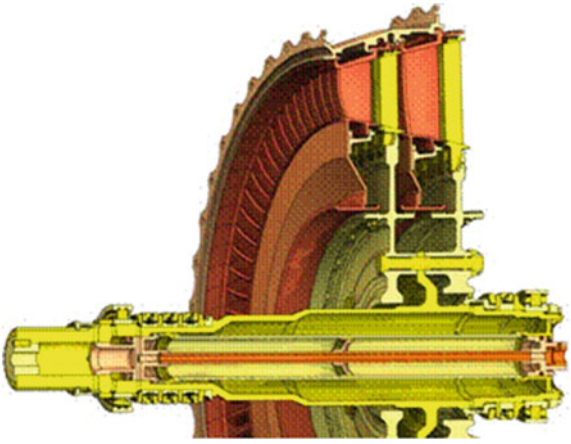

**Fig. 16.6** Two-stage low-pressure turbine of the AI-25 turbojet engine

rotors. The companies that produce the steam turbines, in stationary GTUs also use a big number of stages.

## 16.2 Axial Turbine Nozzle Vanes and Moving Blades

### *16.2.1 Axial Turbine Nozzle Vanes*

The turbine nozzle vanes which are placed on the retaining rings form the **nozzles**, in which the potential energy of the gas is converted into kinetic energy (flow acceleration). There is the inner and outer retaining rings limit of the annular channel of the turbine flow path. In some designs, the turbine casing plays the role of the outer retaining ring.

The nozzle vanes of the first turbine stage are made wider; the subsequent ones are already made in order to reduce the axial dimensions and weight of the turbine. The vanes are twisted in length and have a constant or variable airfoil and a chord length (Figs. 16.7 and 16.8). In the nozzle vanes with a chord increasing towards the periphery, the relative pitch of the vanes along its length is closer to the optimal value [2].

The design of the nozzle vanes depends on the method of attachment and the manufacture. The vanes can be with shelves, pins, ears, etc., solid or hollow (Fig. 16.9).

The nozzle vanes are under significantly lower mechanical loads compared to rotor blades but are under the high-temperature stresses caused by uneven heating. When starting a gas turbine engine and during rapid power gaining, the nozzle vanes are under significant stresses associated with a sharp change in the inlet edges temperature and higher thermal inertia of the massive middle parts. This temperature

**Fig. 16.7** Nozzle vane of GTK-10-4 engine from "Nevsky Zavod"

**Fig. 16.8** Nozzle vane of GTE-45-3 engine from "Turboatom"

difference, even with a relatively small number of cycles, can lead to vanes fatigue destruction.

**The use of hollow vanes** minimizes this temperature difference. Compared to solid vanes, hollow vanes have 3–4 times higher heat resistance, as well as higher reliability and resource.

In addition, the presence of cavities in the vanes provides the possibility of cooling, and also reduces their weight, and reduces metal consumption. However, the hollow vanes have a large thickness of the airfoil and outlet edges, which worsens their gas-dynamic properties.

To increase the nozzle vane's heat resistance during its manufacture the following methods have been applied: (broaching, electromechanical processing, electropolishing, etc.) that do not give the residual tensile deformations.

From casting alloys, the nozzle vanes are made by the **method of lost wax casting**. By casting, both solid vanes and hollow cooled vanes are made.

In the cooled casted vanes, a cooler (most often compressor air) exits either through slotted holes on the side of the airfoil near the outlet edge (which makes it possible to keep the outlet edges thin) or through slotted holes in the outlet edge.

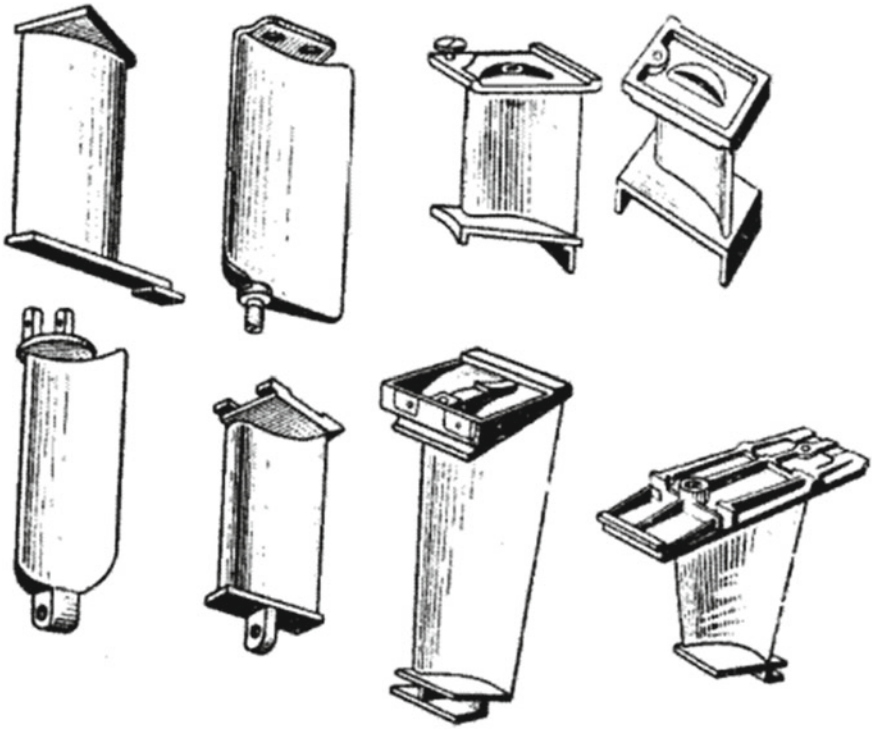

**Fig. 16.9** Nozzle vanes

The hollow nozzle vanes are also made by the **flexible stamping** of sheets which is followed by **welding** along the outlet edge. Using that method, the material consumption is significantly reduced, and the complexity of the production and the cost of the vanes are also reduced.

**The thermocouples** can be mounted in the inlet edges of the nozzle vanes to control the gas turbine engine according to the gas temperature.

Due to significant temperature deformations, the nozzle vanes, as a rule, are not used to transfer the load from the bearing casing to the turbine casing. Other elements are used (studs, struts, etc.) for this aim.

**The methods for attaching the nozzle vanes** to the retaining rings are very different. All methods are divided into single-support mounting and double-support mounting.

**A single-support mounting**, in which the vanes are only connected with one retaining ring (usually with the outer ring, connected rigidly to the engine casing), is sometimes used in the nozzles of the last stages. In Fig. 16.10, the vanes are fixed in the split segment inserts with T-shaped shelves of the same profile (similar to the circumferential mounting of the blades). A gap of 0.2 mm is provided between the

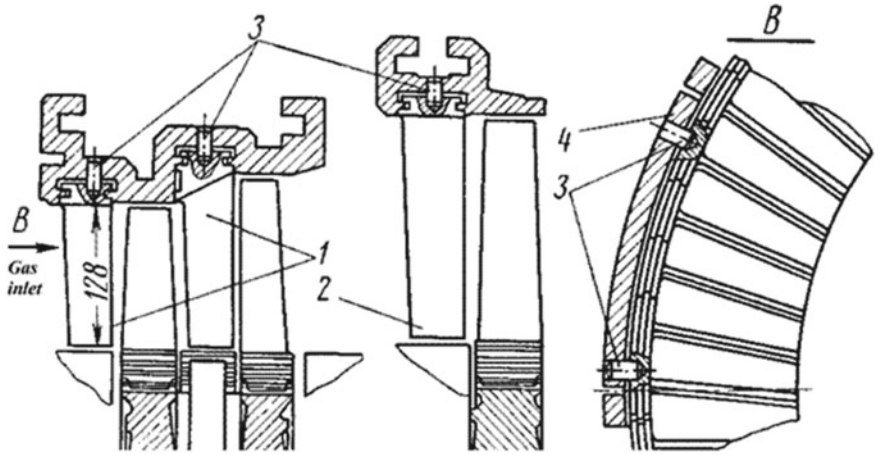


**Fig. 16.10** Nozzle vanes of GT-700-5 engine from "Nevsky Zavod". 1—vanes of the high-pressure turbine; 2—vanes of the low-pressure turbine; 3—radial pin; 4—segment insert

shelves to compensate for the thermal extensions. The last vanes of each segment are fixed by the radial pins.

At the **double-support mounting** (Fig. 16.11), the nozzle vanes are connected both to the outer retaining ring and to the inner one. The double-support mounting is widely used in the nozzles of all stages, where the retaining rings are rigidly attached to the corresponding casing elements [2, 3].

The double-support and single-support mountings of the nozzle vanes can be disassembled and non-disassembled. Accordingly, the nozzles are divided into disassembled and non-disassembled.

**The non-disassembled nozzles** can be made by cast, welding, and with the riveted vanes.

For the **cast nozzles** manufacture, the precision casting method is used. The vanes and retaining rings are usually cast as a single detail, in sections of 2–4 vanes in each (Fig. 16.12). The advantage of this design is its high rigidity. Its disadvantages include the difficulty of grinding the vanes and providing high-quality surfaces; the presence of thermal stresses in the structural elements; the difficulty to repair [4].

In the **welded nozzles**, the vanes are welded to both retaining rings, or to one of the retaining rings for the formation of the movable joint with the other. This design is simple, but it is very time-consuming to manufacture due to the welding of a large number of vanes. At the same time, with such mounting of the vanes, it is difficult to install them accurately before welding, and, in addition, during the welding process, warping of the vanes and violation of the shape of the flow part are possible. Therefore, the welding of the vanes has to be performed in special devices. The replacement of defective vanes is completely impossible.

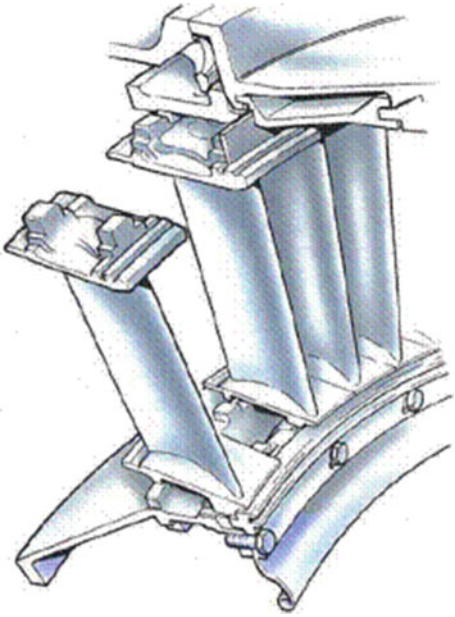

**Fig. 16.11** Nozzles with double-support mounting

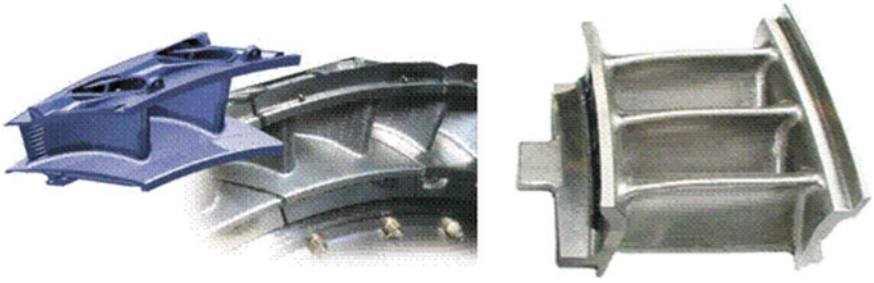

**Fig. 16.12** Cast nozzles

The mounting of the vanes to the retaining rings **by riveting is** technologically simpler. The vanes have protrusions, which after they have been inserted, are riveted into the corresponding protrusions of the retaining rings.

The main advantage of the non-disassembled nozzles is a relatively small number of technological operations for the machining of details. The disadvantages include the difficulty of replacing defective vanes during the repair.

**Disassembled nozzles with double-support mounting** are made either with the rigid mounting of the vanes in one of the retaining rings and with a movable mounting in the other or with movable mounting in both retaining rings.

**The rigid mounting** of the vanes (Fig. 16.13) is usually carried out in the outer retaining ring or in the turbine casing. The rigid mounting is carried out:

- with screws which are passing through the shelf of the vane;
- with the assistance of the shelf, which enters the groove of the retaining ring and is fixed to the casing by a radial pin;
- with using of the protrusion on the shelf of the vane through which the vane is attached to the turbine casing flange.

By use of the **movable mounting in both retaining rings** (so-called *floating vanes*), the circumferential and axial fixation of the vanes can be carried out in various ways, for example, using **special spacers** (Fig. 16.14) [2].

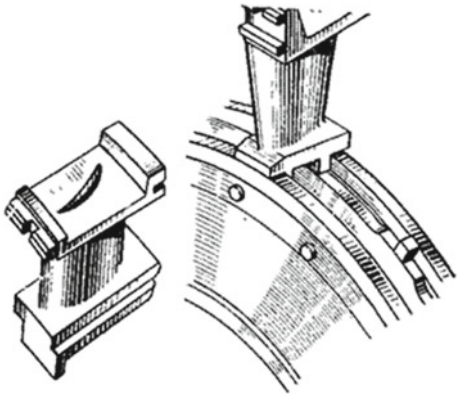

**Fig. 16.13** Nozzle vanes of CS600 engine from "Centrax Ltd."

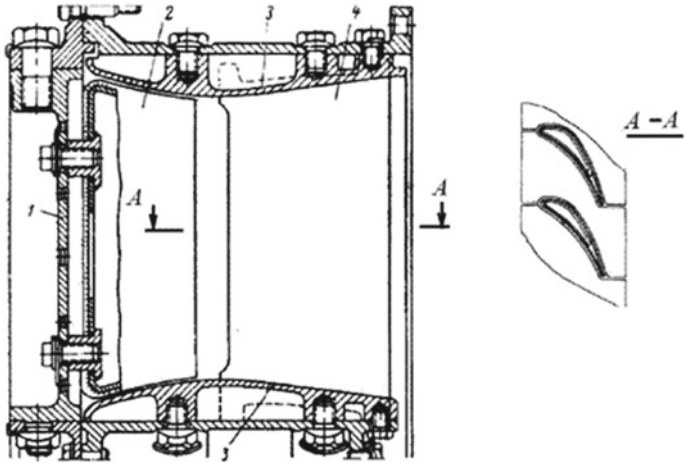


**Fig. 16.14** Nozzles with floating vanes. 1—strut; 2—inlet space; 3—upper and lower spacers; 4—nozzle vane

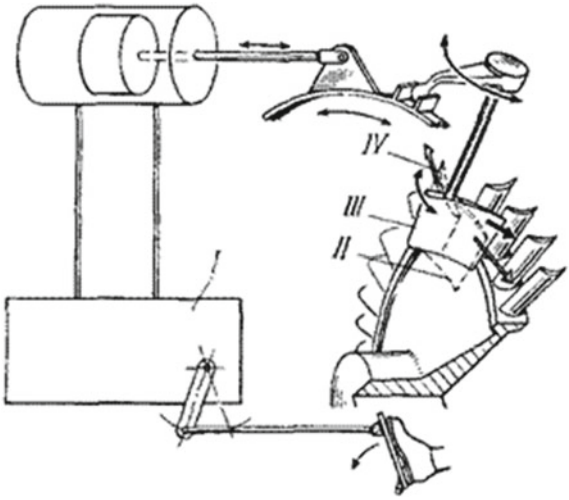


**Fig. 16.15** Rotary nozzle vanes of automobile engine from "Chrysler Corp.". I—regulation system; II—position of the vanes at partial operating modes; III—position of the vanes in full power mode; IV—position of the vanes during braking

Each of the spacers from one side has a profile which is corresponding to the concave surface of the airfoil. Each of the spacers from another side has a profile which is corresponding to the airfoil convex. In this way, two adjacent spacers form a notch which is having the shape of a vane airfoil in which the vane is mounted at one end. Its other end is mounted in a similar notch which is formed by spacers on the opposite side.

The radial fixation of the floating vanes is carried out either by stopping the vanes at the turbine casing (see Fig. 16.14) using a locking ring, or with the assistance of special shelves which are welded to the retaining ring and the cotter pins that are inserted into the holes in the shelves and vanes.

The disassembled nozzles have the following advantages:

- the ability of a good surface grinding and obtaining a high accuracy airfoil;
- lower thermal stresses that arise due to differences in temperature of the airfoils and the retaining rings;
- the ability to replace quickly the damaged vanes during the repair.

To provide higher GTU efficiency in the partial operation modes, in some turbines the nozzle vanes can change their position (rotates) according to the special program. An example is the rotary nozzle vanes of the automobile engine from "Chrysler Corp." (Fig. 16.15).

### *16.2.2 Axial Turbine Moving Blades*

The turbine's moving blades form passages, in which the kinetic energy of the gas is converted into mechanical work.

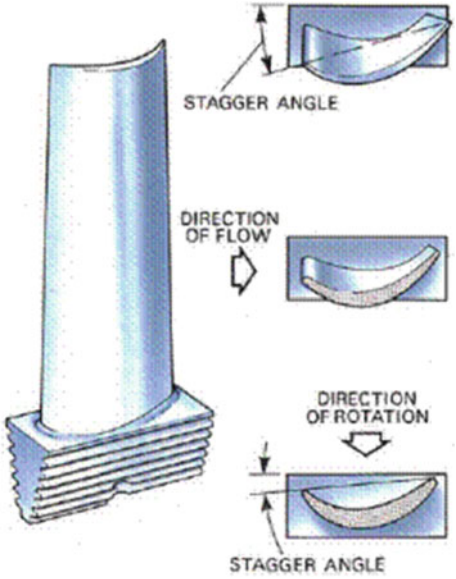


**Fig. 16.16** Twisted blade

Due to the different angles of the gas flow along the airfoil length, the blades are **twisted**, i.e. have a different orientation relative to the flow airfoil (Fig. 16.16). The twisting of the blades increases with their length. For this reason, the blades of the last turbine stages are most tightly twisted (as the longest) [2].

The blades are affected by significant centrifugal and bending forces. They are also under the vibration loads of various natures. To reduce the blade's weight, tensile stresses, and loads on the rotor, the blades are performed with decreasing chords and thicknesses, so that the peripheral section area can be 3–5 times less than the root section area. In this case, the rigidity of the airfoil should be sufficient to maintain the installation angles in the most difficult conditions of work.

Compared to the compressor blades, the turbine blades operate at higher temperatures and are affected by higher static, vibration, and temperature stresses. They are also under simultaneous corrosive and erosive effects of the gas.

Considering the difficult working conditions and the role of the blades in the engine (the reliability and service life of the blades determine largely the reliability and life of the entire engine), strict requirements are imposed on the moving blade design and the method of their mounting at the disk, on their materials and manufacturing technology.

The turbine blades have the same structural elements as the compressor blades, but their geometric shapes and proportions are different. The turbine blades are characterized by thicker, more curved airfoils and by bigger transition parts and roots.

To reduce the leakage through the radial clearance, which is especially important for short blades, the blades are equipped with **shrouding (bandage) shelves**

(Figs. 16.17, 16.18, 16.19 and 16.20). The long blades are also equipped with shrouding shelves, but it is to reduce stress during vibration.

The blades with the shrouding shelves have thicker peripheral airfoils. After mounting the blades on the disk, **the shelves form a split shrouding ring**. A small gap is provided between the shelves in the cold state (0.15–0.25 mm). In working conditions, the shrouding shelves are in contact with each other, while the airfoil of each blade under the action of a centrifugal force is untwisted.

The shrouding shelves are joined together with a slash (Fig. 16.19a) or a straight (Fig. 16.19b) contact surface, and, considering the significant thermal expansion of the blades, they are rarely welded.

The solid shrouding ring is used extremely rarely. It is performed mainly in low-power engines with low temperatures.

On the blades, the airfoil which is tightly twisted and during operation due to the centrifugal forces is under significant untwisting, as a rule, **Z-shaped shrouding shelves** are used (see Fig. 16.19a). However, these shelves are characterized by the increased shear stresses on the contact surfaces, as well as stress concentrators in Z-surfaces. Therefore, for blades with a relatively rigid airfoil, it is more acceptable

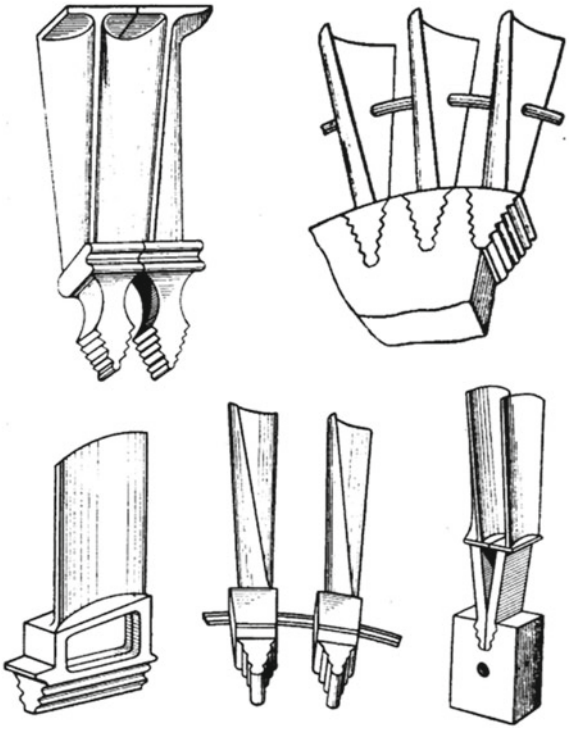

**Fig. 16.17** Turbine blades

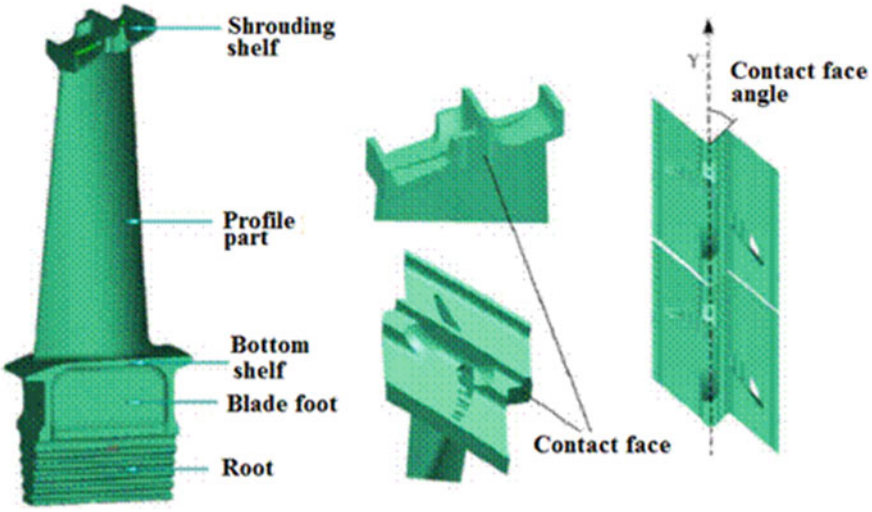


**Fig. 16.18** Blblade with shrouding shelf, root shelf, and elongated root

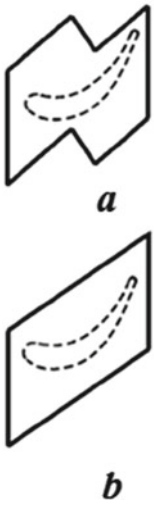


**Fig. 16.19** Z-shaped shrouding shelf (**a**) and shrouding shelf with straight contact surfaces (**b**)

to use the **shrouding shelves with the straight contact surfaces** (see Fig. 16.19b) [2].

The shrouding shelves are often equipped with **sealing ridges** to reduce gas leakage. The weight of the shrouding shelf can be up to 20% of the airfoil weight for the first stage, up to 15% for the second stage, and up to 10% for the subsequent

**Fig. 16.20** Blades with elongated roots

stages. The centrifugal forces, which are provided by the shrouding shelves, give the blade additional tensile loads.

Between the airfoil and the root, the blade has a **root shelf** that improves the transition from airfoil to root. The combination of these shelves limits the turbine flow part at the inner diameter.

Sometimes the blades are made with **elongated roots** (Fig. 16.20). This design provides the reliable isolation of the disk from hot gas, as well as damping the blade vibrations. Blowing elongated roots with cooling air significantly reduces the temperature of the disk and allows the disk to be thinner and lighter [2].

To reduce vibration, the **box-shaped dampers** are sometimes placed between the root shelves. In some designs, for the same purpose, they put the **shrouding tubes** (or wire) through the holes in the roots or in the airfoils (see Fig. 16.17) [2].

To improve the damping of vibration, the blades with the elongated roots **can be installed in pairs (two roots in one groove)** (Figs. 16.17 and 16.21). This constructive solution is often used by "General Electric Co.". In this case, the friction on the root contact surfaces, that occur during vibrations, dampens these vibrations and reduces stresses in the blade.

Nickel-chromium alloys with additives of the different components are used for the manufacture of the blades.

To ensure the high efficiency of the turbine, the blades are **carefully monitored** in the production. The accuracy of the relative position of the sections along the length

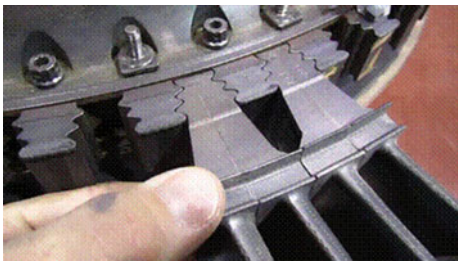

**Fig. 16.21** Mounting of blades in pairs (two roots) in one groove

of the blade and the relative to the root airfoil, as well as the cleanliness of the blades, are verified.

To facilitate the process of rotor balancing, **the blades are divided by weight**. The deviation in the blade weight in one row does not exceed 5–10 g. In the opposite grooves of the disk, the blades with a weight difference of no more than 1–2 g must be installed.

**The axial mounting of the gas turbine blades with a fir-tree root** has received widespread use at present (Figs. 16.22 and 16.23).

The blade is mounted in the disk groove with the assistance of the serrations which are located on the root and, accordingly, on the inner surface of the groove. From moving along the groove, the blade is fixed from one side by protrusion *1* (Fig. 16.23a), and from the other side, by the antenna, which is shown in position before bending *3* and after bending *4*. The movement of the blade in the groove after bending the antennae is 0.1–0.3 mm.

The blades can be locked with a folding plate 7 that keeps them from moving in both directions (Fig. 16.23b), because the antenna can be damaged during engine repair [2].

Other methods of axial fixation of the blades are also used.

In practice, a fir-tree mounting became the best for the blades of the axial turbines.

**Advantages of this mounting**:

- a small-size- the root allows the placement of a large number of blades on the disk;
- a mounting of the blades does not limit the thermal expansion of the disk, so that the temperature stresses in the blades are eliminated, and they are reduced in the rim of the disk;
- during the turbine rotation, the blades can turn slightly in the groove so that the bending stresses will be minimal;
- due to the friction in the lock, the mounting has a good damping ability;
- a possible easy blade replacement and cooling them by blowing air through the gaps in the lock.

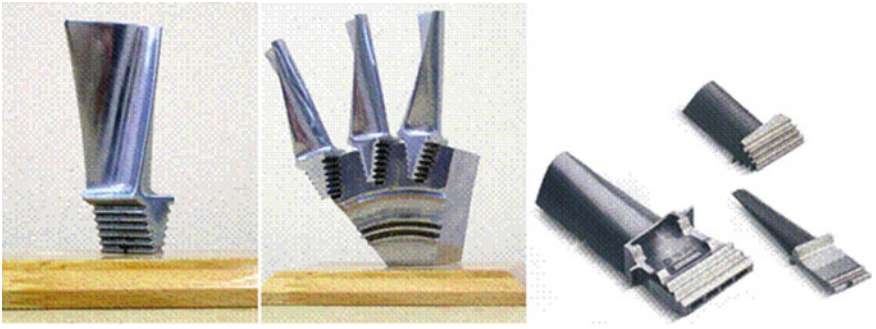

**Fig. 16.22** Blades with a fir-tree roots

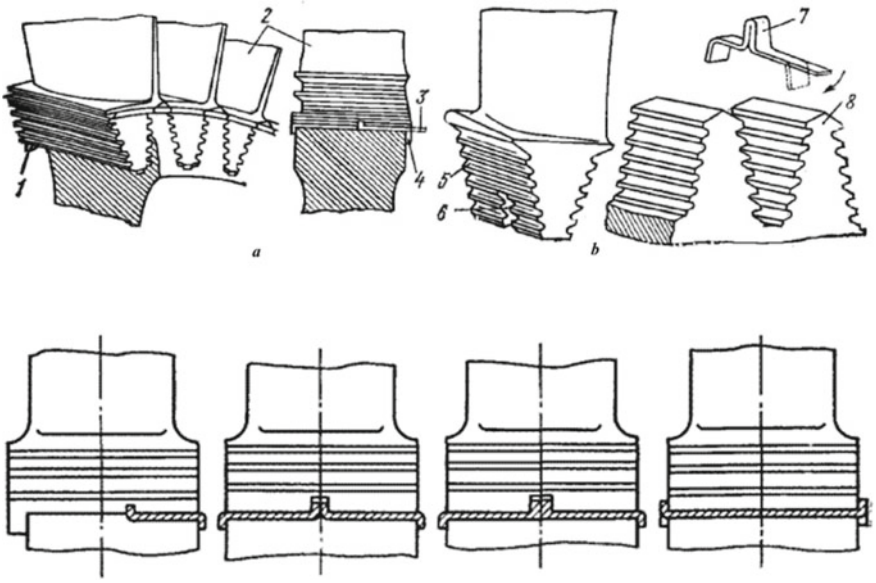


**Fig. 16.23** Fixing of blades with fir-tree roots. *A*—by protrusion and antenna; *b*—by folding plate; 1—protrusion; 2—airfoils; 3—antenna in position before bending; 4—antenna in position after bending; 5—root; 6—groove for fixing of a folding plate; 7—folding plate; 8—disk

**A fir-tree mounting also has such disadvantages**:

- there is a heat transfer from the blade to the disk due to poor contact between them is small;
- there is a large stresses concentration in the serrations of the blades and disk, which can lead to fatigue failure;
- to ensure uniform serration loading, high precision of their manufacture is necessary.

In recent decades, there has been a transition from a large number of serrations in a fir-tree mounting (seven–eight) to a smaller number (three–four). In the latter case, the serrations can be made larger and the stress concentration in them can be reduced.

It is earlier, in low-power engines, the turbine blades could also be mounted in the circumferential grooves **with forked roots on the rivets** and in the individual grooves **with the bulb roots** (Fig. 16.24). Such mountings are characterized by simplicity, a low time of manufacture, and ease of assembly. However, the locks of such mountings were large, the rims of the disks were weakened and large temperature stresses arise in them (because freedom of the thermal expansion was not ensured), especially during a quick start. This led often to the breakage of the blades.

Sometimes (usually in small turbines), the blades are made integrally with the disk by milling. This turbine wheel is called **blisk** (“bladed disk”) (Fig. 16.25). Modern

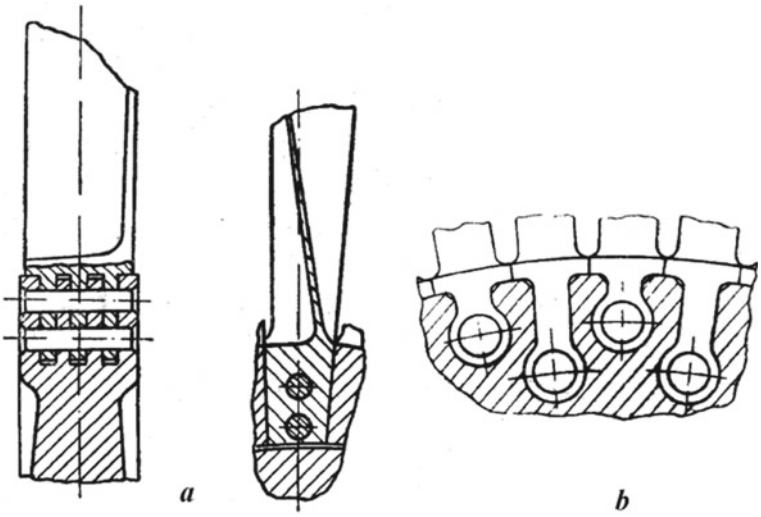


**Fig. 16.24** Types of blade mounting: *a*—with forked roots on rivets; *b*—with bulb roots

**Fig. 16.25** "Blisk" type turbine wheel

blade machines can provide the required manufacturing accuracy and high surface cleanliness. It should be noted that blisk type wheels are not performed only for turbines, but for compressors too [2].

## 16.3 Gas Turbine Blade Cooling

It is clear that the higher the gas temperature before the turbine part, it is the higher the GTU actual efficiency. But the tensile strength of the blade metal and its service life decreases sharply with increasing temperature.

Cooling of the turbine blades allows:

– without changing the gas temperature before the turbine to increase the tensile strength and the service life of the blades, or
– without changing the tensile metal strength to increase the gas temperature before the turbine and to increase the GTU's actual efficiency.

An additional useful effect of cooling is the equalization of the temperature inside the blade, which leads to a decrease in thermal stresses in it and leads to an increase in its service life.

Various methods of blade cooling are used. The **methods of cooling by compressor air** are more widely used, in which air is used as a cooler. It is taken from the engine compressor part. Air during its movement through the internal blade passages cools it and then is discharged in one way or another into the flow part, where it mixes with gas. The movement of air is due to the pressure difference between the inlet compressor point and the outlet turbine point. Most often the first turbine stages with the highest temperatures are cooled.

It should be noted that for air cooling a certain amount of GTU mechanical energy will be spent. Therefore, the compressor air intake leads to a decrease in the power which is produced by GTU (on the amount of mechanical energy which is expended on the cooling air compression). For that reason, the engineers try to take air from the stages, on the one hand, ensuring the pressure difference which is required for movement, and on the other hand, located as close as possible to the compressor beginning.

At present, the **main types of blade cooling** are:

– a convective cooling;
– a combined convective and film cooling;
– a transpiration (porous) cooling.

With **convective cooling**, the cooler (compressor air) moves through the internal blade passages, thereby cooling it. To increase the cooling efficiency, it is necessary (1) to increase the contact surface of the blade with the cooling air and (2) to increase the heat transfer coefficient from the blade to the air. The latter is achieved by maximum turbulization of the air along its movement.

The outflow of the cooling air into the flow part is usually carried out at points of the blade with relatively low-pressure—through the outlet edge or through the upper end (tip) of the blade.

The following design solutions are used to intensify the heat transfer from the blade to the cooling air: a jet blowing, a transverse finning, cylindrical pins, holes, swirling flows ("cyclone cooling"), "vortex matrix", etc. The advantage has the type of heat transfer intensification, in which the required level of the removal heat is achieved at the lowest cooling air consumption.

Figure 16.26 shows some of the simplest schemes of convective cooling with the longitudinal air movement inside the blades, as well as their cooling temperature in height and a chord. The design of the cooled blade with a "vortex matrix" from "Zorya-Mashproekt" is shown in Fig. 16.27.

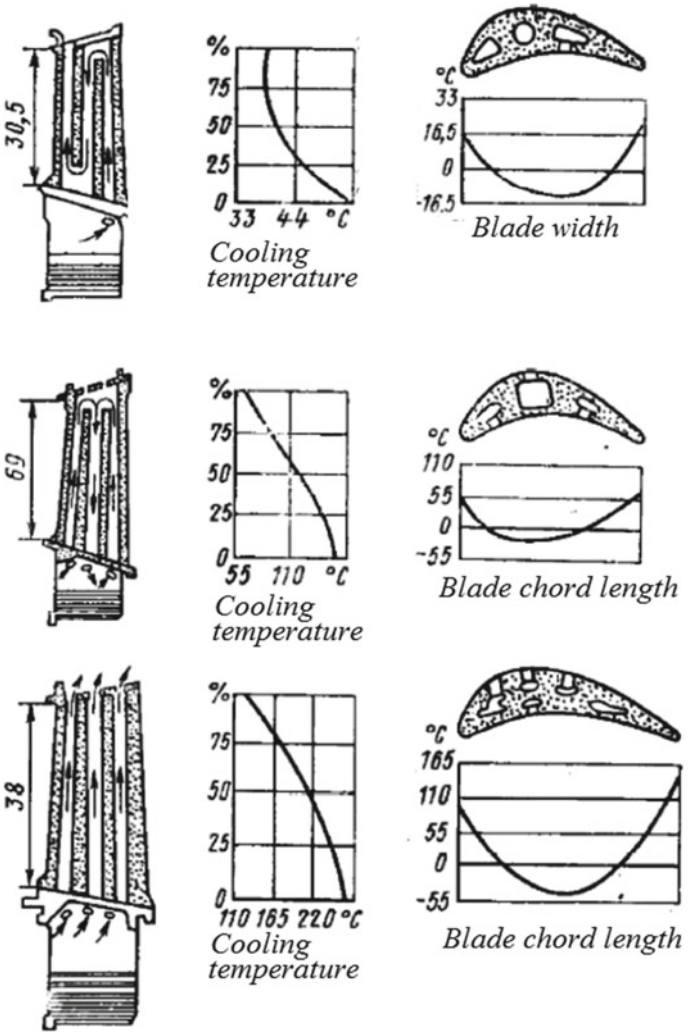


**Fig. 16.26** The simplest convective cooling schemes

Figure 16.28 shows a hollow blade with internal ribs and an insertable deflector (a perforated plate which is designed to distribute evenly the cooling air over the inner surface of the blade), in which the transverse movement of air is carried out [2].

With the **combined convective and film cooling**, a cooler (air) at first cools the internal passages of the blade, and then goes out of the blade through special slots and creates a film of cold air around the outer surface of the blade (Figs. 16.29 and 16.30). An additional protective effect is provided due to the fact that the temperature of the film is significantly lower than the temperature of the main gas flow.

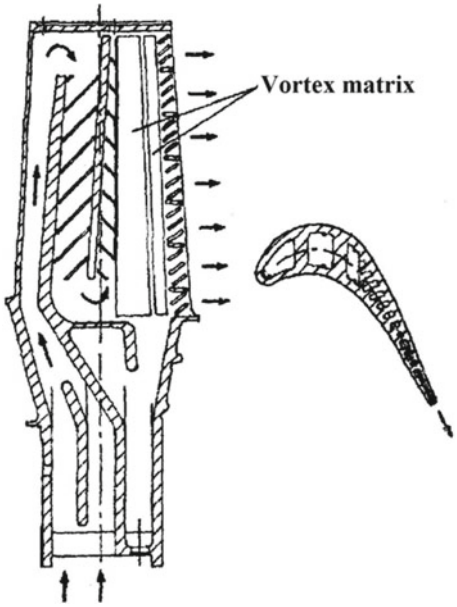


**Fig. 16.27** Cooled blade with a "vortex matrix" from "Zorya-Mashproekt"

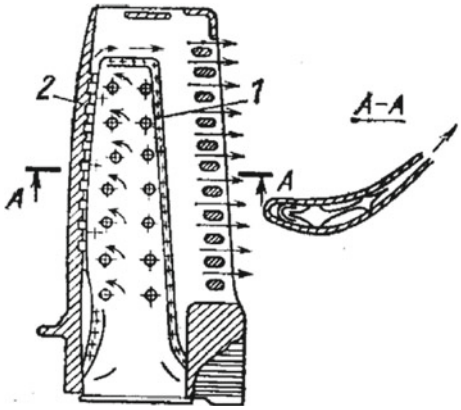


**Fig. 16.28** Cooled blade with a deflector (1) and transverse ribs (2) on the inner surface

The film cooling is the most effective when air is flowing out through the most heated surfaces i.e. the inlet edge, the concave blade surface, etc. The exit of air into these zones requires a little pressure reserve, because these zones are, as a rule, at the same time zones with relatively high-pressure.

Various forms of air exit slots are used: cylindrical, conical, and trapezoidal.

The factors which are affecting the effectiveness of the film cooling are:

– the shape of the exit slots (holes with a diameter of 0.35–1.1 mm are widely used for technological reasons);

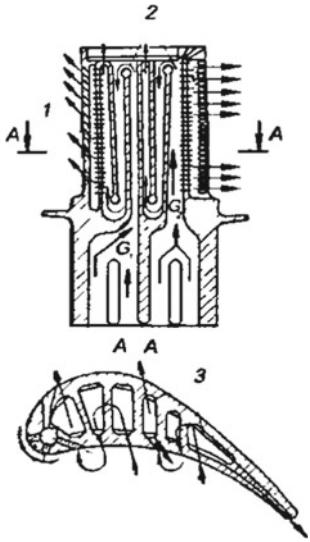


**Fig. 16.29** Blade with convective and film cooling: 1—slots for air exit on the outer surface; 2—inner passages; 3—ribs (heat transfer intensifiers)

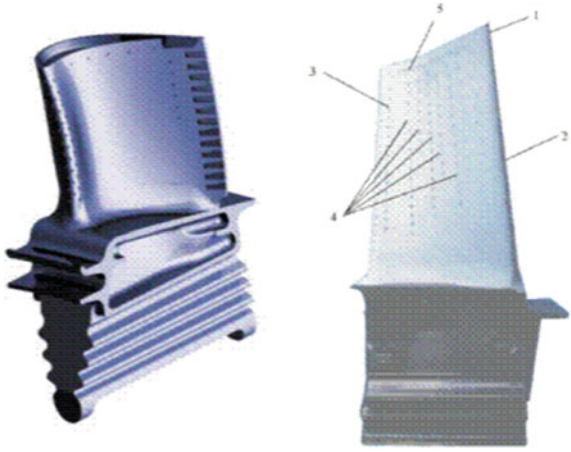


**Fig. 16.30** Blades with convective and film cooling:1—outlet edge; 2—slots in the outlet edge; 3—slots in the inlet edge; 4—slots on the concave surface; 5—slots near the tip of the blade

– the distance between the adjacent slots (for holes this value is usually equal to three diameters);
– the number of slot rows (2–6 for a convex surface, 1–2 for the concave blade surface).

At present, it should be noted that the combined convective and film cooling provides the highest efficiency for blade cooling at the lowest cooling air consumption. Despite its complexity and high manufacturing cost, it is widely used in the first stages of high-temperature gas turbines.

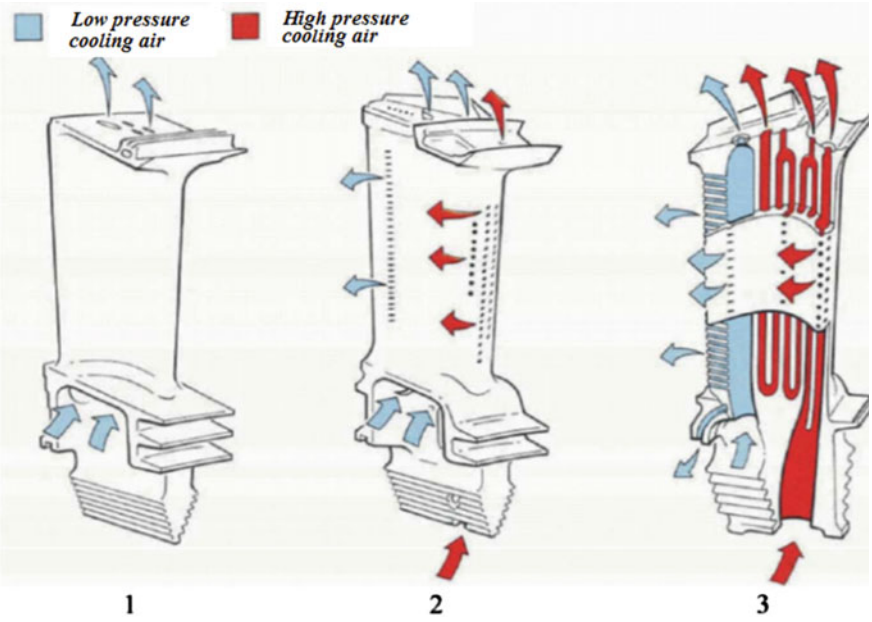


**Fig. 16.31** Development of "Rolls-Royce plc" blade cooling system

Figure 16.31 shows the development of "Rolls-Royce plc" blade cooling system from a single-pass convective scheme 1 to a single-pass convective and film scheme 2 (with a film on the inlet edge and the concave surface near the outlet edge) and then to the multi-pass convection scheme 3 with the intense film cooling [2].

**Transpiration (porous) cooling** is the most promising and should provide the biggest effect from the film.

The blades in this case are made with porous walls. Air from the internal cavities of the blade through numerous pores penetrates to the outer surface, providing a film. Unlike the combined convective and film scheme, this film will be as uniform as possible. The cooling effect of that scheme will be the highest.

Due to technological difficulties, transpiration cooling in its pure form is not used anywhere. The scheme which is close to transpiration cooling is **the "lamilloy" cooling**, which has been developed by the American branch of "Rolls-Royce plc".

That scheme is used for blades the material (so-called *laminate alloy*), which is usually obtained from two to four layers, connected by diffusion soldering (Fig. 16.32). Such material is used to make the blade walls, which are fixed on the rods, ensures the distribution of the cooling air [2].

The layered material allows the choice of the size and shape of the cooling passages and slots, their location, and exit to the outer surface and, therefore, provides the most effective cooling.

An example of such blade ("blade with cooled walls") is shown in Fig. 16.33. The blade has two-layer walls. The thickness of the outer wall is 0.5 mm, and the thickness

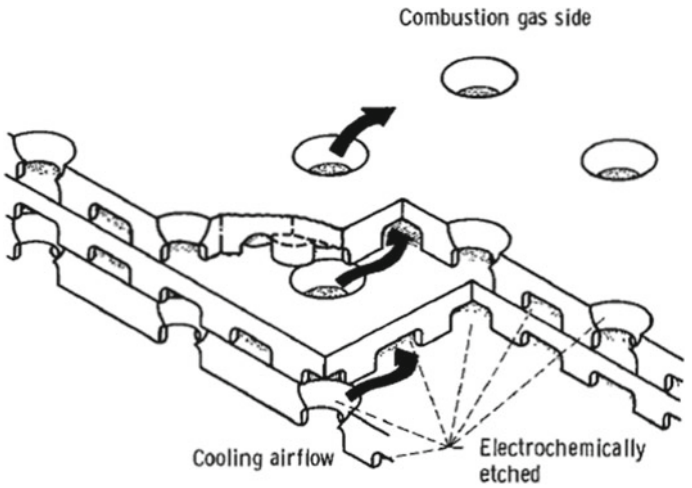


**Fig. 16.32** Scheme of "lamilloy" cooling

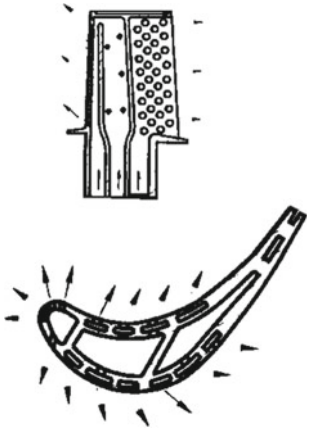

**Fig. 16.33** Blade with cooled walls

of the inner wall is 1 mm. After cooling the inner space between the walls, the air exits evenly to the outer surface through the holes with a diameter of 0.5–1.0 mm, thereby ensuring its film cooling.

It should be noted that the creation of successfully cooled blades is associated with great design and technological difficulties.

## 16.4 Calculation of the GTU Turbine Part

We consider the determination of the main dimensions of the GTU turbine part [4].

GTU turbine part consists of three turbines: high-pressure turbine (HPT), low-pressure turbine (LPT), and power turbine (PT). The dimensions of the turbines are sequentially calculated, starting with HPT. The diagram of the axial turbine is shown in Fig. 16.34.

The calculation of all turbines is carried out according to the same formulas which consider some features.

(1) The following parameters were determined during the thermal calculation of GTU at nominal operating mode:

- a gas flow rate through a turbine $G_t$ (accordingly, $G_{t1}$, $G_{t2}$ and $G_{t3}$);
- temperature before a turbine $T_1$ (accordingly, $T_3$, $T_{3.2}$ and $T_{3.3}$);
- pressure before a turbine $p_1$ (accordingly, $p_3$, $p_{3.2}$ and $p_{3.3}$);
- an air excess coefficient in the combustion chamber $\alpha$.

(2) Specific heat of gas before the turbine:

$$c_{p\,g1} = f(T_1, \alpha).$$

(3) The specific heat ratio for gas before the turbine:

$$k_{g1} = \frac{c_{p\,g1}}{c_{p\,g1} - R_{\text{gas}}},$$

where $R_{\text{gas}} = 0.288 \sim 0.290$ kJ/kg/K is the gas constant.

(4) The medium diameter before a turbine $D_{m\,1}$ is accepted with further clarification in step 26.

For HPT, $D_{m.1}$ is approximately equal to the medium diameter of the flame tube installation.

For LPT, $D_{m.1}$ is approximately equal to the medium diameter before HPT.

For PT, $D_{m.1}$ is a little more than the medium diameter before LPT.

(5) The turbine rotor speed $n_t$ is accepted, based on the GTU design features.

For HPT, $n_t$ is equal to the rotor speed of HPC.

For LPT, $n_t$ is equal to the rotor speed of LPC.

For PT, $n_t$ is equal to the rotor speed of the consumer.

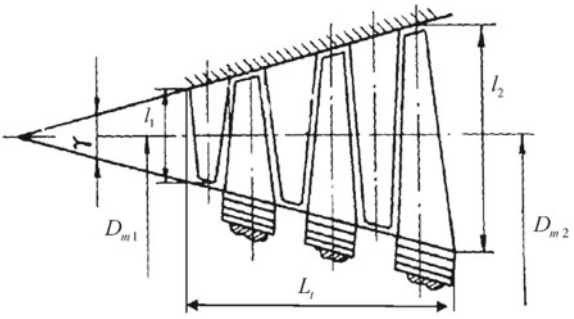


**Fig. 16.34** The diagram of axial turbine

(6) The circumferential velocity at the medium diameter before a turbine:

$$u_1 = \frac{\pi\, D_{m.1}\, n_t}{60}.$$

(7) The axial velocity before a turbine:

$$c_{a1} = (0.30 \ldots 0.40)\ u_1.$$

(8) The specific flow velocity before a turbine:

$$\lambda_{c_{a1}} = \frac{c_{a1}}{\sqrt{\frac{2\,k_{g1}}{k_{g1}+1} R_{\text{gas}}\, T_1 \cdot 10^3}}.$$

(9) The gas-dynamic flow density function before a turbine:

$$q(\lambda_{c_{a1}}) = \lambda_{c_{a1}} \left[ \frac{k_{g1}+1}{2} \left( 1 - \frac{k_{g1}-1}{k_{g1}+1} \lambda^2_{c_{a1}} \right) \right]^{\frac{1}{k_{g1}-1}}.$$

(10) The required flow area before a turbine:

$$F_1 = \frac{G_t \sqrt{T_1}}{\sqrt{\left(\frac{2}{k_{g1}+1}\right)^{\frac{k_{g1}+1}{k_{g1}-1}} \cdot \frac{k_{g1}}{R_{\text{gas}} \cdot 10^3}\ p_1\, q(\lambda_{c_{a1}}) \cdot 10^6}}.$$

(11) Length of the first stage blades:

$$l_1 = \frac{F_1}{\pi\, D_{m.1}}.$$

(12) The outer diameter before a turbine:

$$D_{\text{out.1}} = D_{m.1} + l_1.$$

(13) The inner diameter before a turbine:

$$D_{in.1} = D_{m.1} - l_1.$$

(14) Number of the turbine stages $z_t$ is accepted according to the basic gas turbine engine. For example, such engines of "Zorya-Mashproekt" as UGT3000, UGT6000, UGT10000, UGT15000, and UGT25000 have a single-stage HPT and a single-stage LPT.

Depending on the application, the number of stages of a power turbine $z_{t3}$ can be from 2 to 6.

(15) The following parameters were determined during the thermal calculation of GTU at nominal operating mode:

- pressure after a turbine $p_2$ (accordingly, $p_{4.1}$, $p_{4.2}$ and $p_4$);
- temperature after a turbine $T_2$ (accordingly, $T_{4.1}$, $T_{4.2}$ and $T_4$).

(16) Specific heat of gas after a turbine:

$$c_{p\,g2} = f(T_2, \alpha).$$

(17) The specific heat ratio for gas after a turbine:

$$k_{g2} = \frac{c_{p\,g2}}{c_{p\,g2} - R_{\text{gas}}}.$$

(18) The axial velocity after a turbine:

$$c_{a2} = (1.00 \ldots 1.05)\, c_{a1}.$$

(19) The specific flow velocity after LPC:

$$\lambda_{c_{a2}} = \frac{c_{a2}}{\sqrt{\frac{2\,k_{g2}}{k_{g2}+1} R_{\text{gas}}\, T_2 \cdot 10^3}}.$$

(20) The gas-dynamic flow density function after a turbine:

$$q(\lambda_{c_{a2}}) = \lambda_{c_{a2}} \left[ \frac{k_{g2}+1}{2} \left( 1 - \frac{k_{g2}-1}{k_{g2}+1} \lambda_{c_{a2}}^2 \right) \right]^{\frac{1}{k_{g2}-1}}.$$

(21) The required flow area after a turbine:

$$F_2 = \frac{G_t \sqrt{T_2}}{\sqrt{\left(\frac{2}{k_{g2}+1}\right)^{\frac{k_{g2}+1}{k_{g2}-1}} \cdot \frac{k_{g2}}{R_{\text{gas}} \cdot 10^3}\; p_2\, q(\lambda_{c_{a2}}) \cdot 10^6}}.$$

(22) The layout of the turbine stages choice. The most popular is the layout with a constant medium diameter $D_m = \text{const}$. For a power turbine, the layout with a constant inner diameter or the layout with a constant outer diameter can be adopted too.

If we accept the layout with a constant medium diameter for all three turbines, then medium diameter after turbine:

$$D_{m.2} = D_{m.1}.$$

(23) Length of the last stage blades:

$$l_2 = \frac{F_2}{\pi\, D_{m.2}}.$$

(24) The inner diameter after the turbine:

$$D_{in.2} = D_{m.2} - l_2.$$

(25) The outer diameter after the turbine:

$$D_{\text{out.2}} = D_{m.2} + l_2.$$

(26) At this step we must check the equation:

$$\frac{D_{m.2}}{l_2} > 3.5.$$

If this equation is not fulfilled, then the turbine has an unacceptably big length of the blades. Therefore, we must return to step 4 and increase the medium diameter of the turbine $D_{m1}$, an increase in the medium diameter $D_{m1}$ improves the fulfillment of this equation.

(27) The medium diameter of the turbine:

$$D_{m.t} = 0.5\,(D_{m.1} + D_{m.2}).$$

(28) The medium length of the turbine blades:

$$l_{m.t} = 0.5\,(l_1 + l_2).$$

(29) The ratio:

$$\lambda_t = \frac{D_{m.t}}{l_{m.t}}.$$

(30) The coefficient $\bar{\delta}_t = f(\lambda_t)$ is determined by Table 16.1.

(31) The axial dimension of the single turbine stage:

$$b_{st.t} = \bar{\delta}_t l_{m.t}.$$

(32) The axial dimension of the turbine main casing:

**Table 16.1** Values of the coefficients $\bar{\delta}_t$

| $\lambda_t$ | 4 | 5 | 6 | 7 | 8 | 9 | 10 | 11 | 12 | 13 | 14 | 15 | 16 | 17 | $\geq 18$ |
|---|---|---|---|---|---|---|---|---|---|---|---|---|---|---|---|
| $\bar{\delta}_t$ | 0.62 | 0.77 | 0.91 | 1.05 | 1.17 | 1.27 | 1.37 | 1.46 | 1.53 | 1.60 | 1.66 | 1.71 | 1.74 | 1.79 | 1.82 |

$$L_t = z_t b_{st.t}.$$

(33) The axial dimension of the intersection between LPT and PT:

$$L_{\text{int}} \approx (0.35 \ldots 0.40)\, D_{\text{out.2}}^{\text{LPT}}.$$

(34) The axial dimension of the rear bearing casing for the power turbine:

$$L_r \approx (0.30 \ldots 0.35)\, D_{\text{out.2}}^{\text{PT}}.$$

## References

1. Romanovsky GF, Serbin SI, Patlaychuk VM (2016) Gas turbine plants. Part 1.General structure and classification. Publisher NUS, Mykolaiv, 216 p. (in Ukrainian)
2. Romanovsky GF, Serbin SI, Patlaychuk VM (2017) Gas turbine plants. Part 2. Structural elements. Publisher NUS, Mykolaiv, 196 p. (in Ukrainian)
3. Romanovsky GF, Serbin SI, Patlaychuk VM (2005) Modern gas turbine units. Volume 1. Production units of Ukraine and Russia. Publisher NUS, Mykolaiv, 344 p. (in Ukrainian)
4. Romanovsky GF, Washchilenko NV, Serbin SI (2003) Theoretical basics of ship gas turbine designing. Publisher USMTU, Mykolaiv, 304 p. (in Ukrainian)

# Chapter 17
# Improving the Efficiency of the Gas Turbine Units


The main disadvantage of a simple cycle gas turbine unit is a lower efficiency compared to other types of power plants, or, in other words, a higher specific fuel consumption. So, for example, the actual efficiency of modern gas turbine units with a power of 3 MW or more is 28–42%, diesel power plants with LSE and MSE 46–54% and steam turbine power plants 30–43%.

We consider the main directions of GTU efficiency increasing [1–3].

(1) **Improving the efficiency of the gas turbine unit structural elements**

A gas turbine unit is a combination of several structural parts: a compressor, a combustion chamber, a turbine, a gear, various service systems, etc. Each of them is a complex system consisting of many heterogeneous elements. The efficiency of each element affects directly the overall efficiency of the gas turbine unit. The operation by use of the improving GTU structural elements is ongoing and every year their effectiveness is becoming higher.

(2) **The increase of the gas temperature behind the combustion chamber**

It is clear, that an increase of the gas temperature $T_3$ causes an increase in the actual GTU efficiency.

It is theoretically possible to increase the gas temperature behind the combustion chamber to its optimum value in the combustion zone (2,000–2,200 K). However, we know that an increase in the gas temperature leads to a sharp decrease in the long-term strength of the metal from which the turbine blades are made. This in turn leads to a sharp reduction in the service life of the turbine.[1]

Therefore, the increase of the gas temperature behind the combustion chamber should be accompanied (1) by the creation of new heat-resistant alloys (based on

[1] Very oftensuch a choice is made: either higher GTU efficiency due to a higher gas temperature $T_3$ and a shorter service life (as in aircraft engines), or a longer service life due to a lower gas temperature $T_3$ and lower GTU efficiency (as in stationary power plants).



K. Liu et al. (eds.), *Gas Turbines Structural Properties, Operation Principles and Design Features*, https://doi.org/10.1007/978-981-99-0977-3_17

nickel, chromium, cobalt, tungsten, molybdenum, hafnium) and (2) by the improvement of the cooling systems for the turbine blades. The operation in both of these fields is ongoing.

(3) **The complication of the GTU thermal scheme**

During the XXth century, different methods have been developed to complicate the thermal scheme and thermodynamic cycle of the gas turbine units. All of them more or less led to an increase in the efficiency of GTUs.

It should be noted that the complication of the GTU thermal scheme is the most promising way and gives the biggest increase in efficiency.

In order to increase efficiency, the thermal scheme of GTUs is complicated by using additional heat exchangers.

**The main directions of GTU complications** are:

- the air heating in the recuperator by the exhaust gas;
- the intermediate air cooling between compressors;
- the intermediate gas heating between turbines;
- the heat recovery of the exhaust gas.

In some cases, several of these directions can be realized at the same time.

## 17.1 Gas Turbine Units with Recuperators

In GTU with a recuperator, the exhaust gas is used for heating air before the combustion chamber. It should be recalled that the temperature of the exhaust gas in modern simple cycle GTUs is 650–900 K. The diagram of GTU with the recuperator is shown in Fig. 17.1 [1].

A recuperator is a surface heat exchanger which is placed at the movement of air between the compressor and the combustion chamber, and at the movement of gas between the last turbine and the exhaust. During the heat exchange, the air temperature increases and the temperature of the exhaust gas decreases (Fig. 17.2).

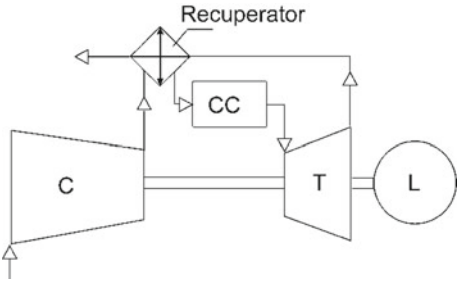


**Fig. 17.1** GTU with recuperator

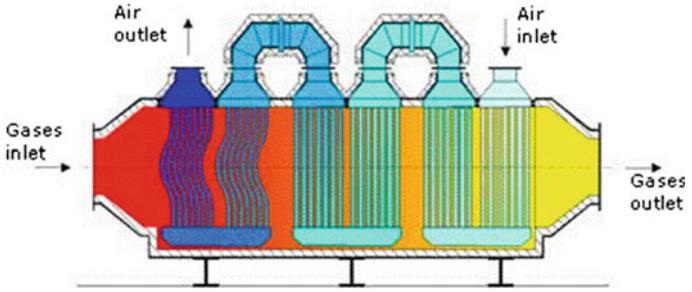


**Fig. 17.2** Diagram of recuperator

An increase in air temperature before the combustion chamber reduces the amount of fuel that needs to be burned in it to heat the gas. Therefore, the efficiency of the gas turbine unit increases.

By using a recuperator, it is possible to increase GTU efficiency 1.20–1.25 times and this way of efficiency increase is much simpler than increasing GTU elements' efficiency or increasing the gas temperature behind the combustion chamber.

An important advantage of using a recuperator is the decreasing of optimal compressor pressure ratio $\pi_c$ in GTU (from 15 to 25 as in a simple cycle to 5–15).

The disadvantages of such GTUs are:

- significant size and weight of the recuperator;
- malfunctions in the recuperator operation (breakdowns due to thermal stresses, air leakage into the exhaust, etc.);
- significant pressure losses during air and gas movement.

An example of GTU with a recuperator is **Mercury 50** engine from "Solar Turbines Inc." (Fig. 17.3). The engine has 4.6 MW power, single-shaft rotor, 10-stage axial compressor, two-stage turbine, the gas temperature behind the combustion chamber is equal to 1436 K, compressor pressure ratio $\pi_c = 9.9$. The actual efficiency of Mercury 50 is 38.5% [1].

Since 1979, the "AVCO Lycoming Co." (and then "Honeywell International, Inc.") produced the 1120 kW **AGT1500** tank gas turbine engine (Fig. 17.4). The engine has a three-shaft rotor, 5-stage axial LPC, axial-centrifugal (4 + 1) HPC, single-stage HPT and LPT, two-stage power turbine, the initial gas temperature is equal to 1466 K, compressor pressure ratio $\pi_c = 14.5$. The actual efficiency of AGT1500 is 28% [1].

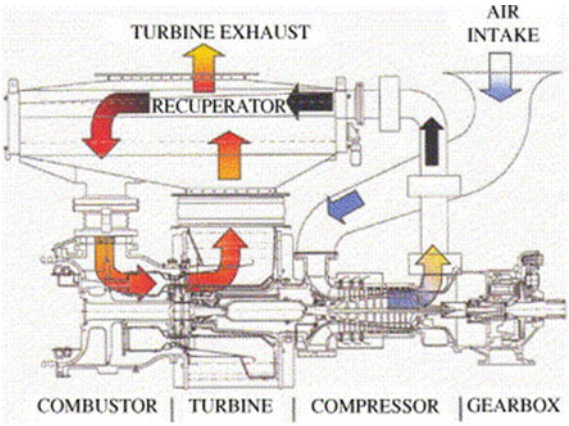


**Fig. 17.3** "Mercury 50" from "Solar Turbines Inc."

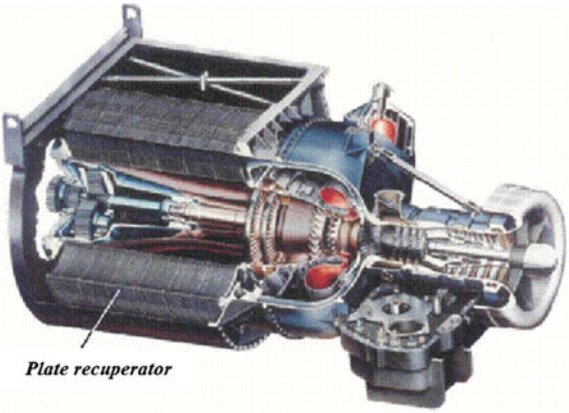


**Fig. 17.4** AGT1500 from "Honeywell International, Inc."

## 17.2 Gas Turbine Units with Intercooling

The intermediate air cooling between the compressors (so-called *intercooling*) is used to reduce the mechanical work which is required to compress the air in the second compressor (Fig. 17.5).

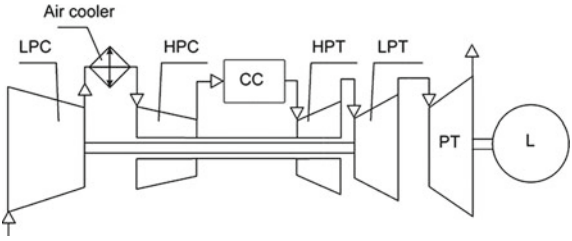


**Fig. 17.5** GTU with intercooling

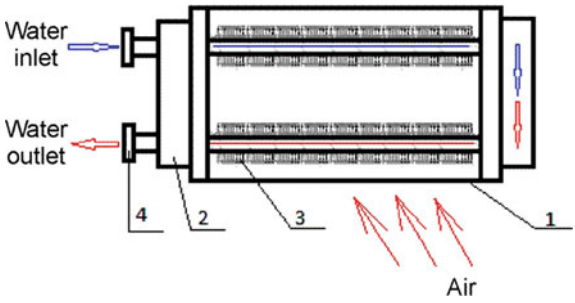


**Fig. 17.6** Diagram of simplest air cooler: 1—casing; 2—water intake; 3—tubular heat exchanger with finning on the air side; 4—flange

The intermediate air cooling necessitates additional heat exchanger use (an air cooler) and a special water cooling system. The attempts to use the atmospheric air as a cooler are rarely made, as a rule, only in some transport (automobile) GTUs.

Due to the big difference in density of water and air, the heat transfer coefficient from the waterside is many times higher than the heat transfer coefficient from the air side. For this reason, to reduce the size and weight of these coolers, most of them use tubular heat exchanger surfaces with finning on the air side (Fig. 17.6) [1].

The mechanical work spent on compressing air in the compressor stages is directly proportional to the temperature of the air which is entering them. Because the air heats up during compression, it is necessary to spend more and more work from stage to stage in order to increase the pressure by the same ratio.

The mechanical work spent on compressing the air is taken from the GTU turbine. Therefore, by applying the intermediate air cooling, we will reduce the required compression work in the stages which are located after the air cooler, and thereby the useful power of the gas turbine unit and its efficiency will increase.

On the other hand, because the air will enter the combustion chamber at a lower temperature, there is a need to increase the consumption of the burned in the combustion chamber fuel to heat gas. That leads to a decrease in GTU efficiency.

From the above information, it follows that **the use of intercooling ambiguously affects the GTU efficiency**. In some cases, the efficiency may increase, and in some cases, it may decrease. We must calculate thoroughly the parameters of the engine to find out what effect (positive or negative) we will obtain.

The useful effect of intercooling will be bigger, the compressor efficiency will be worse, the gas temperature behind the combustion chamber will be lower, and the compressor pressure ratio in GTU will be bigger.

An example of GTU with intercooling is the **LMS100** engine from "General Electric Co." (Fig. 17.7). The intercooling made it possible to increase the compressor pressure ratio to 40, which together with an initial gas temperature of 1653 K ensured efficiency of 45% [1].

The standard layout provides the water cooling of the compressor air. In places of operation with a lack of water resources provides cooling of the compressor air by atmospheric air.

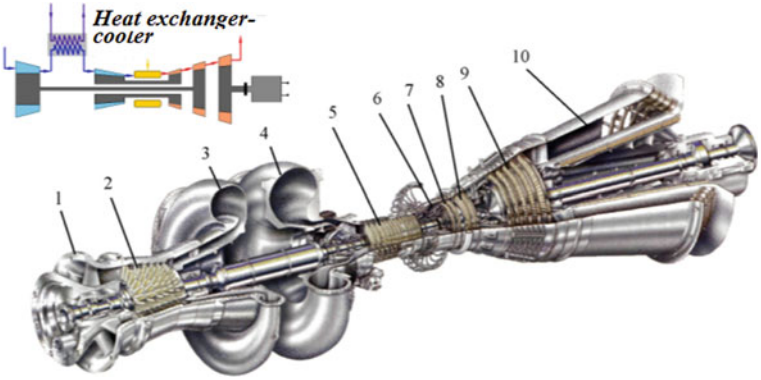


**Fig. 17.7** 100 MW LMS100 engine from "General Electric Co.": 1—inlet casing; 2—6-stage LPC; 3—air duct to cooler; 4—air duct from cooler; 5—14-stage HPC; 6—combustion chamber; 7—2-stage HPT; 8—2-stage LPT; 9—5-stage power turbine; 10—gas exhaust

**The intermediate air cooling can be carried out** not only in a heat exchanger, as previously considered but also **by water which is injected directly into the airflow between the compressors**. The air cooling will occur due to the evaporation of the water drops in the hot air volume. For rapid evaporation, the spray system must ensure the size of drops is less than 20 μs.

A similar diagram is realized in the 48 MW **LM6000PC SPRINT** engine which is produced by "General Electric Co.": "SPRINT" is an abbreviation of "SPRay INTercooling". Water is sprayed through 24 nozzles which are located between the compressors (Fig. 17.8) [1, 4].

The SPRINT system is the most effective when the engine is operated in the hot season when an increase in the atmospheric air temperature leads to a significant decrease in the generated power. At an air temperature of 15 °C, the water injection

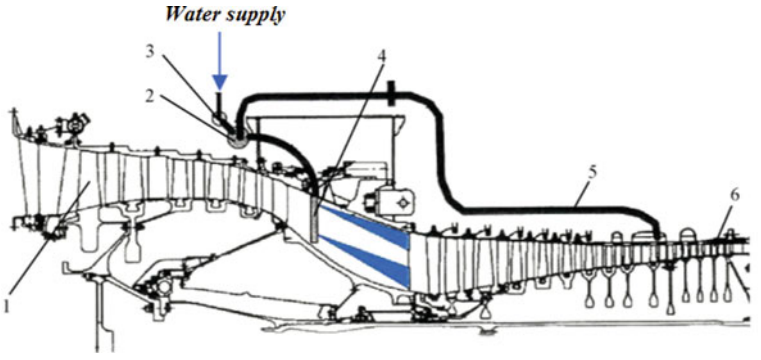


**Fig. 17.8** Spray intercooling of LM6000PC SPRINT engine from "General Electric Co.". 1—5-stage LPC; 2—atomizing air manifold; 3—water manifold; 4—spray nozzles; 5—air extraction from 8th stage of HPC for spraying water; 6—14-stage HPC

leads to an increase of GTU power by 9%; at a temperature of 32 °C, the power as a result of the water injection increases by 20%.

The useful effect of the intercooling increases sharply when it is used together with a recuperator (Fig. 17.9).

"Rolls Royce plc" for the needs of the Navy in the last years of the XX century created a 25 MW gas turbine unit WR-21 (Fig. 17.10). That engine has high efficiency both in nominal and partial operating modes (42.3% at the nominal mode and 41.4% at the mode of 0.4 of the nominal) [1].

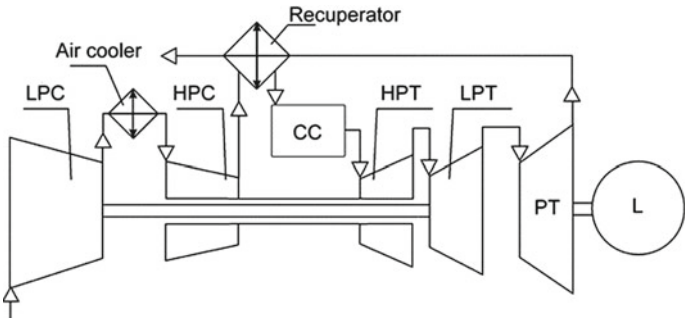


**Fig. 17.9** GTU with intercooling and recuperator

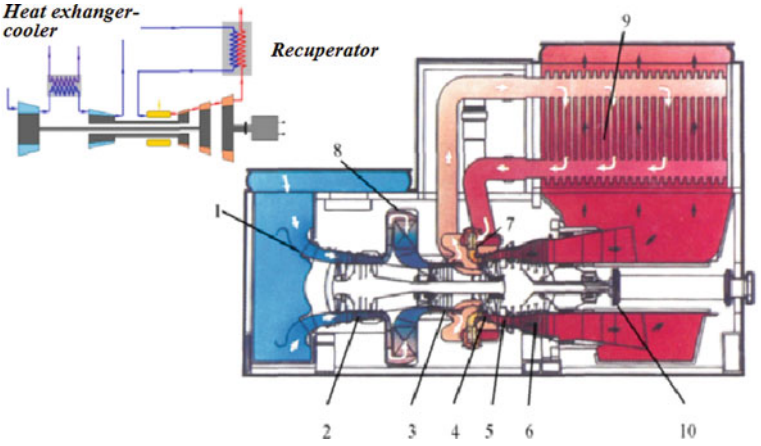


**Fig. 17.10** 25 MW WR-21 engine from "Rolls-Royce plc". 1—inlet casing; 2—7-stage LPC; 3—6-stage HPC; 4 and 5—single-stage HPT and LPT; 6—5-stage power turbine; 7—combustion chamber; 8—air cooler; 9—recuperator; 10—output shaft

## 17.3 Gas Turbine Units with Sequential Combustion

The intermediate heating of gas between turbines allows for increasing the power which is produced by a gas turbine unit.

To provide sequential combustion, such GTU has additional combustion chambers (Fig. 17.11). Because the air excess coefficient of GTU is 2.5–4.0, the oxygen content in the gas is quite enough for the normal operation of these chambers.

The total number of combustion chambers which are sequentially operating must be no more than two because each additional chamber complicates significantly the control of GTU.

The heating of gas in the additional combustion chamber before the power turbine increases the potential energy of the gas, which can be converted into mechanical work in this turbine. That in turn leads to an increase in the useful power and efficiency of the gas turbine unit.

However, the use of an additional combustion chamber means an increase in the total fuel consumption in GTU, which leads to a decrease in efficiency.

From the above information, it follows that **the use ambiguously of intermediate heating affects the GTU efficiency**. In some cases, the efficiency may increase, and in some cases, the efficiency may decrease.

The examples of GTUs with sequential combustion are GT24 (192 MW) and GT26 (297 MW) engines from "Alstom S.A." (Fig. 17.12). The engines have a single-shaft rotor. The 22-stage axial compressor provides the pressure ratio $\pi_c = 32$. The first turbine has a single-stage; the second turbine has four stages. At an initial gas temperature of 1528 K, the engine efficiencies are respectively: 37.6 and 39.0% [1, 4].

Intermediate gas heating is used widely in aircraft turbojet and turbofan engines for a short-term sharp increase in the thrust and flight speed. The additional combustion chamber is called an **afterburner** and is directly placed before the jet nozzle. The use of the afterburner leads to a decrease in engine efficiency.

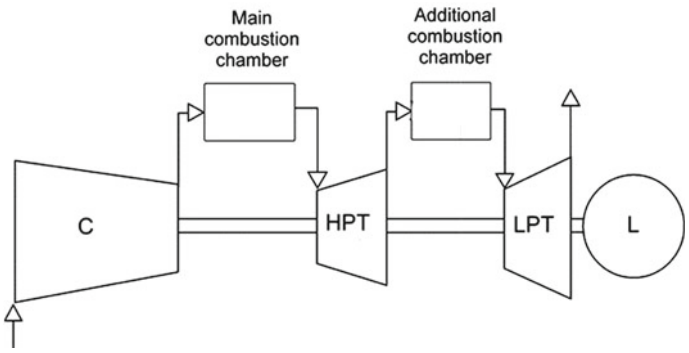


**Fig. 17.11** GTU with sequential combustion

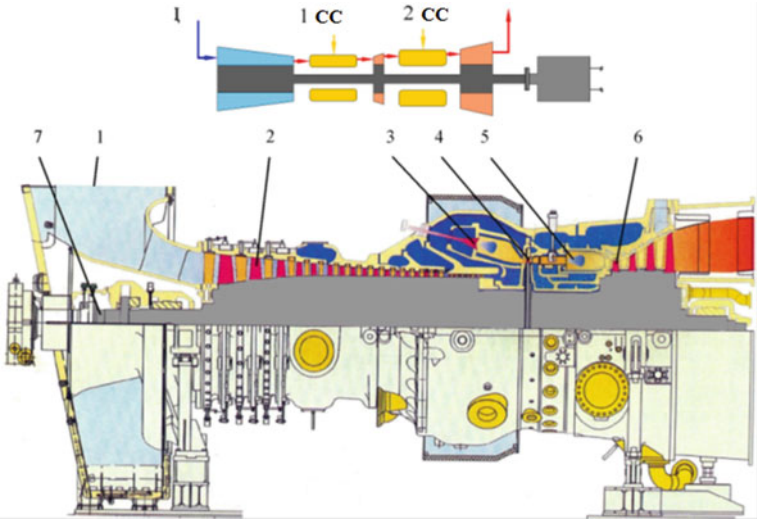


**Fig. 17.12** Layout of GT24 and GT26 engines from "Alstom S.A.". 1—inlet casing; 2—22-stage compressor; 3—combustion chamber; 4—single-stage HPT; 5—additional combustion chamber; 6—4-stage LPT; 7—output shaft

## 17.4 Gas Turbine Plants with Heat Recovery Steam Generators

At present the temperature of the exhaust gases from the simple cycle GTUs is 650–900 K. Therefore, the exhaust gas has a significant amount of thermal energy, which can be used. It should be noted that the tendency to increase the gas temperature behind the combustion chamber leads to an increase in the exhaust gas temperature. Therefore, the thermal energy of the exhaust gas during the GTU development will increase.

The utilization of the exhaust thermal energy consists of its use for producing steam or heating water. This is structurally ensured by the use of the **heat recovery steam generator (HRSG)** with a piece of special service equipment (Fig. 17.13) [1].

Sometimes, to increase the steam temperature, a small amount of fuel is re-burned in the duct between the engine and the HPSG.

At present, utilization of exhaust thermal energy is the most effective way to increase the efficiency of the gas turbine units.

The received in HRSG steam can be used:

– for heating of buildings or industrial needs;
– for producing the additional power in a steam turbine;
– for producing the additional power in the GTU turbine.

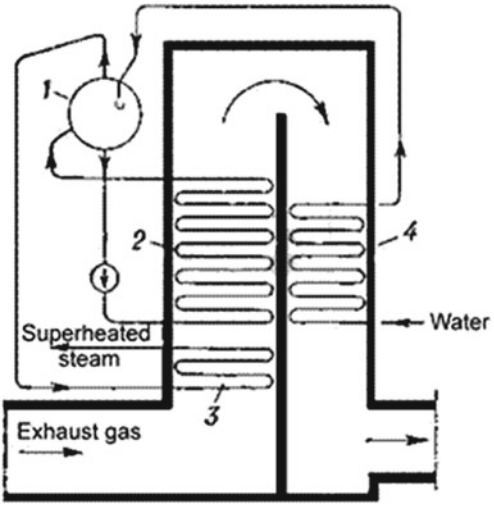


**Fig. 17.13** Scheme of simplest HRSG. 1—steam separator; 2—evaporator; 3—superheater; 4—economizer

## Combined heat and power plants

The power plants in which the steam or hot water which have been produced in HRSG is used for heating buildings or industrial needs are called **combined heat and power (CHP) plants**. They have also the name **cogeneration plants**.

The term "cogeneration" means that a gas turbine plant generates jointly mechanical energy (on the engine output shaft) and thermal energy (in the form of steam or hot water which is supplied to the consumer) (Fig. 17.14). The mechanical power in such plants is determined by the power of the gas turbine engine, and the value of the thermal power can vary widely depending on the HRSG type.

The modern cogeneration plants have a high utilization rate of fuel energy (75–85%) and are the most effective power plants for industry and public utilities, where

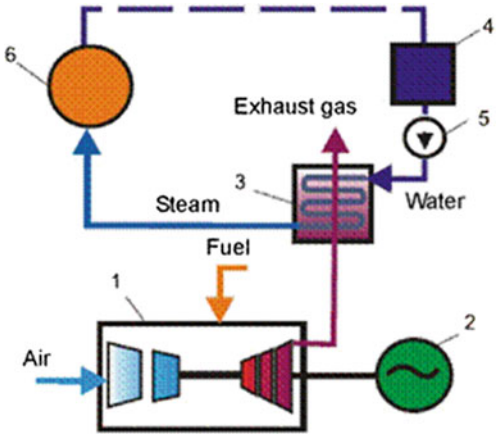


**Fig. 17.14** Diagram of combined heat and power plant. 1—engine; 2—generator; 3—HRSG; 4—water tank; 5—pump; 6—consumer of heat energy

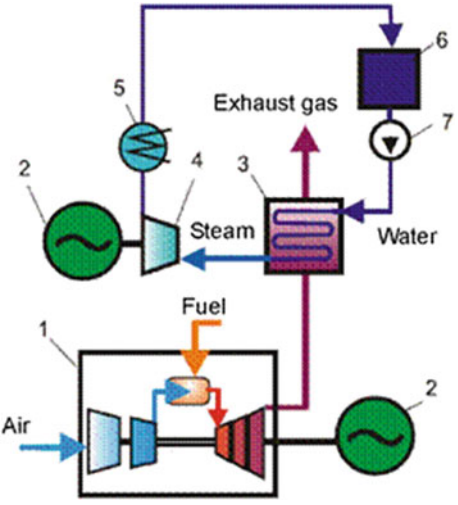


**Fig. 17.15** Scheme of multi-shaft combined cycle power plant. 1—engine; 2—generator; 3—HRSG; 4—steam turbine; 5—condenser; 6—water tank; 7—pump

there is a constant need for both electrical and thermal energy in the form of hot water or steam.

### Combined cycle power plants

A power plant, in which the steam from HRSG is used to produce the additional power in a steam turbine, is called **combined cycle power plant (CCPP)** (Fig. 17.15). Sometimes they are called **combined cycle gas turbines (CCGT)** [1].

These plants can have a multi-shaft or a single-shaft layout.

**A multi-shaft CCPP** may consist of one gas turbine engine and one steam turbine (see Fig. 17.15) or may consist of two gas turbine engines and one steam turbine.

**A single-shaft CCPP** scheme is considered to be more promising at present. Its characteristic feature is the placement of a gas turbine engine and a steam turbine in line with a common shaft that drives one common generator (Fig. 17.16). A typical arrangement of the single-shaft CCPP equipment is engine—electric generator—*SSS* (Synchro-Self-Shifting) *clutch*—steam turbine. The *clutch* of this type provides the possibility of the completely independent operation of the gas turbine engine.

At present, the combined cycle power plants are produced with HRSGs that generate steam of single pressure, dual pressure, or triple pressure. Dual pressure and triple pressure CCPPs provide more effective utilization of the exhaust thermal energy and have higher efficiency.

Triple pressure CCPPs are often performed with intermediate steam superheating (so-called *reheating of steam*). This is mainly done to reduce steam humidity at the last stages of the turbine.

Due to the complexity, considerable size, weight, and cost, the combined cycle power plants are mainly used in electric power generation. In the XXth century, CCPP received some applications in marine transport. So, for example, "Zorya-Mashproekt" developed the **M25** combined cycle power plant **for container ships**

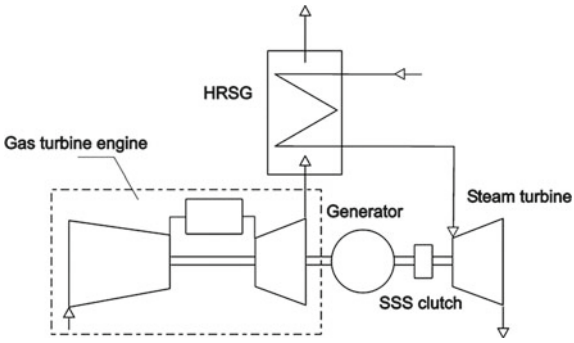


**Fig. 17.16** Diagram of single-shaft CCPP

**of the "Atlantic" type**. Four such ships were built in Mykolayiv. Ukraine, from 1979 to 1987.

The container ship has two propellers (Fig. 17.17). Two M25 with a total power of 37 MW provide a speed of 25 knots (Fig. 17.18).

In the 80s in Mykolayiv, three missile cruisers of the "Atlant" type were built. All of them were equipped with M21 combined cycle power plant.

It should be noted that at present CCPPs are considered as the most efficient and environmentally friendly type of power plant. In the latest stationary CCPPs, the actual efficiency exceeded 60%. It is significantly higher than in the steam turbine plants by use of both organic and nuclear fuel.

It should be noted that the complication of GTU by using HRSG, the steam turbines and the additional equipment increases significantly its size, weight and cost, worsens its maneuverability and reliability, and complicates the maintenance and operation.

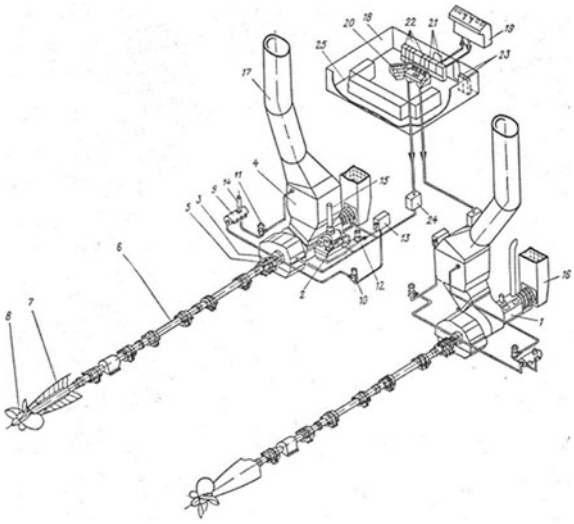

**Fig. 17.17** Power plant of "Atlantic" container ships

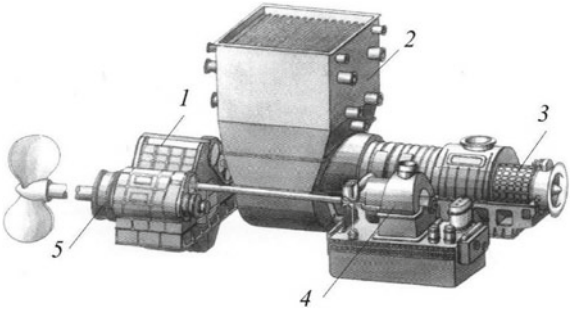


**Fig. 17.18** M25 gas turbine unit. 1—gear; 2—HRSG; 3—gas turbine engine; 4—steam turbine; 5—clutch

So, for example, the total weight of the M25 plant is equal to 143 tons. The weight of the engine together with the frame, the air intake, and the gas exhaust devices is only 19 tons (13% of total weight). The weight of HRSG with the pumps and the steam separator is 45 tons (31.5%). The weight of the gear with the clutch is 55 tons (38.5%). The weight of the steam turbine is 22.7 tons (16%).

### Cheng Cycle Power Plants

The power plants, in which the steam from HRSG is used to produce additional power in the turbine of the GTU, are called **Cheng cycle power plants** (Fig. 17.19) [1].

In such plants, steam from HRSG is sent to the dilution zone of the GTU combustion chambers, where it is mixed with gas. The resulting gas-steam working fluid moves through GTU turbine and produces mechanical energy. The consequence of the increased working fluid flow is an increase in the power output and the GTU efficiency.

Such power plants were named after American scientist and professor of the University of Santa Clara (California, USA) Dah Yu Cheng who patented them in 1976.

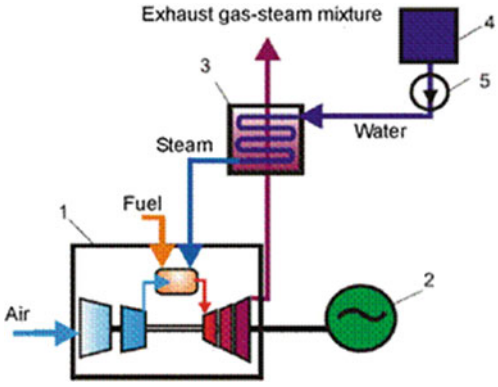


**Fig. 17.19** Scheme of Cheng cycle power plant. 1—engine; 2—generator; 3—HRSG; 4—water tank; 5—pump

In 1984, the first Cheng cycle power plant was commissioned at San Jose State University (USA). At present, the total number of such plants is already several hundred.

**The main advantage** of Cheng cycle power plants in comparison with **CCPP** is the absence of a steam turbine, which simplifies greatly the maintenance and operation, and reduces the total weight, size, and cost of the plant.

**The main disadvantages** of these plants include a complex control system, a salt deposition on the turbine blades, and significant consumption of water.

In Cheng cycle power plants the exhaust steam with gas goes into the atmosphere. For plants with the power of 16–25 MW, the water consumption is 20–30 t/h. Therefore, a special water preparation station is required.

To reduce the consumption of water, "Zorya-Mashproekt" created the special "**Aquarius" technology**, which allows the extracting of the steam from the exhaust gas-steam mixture and returning it to a cycle.

## References

1. Romanovsky GF, Serbin SI, Patlaychuk VM (2005) Modern gas turbine units. Volume 1. Production units of Ukraine and Russia. Publisher NUS, Mykolaiv, 344 p. (in Ukrainian)
2. Giampaolo T (2006) Gas turbine handbook: principles and practices. 3rd edn. The Fairmont Press, 437 p
3. Boyce MP (2006) Gas turbine engineering handbook, 3rd edn. Elsevier Inc., 936 p
4. Romanovsky GF, Serbin SI, Patlaychuk VM (2008) Modern gas turbine units. Volume 2. Production units of Western European countries, America and Asia. Publisher NUS, Mykolaiv, 420 p. (in Ukrainian)